NOVEL CRYSTALLINE FORMS OF ACTIVE PHARMACEUTICAL INGREDIENTS

A Thesis Submitted to the University of Hyderabad in partial fulfillment of the Award of PhD Degree in Chemistry

By

Nagula Rajesh Goud

School of Chemistry

University of Hyderabad

Hyderabad 500046, Andhra Pradesh, India

June 2013

DEDICATION

To

Amma & Nanna

CERTIFICATE

This is to certify that the thesis entitled **"Novel Crystalline Forms of Active Pharmaceutical Ingredients"** submitted by **Nagula Rajesh Goud** bearing Regd. No. 08CHPH07 in partial fulfillment of the requirements for the award of Doctor of Philosophy in Chemistry is a bonafide work carried out by him under my supervision.

The thesis has not been submitted previously in part or in full to this or any other University or Institution for the award of any degree or diploma.

Prof. Ashwini Nangia
Thesis Supervisor

Dean
School of Chemistry

DECLARATION

I, **Nagula Rajesh Goud**, hereby declare that this thesis entitled **"Novel Crystalline Forms of Active Pharmaceutical Ingredients"** submitted by me under the supervision of **Professor Ashwini Nangia** is a bonafide research work. I also declare that it has not been submitted previously in part or in full to this University or any other University or Institution for the award of any degree or diploma.

Hyderabad

Date:

Signature:

Name: **Nagula Rajesh Goud**

Regd. No. 08CHPH07

ACKNOWLEDGEMENTS

I express my deep sense of gratitude and profound thanks to **Prof. Ashwini Nangia** for his inspiring guidance and constant encouragement throughout the course of this research work. I have been able to learn a great deal in this fascinating field of research through his inspiring lectures and thought provoking discussions, and I consider my association with him a rewarding experience.

I thank Prof. M. V. Rajasekharan, Dean, School of Chemistry, former Deans Prof. D. Basavaiah, Prof. M. Periasamy and faculty for their co-operation in providing facilities in the School. I thank Prof. Gautam R. Desiraju for his inspiring lectures and motivation.

I am thankful to Dr. Chelli. Janardhana, Dr. K. Anil Kumar, Dr. G. Nageshwara Rao, Dr. Jagadeeshwara Rao, Dr. B. Shiva Kumar, Prof. M. Anil Kumar, Prof. Krupanidhi, and all other lecturers who taught me throughout my career. My sincere thanks to Dr. Sailesh Srivastava, Uday Kumar, and other teachers from Sri Satya Sai Higher Secondary School and my school teachers Mr. Sharma, Mr. Suresh, Mr. Narsimha rao, Smt. Kameshwari, Mr. Guruvaiah and all others for guiding me through my school and college education. My sincere regards to Prof. Javed Iqbal of ILS for his encouragement.

I am grateful to CSIR, New Delhi, for providing fellowship support. I thank UGC and DST for providing instrumentation and infrastructure facilities at the School of Chemistry.

I thank each and every non-teaching staff of the School of Chemistry, CIL, and Administrative section for their assistance on various occasions. I take this opportunity to thank Dr. P. Raghavaiah for his kind help in acquiring the Single crystal data on various occasions. I thank Mr. Satyanarayana, Smt. Vijayalakshmi and Turabuddin for their help in recording NMR spectra. I thank Mr. Mallaya Shetty garu, Kumar, A. V. Ramana, Mr. Vijay Bhaskar, Mr. Dilip, Mr. Sai, Mr. Sharma, Mr. Jayaram, Mr. Desbandu, Mr. Durgesh, Mr. Shetty and Mr. Naik for their cooperation.

It gives me immense pleasure to thank my lab mates Dr. Jagadeesh Babu, Dr. Bipul Sarma, Dr. Ranjit Thakuria, Dr. Naba Kamal Nath, Dr. Palash Sanphui, Dr. Suryanarayan, Kalyan, Maddileti, Sudalai, Geetha, Suresh, Swapna, Sudhir and Ronak for their help, cooperation and maintaining a cheerful atmosphere in the lab. My

association with them is unforgettable and cherishable. I appreciate the support of Sreenu, Uday, Sumanth, Swarupa, Raghavender, Srikanth, Chaitanya, Viswanath, Dr. Ruchi, Dr. Soumendra Rana and Dr. Damandeep on various occasions. I would like to thank Dr. Saikat Roy, Dr. Prashanth, Dr. Tejender and Dr. Balakrishna Reddy for their help and encouragement.

My stay on this campus has been pleasant with the association of many students, Prabhakar anna, Phani pavan anna, Ramesh anna, Anji anna, DK anna, Ramu anna, Satpal bhai, Rajagopal, Tirupathi, Sashi, Ramu Yadav, Gangadhar, Nanda Kishore, Naveen, Kishore, Pavan, Chary, Swamy, Shiva, Sanathan, Narayana, Chandu, Bharath, Sridevi, Ram, Kishore, Anand, Praveen, Ganesh, Vignesh, Sudhangshu, Mousami, Balu, Nagaraju, Srinivas, Ganesh, Vikranth, Chary, Kondalu, Gupta, Balaswamy, Santosh, Ashok, Jallu Kumar and all others whose names are not mentioned due to lack of space.

I would like to thank my SSIHL friends, Giddi, Hema, Goutam Raju, Sreenivas Raju, Govinda Narayan, Sampath, Rama Krishna, Sunil, Sivaram Raju, Pratap, Ranganath, Manoj, Aravind, Raj Bhushan, Raghava, Varma, Debashis, Arun, Pavan, Ajay, Shiva for their ever willing support and encouragement. I would like to thank my Gurukulam friends, Koti, Karun, Karri, Sharath, Sivaram, SSR, Nandu, PSN, Chanakya, YG, Ravi Kiran, TVS, Dilip, VNA, Nalini and Pavani for their wonderful friendship.

I would like to express my love and gratitude to Bhagawan Sri Sathya Sai Baba, who is my source of inspiration, and has taught me the basic principles of life. His teachings enabled me to cultivate patience and perseverance to endure challenges in life.

My heartfelt thanks to Nanamma and Ammamma for their blessings. I would like to take this opportunity to appreciate the support from my relatives, kamala pinni, Rajeshwar babai, Padma pinni, Venu babai, Aruna pinni, Ashok babai, Shantha pinni, Naresh babai, and my cousins, Puppy, Nishu, Nani, Chinna, Teja, Sachin, Choti, Chikki and Dimple.

The unconditional love of my Amma & Nanna and their blessings made me what I am today and I owe everything to them. Dedicating this thesis to them is a minor recognition to their boundless love and affection. The love and support i received from my brother Prashanth & sister Pranitha are invaluable. I feel immensely blessed to have them as siblings.

–Rajesh

SYNOPSIS

This Thesis entitled "**Novel Crystalline Forms of Active Pharmaceutical Ingredients**" consists of eight chapters

CHAPTER ONE

Introduction to Crystal Engineering and Pharmaceutical Solids

The subject of 'Crystal Engineering' aims to understand and design novel solid forms of molecules with predefined properties by methodically altering their intermolecular interactions. Complex solid state assemblies are systematically downsized into supramolecular synthons comprising complementary functional groups that are held together by a range of non-covalent interactions. Apart from the Electrostatic, π-stacking, Halogen bonding, and Van der Waals forces, Hydrogen bonding is the primary directional interaction, known for its pivotal role in complementing crystal engineering principles for supramolecular synthesis. Today the concept of crystal engineering is widely applied to design functional solids encompassing the areas of host-guest complexes, network solids, metal-organic frameworks and coordination polymers. Nevertheless, crystal engineering is popular among academic and industrial chemists for its ability to design novel pharmaceutical solids for drug development.

The advantage of a pharmaceutical solid formulation lies in its convenience to patients, mode of administration, ease of manufacture and storage. A solid formulation may contain the drug molecule either as a polymorph/mixture, salt, amorphous form, or solvate/hydrate blended with excipients. By the virtue of their hydrophilic/hydrophobic nature, pharmaceutical solid forms can exhibit a wide spectrum of physicochemical properties like solubility, dissolution, stability and bioavailability. Consequentially, they have a significant role in developing optimal formulations of a drug for better therapeutic effect and drug-patient compatibility.

Based on the adapted design strategies and experimental procedures, a pharmaceutical solid may exist in a single or a multi component form. Multi component solids of a drug may be in the form of a 'Salt' where the components are held together by ionic

interactions, or ‘Hydrate/ Solvate’ where the crystal lattice of drug molecule contains stoichiometric amounts of solvent or water molecules. API’s can also be modified into ‘Cocrystals’, a recently popularized multicomponent system where the stoichiometric components are solids at ambient conditions and are held together by non-covalent interactions. ‘Eutectics’ and ‘Solid Solutions’ are much less explored and poorly understood multicomponent systems for pharmaceutical applications. While solid solution is a homogeneous phase of two or more solids with variable stoichiometry, eutectics are defined as a conglomerate of solid solutions. Although eutectics exhibit fixed stoichiometry, they differ from cocrystals in terms of molecular interactions; i.e. unlike cocrystals cohesive forces prevail over adhesive interactions retaining the parent lattice structure. Except eutectics and solid solutions all the multicomponent and single component phases are capable of exhibiting ‘polymorphism’, effectively multiplying the structural landscape of a molecule. The phenomenon of Polymorphism by which a molecule adopts more than one crystalline arrangement and the aperiodic ‘amorphous phase’ where the periodicity is restricted to the nanoscale level is often observed in both single and multicomponent systems. Therefore, thorough screening of a drug molecule may result in any of the above mentioned solid forms for pharmaceutical applications. Diversity in the nature of pharmaceutical solid forms is essential because the pathological profile of a disease/infection might demand different formulations of a drug at various stages for effective treatment. In such cases, the wide range of physicochemical properties offered by the solid forms of an API would prove highly beneficial.

In essence, this chapter deals with the brief description of crystal engineering principles and pharmaceutical solids forms. It acts as a prelude to the working chapters of this thesis which deal with identifying novel heterosynthon for solid form development and discovering various pharmaceutical solid forms with promising physicochemical properties.

CHAPTER TWO

Sulfonamide-Pyridine-*N*-Oxide Heterosynthon in Cocrystal Design

The concept of supramolecular synthon has a significant role to play in rational cocrystal design. Using synthon concept complex supramolecular architectures in crystals can be systematically downsized into robust intermolecular interactions between complementary functional groups of molecules. Therefore, apart from the utilization of known synthons, discovering novel heterosynthons for unexplored functional groups is absolutely essential in designing cocrystals for pharmaceutical applications.

Sulfonamides occupy a place of prominence in drug molecules, being the common functional moiety in sulfa drugs. Whereas a few isolated cases of sulfonamide hydrogen bonding to other functional groups, such as COOH, $CONH_2$, urea, etc., are reported, there is no specific heterosynthon associated with the SO_2NH_2 group. Our objective was to develop a reliable heterosynthon for sulfonamide moiety using a complementary and robust functional group. For this purpose we chose Pyridine-*N*-oxide as complementary hydrogen bond acceptor. An advantage with pyridine-*N*-oxide compared to COOH and $CONH_2$ as a complementary functional group is that homosynthon competition is minimal in pyridine-*N*-oxide because it lacks strong donor groups of its own. In addition, the Cambridge Structural Database does not contain even a single hit of a primary sulfonamide and pyridine-*N*-oxide functional group in the same crystal structure, suggesting that this class of heteromeric cocrystals is completely unexplored. We have explored the probability of forming reliable heterosynthon by cocrystallizing model sulfonamides and a drug molecule, Furosemide with pyridine-*N*-oxides by using the traditional solution crystallization, liquid assisted grinding and slurry grinding methods. We were successful in obtaining six cocrystals containing sulfonamide and pyridine-*N*-oxide moieties (Scheme 1).

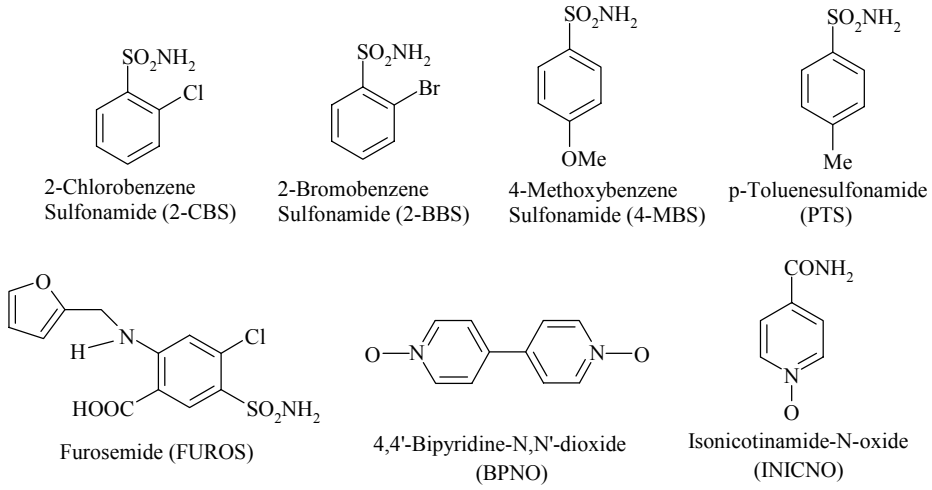

2-CBS–BPNO (1:1) **2-BBS–BPNO (1:0.5)** **4-MBS–BPNO (1:0.5)**

PTS–BPNO (2:1) **FUROS–BPNO–H_2O (1:1:0.25)** **FUROS–INICNO (1:1)**

Scheme 1 Chemical structures of Sulfonamides and Pyridine-*N*-oxides successful in forming cocrystals.

Crystal structure analysis revealed that the exact geometry of the sulfonamide motif, i.e. discrete N–H···O (D), cyclic motifs $R^2_4(8)$ or $R^2_2(4)$ varies from one structure to another and it is difficult to anticipate their presence in a particular structure. Perhaps the non-planarity of the SO_2NH_2 group prevents the formation of a two-point motif with an aromatic partner group. Nevertheless, the heteromeric N–H···$O_{N\text{-oxide}}$ one-point synthon is the recurring interaction in all the structures. Interestingly, barring FUROS-BPNO the characteristic sulfonamide dimer, a prominent motif in parent sulfonamide structures is absent in all the cocrystals. The unique nature of the novel cocrystals were further established using IR, Raman, PXRD and DSC techniques. In essence, we have discovered a novel heterosynthon between primary sulfonamide and pyridine-*N*-oxide functional groups. The recurring N–H···$O_{N\text{-oxide}}$ heteromeric interaction was successful in breaking the stable homomeric sulfonamide dimer of parent sulfonamides in order to form cocrystals. The scope of this model study will be easily extendable to prepare pharmaceutical solids. The fact that pyridine-*N*-oxide functional group is present in some anti-HIV and anti-cancer drug molecules and discovery candidates, cocrystallizing them with sulfonamide drug molecules can form two-drug cocrystals. They may synergistically influence each other in minimizing their therapeutic dosage and enhance their efficacy in patients.

CHAPTER THREE

Solubility and Stability advantage of Aceclofenac Salts

Aceclofenac (ACF hereafter) (2-[2, 6-dichlorophenyl) amine] phenylacetoxyaceticacid) is an orally effective non-steroidal anti-inflammatory drug (NSAID) which was found to possess remarkable anti-inflammatory, analgesic and antipyretic properties. It belongs to the class of phenyl acetic acid and was found to be the most tolerated drug among NSAIDs with a lower incidence of adverse gastrointestinal effects. It is a BCS class II drug with poor aqueous solubility of 0.058mg/mL. In literature, attempts towards increasing the solubility of ACF were made through the formation of Salts, Cocrystal and Solid dispersion techniques. Nevertheless, it is still marketed in its neutral form. On the downside, ACF is reported to undergo degradation in strongly acidic or basic conditions. A schematic representation of the degradation process is shown below (Scheme 2).

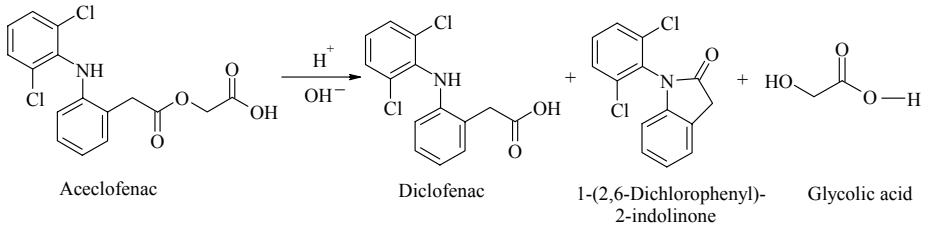

Scheme 2 Degradation process of Aceclofenac under strongly acidic or basic conditions.

Since salt formation is not a straight forward strategy for ACF due to its inherent nature to undergo degradation, cautious selection of coformers which can improve its solubility without affecting its stability is very important. With this background, we chose to cocrystallize ACF with mild GRAS coformers. During attempted cocrystallization with various coformers we obtained novel salts with Piperazine (PIP), Cytosine (CYT), L-Lysine (LYS) and γ-Amino Butyric acid (GABA). In addition we also discovered a salt hydrate with piperazine and a cocrystal hydrate with bipyridine (BIP). As a result, the problem of drug cyclization to give the inactive indolinone by-product is avoided in the mild conditions of salt formation. All the solid forms have been characterized with various spectroscopic, diffraction and thermal methods. Single crystal analysis of ACF was found to contain a rare catemeric O−H···O synthon stabilized by auxiliary C−H···O and Cl···O interactions. Heteromeric O−H···N interactions are commonly observed in

other salts and cocrystal, differing in terms of the extent of proton transfer. Solubility advantage of these solid forms was ascertained through solubility and dissolution studies in 25% EtoH-Water medium. Equilibrium solubility experiments performed for 48hrs showed that except ACF-PIP and ACF-GABA the other solid forms were stable. The stable ACF-CYT, ACF-PIP-HYD and ACF-LYS salts exhibited 16.3, 3.5 and 156.5 times higher solubility than ACF. Dissolution experiments performed in the same media revealed that ACF-LYS has 135 fold higher IDR than ACF followed by ACF-GABA (112.7), ACF-CYT (11.6), ACF-PIP (3.4), and ACF-PIP-HYD (2.6). As expected, ACF-PIP converted to its hydrate and ACF-GABA dissociated into the starting components in the IDR experiment. Intrinsic dissolution rate curves are displayed in Figure 1.

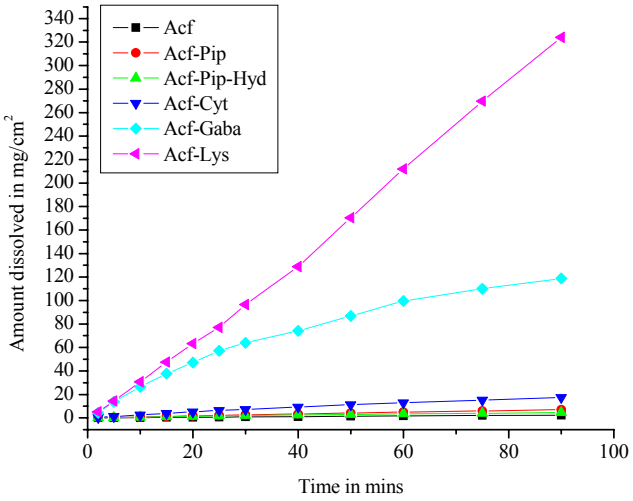

Figure 1 Intrinsic dissolution rate curves of ACF salts in 25% EtOH–water solution.

In order to assess the stability advantage, ACF and its solid forms were exposed to accelerated ICH conditions of 40°C temperature and 75% relative humidity. All the solid forms were characterized by PXRD at regular intervals for 8 months. Based on the characteristic peak positions, stability of the samples to the set humidity conditions was assessed. While ACF-CYT, ACF-PIP-HYD, ACF-LYS and ACF-GABA were found to be equally stable as that of the reference ACF drug throughout the 8 months period, ACF-PIP converted to its hydrate in 3 days. The primary objective of this work was to improve the solubility of ACF without affecting its stability or cause chemical transformation. This was achieved through salt formation using mild basic coformers

which showed significant solubility enhancement in 25% EtoH-Water medium and good stability in accelerated ICH conditions.

CHAPTER FOUR

Polymorphism in Sulfacetamide-Acetamide Cocrystal

Sulfacetamide (SACT hereafter) belongs to the class of sulfonamide antibacterial drugs and is well known for treating ophthalmic injuries and dermatitis. Recent reports indicate that it may act as antifungal drug by a CYP51A1-independent mechanism. SACT is active against both Gram-positive and Gram-negative bacteria. In order to explore the solid form diversity and the structural landscape of SACT, we resorted to cocrystallization strategy. Various techniques like mechanochemical grinding, slurry grinding and fast evaporation methods were used to generate cocrystals. On subjecting SACT and various GRAS coformers to these techniques in stoichiometric ratio, we obtained two polymorphs of a 1:1 SACT-Acetamide (ACT) cocrystal.

A CSD search for molecules with $–SO_2NHCO–$ skeleton showed 1528 hits. Among them only five single component and two multi-component systems exhibited polymorphism. Therefore polymorphism in this group of compounds is rare with only a couple of reported cases apart from SACT-ACT cocrystal polymorphs documented in this chapter. Both the SACT-ACT polymorphs were characterized using various analytical techniques like Single crystal and powder XRD, FT-IR, FT-Raman, Differential scanning calorimetry (DSC), Hot stage Microscopy (HSM), variable temperature powder X-ray diffraction (VT-PXRD) and ss-NMR. Crystal structure analysis revealed that both the polymorphs are sustained by a prominent tetrameric unit (Figure 2). Other hydrogen bonding interactions significantly vary the 1D and 2D packing modes of both the polymorphs. With minimum conformational differences this polymorphic system is classified under synthon and packing polymorphs.

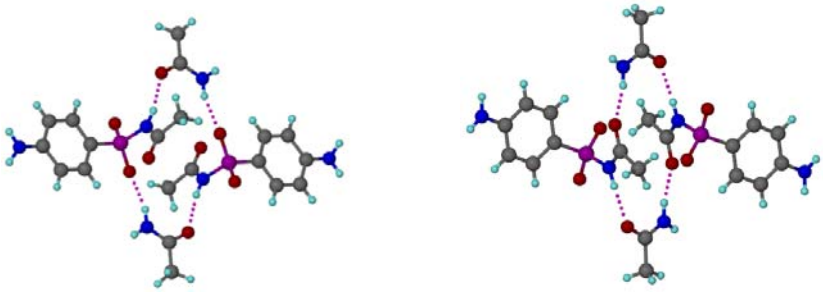

(a) (b)

Figure 2a) Tetrameric ring motif in SACT-ACT form 1 sustained by two each of N–H···$O_{sulfonamide}$ and N–H···$O_{carbonyl}$ interactions. **2b)** The corresponding interactions in SACT-ACT form 2 are all of N–H···$O_{carbonyl}$ type.

Stability relationship based on the density rule revealed that form 2 is more stable compared to form 1 based on higher calculated density (Form 1 – 1.323 g cm^{-3} *vs.* form 2 – 1.365 g cm^{-3}) and packing fraction (form 1 – 63.8% *vs.* form 2 – 66%). Experimental phase stability over the entire temperature range was studied using thermal, grinding and slurry techniques. While the DSC analysis of SACT-ACT Form 1 showed a single melting endotherm at 106.5°C, the corresponding thermogram of form 2 showed a endothermic transition to the high temperature phase form 1 (confirmed by VT-PXRD) between 79-83°C before melting at 106.5°C. Application of heat of transition rule suggested an enantiotropic relationship between the polymorphs. Based on the thermal experiments form 2 was shown to be the stable phase below the transition point and vice-versa. Slurry and grinding experiments on the individual phases and 1:1 mixtures of both the polymorphs established form 2 as the thermodynamic phase and form 1 as the metastable kinetic modification. Solubility advantage of the cocrystal polymorphs in comparison to the parent API was ascertained by performing solubility and dissolution experiments in pH 7 buffer media. Although both the polymorphs were found to be unstable in equilibrium solubility conditions, dissolution experiments showed that SACT-ACT form 1 has 1.57 times and SACT-ACT form 2 has 1.27 times higher IDR compared to SACT. In this chapter we have highlighted the importance of systematic characterization of cocrystal polymorphs in order to establish the stable modification. Establishing stability relationship between polymorphs would not only prove to be

extremely beneficial in overcoming accidental phase transformations but also help in judicious selection of the optimal solid form for pharmaceutical development.

CHAPTER FIVE

Fast Dissolving Eutectic Compositions of Curcumin

Curcumin (diferuloylmethane) is the active ingredient of the dietary Indian spice turmeric. It is a hydrophobic polyphenol derived from the rhizome of the herb curcuma longa having diverse pharmacological activities, such as anti-inflammatory, antioxidant, and anticancer. Despite being safe at high doses of 12g/day in humans, the therapeutic effectiveness of curcumin is limited by very low solubility (7.8mg/L) and poor bioavailability in the aqueous medium. In literature, the stability and bioavailability of curcumin has been enhanced through adjuvants like piperine and novel drug delivery platforms such as nanoparticles etc. Recently, we discovered polymorphs and cocrystals of curcumin which enhanced its solubility. Encouraged by these preliminary results we performed co-crystallization of curcumin with several GRAS coformers. Mechanochemical grinding of curcumin and the coformer in stoichiometric ratio gave binary eutectic compositions (Scheme 4). The novel eutectic compositions of curcumin were identified by thermal techniques (DSC) and the absence of cocrystal products characterized by their unique molecular packing and intermolecular interactions were confirmed by powder X-ray diffraction and IR-Raman spectroscopy.

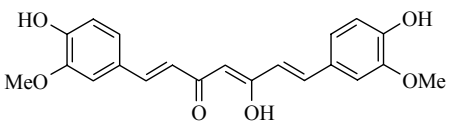

CUR

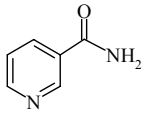

NAM

1:2 Eutectic by ^{1}H NMR

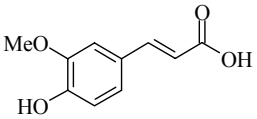

FA

1:1 Eutectic by ^{1}H NMR

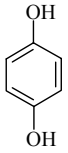

HQ

1:1 Eutectic by ^{1}H NMR

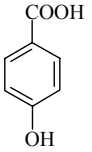

PHBA

1:1 Eutectic by ^{1}H NMR

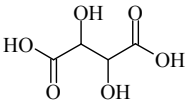

L -TA

1:1 Eutectic by ^{1}H NMR

Scheme 4 Curcumin and coformers discussed in this study. The stoichiometry of curcumin–coformer was determined by ^{1}H NMR and the eutectic nature established by DSC.

Eutectic compositions are conglomerates of solid solutions. As a result, the individual parent lattice structure remains unaffected in the product eutectic composition. Weak intermolecular interactions and unfulfilled bonds mark the interphase interactions of solid solution domains. As a result of negligible heteromeric interactions, is not possible to differentiate the eutectic phases from their starting components using diffraction or spectroscopic techniques. Nevertheless, the excess thermodynamic functions resulting from the random molecular arrangement lowers the eutectic melting point compared to the parent compounds. Similar observations were made in relation to the curcumin eutectics. While the diffraction and spectroscopic techniques showed negligible differences from their parent compounds, their DSC thermograms showed a characteristic lower melting point. More importantly, DSC was able to distinguish between the eutectic formed from grinding and on heating. Eutectic formed on grinding – a 'preformed eutectic' showed a distinct lower melting point compared to physical mixture which formed a eutectic on heating. The increased contact surface area between the components after grinding induces weaker eutectic interactions (a preformed eutectic), which requires lower activation energy to reach the melting temperature. In the physical mixture, however, the contact area between the components is less and so larger activation energy is required to bring the components together for inducing weak interactions (eutectic on heating). The excess activation energy required for the physical mixture gives it a slightly higher T_{onset} value compared to that of the ground mixture.

Due to its excess thermodynamic functions, a eutectic confer higher solubility to the parent compound. The solubility advantage of curcumin eutectics is ascertained in 40% EtOH-water medium. It was not possible to obtain equilibrium solubility (at 24, 48 h) because the eutectic components dissociated after some time due to incongruent solubilities of the components. IDR experiments on curcumin eutectics for 7hrs showed that CUR-NAM has 10.6 fold higher IDR than curcumin and the other eutectics CUR–FA, CUR–HQ, CUR–PHBA, and CUR–TA showed less dramatic accelerations of 6.8, 5.6, 4.4, and 2.1 times respectively. In addition, powder dissolution (PD) was performed on the curcumin eutectic compositions with a near uniform particle size (25-75 micron) distribution. The PD rates for 120 min (peak solubility) of CUR–FA 244 mg/L > CUR–

TA 226 mg/L > CUR–HQ 219 mg/L > CUR–PHBA 214 mg/L > CUR–NAM 197 mg/L > CUR 99 mg/L are different from those of IDR experiments probably due to the effect of variable particle size. The ultimate aim of this work was to increase curcumin solubility through physical form modification, and this objective was achieved through binary eutectic compositions. Our binary eutectic compositions were found to be stable at ambient conditions of 35°C and 40% RH for over 6 months. Given their crystalline nature they are less likely to undergo spontaneous phase transformations compared to amorphous forms. Hence eutectics confer both solubility and stability advantage, similar to cocrystal counterparts.

CHAPTER SIX

Novel Cocrystals of Sulfacetamide

Sulfacetamide (SACT hereafter) is a sulfonamide antibiotic useful in the treatment of various ocular infections like trachoma, blepheritis, conjunctivitis, and corneal ulcer apart from being a potential antifungal agent. It has high solubility of 12.5mg/mL. SACT is supplied either as ointment or eye drops for the treatment of ocular infections. As a result of reflex blinking and tear flow from eyes, the concentration of SACT falls by one-tenth of its starting value within 4-20 mins. As a result only a small extent of drug is absorbed and the duration of therapeutic action is quiet short. In literature, extended release formulations using bioadhesive microspheres, nanosuspensions etc were proposed as solutions to this problem. Remington et. al. has noted that preparing a less soluble form of a high soluble drug is a facile method for producing extended release dosage forms. Encouraged by the ability of cocrystals in modulating the solubility of drug molecules, we have explored the structural landscape of SACT with an idea that the resulting pharmaceutical cocrystals would have the appropriate hydrogen bonding patterns for lowering its solubility. Using mechanochemical grinding, slurry grinding, fast evaporation and solution crystallization techniques we obtained variable Z′ cocrystals with theophylline (THEO, 2:2), isonicotinamide (INIC, 1:2), caffeine (CAF, 1:1), bipyridine (BIP, 1:0.5) and a salt with 4-aminopyridine (4AP, 1:1). Numerous hypotheses like synthon frustration, twisted conformation of the parent molecule, internal symmetry, donor acceptor imbalance etc. were proposed to be the reasons for the

occurrence of variable Z″ phenomenon. These cocrystals were characterized by thermal, spectroscopic and diffraction methods.

Solubility and dissolution studies on pharmaceutical cocrystals of SACT (SACT-CAF, SACT-THEO, and SACT-INIC) were performed in pH 7 buffer media and the concentration was measured using HPLC at 254 nm. Equilibrium solubility studies showed that apart from SACT, only SACT-CAF was stable at the end of the experiment. Other cocrystals converted into starting components. The stable SACT-CAF showed a lower equilibrium solubility of 8.64 g/L as compared to 14.54 g/L of SACT. While the dissolution experiments on SACT-CAF (1.49 mg/cm^2/min, 0.68 times) and SACT-INIC (1.39 mg/cm^2/min, 0.64 times) showed lower IDR compared to SACT (2.18 mg/cm^2/min), SACT-THEO (2.18 mg/cm^2/min) had similar dissolution profile as parent drug (Figure 3). Solubility studies indicate the lowering in solubility profiles of SACT on forming cocrystals. SACT-CAF cocrystal with its lower solubility and stability during equilibrium solubility and dissolution experiments can be a suitable solid form for preparing extended release formulation of SACT.

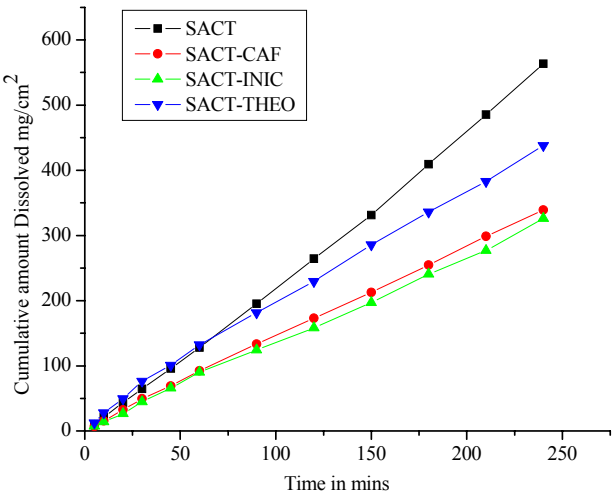

Figure 3 Dissolution profile of SACT and its Cocrystals.

CHAPTER SEVEN

Relative Stability of Atovaquone Polymorphs

Atovaquone, trans-2-[4-(4-chlorophenyl)cyclohexyl]-3-hydroxy-1,4-naphthalenedione (ATV hereafter) belongs to the class of naphthoquinones with specific activity against Pneumocystis carinii. It is a potent antimalarial and antibacterial drug. The antimalarial activity of ATV has been attributed to its interference with mitochondrial electron transport in the parasite, specifically at the cytochrome C reductase complex, that results in a collapse of the mitochondrial activity. In literature, four polymorphs and various derivatives of ATV are reported. Two of the polymorphs were characterized using single crystal analysis. By the virtue of their unique solid state assemblies, polymorphs exhibit different physico-chemical properties (e.g. melting point, solubility, stability, bioavailability etc.). Therefore a thorough investigation into their stability relationships is essential for optimizing a desired polymorph for solid form development. Malpezzi and coworkers proposed the stability order for Form 1 and 2 of ATV. Based on thermal and kinetic experiments, they have concluded form 2 as the thermodynamic phase and form 1 as kinetic modification. The lower density and kinetic methods of obtaining form 2 intrigued us to revisit the stability relationships along with another polymorph of ATV. All the three polymorphs were obtained using slow evaporation, slurry and crash cooling techniques. DSC analysis of ATO polymorphs revealed that form 1 and form 3 undergo phase transition to the high temperature phase form 2. Therefore form 1 and form 3 are enantiotropically related to form 2 with form 1 to form 2 conversion having higher heat of transition. Individual and competitive slurry grinding and mechanochemical grinding experiments revealed that both form 2 and form 3 convert to form 1, establishing form 1 as the thermodynamic phase. Competitive slurry and grinding experiments on form 2 and form 3 showed that form 2 converted to form 3, establishing form 3 as the stable phase next to form 1. These results are in contrast to the stability order proposed by Malpezzi et. al. where form 2 was shown as the thermodynamic phase. Our stability order was rationalized using a E-T diagram (Figure 4). According to the E–T diagram, the stability order at absolute zero (–273 °C) is form 1 < form 3 < form 2, between 130-187.5°C it is form 1 < form 2 < form 3, and above 188°C it is form 2 < form 1 < form 3, i.e. form 1 is the thermodynamic form at ambient conditions. In addition the poor solubility of ATV was addressed by forming a piperazine salt which showed 18 times higher solubility

compared to the commercial form 1. In short, this chapter highlights the importance of establishing the relative stability of drug polymorphs by thorough characterization in the typical conditions of pharmaceutical processing (crystallization, milling etc.) and storage (temperature and relative humidity around 25 °C and 50% respectively), apart from improving its solubility through salt formation.

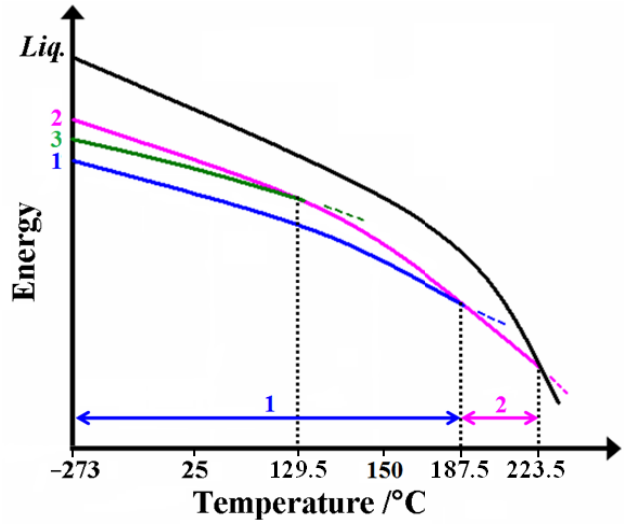

Figure 4 Semi-quantitative E–T diagram to show the relative stability and polymorphic transformations of ATV polymorphs. At –273 °C form 1 is the stable form. Between 25-187.5 °C, form 1 has the lowest free energy; form 2 is stable after 187.5 °C before it melts at 224°C.

CHAPTER EIGHT

Conclusions and Future Prospects

Crystal engineering principles and hydrogen bonding rules form the basic design elements of diverse pharmaceutical solids. These design elements represent the recurring theme of this thesis where different solid forms like polymorphs, cocrystals, salts, eutectics etc were discovered for pharmaceutical applications. In chapter 2, a novel heterosynthon between Sulfonamides and Pyridine-*N*-oxides was identified. Its application towards forming cocrystals of sulfonamide containing drug molecules was exemplified by forming cocrystals with anti-diuretic drug Furosemide. In chapter 3,

Solubility of pH labile drug molecule Aceclofenac was improved by forming salts with mild coformers. The long term stability of these salts was established through accelerated humidity experiments. In chapter 4, the importance of establishing relative stability of multicomponent polymorphs was exemplified through Sulfacetamide-acetamide 1:1 cocrystal. In chapter 5, a rare case of eutectic formation through mechanochemical grinding was highlighted. Novel eutectic compositions of bio-active molecule curcumin were discovered through mechanochemical grinding and their ability to improve the solubility of parent compound was shown through solubility experiments. In chapter 6, the solubility modulating ability of cocrystals was highlighted through novel Sulfacetamide cocrystals. The resulting cocrystals showed similar to low solubility compared to Sulfacetamide. This ability of cocrystals may find application in developing extended release formulations of the parent drug. In chapter 7, the importance of establishing stability relationship between single component polymorphs was highlighted through three polymorphs of a drug molecule Atovaquone. The effect of modulating the drug solid state assembly on its physicochemical properties was exemplified by forming a piperazine salt which showed improved solubility.

CONTENTS

CHAPTER ONE

INTRODUCTION TO CRYSTAL ENGINEERING AND PHARMACEUTICAL SOLIDS

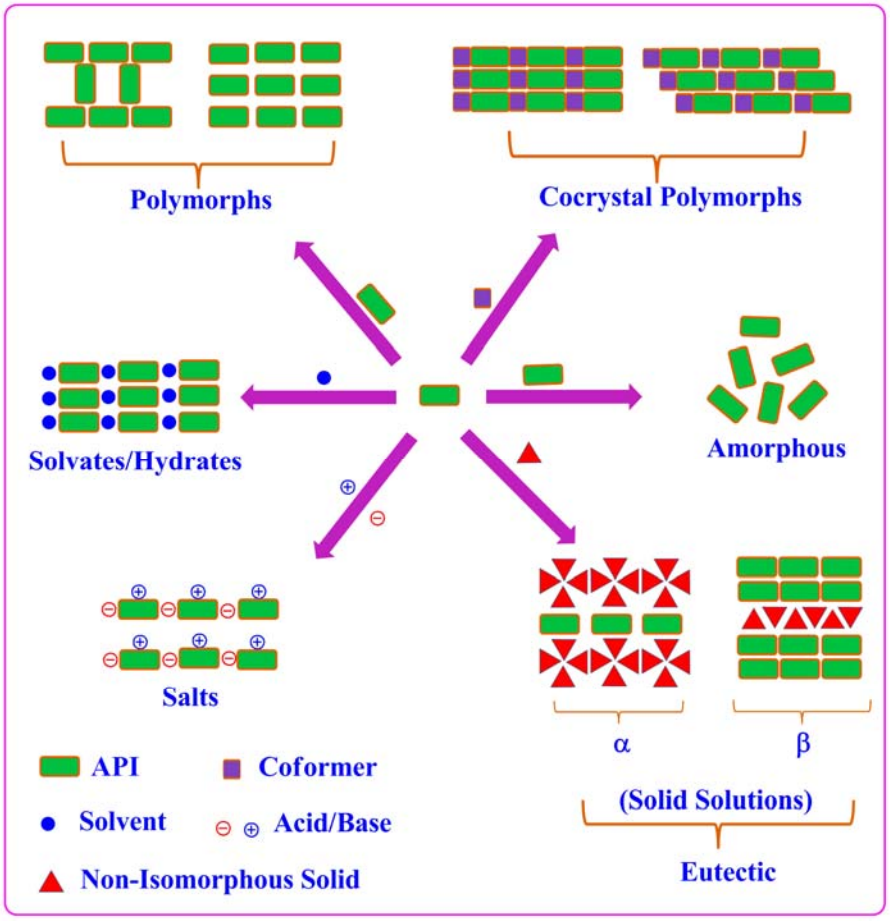

Schematic representation of various solid forms studied in this thesis. A pharmaceutical solid formulation contains an 'Active Pharmaceutical Ingredient' (API) as a polymorphic form/mixture, salt, hydrate/solvate, complex, cocrystal, eutectic or an amorphous solid.

"It has been recognized that hydrogen bonds restrain protein molecules to their native configurations, and I believe that as the methods of structural chemistry are further applied to physiological problems it will be found that the significance of the hydrogen bond for physiology is greater than that of any other single structural feature."

– Linus Pauling, The Nature of the Chemical Bond and the Structure of Molecules and Crystals (1939).

1.1 Molecule to Supermolecule – A Paradigm Shift

Ever since Friedrich Wöhler synthesized urea[1] from ammonium cyanate in 1828, the concept of molecule has been of paramount importance in chemistry. Through the efforts of classical chemists then, molecule was fortified as a decisive factor in understanding the physicochemical properties of a compound. Nevertheless, some of the fundamental properties of a compound such as its melting point are bulk properties and depend on the assembly of molecules rather than the molecule itself. Hence a shift from this classic thought towards 'supramolecular chemistry[2]' was imminent. Supramolecular chemistry, also known as 'non-covalent chemistry' or 'Lego chemistry' aims to build complex chemical systems from simple molecules held together by non-covalent interactions. The philosophical roots for supramolecular chemistry were laid by Emil Fischer in 1894 when he compared the enzyme-substrate interactions to a 'Lock and Key' mechanism[3]. This model later formed the fundamental principles of now popular molecular recognition and host-guest chemistry. The first modern stimulation of supramolecular thought occurred when H. M. Powell in 1948 discussed the organic crystal of hydroquinone clathrates as a network[4]. The serendipitous discovery of crown ethers by Pedersen in 1967, followed by subsequent pioneering work of Donald Cram and Jean-Marie Lehn in developing molecules with structure-specific non-covalent interactions and high selectivity laid the foundation for the modern supramolecular chemistry. In 2002, Jean-Marie Lehn gave the functional definition[5] of supramolecular chemistry as: "*Supramolecular Chemistry aims at developing highly complex chemical systems from components interacting by non-covalent intermolecular forces*". Today, many areas like template-directed synthesis, complexation, biomimetics, molecular imprinting,

dynamic covalent chemistry and molecular self-assembly find inspiration from the concepts of supramolecular chemistry[2,5]. Molecular self assembly in particular is broadly classified into 1) solution state dynamics of host-guest molecules which seek inspiration from the complex enzymatic reactions in biological systems referred to as molecular recognition and 2) understanding and designing solid-state intermolecular interactions which is popularly known as 'Crystal Engineering[6]'.

1.2 Crystal Engineering

Molecular crystals have interesting physical and chemical properties that are not associated with other categories of crystalline substances. These properties are closely related to the internal periodic arrangement of molecules. The desire to understand the intermolecular interactions that prevail in the molecular solids in order to apply them in designing solid-state assemblies with tailor-made properties have given birth to the subject of crystal engineering. In 1989, Desiraju defined crystal engineering[6a] as "*the understanding of intermolecular interactions in the context of crystal packing and the utilization of such understanding in the design of new solids with desired physical and chemical properties*". Ever since Pepinsky[7] coined the term crystal engineering in 1955 in the context of crystallization of organic ions with metal-containing complex ions, it has inspired the development of solid forms in pharmaceuticals[8a], metal-organic frameworks[8b] and nanostructures[8a]. The quest of crystal engineering to answer the fundamental question: "*Given the molecular structure of a compound, what is its crystal structure?*" has significantly narrowed the gap in predicting crystal structures of compounds from their molecular structures and vastly contributed to the understanding of intermolecular interactions in designing solid forms with predefined properties. The evolution of crystal engineering into a subject may be classified into two phases. One of the major contributions to the first phase was by Robertson[9] through his work on aromatic hydrocarbons. He has surveyed a large number of polynuclear aromatic hydrocarbons and classified them into two categories based on molecular thickness and area. Compounds are classified under first category when their molecular thickness is comparable to molecular area. Hydrogen rich

molecules like naphthalene and anthracene come under this group. In the second category, exemplified by coronene and ovalene, the molecular thickness is smaller than molecular area. In essence, Robertson performed the first systematic experiment in crystal engineering. He crystallized aromatic hydrocarbons, solved their crystal structures and correlated their molecular structure to crystal structure. Another significant contribution to this phase of crystal engineering was made by Schmidt and coworkers[10] at the Weizmann institute 1950-1970. They systematically established a link between molecular structure and reactivity through studies on the 2+2 cycloaddition reactions of trans-cinnamic acids to cyclobutanes. Based on their observations on dichloro substituted aromatic molecules where the crystal structure has a tendency to adopt a short axis of 4Å, they synthesized alkenes (trans-cinnamic acids) that would undergo photodimerization to cyclobutanes. They have crystallized α, β and γ forms of trans-cinnamic acids and irradiated them in the solid state. They found that α and β forms where the intermolecular distance is about 4Å had undergone cycloaddition reaction whereas the γ form was photo stable (Scheme 1.1).

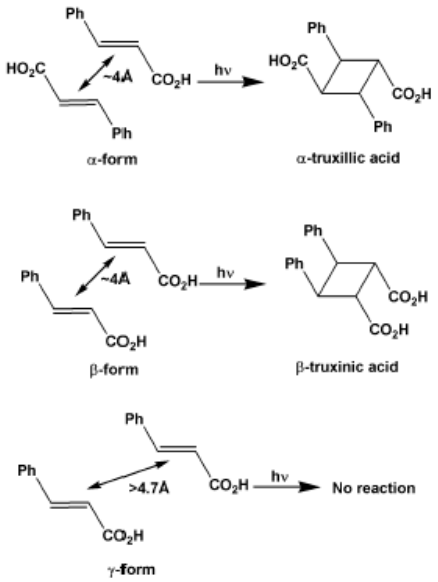

Scheme 1.1 Photo irradiation of α, β forms of trans-cinnamic acid with intermolecular distance of 4Å has photodimerized to α and β truxillic acid respectively, whereas γ form with intermolecular distance of >4.7Å was photo stable (adapted from ref. 10)

In late 1980s the next phase of crystal engineering began. Major contributions to this phase included an article by Ermer[11] on the crystal structure of adamantane-1,3,5,7-tetracarboxylic acid. He interpreted the crystal structure of this molecule in terms of interpenetrated networks which could be defined as a pioneering work for describing crystals using topological approach. Subsequently, in 1990 Robson[12] studied coordination compounds based on the theme of interpenetration which paved the way to the investigations on coordination polymers and metal-organic framework structures (MOFs). In short, the initial interest in crystal engineering was to understand and design organic solids. Today[8a,13], it is a mainstream interdisciplinary field influencing diverse areas like self-assembly in molecular crystals, coordination polymers, metal-organic frameworks, nanostructures etc. through hydrogen bonding, van der Waals interactions, electrostatic and metal-coordination bonding.

1.3 Intermolecular interactions

A 'crystal' is a periodic arrangement of millions of molecules at an amazing level of precision. It is defined by Dunitz as '*supermolecule par excellence*'[14] while Lehn termed it as '*a very large supermolecule indeed*'[2b]. The intermolecular interactions that bind molecules in a crystal lattice are broadly classified into two types: the isotropic medium range forces (C···C, C···H, H···H interactions) that influence the close packing based on size and shape of molecules and anisotropic long range forces (O–H···O, N–H···O, C–H···O, halogen···halogen etc) which are electrostatic and include hydrogen bonds and heteroatom interactions. The importance of isotropic interactions is highlighted by A. I. Kitaigorodskii[15a] who postulated the atom-atom potential method[15b] for intermolecular interactions in crystal structures. This model describes crystals as being derived from efficient utilization of space during their formation, hence it is also popularly known as the 'principle of close packing'.

Hydrogen bond[16] is the most important of all the anisotropic interactions. It is a unique phenomenon in both structural chemistry and biology. The earliest references to this concept which could be termed hydrogen bond according to the current understanding was made by Werner[17a] (1902) and Hantzsch[17b] (1907) who referred to the intermolecular interactions between ammonium salts by the term *Nebenvalenz* (secondary valence). It was however the

chapter on hydrogen bonding in '*The nature of chemical bond*[18]' (Pauling, 1939) that drew the subject of hydrogen bonding into the chemical mainstream. The current definition[19] (2010) states that "*The hydrogen bond is an attractive interaction between a hydrogen atom from a molecule or a molecular fragment X-H in which X is more electronegative than H, and an atom or a group of atoms in the same or a different molecule, in which there is evidence of bond formation*". Depending on the electronegativity of atoms to which it is bound either through covalent or non-covalent interactions, a hydrogen bond can exist with a continuum of strengths. For practical reasons it is essential to classify hydrogen bonds[20] based on their energy range (Table 1.1)

Table 1.1 Some properties of very strong, strong and weak hydrogen bonds

	Very strong	Strong	Weak
Bond Energy (Kcal/mol)	15-40	4-15	< 4
Examples	[F–H···F⁻]	O–H···O=C	C–H···O
IR *vs* relative shift	>25%	5-25%	< 5%
Bond lengths	H–A ≈ X–H	H···A > X–H	H···A >> X–H
Lengthening of X-H (Å)	0.05–0.2	0.01–0.05	≤ 0.01
D (X···A) range (Å)	2.2–2.5	2.5–3.2	3.0–4.0
d (H···A) range (Å)	1.2–1.5	1.5–2.2	2.0–3.0
Bonds shorter than vDW	100%	Almost 100%	30-80%
θ (X–H···A) range (°)	175–180	130–180	90–180
kT (at room temp.)	>25	7-25	<7
Effect on crystal packing	Strong	Distinctive	Variable
Covalency	Pronounced	Weak	Vanishing
Electrostatics	Significant	dominant	moderate

Adapted from ref. 20.

1.4 Supramolecular synthons and Cambridge structural database

In 1967, in a seminal paper describing synthetic strategies for constructing complex molecules, E. J. Corey[21] coined the term 'Synthon'. He defined synthon as "*Structural units within molecules which can be formed and/or assembled by known or conceivable synthetic operations*". Right from its inception, a synthon was considered as a part of the molecule which contains vital information about the bond connectivity and stereochemical information. Using these synthon strategies in constructing a complex molecule with due

consideration to its stereochemical preferences is popularly known as "Retrosynthesis". However, in later years this term fell into disuse as explained by Corey himself[22a] and Seebach[22b] in 1990 since it degenerated into a descriptor of synthetic intermediates. In 1989, Desiraju through his excellent monograph[6a] recognized crystal engineering as a supramolecular equivalent of organic chemistry. In order to simplify the complex supramolecular architectures which is a result of the compromise between isotropic and anisotropic interactions, Desiraju revived and modified the term as 'Supramolecular synthon[23]'. It is defined as "*structural units within supermolecules which can be formed and/or assembled by known or conceivable intermolecular interactions".* The supramolecular synthon approach is advantageous in the sense that it considerably simplifies the understanding of crystal structures. In order to understand and design the robust supramolecular synthons, it is important to recognize the appropriate functional groups that would result in a high yielding supramolecular reaction[24]. Since the operating intermolecular interactions are weak in nature, designing a crystal structure effectively becomes a synthon design[13a, 23] which is possible through a vast knowledge of intermolecular interactions in various crystal structures.

The Cambridge structural database[25a] (CSD) is the world's repository for small-molecule organic and metal-organic crystal structures. It contains over 500,000 structures determined by various X-ray and neutron diffraction techniques. This large source of data is invaluable in establishing molecular dimensions of a crystal structure, understanding the 3-dimensional conformation of molecules in a crystal and the intermolecular interactions that bind them[32b,c]. CSD plays a pivotal role in establishing the synthon robustness between two different functional groups based on the number of crystal structures that are deposited with synthon formation between these functional moieties. Since the synthon formation between the complementary groups can be determined irrespective of the nature (single or multiple arrays) of hydrogen bonding interactions, the probability outcome is invaluable in selecting a robust synthon for designing crystal structures. It may be noted that recognition between unlike functional groups (e.g. acid–pyridine) has far greater probability of formation than synthons between identical functional groups (e.g. acid dimer, amide dimer). In a timely follow through, Zaworotko[26] sub-classified synthons as homosynthons and heterosynthons based on the interacting functional groups. If supramolecular synthon is formed between the

same functional group it is a homosynthon, and between two different functional groups it is called as heterosynthon. Heterosynthons like acid–pyridine[27a], phenol–pyridine[27b], phenol–amine[27c], acid–amide[27d], aminopyridine–acid[27e] and amide–pyridine-*N*-oxide[27f] are well exploited in crystal engineering because of their strength and probability of formation (Scheme 1.2).

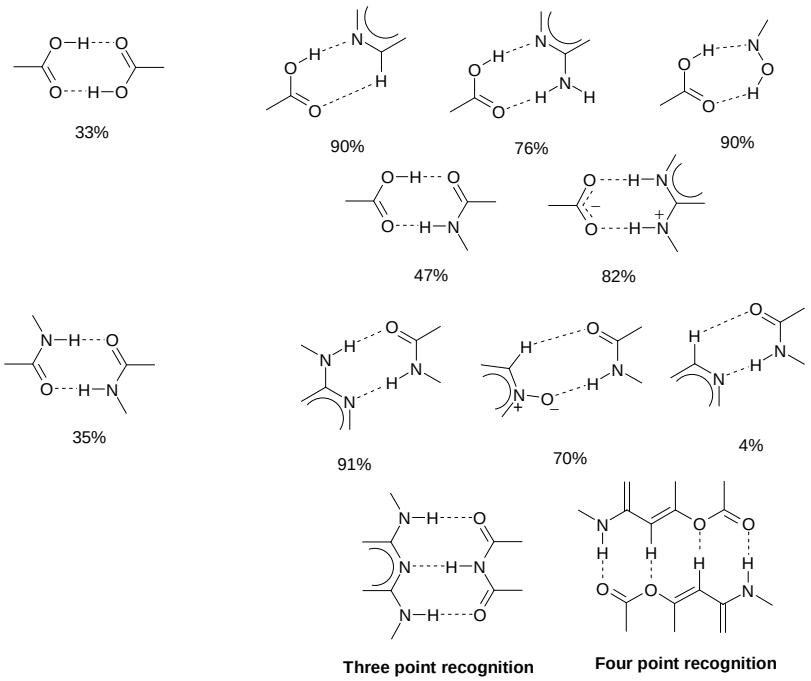

Scheme 1.2 Some examples of supramolecular synthons with their probabilities calculated from CSD statistical study (adapted from ref. 23).

1.5 Solid-State Chemistry of Pharmaceutical Solids

Currently, about 80% of the marketed drugs are sold as tablets[28]. This is not surprising since a solid formulation would ensure ease of manufacture, transport, storage and overall drug-patient compatibility. Nevertheless, variation in the nature of drug molecules because of vast differences in their molecular skeleton and bulk scale properties do not comply with a one size fits all type of solid form for their targeted site of action. Developing an optimal solid

formulation, at times it may even amount to stabilizing unconventional solid forms is essential in order to secure maximum therapeutic efficacy. For example, Novobiocin[29a,b] is marketed in its amorphous form due to its superior blood plasma levels compared to the conventional crystalline form. Similarly, anti-HIV drug Darunavir[29c] is marketed as its unconventional ethanol solvate as a result of its better physicochemical properties. Of late, the usage of high-throughput technology and combinatorial chemistry[30] for lead molecule synthesis has only increased the necessity for developing various solid forms of a drug molecule. Although, these techniques have increased the number of new chemical entities (NCEs) enormously, their corresponding physicochemical properties have decreased drastically. Therefore discovering and optimizing diverse solid forms of a drug molecule is essential to achieve optimal bioavailability. In order to do so it is necessary to understand the nature of these solid forms in terms of their molecular packing, stability, physicochemical properties etc. The following sections give a brief introduction to various solid forms that are studied in this thesis.

1.5.1 Amorphous Forms

Amorphous solid forms occupy a prominent place in pharmaceutical industry with their ability to improve solubility and dissolution rate of Active Pharmaceutical Ingredients (APIs)[31]. But unlike crystalline phases, amorphous compounds do not show a regular diffraction pattern. These aperiodic solid forms can be produced by several techniques such as melt quenching, spray- and freeze-drying, milling, wet granulation[31b] etc. and recently manual grinding[31c] was shown to result in amorphous salts. Of late 'Co-amorphous[32]' compounds – amorphization of two or more neutral compounds in stoichiometric ratio are becoming popular for their ability to enhance parent drug solubility (Figure 1.1).

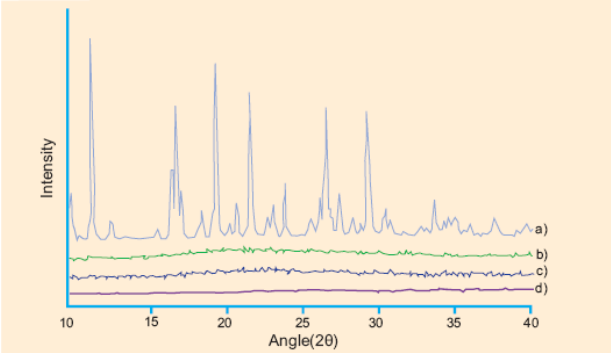

Figure 1.1 Powder X-ray diffraction scans of **a)** crystalline indomethacin, **b)** amorphous indomethacin (melt–quenched), **c)** co-amorphous compound of indomethacin and neusilin US2, **d)** Neusilin US2. (adapted from ref. 32c)

An amorphous solid is characterized by its glass transition temperature (T_g). It is the temperature at which a glassy material (plastic) is converted to rubbery phase retaining some properties of the liquid[31b]. Similar to their crystalline counterparts, amorphous forms are also known to exhibit polymorphism[33]. For example, polyamorphism in H_2O is extensively studied[34], but the data interpretation remains controversial since the diffraction pattern does not show any Bragg lines. On one hand the excess thermodynamic functions of amorphous phases confer solubility/dissolution advantage to the poorly soluble APIs. Various drug products like Lopinavir, Cefuroxime axetil, Itraconazole, Quinapril hydrochloride etc., are marketed either as purely amorphous phases or in combination with other solid forms[44a]. But on the other hand, the higher entropy and enthalpy can be disadvantageous since they make the amorphous solid forms highly unstable. Several excipients such as methyl cellulose, alginic acid, polyvinyl pyrrolidone (PVP), polyethylene glycol (PEG) etc[31b] have been developed to stabilize the amorphous forms. Recently, Chen et. al.,[35] identified the structure of amorphous aluminoborane compound, AlB_4H_{11} by combining density functional based approach with experimental measurements using IR, NMR and neutron vibrational spectroscopy (NVS). Application of these techniques in dissecting the lattice structure of pharmaceutical amorphous solid forms may be helpful in better understanding of their molecular packing and intermolecular interactions which in turn may be helpful in greater application of these solid forms for enhanced drug efficacy.

1.5.2 Polymorphism

The term polymorphism[36] is derived from Greek (*Poly* = many, *morph* = form) specifying the diversity in nature. According to the oxford dictionary this term first appeared in 1656 in relation to the diversity of fashion[36a]. In the context of crystallography it is generally credited to Mitscherlich[37a] (1822, 1823) who recognized different crystal structures of the same compound in a number of arsenate and phosphate salts. In layman terms polymorphism may be defined as the 'existence of a chemical compound in different crystalline arrangements' and the different crystal forms are known as 'polymorphs'. Berzelius[37b] first coined the term allotropism to describe the phenomenon of existence of an element in different crystal structures known as allotropes. For example, Tin exists as two allotropes. While the β form is metallic and stable above 18°C, the α form is non-metallic and stable below 18°C (Figure 1.2). Similarly polymorphism, in the context of material science describes the existence of a compound in different crystal structures. Therefore in a broad sense what allotropes and allotropism is to an element so are polymorphs and polymorphism to a compound[36a].

α-Tin

β-Tin

Figure 1.2 α and β forms, the two allotropes of Tin. It is interesting to note that allotropism in tin had a link to Napoleon Bonaparte. In the chilling winter of 1812, the highly decorated and shining buttons on the uniform of Napoleon's soldiers (made of tin) crumbled to dirty grey and the soldiers believed that it is the wrath of God; their morale became so low that they faced a pathetic defeat at the gates of Moscow. The scientific reason for the crumbling of the buttons is that at subzero temperatures of Moscow, the metallic white tin underwent a allotropic transition to the stable but nonmetallic grey tin, thus reducing the decorum of the mighty soldiers (adapted from ref. 37c).

According to the widely accepted definition of McCrone[36b], polymorphism is defined as "*a solid crystalline phase of a given compound resulting from possibility of at least two different arrangements of the molecules of the compound in a solid state*". However, this definition does not include polymorphs involving different molecular conformations and dynamic isomers like tautomers[38]. A safe criterion for polymorphism would be if the crystal structures are different but lead to identical liquid and vapour states. Just as different allotropes of carbon exhibit differences in strength and conductivity, polymorphs of a compound exhibit significant differences in physico-chemical properties, such as melting point, compressibility, flowability, stability, solubility, dissolution rate and bioavailability which form an important criteria for the selection of stable polymorph for optimal drug delivery[36].

1.5.2.1 Classification of polymorphs

In literature, polymorphs (single or multicomponent) are synonymously called as 'forms', 'modifications' or 'phases' and represented as numerals or alphabets[36a]. In terms of structural differences polymorphs may be broadly classified into three types i) Packing polymorphism[39] ii) Conformational polymorphism and iii) Synthon polymorphism (Figure 1.3). In a broader sense all polymorphs may be classified under packing polymorphism since all the polymorphs differ in their packing by default. Nevertheless, it would be a gross classification since it would not account for the structural differences in terms of intermolecular interactions and molecular flexibility. When the packing differences are mainly due to the variation in the conformation of molecules, they are known as conformational polymorphs[40], for example, chiral and racemic tetramorphs of t-butyl fuchsone[40b] (Figure 1.4). A metastable conformation may be stabilized by stronger hydrogen bonds in the crystal structure while a stable conformer may not be able to form strong hydrogen bonds. The overall stability of a polymorph is accounted by the conformational energy and lattice energy (total) for a given polymorphic system. The energy compensation towards overall energy minimization in a polymorphic system is referred to as systematic effect. This phenomenon was recently reviewed by Nangia[40a] with several examples of

conformational polymorphs. When the packing differences are mainly due to the differences in the intermolecular interactions of molecules then they are termed as synthon polymorphs[41]. For example, carbamazepine molecules propagate through amide dimer in Form IV and amide catemer in form V[41a,b] (Figure 1.5). This classification is subjective and in any polymorphic system two or more types of polymorphism coexist. For example, conformational and synthon polymorphism differentiate the trimorphs of anti-diuretic drug Furosemide[42a] and synthon and packing polymorphism coexist in the tetramorphs of anti-tubercular drug Pyrazinamide[42b](Figure 1.6).

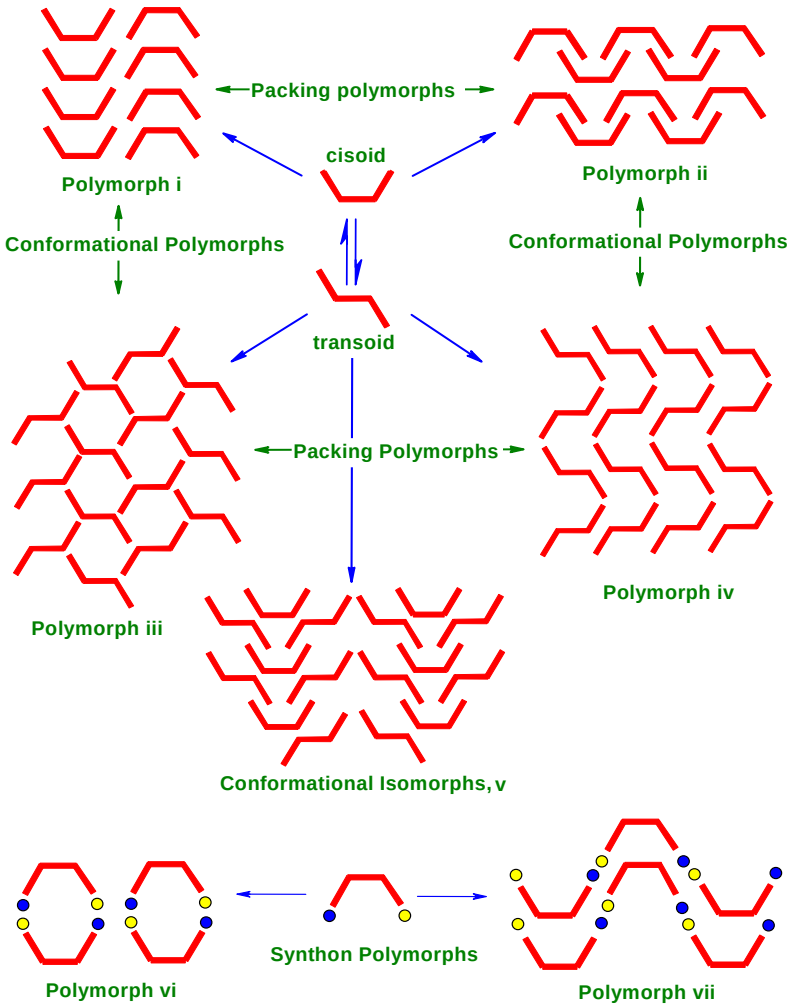

Figure 1.3 Schematic representation of different kinds of polymorphs (adapted from ref. 40a).

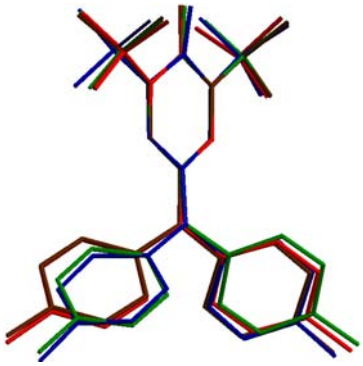

Figure 1.4 Molecular overlay of the tetramorphs of t-butyl fuchsone showed significant conformational differences, form I (blue), form II (brown), form III (green) and form IV (red), (adapted from ref.40b).

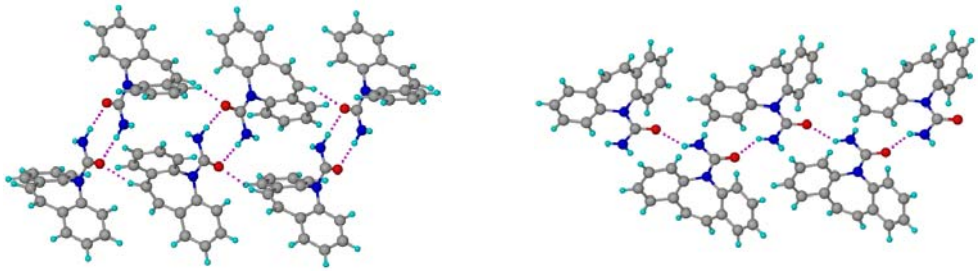

(a) (b)

Figure 1.5a) Amide dimer in form IV of Carbamazepine, **b)** Amide catemer in Form V of Carbamazepine (adapted from ref.41a,b).

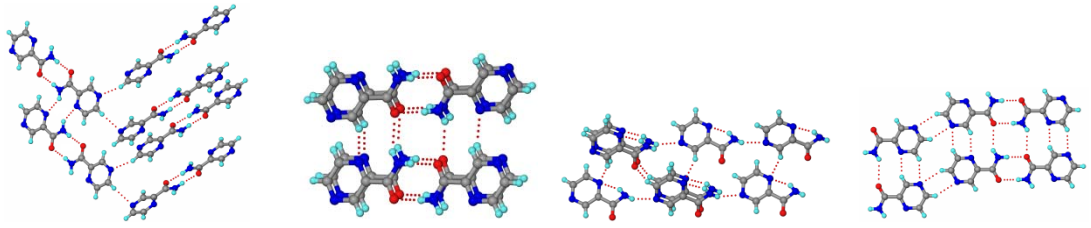

α β γ δ

Figure 1.6 Synthon and packing polymorphism in Pyrazinamide. In α polymorph, zigzag tapes formed by $R^2_2(8)$ N–H···O and $R^2_2(10)$ N–H···N hydrogen bonds are connected

orthogonally to 2_1 screw related tapes through C–H···N interactions in a 3D arrangement. The β polymorph has non-planar $R^2_2(8)$ N–H···O dimers that make a helix along the *b*-axis through anti N–H···O and C–H···N interactions. In γ polymorph, 1D tapes assembled via N–H···N hydrogen bonds of $C(6)$ notation are connected through C–H···O and C–H···N interactions. In δ polymorph, carboxamide tapes formed by $R^2_2(8)$ dimer and $C(4)$ catemer N–H···O synthons and $R^2_2(6)$ C–H···N synthons make 2D sheets (adapted from Ref. 42b).

When polymorphs crystallize simultaneously in the same flask under identical crystal growth conditions from the same solvent, they are termed as concomitant polymorphs[43]. This phenomenon occurs when the crystallizing polymorphs have almost similar energies. Concomitant polymorphism is exemplified by benzamide which incidentally is also the first example of a polymorphic organic substance reported by Wöhler and Liebig in 1832[43]. When the tautomers of a compound rapidly interconvert in solution or in melt but crystallize as polymorphs in their solids then the phenomenon is known as tautomeric polymorphism[44], example, Omeprazole[44a]. The term Desmotropy[44b] is synonymous with tautomeric polymorphism.

1.5.2.2 Generation of polymorphs

Solution crystallization is a traditionally used method for polymorph generation. Solution crystallization conditions can be systematically varied by changing solvents (or solvent mixtures), temperature, supersaturation, stirring, slurrying, cooling rate, seeding, use of antisolvent etc. Recent approaches for polymorph generation include crystallization with structurally related additives[45a], epitaxial growth[45b], melting[45c], sublimation[45d], laser induced nucleation[45e], crystallization in capillaries[45f], mechanical grinding[45g], using supercritical liquids[45h] etc. Interestingly, many novel polymorphs of drug molecules and bioactive compounds were obtained serendipitously on cocrystallization[47] as observed in the case of curcumin[46] where Form II crystals were obtained on attempted cocrystallization with 4-hydroxypyridine. This strategy has undergone renaissance in recent years where tailor-made additives[48] were used in recent years for exclusive crystallization of desired polymorph.

1.5.2.3 Kinetic Vs. Thermodynamic Polymorph

Polymorphism results from the interplay of thermodynamic functions (free energy, enthalpy and entropy) and kinetic factors (activation energy, temperature, supersaturation, rate of evaporation etc.) that govern the crystallization process[36]. The role of nucleation governed by the Ostwald's law of stages is vital in predicting the nature of polymorphic outcome of a molecule[47]. The Curtin-Hammett principle[48] states that "*for a pair of reactive intermediates or reactants that interconvert rapidly, each going irreversibly to a different product, the product ratio will depend both on the difference in the energy between the two conformers and the free energy of the transition state going to each product*". This definition is equally applicable to crystallization process where kinetically favored crystal is obtained faster because the activation energy required to achieve this state is lower, whereas the thermodynamic polymorph is obtained later due to higher activation energy requirement. Nevertheless, the polymorph obtained at the end is the most stable since its thermodynamic state is lowest in energy. If the same crystal structure is kinetically and thermodynamically favored, then polymorphism is less likely[49a]. At molecular level, close packing and intermolecular interactions are the competing factors that determine the polymorphic outcome. Thermodynamic polymorph is favored when close packing dominate the intermolecular interactions. Similarly, kinetic polymorph is favored when the crystal nucleus is stabilized by intermolecular interactions. It is highly unlikely to observe polymorphism in crystal systems where the best interactions are accompanied by the best packing. Examples like naphthalene and D-glucose belong to this category where polymorphism is not observed so far[49a]. Recently, polymorphs of a monosaccharide, D-ribose were solved using powder and single crystal diffraction techniques[49b].

1.5.2.4 Polymorphism in pharmaceutical industry

Polymorphism has received particular attention in the recent literature because of its importance in drug substances and pharmaceutical formulation[29a]. Solubility and dissolution rate are important physico-chemical properties that have a direct influence on the physiological performance of the drug. Dissolution rate in particular is often the rate determining step which directly affects the drug bioavailability[36]. There are numerous

examples where the bioavailability of polymorphs varies significantly. For example, 6-mercaptopurine[50] (6-MP) is an immunosuppressive drug. Plasma concentration of form I and Form III of 6-MP after intravenous administration of 50mg/kg to rabbits showed that the extended bioavailability (EBA) of form III is 1.5 times higher than form I.

Different structures and properties make polymorphs patentable.[51] If a generic pharmaceutical company discovers a novel crystal form of an already marketed drug, it will gain an early access into the market place; therefore, the innovator companies must find out all possible polymorphs of the drug and patent them in order to extend their monopoly in pharmaceutical industry and to protect their product. A well-known example is the polymorphs of anti-ulcer drug Ranitidine hydrochloride.[36] Glaxo obtained a patent on the two polymorphs (I followed by II) of Ranitidine hydrochloride. In the mid 1990s, as the patent on the drug (form I) was approaching expiration, other companies began preparing to market a cheaper, generic versions of form I. But the generic manufacturers were not able to crystallize form I exclusively as it was always crystallizing as a mixture of form I and form II. This kept the generic companies products off the market for several years and during that period Glaxo was making $10 million in sales each day on this blockbuster drug. Ultimately, Novopharm could find a method to prepare form I exclusively with non-detectable amounts of form II, and won the battle. Since then generic entry was made into the market. Cefadroxil, Terazosin hydrochloride and Aspartame are other well known examples of patent issues surrounding polymorphism.[36]

1.5.3. Solvates and Hydrates - Pseudopolymorphism

Pseudopolymorphism[51] is defined as a phenomenon wherein a "*Compound is obtained in crystalline forms that differ in the nature or stoichiometry of included solvent molecules*" and the resulting solid forms are known as pseudopolymorphs. Terms like hydrate, solvate and solvatomorphs are synonymous with pseudopolymorphs. A molecular solid can form solvates with different stoichiometries of the same solvent[52], for example, mono and 2/3 hydrate of ergot alkaloid Tergurid[52a]. It may also form a series of solvates with different solvent molecules, for example, Sulfathiazole forms over hundred solvates with various

solvents[52b]. Even more a solvated structure can even exist as polymorphs, for example, α and β forms of Indantrione 1,2-dioxime[52c] (IND) methanol solvate (Figure 1.7).

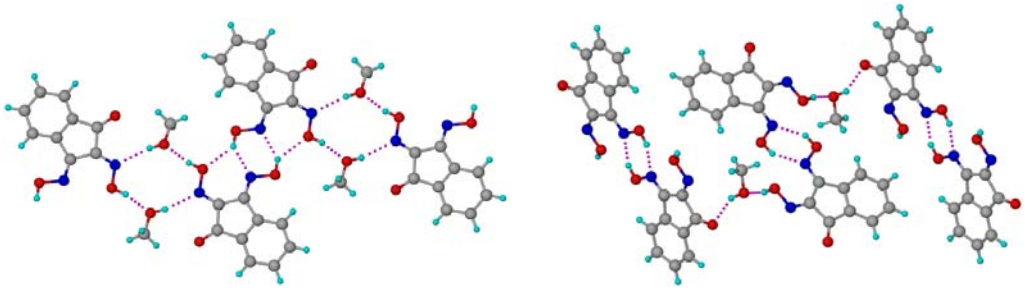

IND-MeOH solvate α form IND-MeOH solvate β form

Figure 1.7 In α form guest molecules bridge the dimeric units of IND through O–H···N and O–H···O hydrogen bonds resulting in the centrosymmetric cyclic assembly. In β form dimeric units of IND are linked by a single MeOH molecule extending the assembly through O–H···O hydrogen bonds (adapted from ref.52c).

The choice between solvated or unsolvated forms of a drug will depend on its pharmaceutical properties like stability under different conditions, shelf life etc. Various drug molecules are currently marketed as solvates/hydrates, for example, Indinavir sulfate[53a] is marketed as its ethanol solvate and Paroxetine hydrochloride[53b] is marketed as its hemihydrate. Depending on their effect on the crystal lattice, desolvation of the solvated structures can be of two types: 1) these solvents have minimum interactions with the parent molecule in the crystal lattice, hence desolvation does not affect the overall crystal structure, for example, solvates of cephalosporine[54a]. 2) In these crystal structures solvent molecules are bound to the parent molecules through strong intermolecular interactions, hence their desolvation may result in novel polymorphs of the guest free form. For example, Spironolactone[54b] form I and II was obtained by varying the desolvation rates of its ethanol solvate. In essence, solvate/hydrate formation can have diverse applications in pharmaceutical industry.

1.5.4 Pharmaceutical Salts

Salt formation is the most common and effective method for improving the physicochemical properties of drug molecules[29a,55]. The 'rule of three[56]' is a useful guide to predict salt formation between organic acids and bases. Nangia and coworkers[56b] tested this hypothesis by forming salts and cocrystals between several acid and pyridine containing molecules and concluded that the carboxylic acid–pyridine O–H···N interaction will be neutral when $\Delta pK_a < 0$ and it will have an intermediate H bond character, O–H···N and/or N^+–H···O^-, when the transition range $0 < \Delta pK_a < 3.75$. The interaction will be ionic N^+–H···O^- when $\Delta pK_a > 3.75$. Similar observations were echoed by Childs and Stahly[56b] in their analysis of 20 complexes of theophylline with COOH partners. The Orange book database[56c] lists various drugs products approved by the US-FDA, and the frequency of counterions used for salt formation over different decades. Therefore, the orange book is an excellent source of information on counterions based on their usage.

Salt formation has diverse implications in pharmaceutical industry. Salt formation confers solubility and thermal stability to drug molecules. For example, the poor solubility and low melting point of antiulcer drug Ranitidine was overcome by forming hydrochloride salt of the drug which showed very high solubility (1g/mL) and improved melting point (136°C). The plethora of counterions provides ample options for developing the optimal solid formulation for maximal therapeutic efficacy[55]. For example, Perindopril[58a], an angiotensin-converting enzyme (ACE) inhibitor widely used in cardiovascular therapeutics is available as a salt of tert-butylamine (erbumine), which is freely soluble in water and in ethanol (96%), and has a shelf-life of approximately two years. However, it is known that Perindopril requires special packaging in countries with high temperature and relative humidity. Telejko and coworkers[58a] reported that the arginine salt, in comparison with the erbumine salt, was more stable and led to a 50% increase in shelf-life, an important step for distribution of this drug in the developing world. The safety profile of the parent drug can also be altered by switching an ionic salt counter-ion. For example, the acute oral toxicity of propoxyphene was halved when prepared as the napsylate salt rather than the hydrochloride salt.[58b] On the downside salts tend to be more hygroscopic and restricted to drugs with

ionizable functional groups. These issues warrant the need for other techniques for pharmaceutical solid form development. Of late techniques like solid dispersions, nanoparticles, inclusion complexes seem to be very promising in addressing the poor physicochemical properties of drug molecules.

1.5.5 Pharmaceutical Cocrystals

Crystal engineering principles[6,8a] and hydrogen bonding rules are the primary design elements for cocrystal formation. A cocrystal[55d] may be defined as "a stoichiometric multi-component system where the individual components are held together by heteromeric interactions like hydrogen bonds and are solids at room temperature". Although the use of cocrystals in altering the physico chemical properties of pharmaceutically active compounds was reported as early as 1946, when Krantz et al.[59a] found that the stoichiometric (1:1) cocrystal containing the sodium salt of theophylline and glycine increased the water solubility of the API, it is only around the year 2000 that its importance was fully appreciated in the current context and popularized as 'Pharmaceutical cocrystals[60]'. A pharmaceutical cocrystal follows the definition of a simple cocrystal except that the individual components are generally an Active Pharmaceutical Ingredient (API) and a coformer which was assigned a GRAS status[60a,b] by the FDA. They have primarily attracted the attention of both academic and pharmaceutical chemists with their ability to modulate the solubility and dissolution rates of active pharmaceutical ingredients. Cocrystals can be synthesized by different methods wherein the components are mixed together and subjected to solution crystallization, co-sublimation, co-melting, solid state grinding, liquid assisted grinding, slurry crystallization, reaction crystallization, spray drying etc.[60] Recently novel techniques like inkjet printing[60d] and crystallization at solvent-solvent interface[60e] were used to form cocrystals. Coformers play a decisive role in influencing the physicochemical properties of a cocrystal which ultimately affects the parent drug. With few exceptions, it was observed that a high melting coformer always produces a high melting cocrystal and a high soluble coformer confers higher solubility to a cocrystal[60f].

Recently, Nangia et al.[55c] proposed a model explaining the role of coformer in improving the solubility of cocrystals, based on 'spring and parachute' model of amorphous forms.[61] According to the model, a cocrystal containing a high soluble coformer can facilitate faster dissolution of a low soluble component. This happens via the fast release of high soluble coformer into aqueous medium that results in the dissociation of cocrystal, thereby leaving behind the low soluble component in an amorphous/randomized state, which understandably leads to an increase in the free energy of the system, ultimately leading to an improvement of solubility/dissolution of the low soluble component (Figure 1.8).This model conforms that high solubility coformers will give rise to high solubility cocrystals and vice-versa. If the coformer has low water solubility, it does not dissociate from the lattice easily and in effect can control the solubility/dissolution of the drug like the cocrystals of anti-lung cancer agent Hexamethylenebisacetamide[60b] with sebacic acid and dodecanedioic acid.

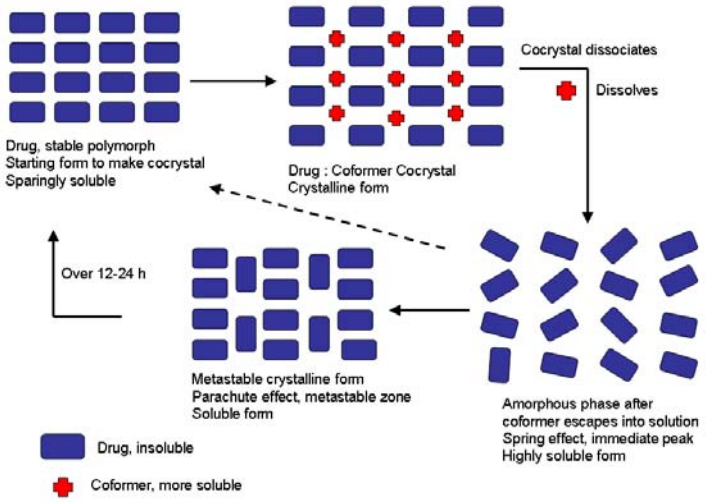

Figure 1.8 Nangia's model of solubility enhancement of a drug through a pharmaceutical cocrystal (adapted from ref.55c).

Conventionally, salts have been used to enhance solubility of drug molecules but cocrystals have the ability to modulate the solubility of an API either way (increase or decrease). Numerous literature reports highlight the solubility enhancing ability of cocrystals. For example, Itraconazole-maleic acid[62] cocrystal has about 20 times higher solubility compared

to the parent API which is comparable to that of the marketed amorphous form. In 1973, Higuchi[59b] reported that the 1:1 and 1:2 complexes of caffeine with gentisic acid could reduce the dissolution rate of caffeine, highlighting the solubility lowering ability of cocrystals which might be useful in making slow release dosage forms. Of late, polymorphism in cocrystals[60e], and cocrystallization between organic compounds and an inorganic salt also known as 'Ionic Cocrystals[63]' have become popular not only for diversifying the structural landscape of an API but also due to their ability to confer solubility/dissolution advantage. Apart from solubility modulation, cocrystals were used for various other applications as summarized below[64] (Figure 1.9). Recently, the US-FDA has published 'draft guidance on pharmaceutical cocrystals[65]' from the perspective of looking at them as intellectual property and hopefully a cocrystal formulation of a drug will be a reality in the near future.

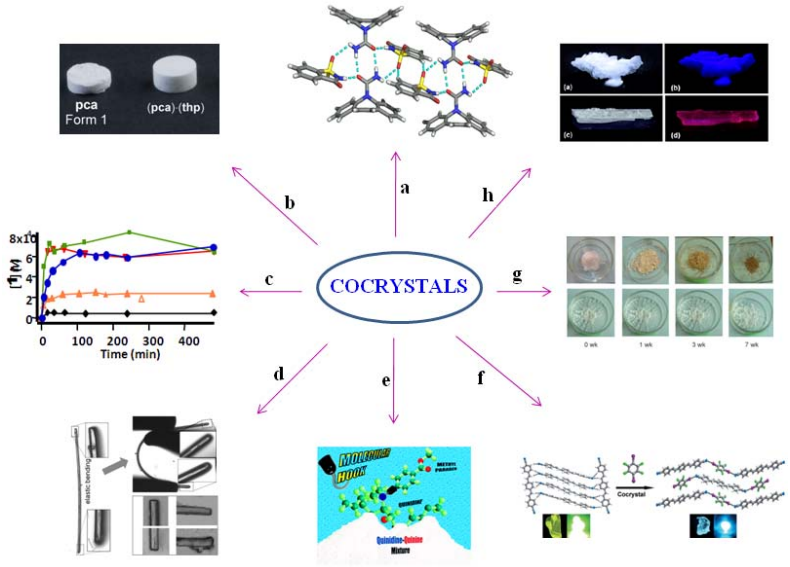

Figure 1.9 Some of the diverse applications of cocrystals **a)** unlike the parent drug carbamazepine, its cocrystal with saccharin was stable to hydration in a 24hrs slurry experiment, (ref. 64b) **b)** Tabletability of paracetamol was improved by forming cocrystal with theophylline, (ref. 64g) **c)** Cocrystal of itraconazole with maleic acid showed 20 times more solubility compared to parent drug. (ref.62) **d)** Highly flexible and elastically bendable cocrystal was formed on cocrystallizing caffeine with 4-chloro-3-nitrobenzoic acid (ref. 64c)

e) Methyl paraben acted as 'molecular hook by selectively forming cocrystal with quinidine from a mixture of quinidine-quinine stereoisomers. (ref. 64d) **f)** Cocrystal strategy tuned the luminescent properties of stilbene type organic molecules (ref. 64e) **g)** unlike temozolomide, its cocrystal with succinic acid showed good physical stability. (ref. 64a) **h)** Cocrystallization turned on the phosphorescence of phenanthrene (ref. 64f).

1.5.6 Eutectic Compositions

Limited aqueous solubility of emerging new chemical entities as well as older drug molecules, represent a barrier to solid oral dosage form development[29a]. Although the above solid forms like salts, cocrystals, polymorphs, pseudopolymorphs and amorphous forms are conventionally employed to overcome solubility problems, a universal solution still proves elusive. Binary eutectic compositions[66] with their excess thermodynamic functions[67] can act as alternate solid forms for solubility modulation. Their poorly understood internal structure has dissuaded researchers from exploring this strategy. Nevertheless, if further explored, eutectic mixtures can be promising as alternate strategies for solubility enhancement. Generally, alloys are classified into two categories, i) Isomorphous or solid solution alloys[66], ii) Non-isomorphous or eutectic alloys[66]. Both solid solution and eutectic alloys were prepared using fusion methods, hence it would be relevant to describe them using solid-liquid phase-diagrams[66,68]. A solid solution is formed by isomorphous solids in accordance with Hume-Rothery rules (same crystal structure, size, elctronegativity and valence)[66]. In solid solutions, by virtue of their structural similarities, the individual components form continuous solid solutions ranging from 1:99 to 99:1 ratios keeping the homogeneity of the phase intact. They are best represented through the solid-liquid phase diagram of Cu-Ni alloy[66] (Figure 1.10). Given their close atomic numbers and same 'face centered cubic' crystal structure, Cu (Z = 29) and Ni (*Z* = 28) atoms randomly distribute without affecting the FCC structure. They form homogeneous phases (α, in Figure 1.10) without any interatomic boundaries between the components. Also a solid solution exhibits a range in melting or freezing point[66]. The temperature below which it is a solid is known as 'solidus' and 'liquidus' is the temperature where the material is in liquid form. In the intermediate temperature range both solid and liquid phases coexist (Figure 1.10).

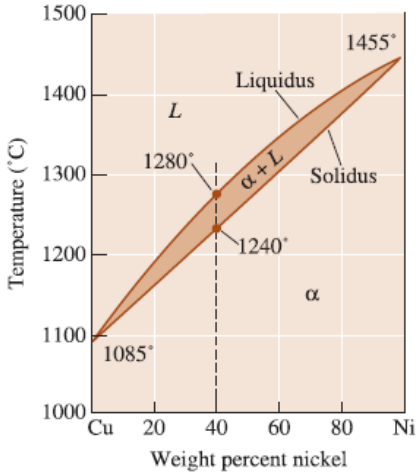

Figure 1.10 Phase diagram of Copper-Nickel solid solution alloy. This 40:60 Cu-Ni solid solution exhibits a melting range of 1240-1280°C. (adapted from ref. 66c).

When the interacting components are non-isomorphous and the interaction is dominated by misfit or mismatch of components then they result in eutectic alloys. In Greek '*Eutectos*' means easily fused[66]. Eutectics may be defined as "a specific composition of constituents in a mixture of elements or compounds which exhibits the lowest melting point than any other composition of the constituents[69]. Unlike solid solutions, the dissolution of non-isomorphous components of eutectic has a solubility limit. Hence they cannot form continuous solid solutions. This case is best exemplified by Tin-Lead eutectic alloy (Figure 1.11a).

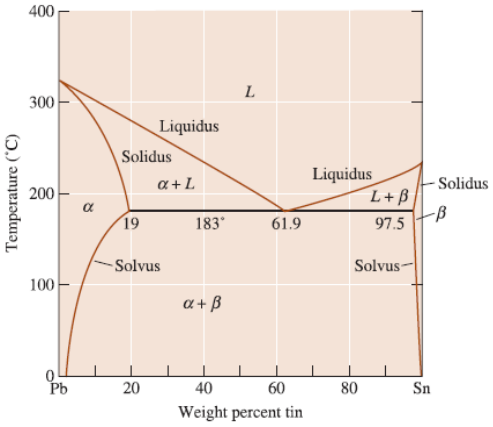

(a)

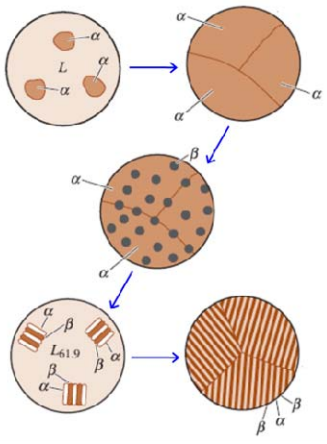

(b)

Figure 1.11a) Phase diagram and **b)** microstructure of Lead-Tin eutectic alloy showing solidification and growth of solid solutions (adapted from ref. 66c).

Although Sn-Pb alloy forms a solid solution like Cu-Ni alloy, the extent of homogeneity is limited by the difference in the physical and chemical parameters of Sn (Z = 50, tetragonal) and Pb (Z = 82, cubic). Since Sn is smaller in size compared to Pb, about 19% of Sn can dissolve in to the crystal lattice of Pb without affecting its crystal structure. This (19:81) % of Sn-Pb system forms a homogenous solid solution represented as α (Figure 1.11a). Similarly, Pb can be accommodated into the crystal lattice of Sn, but given its large size its solubility is limited to 2.5%. Therefore a (2.5:97.5) % of Pb in Sn forms a uniform solid solution (β, Figure 1.11a). When either of the elements exceed the solubility limits, they cause strain and disorganization in the crystal lattice of the solid solutions[66,68]. In order to resolve this issue, the system reorganizes into a definite arrangement of α and β phases where the individual phases represent a solid solution retaining the crystal lattice of the major component. This reorganized arrangement on solidification result in a eutectic composition (Figure 1.11b). Hence eutectics are also known as 'Conglomerates of solid solutions[66,68]. The microstructure of eutectic mixtures represent domains of two or more phases. The interphase boundaries are composed of imperfect atomic arrangements and weak intermolecular forces. As a result, eutectics have excess thermodynamic functions which result in their lower melting point[67]. When the ratio of tin and lead are in 61.9% and 38.1%, the alloy has lowest melting point (183 °C) than its parent elements (Tin = 232 °C, Lead = 327 °C) and also other compositions (Figure 1.11a) and displays the characteristic eutectic microstructure. The microstructure of Sn-Pb system adopts a lamellar arrangement. In literature several other microstructures are reported (Figure 1.12).

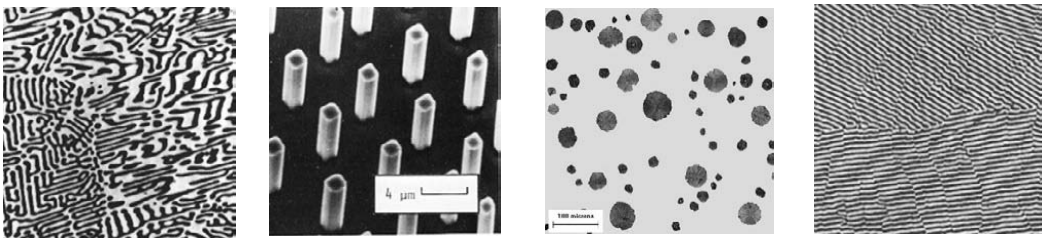

Figure 1.12 Various microstructures in eutectic systems. **a)** Irregular microstructure in Mg-Mg_2Sn eutectic. The dark phase is the faceted Mg_2Sn, **b)** Rod shaped faceted/non-faceted microstructure in Ni-NbC eutectic, **c)** Divorced microstructure in Fe-spheroidal graphite eutectic, **d)** Lamellar arrangement in Sn-Pb system(adapted from ref.66d).

1.5.6.1 Importance of eutectics in pharmaceutical development

Eutectic compositions represent those long known class of compounds which are often neglected by pharmaceutical chemists due to their poorly understood internal structure especially in the organic compounds. Nevertheless, from the classic NaCl/water eutectic[69a] to the more recent energy storage purposes[70a], eutectics are part of the everyday life (Scheme 1.3).

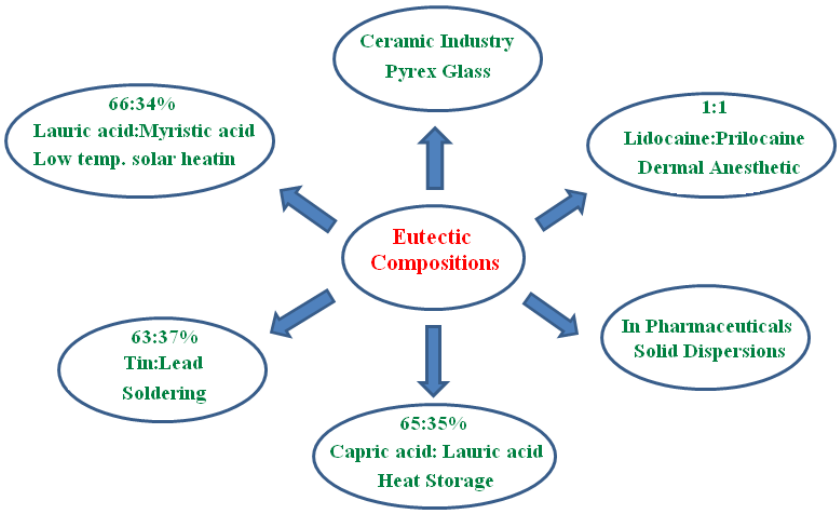

Scheme 1.3 Various applications of eutectics in everyday life (adapted from ref.70).

In pharmaceuticals, it was observed that in the process of grinding and milling the drug molecules form eutectics with other constituents like excipients[71]. Chiou and colleagues[72a] have reported that a eutectic composition of antifungal drug Griseofulvin with succinic acid (55% w/w of Griseofulvin) have shown 6-7 times faster dissolution rate compared to pure Griseofulvin (Figure 1.13). Eutectic mixtures have also been shown to improve the permeability of drug molecules[72]. Hence eutectics confer both solubility and bioavailability advantage on the drug molecules. Solid dispersions[66] due to their amorphous nature are likely to undergo phase transformation under the pharmaceutical processing and storage conditions. Whereas eutectics are highly crystalline compounds hence they do not have any disadvantages associated with phase transformation.

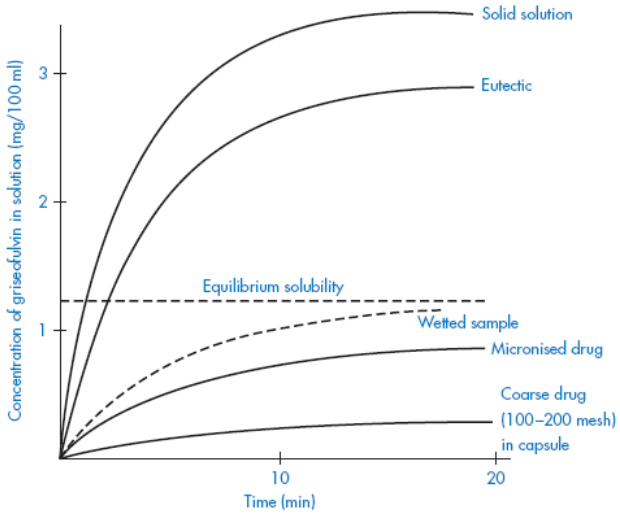

Figure 1.13 Rate of dissolution of Griseofulvin- succinic acid solid solution, eutectic mixture and crystalline material. The dissolution rate of Griseofulvin was improved by 6-7 times on forming eutectic (adapted from ref.72a).

Inspite of all the above advantages, eutectics are not popular as solid forms for pharmaceutical development due to their poorly understood internal molecular arrangement. However careful analysis of literature[66,68] reports and our own work[666a,b] on eutectics showed that there is a certain design aspect in the formation of eutectic compositions. It was found that 1. Lack of auxiliary interactions, 2. Misfit or mismatch of components, 3. Internal

symmetry in the molecules, 4. Molecular similarity seems to play a prominent role in the eutectic formation. These observations are elaborated in chapter 5. On comparing the solid forms described in previous sections it becomes clear that in salts/cocrystals adhesive interactions dominate cohesive forces which can be distinguished by various diffraction and spectroscopic techniques. On the other hand, in eutectics cohesive interactions are more prominent compared to adhesive interactions. Therefore, cocrystallization experiments can result in the formation of cocrystals/eutectics, depending on the dominating (cohesive/adhesive) interactions[55]

The inability of eutectics to produce single crystals for X-ray diffraction has made the understanding of their internal structure difficult. Unlike cocrystals, where the internal arrangement is homogeneous, the complex heterogeneous arrangement in eutectics comprised of domains of solid solutions held by weak interphase interactions might be the plausible reason for not obtaining single crystals. Of late, specific techniques like atomic pair distribution function (PDF) approach[73a,b] and extended x-ray absorption fine-structure spectroscopy (EXAFS)[73c,d] are used to analyze the local structure of materials. PDF is obtained from a total scattering powder diffraction pattern via a Fourier transform. Since the total scattering is composed of Bragg as well as diffuse scattering contributions, it contains local, medium range and long range structural information. Similarly, EXAFS is used to determine the distances, coordination number, and the nature of the neighbors of the absorbing atoms. Therefore these techniques may be helpful in dissecting the microstructure of a eutectic composition by analyzing the short range interactions comprising their interphase boundaries. In all, analyzing the complex microstructure of a eutectic composition is a huge challenge for a pharmaceutical chemist. Nevertheless, this poorly understood area is worth exploring since significant understanding of its internal arrangement would not only widen the horizons of solid form screening strategies but would also be important in 'Intellectual property management'[29a].

1.6 Conclusions

In this chapter we have briefly explored the origin and evolution of crystal engineering as a primary design element in developing pharmaceutical solid forms. Through various sections on intermolecular interactions and supramolecular synthons we have highlighted the importance of isotropic and anisotropic interactions in the growth of complex supramolecular architectures. This understanding would be vital in the context of 'pharmaceutical form development' since it would enable the design of several solid forms with varying strengths of intermolecular interactions such as polymorphs, amorphous forms, salts, cocrystals and solid solutions/eutectics for better therapeutic effect.

An API can give rise to a multitude of crystal forms upon solid form screening. A review of these solid forms was provided in various sections of this chapter which would highlight the inherent differences in the structural aspects among these crystalline forms. By virtue of their uniqueness, these solid forms would result in varied physico-chemical properties which are of paramount importance for optimal solid form selection and development. Since there is no single solution to the problems arising from the physico-chemical behavior of various drug molecules, it is absolutely essential to screen for all the possible solid forms (polymorphs, amorphs, salts, solvates, cocrystals, eutectics), which through their unique physicochemical properties would provide specific and desirable applications in different systems. In the following chapters, chapter 2 deals with the discovery of novel sulfonamide-pyridine-*N*-oxide heterosynthon, chapter 3 describes the solubility enhancement of Aceclofenac drug through salts, chapter 4 explores polymorphism in sulfacetamide-acetamide cocrystal, chapter 5 discusses the solubility enhancement of curcumin through binary eutectic compositions, chapter 6 describes the solubility modulating ability of novel sulfacetamide cocrystals and chapter 7 explores the relative stability of Atovaquone polymorphs. In essence, this thesis deals with the application of crystal engineering principles in designing and discovering different solid forms of drug molecules and their application towards addressing their poor physicochemical properties.

1.7 References

1. F. Wöhler, *Annalen der Physik und Chemie,* 1828, **88**, 253-256.
2. (a) J.-M. Lehn, *Pure Appl. Chem*., 1978, **50**, 871. (b) J.-M. Lehn, *Supramolecular Chemistry: Concepts and Perspectives*, VCH: Weinheim, 1995.
3. E. Fischer, *Chem. Ber.,* 1894, **27**, 2985-2993.
4. D. E. Palin and H. M. Powell, *J. Chem. Soc.,* 1948, 571-574.
5. J.-M. Lehn, *Proc. Nat. Acad. Sci.,* 2002, **99**, 4763-4768.
6. (a) G. R. Desiraju, *Crystal Engineering: The Design of Organic Solids*, Elsevier, Amsterdam, 1989. (b) G. R. Desiraju, *J. Chem. Sci*., 2010, **122**, 667. (c) G. R. Desiraju, J. J. Vittal and A. Ramanan, *Crystal Engineering. A Textbook,* World Scientific Publishing, Singapore, 2011.
7. R. Pepinsky, *Phys. Rev.,* 1955, **100**, 52.
8. (a) E. R. T. Tiekink, J. J. Vittal and M. J. Zaworotko, *Organic Crystal Engineering: Frontiers in Crystal Engineering*, John Wiley & Sons, Ltd., West Sussex, 2010. (b) J. Graetz, *Chem. Soc. Rev.,* 2009, **38**, 73-82.
9. J. M. Robertson, *Organic Crystals and Molecules*, Cornell University Press, 1953.
10. (a) M. D. Cohen and G. J. M. Schmidt, *J. Chem. Soc.,* 1964, 1996-2000. (b) G. J. M. Schmidt, *Pure Appl. Chem.,* 1971, **27**, 647-678.
11. O. Ermer, *J. Am. Chem. Soc.,* 1988, **110**, 3747-3754.
12. (a) B. F. Hoskins and R. Robson, *J. Am. Chem. Soc.*, 1990, **112**, 1546. (b) B. F. Hoskins and R. Robson, *J. Am. Chem. Soc.*, 1989, **111**, 5962.
13. (a) G. R. Desiraju (Ed.), *Crystal Design: Structure and Function, Perspectives in Supramolecular Chemistry*, Vol **7**. Wiley & Sons, 2003. (b) E. Weber (Ed.), *Design of Organic Solids*, Springer-Verlag, Berlin, 1998. (c) M. D. Hollingsworth, *Science,* 2002, **295**, 2410. (d) L. Brammer, *Chem. Soc. Rev.,* 2004, **33**, 476. (e) B. Moulton and M. J. Zaworotko, *Chem. Rev*., 2001, **101**, 1629. (f) D. Philip and J. F. Stoddart, *Angew. Chem. Int. Ed.,* 1996, **35**, 1154.
14. (a) J. D. Dunitz, *Pure Appl. Chem*. 1991, **63**, 177.

15. (a) A. I. Kitaigorodskii, *Molecular crystals and molecules*, Academic Press, New York, 1973. (b) A. J. Pertsin and A. I. Kitaigorodskii, *The Atom-Atom Potential Method*, Springer-Verlag, 1987.
16. (a) T. Steiner, *Angew. Chem. Int. Ed.,* 2002, **41**, 48-76. (b) G. R. Desiraju, *Acc. Chem. Res.,* 1991, **24**, 290-296. (c) G. A. Jeffrey and W. Saenger, *Hydrogen Bonding in Biological Structures*, Springer-Verlag, Berlin, 1991.
17. (a) A. Werner, *Leibig's Annalen der Chemie*, 1902, **322**, 261-97. (b) A. Hantzsch, *Chemische Berichte*, 1910, **43**, 3049-76.
18. L. Pauling, *The Nature of Chemical Bond*, Cornell University Press, Ithaca, New York, 1939.
19. E. Arunan, G. R. Desiraju, R. A. Klein, J. Sadlej, S. Scheiner, I. Alkorta, D. C. Clary, R. H. Crabtree, J. J. Dannenberg, P. Hobza, H. G. Kjaergaard, A. C. Legon, B. Mennucci and D. J. Nesbitt, *Pure Appl. Chem*., 2011, **83**, 1619-1636.
20. G. R. Desiraju and T. Steiner, *The Weak Hydrogen Bond: In Structural Chemistry and Biology*, Oxford University Press, New York, 1999.
21. E. J. Corey, *Pure Appl. Chem*. 1967, **14**, 19.
22. (a) E. J. Corey. *Chem. Soc. Rev.,* 1988, **17,** 111. (b) D. Seebach, *Angew Chem Int. Ed. Engl.,* 1990, **29**, 1320.
23. G. R. Desiraju, *Angew. Chem*. *Int. Ed. Engl.* 1995, **34**, 2311.
24. C. B. Aakeröy, A. M. Beatty and B. A. Helfrich, *J. Am. Chem. Soc.* 2002, **124**, 14425.
25. (a) Cambridge Structural Database, CSD, version 5.34, ConQuest 1.15, May 2013 update. (b) F. H. Allen, *Acta Crystallogr*. *Sect. B,* 2002, **58**, 380. (c) F. H. Allen and W. D. S. Motherwell, *Acta Crystallogr. Sect. B,* 2002, **58**, 407.
26. R. D. B. Walsh, M. W. Bradner, S. Fleishman, L. A. Morales, B. Moulton, N. Rodríguez-Hornedo, M. J. Zaworotko, *Chem Commun*, 2003, 186.
27. (a) B. R. Bhogala, S. Basavoju and A. Nangia, *Cryst. Growth Des*., 2005, **5**, 1683. (b) P. Vishweshwar, A. Nangia and V. M. Lynch, *CrystEngComm,* 2003, **5**, 164. (c) V. R. Vangala, R. Mondal, C. K. Broder, J. A. K. Howard and G. R. Desiraju, *Cryst. Growth Des.,* 2005, **5**, 99. (d) L. S. Reddy, P. M. Bhatt, R. Banerjee, A. Nangia and G. J. Kruger, *Chem. Asian J.* 2007, **2**, 505. (e) J. A. Bis and M. J. Zaworotko, *Cryst.*

Growth Des., 2005, **5**, 1169. (f) L. S. Reddy, N. J. Babu and A. Nangia, *Chem Commun,* 2006, 1369.

28. A. M. Thayer, *Chem Eng News*, 2010, **88**, 13-18.
29. (a) S. R. Byrn, R. R. Pfeiffer and J. G. Stowell, *Solid-State Chemistry of Drugs*; SSCI, West Lafayette, IN, 1999. (b) J. D. Mullins and T. J. Macek, *J. Pharm. Sci*., 1960, **49**, 245. (c) http://www.drugs.com/ppa/darunavir-ethanolate.html
30. C. G. Smith and J. J. O'Donnell, *The Process of New Drug Discovery and Development*, Informa, New York, 2006.
31. (a) L. R. Hilden and K. R. Morris, *J. Pharm. Sci*., 2004, **93**, 3. (b) L. Yu, *Adv. Drug Deliv. Rev*., 2001, **48**, 27. (c) R. Thakuria and A. Nangia, *CrystEngComm*, 2011, **13**, 1759. (d) J. F. Willart and M. Descamps, *Mol. Pharmaceutics*, 2008, **5**, 905-920.
32. (a)http://www.fujichemical.co.jp/english/newsletter/images/1001/Fuji_Email%20Blast_Neusilin.pdf. (b) Q. Wang, S. Li, X. Che, X. Fan and C. Li, *Asian J. Pharm. Sci.,* 2010, **5**, 188-193. (c) D. Bahl and R. H. Bogner, *Pharm. Res*., 2006, **23**, 2317-2325.
33. (a) P. H. Poole, T. Grande, C. A. Angell and P. F. McMillan, *Science*, 1997, **275**, 322. (b) J. Kieffer, *J. Phys. Chem.*, *B* 1999, **103**, 4153.
34. (a) D. Mishima, L. E. Calvert and E. Whalley, *Nature,* 1984**, 310**, 393. (b) J. P. Johari, A. Hallbrucker and E. Mayer, *Nature,* 330**, 1987**, 552.
35. X. Chen, Y. Zhang, Y. Wang, W. Zhou, D. A. Knight, T. B. Yisgedu, Z. Huang, H. K. Lingam, B. Billet, T. J. Udovic, G. M. Brown, S. G. Shore, C. Wolverton and J-C. Zhao, *Chem. Sci.,* 2012, **3**, 3183-3191.
36. (a) J. Bernstein, *Polymorphism in Molecular Crystals*; Clarendon, Oxford, U. K., 2002. (b) J. Haleblian and W. McCrone, *J. Pharm. Sci*., 1969, **58**, 911. (c) H. G. Brittain, *Polymorphism in Pharmaceutical Solids*, Informa Health Care, New York, 2009.
37. (a) E. Mitscherlich, *Abhl. Akad. Berlin*, 1822-1823, 43. (b) J. Berzelius, *Jahresbericht*, 1844, **23**, 44-55. (c) R. Purohit and P. Venugopalan, *Resonance*, 2009, 882.
38. a) P. Corradini, *Chem. Ind. (Milan)*, 1973, **55**, 122. (b) J. Bernstein and A. T. Hagler, *J. Am. Chem. Soc*., 1978, **100**, 673.

39. D. E. Braun, T. Gelbrich, V. Kahlenberg, G. Laus, J. Wieser and U. J. Griesser, *New J Chem.,* 2008, **32**, 1677-1685.
40. (a) A. Nangia, *Acc. Chem. Res*., 2008, **41**, 595. (b) N. K. Nath, S. Nilapwar and A. Nangia, *Cryst. Growth Des.,* 2012, **12**, 1613-1625.
41. (a) R. K. Harris, P. Y. Ghi, H. Puschmann, D. C. Apperley, U. J. Griesser, R. B. Hammond, C. Ma, K. J. Roberts, G. J. Pearce, J. R. Yates and C. J. Pickard, *Org. Process Res. Dev.,* 2005, **9**, 902-910. (b) J-B. Arlin, L. S. Price, S. L. Price and A. J. Florence, *Chem. Commun*., 2011, **47**, 7074-7076.
42. (a) N. J. Babu, S. Cherukuvada, R. Thakuria and A. Nangia, *Cryst. Growth Des*., 2010, **10**, 1979. (b) S. Cherukuvada, R. Thakuria and A. Nangia, *Cryst. Growth Des.,* 2010, **10**, 3931-3941.
43. F. Wöhler and J. Liebig, *Annal. Pharm.*, 1832, **3**, 249.
44. (a) P. M. Bhatt and G. R. Desiraju, *Chem. Commun,* 2007, 2057-2059. (b) J. Elguero, *Cryst. Growth Des.,* 2011, **11**, 4731-4738.
45. (a) P. K. Thallapally, R. K. R. Jetti, A. K. Katz, H. L. Carrell, K. Singh, K. Lahiri, S. Kotha, R. Boese and G. R. Desiraju, *Angew. Chem. Int. Ed.*, 2004, **43**, 1149. (b) C. A. Mitchell, L. Yu and M. D. Ward, *J. Am. Chem. Soc.*, 2001, **123**, 10830. (c) D. Das and L. J. Barbour, *J. Am. Chem. Soc.,* 2008, **130**, 14032-14033. (d) N. K. Nath, H. Aggarwal and A. Nangia, *Cryst. Growth Des.,* 2011, **11**, 967-971. (e) X. Sun, B. A. Garetz and A. S. Myerson, *Cryst. Growth Des.*, 2006, **6**, 684. (f) J. L. Hilden, C. E. Reyes, M. J. Kelm, J. S. Tan, J. G. Stowell and K. R. Morris, *Cryst. Growth Des.*, 2003, **3**, 921. (g) A. V. Trask, N. Shan, W. D. S. Motherwell, W. Jones, S. Feng, R. B. H. Tan and K. J. Carpenter, *Chem. Commun.* 2005, 880. (h) A. Bouchard, N. Jovanović, G. W. Hofland, E. Mendes, D. J. A. Crommelin, W. Jiskoot and G. Witkamp, *Cryst. Growth Des.*, 2007, **7**, 1432.
46. (a) P. Sanphui, N. R. Goud, U. B. R. Khandavilli, S. Bhanoth and A. Nangia, *Chem Commun*, 2011, **47**, 5013-5015.
47. W. F. Ostwald, *Z. Phys. Chem.,* 1897, **22**, 289.
48. http://en.wikipedia.org/wiki/Curtin%E2%80%93Hammett_principle

49. (a) G. R. Desiraju, *Nature Materials*, 2002, **1**, 77. (b) D. Sisak, L. B. McCusker, G. Zandomenegi, B. H. Meier, D. Blaser, R. Boese, W. B. Schweizer, R. Gilmour and J. D. Dunitz, *Angew. Chem. Int. Ed.,* 2010, **45**, 4503-4505.
50. T. Yokoyama, T, Umeda, K. Kuroda, T. Kuroda and S. Asada, *Chem Pharm Bull,* 1981, **29**, 194-199.
51. A. Nangia and G. R. Desiraju, *Chem Commun.,* 1999, 605-606.
52. (a) B. Kratochvil, J. Novotny, M. Husak, J. Had, J. Stuchlik and A. Jogorov, *Collect. Czech. Chem. Commun.,* 1994, **59**, 149-158. (b) A. L. Bingham, D. S. Hughes, M. B. Hursthouse, R. W. Lancaster, S. Travener and T. L. Threlfall, *Chem Commun.,* 2001, 603. (c) M. Suzuki and K. Kobayashi, *Cryst. Growth Des.,* 2011, **11**, 1814-1820.
53. (a) J. Lin, D. Ostovic and J. Vacca, *Pharm. Biotechnol.,* 1998, **11**, 233-255. (b) http://www.gsk.com.au/resources.ashx/prescriptionmedicinesproductschilddataproinfo/1580/FileName/1FEC0F4C187D4D00DDE44D79CF7C72EA/Aropax_PI_007_approved.pdf
54. (a) R. R. Pfeiffer, K. S. Yang and M. A. Tukker, *J. Pharm. Sci*., 1970, **59**, 1809. (b) B. Nicolai, P. Espeau, R. Ceolin, M.-A. Perrin, L. Zaske, J. Giovannini and F. Leveiller, *J. Therm. Anal. Calorim.,* 2007, **90**, 337-339.
55. (a) Y. Qiu; Y. Chen and G. G. Z. Zhang, Eds., *Developing Solid Oral Dosage Forms. Pharmaceutical Theory and Practice*, Academic Press, New York, 2009; (b) (c) N. J. Babu and A. Nangia, *Cryst. Growth Des.*, 2011, **11**, 2662. (d) N. Schultheiss and A. Newman, *Cryst. Growth Des.*, 2009, **9**, 2950.
56. (a) B. Sarma, N. K. Nath, B. R. Bhogala and A. Nangia, *Cryst. Growth Des*. 2009, **9**, 1546. (b) S. L. Childs, G. P. Stahly and A. Park, *Mol. Pharmaceutics,* 2007, **4**, 323. (c). G. S. Paulekuhn, J. B. Dressman and C. Saal, *J. Med. Chem*. 2007, **50**, 6665.
57. (a) S. M. Berge, L. D. Bighley and D. C. Monkhouse, *J. Pharm. Sci*., 1977, **66**, 1. (b) S. Sweetana and J. M. Akers, *J. Pharm. Sci. Tech*., 1996, **50**, 330.
58. (a) E. Telejko, *Curr Med Res Opin*, 2007, **23**, 953-960. (b) P. L. Gould, *Int. J. Pharm.,* 1986, **33**, 201-217. (c) V. M. Raumer, J. Dannappel and R. Hilfiker, *Chem. Today*, 2006, **24**, 41-44.

59. (a) J. C. Krantz, J. M. Holbert, H. K. Iwamoto and C. J. Karr, *J. Am. Pharm. Assoc.*, 1947, **36**, 248-250. (b) T. Higuchi and I. H. Pitman, *J. Pharm. Sci.*, 1973, **62**, 55.
60. (a) P. Vishweshwar, J. A. McMahon, J. A. Bis and M. J. Zaworotko, *J. Pharm. Sci*., 2006, **95**, 499. (b) C. B. Aakeröy, S. Forbes and J. Desper, *J. Am. Chem. Soc.*, 2009, **132**, 17048. (c) A. Alhalaweh and S. P. Velaga, *Cryst. Growth Des*., 2010, **10**, 3302. (d) A. B. M. Buanz, R. Telford, I. J. Scowen and S. Gaisford, *CrystEngComm*, 2013, **15**, 1031-1035. (e) M. D. Eddleston, S. Sivachelvam and W. Jones, *CrystEngComm*, 2013, **15**, 175-181. (f) M. K. Stanton, R. C. Kelly, A. Colletti, Y.-H. Kiang, M. Langley, E. J. Munson, M. L. Peterson, J. Roberts and M. Wells, *J. Pharm. Sci.*, 2010, **99**, 3769.
61. S. M. Berge, L. D. Bighley and D. C. Monkhouse, *J. Pharm. Sci*., 1977, **66**, 1.
62. J. F. Remenar, S. L. Morissette, M. L. Peterson, B. Moulton, J. M. MacPhee, H. R. Guzman and O. Almarsson, *J. Am. Chem. Soc.,* 2003, **125**, 8456.
63. D. Braga, F. Grepioni, L. maini, S. Prosperi, R. Gobetto and M. R. Chierotti, *Chem Commun.,* 2010, **46**, 7715-7717.
64. (a) N. J. Babu, P. Sanphui and A. Nangia, *Chem. Asian J.,* 2012, **10**, 2274. (b) M. B. Hickey, M. L. Peterson, L. A. Scoppettuolo, S. L. Morrisette, A. Vetter, H. Guzman, J. F. Remenar, Z. Zhang, M. D. Tawa, S. Haley, M. J. Zaworotko and O. Almarsson, *Eur. J. Pharm. Biopharm.,* 2007, **67**, 112. (c) S. Ghosh and C. M. Reddy, *Angew. Chem. Int. Ed.,* 2012, **51**, 10319. (d) M. Khan, V. Enkelmann and G. Brunklaus, *J. Am. Chem. Soc.,* 2010, **132**, 5254. (e) D. Yan, A. Delori, G. O. Lloyd, T. Friscic, G. M. Day, W. Jones, J. Lu, M Wei, D. G. Evans and X. Duan, *Angew. Chem. Int. Ed.,* 2011, **50**, 12483. (f) X. Pang, H. Wang, X. R. Zhao and W. J. Jin, *CrystEngComm*, 2013, **15**, 2722-2730. (g) S. Karki, T. Friščić, L. Fábián, P. R. Laity, G. M. Day and W. Jones, *Adv. Mater.*, 2009, **21**, 3905.
65. http://www.fda.gov/downloads/Drugs/.../Guidances/UCM281764.pdf.
66. (a) S, Cherukuvada and A. Nangia, *CrystEngComm*, 2012, **14**, 2579-3588. (b) N. R. Goud, K. Suresh, P. Sanphui and A. Nangia, *Int. J. Pharm.,* 2012, **439**, 63-72. (c) D. R. Askeland and P. P. Fulay, *Essentials of Materials Science and Engineering*, 2nd ed., Cengage Learning, 2009. (d) W. D. Callister Jr., *Fundamentals of Materials*

Science and Engineering, John Wiley & Sons, 2001. (e) D. M. Stefanescu, *Science and Engineering of Casting Solidification*, 2nd Ed., Springer, 2009.

67. (a) S. S. Das, N. P. Singh, T. Agrawal, P. Gupta, S. N. Tiwari and N. B. Singh, *Mol. Cryst. Liq. Cryst.*, 2009, **501**, 107. (b) N. B. Singh, S. S. Das, N. P. Singh and T. Agrawal, *J. Cryst. Growth*, 2008, **310**, 2878.
68. M. D. Moore and P. L. D. Wildfong, *J. Pharm. Innov.*, 2009, **4**, 36.
69. (a) http://en.wikipedia.org/wiki/Eutectic_system;
    (b) http://www.drugs.com/dict/eutectic.html;
70. (a) A. Karaipekli and A. Sari, *J. Indus. Engi. Chem.*, 2010, **16**, 767. (b) L. Shilei, Z. Neng and F. Guohui, *Ener. Build.*, 2006, **38**, 708. (c) B. F. J. Broberg and H. C. A. Evers, *US Pat.*, 4529601, 1985. (d) A. Sari, *App. Therm. Eng.,* 2005, **25**, 2100.
71. M. Bi, S. -J. Hwang and K. R. Morris, *Ther. Acta*, 2003, **404**, 213.
72. (a) W. L. Chiou and F. Niazi, *J. Pharm. Sci.,* 1976, **65**, 1212. (b) C. W. Park, H. M. Mansour, T. O. Oh, J. Y. Kim, J. M. Ha, B. J. Lee, S. C. Chi, Y. S. Rhee and E. S. Park, *Int. J. Pharm.*, 2012, **436**, 652-658.
73. (a) T. Proffen, K. L. Page, S. E. McLain, B. Clausen, T. W. Darling, J. A. Tencate, S. Y. Lee and E. Ustundag, *Z. Kristallogr.* 2005, **220**, 1002-1008. (b) V. Petkov, M. Gateshki, J. Choi, E. G. Gillan and Y. Ren, *J. Mater. Chem.,* 2005, **15**, 4654. (c) A. M. Beale and B. M. Weckhuysen, *Phys. Chem. Chem. Phys.*, 2010, **12**, 5562-5574. (d) S. Cammelli, D. L. Hecht, C. Degueldre, J. Bertsch and R. Frahm, *J. Phys. Conf. Ser.,* 2009, **190**, 12027.

CHAPTER TWO

SULFONAMIDE-PYRIDINE-*N*-OXIDE HETEROSYNTHON IN COCRYSTAL DESIGN

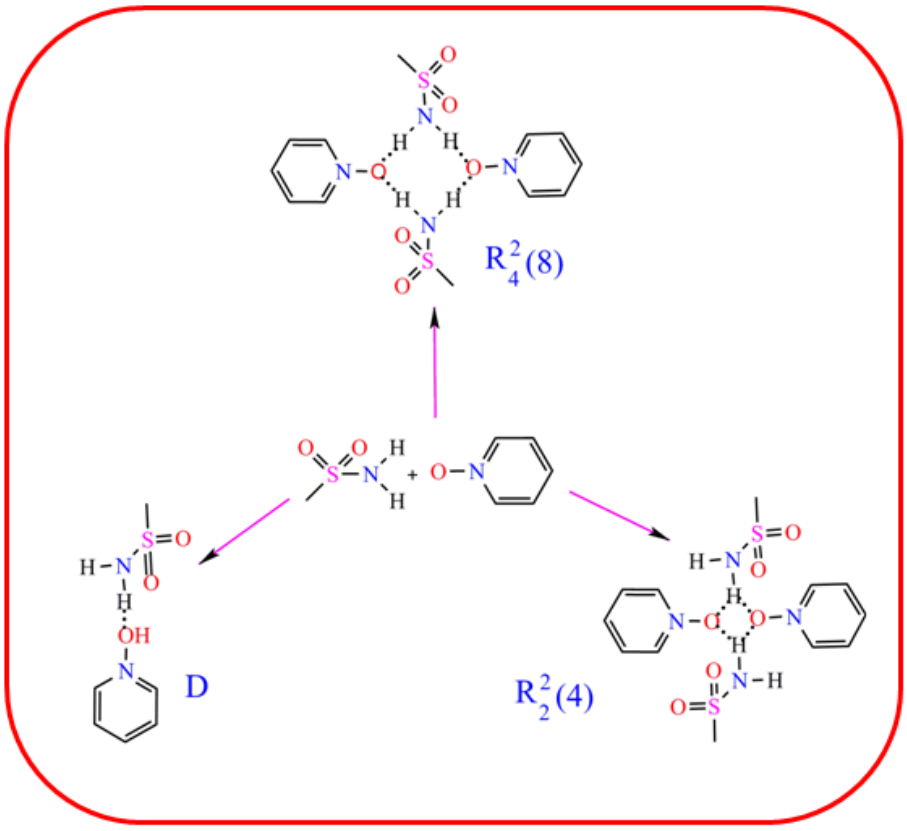

Synthon patterns observed in Sulfonamide-Pyridine-N-Oxide Cocrystals described in this chapter. This novel heterosynthon was successful in disrupting the prominent homodimer of the parent sulfonamides for cocrystal formation.

2.1 Introduction

The discovery of quinhydrone by Wöhler[1] in the year 1844 is officially regarded as the birth of a new class of compounds called cocrystals[2]. For greater part of the last century, cocrystals represented those little studied and vastly neglected set of compounds. However, in the past decade they have attracted the attention of pharmaceutical chemists with their ability to modulate physicochemical properties of drug molecules[3]. Through noncovalent interactions a second component is introduced into the crystal lattice of active pharmaceutical ingredient which can alter its solid state assembly and thereby its physico-chemical properties. This advantage of cocrystals in addressing the solubility, dissolution and stability issues of APIs without altering their chemical structure has since proved to be a promising alternative to chemical modifications like salts.

The concept of 'Supramolecular Synthon[4]' lies at the heart of rational cocrystal design. This term was introduced by Desiraju in the realm of supramolecular chemistry in order to bring the subject of crystal engineering[4,5] into the mainstream of organic chemistry. By doing so, crystals are projected as supramolecular equivalents of molecules and crystal engineering as the supramolecular equivalent of organic synthesis. Using the synthon concept, the complex supramolecular architectures in crystals were systematically downsized into robust intermolecular interactions between complementary functional groups of molecules. This approach was hugely complemented by Etter's hydrogen bond rules[6], which state that, (1) *all acidic hydrogens available in a molecule will be used in hydrogen bonding in the crystal structure of that compound.* (2) *All good proton acceptors will be used in hydrogen bonding when there are available hydrogen bond donors.* (3) *The best hydrogen bond donor and the best hydrogen acceptor will preferentially form hydrogen bonds to one another.* These design elements are immensely useful in simplifying the complex arrangement of molecules that are possible in the presence of multiple competing functional groups. In combination, both crystal engineering principles and hydrogen bonding rules were highly effective in providing rational strategies in the form of supramolecular synthon for the construction of binary/ternary cocrystals for supramolecular synthesis and pharmaceutical solids. Numerous groups all over the world have exploited this concept of supramolecular synthon concept for

understanding intermolecular interactions and quantifying the functional group robustness. In 2000, Steiner[7] carried out a database study on the competition of 34 different hydrogen bond acceptors (O, N, S, halogen and π-acceptors) for the strong carboxyl donor. Carboxylic groups are among the best investigated hydrogen bond functional groups[8]. With strong hydrogen bond donor as well as an acceptor sites they can readily form cyclic dimers (85%) or open arrays or catemer (15%). However the probability drops to 33% for dimer and 2.8% for catemer in presence of other functional groups. Acid–pyridine heterosynthon is the most popular and frequently occurring hydrogen bond motif in the CSD, and has an occurrence probability of over 90% compared to <50% frequency for other strong hydrogen bond synthons, such as acid–acid, amide–amide, and acid–amide (Scheme 2.1). These robust heterosynthons were extensively utilized by the groups of Nangia[8a, 9], Aakeroy[10], Zaworotko[8b,11], Jones[12] etc. to construct binary/ternary /quaternary cocrystals.

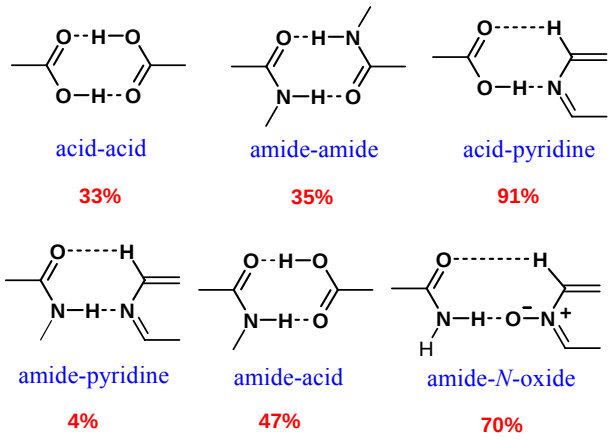

Scheme 2.1 Strong hydrogen bond synthons with their occurrence probability indicated in the presence of other competing functional groups

The supramolecular synthon concept was also explored by several groups in order to understand the synthon competition and structure directing roles of various functional groups. Aakeröy and co-workers[13] studied the structure directing competition between hydrogen and halogen bond donors by synthesizing novel azobipyridine derivatives and cocrystallizing them with a series of bifunctional donor molecules comprising an activated halogen bond donor (I or Br) as well as a hydrogen bond donor (acid, phenol or oxime) on

the same back bone. They have highlighted the importance of binding site location on the acceptor molecules as a direct influence over the structural balance between hydrogen and halogen bond donors. Moorthy and co-workers[14] have highlighted the importance of weak inter-halogen (Cl···Cl, Br···Br) and C–H···X interactions in directing the self-assembly of substituted benzoic acids. Bis et. al.[15] studied the synthon competition between Hydroxy, Pyridine and Cyano containing compounds and observed that persistent hydroxyl···pyridine hydrogen bonds were formed in cocrystals that also contain Cyano acceptor. Nangia and co-workers[16] reported synthon competition and cooperation in molecular salts of hydroxybenzoic acids and aminopyridines. Supramolecular synthons strategy was also exploited to discover novel synthons for cocrystal design. Brooks et. al.[17] identified the novel ortho-Phenylenediamine bis-urea carboxylate supramolecular synthon and demonstrated its robustness in a variety of systems. Maguire and co-workers[18] discovered the intermolecular S=O···H–C–S=O hydrogen bonding in sulfoxides and sulfones and the robustness was determined based on the level of oxidation at sulphur, steric and electronic effects of substituents on the aryl rings and methyl substitution α to the sulphur functional group. In short, the concept of supramolecular synthon enables deeper understanding of intermolecular interactions, synthon robustness and developing novel heterosynthons for cocrystallization.

2.2 Design of Novel Sulfonamide-Pyridine-*N*-Oxide heterosynthon

The sulfonamide group occupies a place of prominence in drug molecules, being the common functional moiety in many antibacterials, diuretics, anticonvulsants and dermatologicals[19]. It is the primary target for forming cocrystals among these classes of drug molecules. Whereas a few isolated cases of sulfonamide hydrogen bonding to other functional groups, such as COOH, $CONH_2$, urea, etc., are reported[20] there is no specific heterosynthon associated with the SO_2NH_2 group. We chose to address this problem by finding a complementary functional group with good basicity so that its better acceptor strength would result in a robust heterosynthon. For this we have analyzed certain basic coformers like pyridine, amide, pyridine-*N*-oxide etc. Among these, pyridine-*N*-oxide was chosen as the complementary functional group for SO_2NH_2 group based on the better

acceptor strength of its anionic oxygen. The pK_{HB} values of pyridine N, amide O and *N*-oxide O^- are 1.86, 1.96 and 2.70 (increasing basicity). Moreover, electrostatic surface potential (ESP) charges at the electronegative atoms (e.g. isonicotinamide: N –43.7, O –47.4 kcal mol^{-1}; isonicotinamide *N*-oxide: O^- –53.3, O –43.1 kcal mol^{-1}) parallel the same trend. An additional advantage with pyridine-*N*-oxide compared to COOH and $CONH_2$ as a complementary functional group is that homosynthon competition is minimal because the pyridine-*N*-oxide lacks strong donor groups of its own (Scheme 2.2)

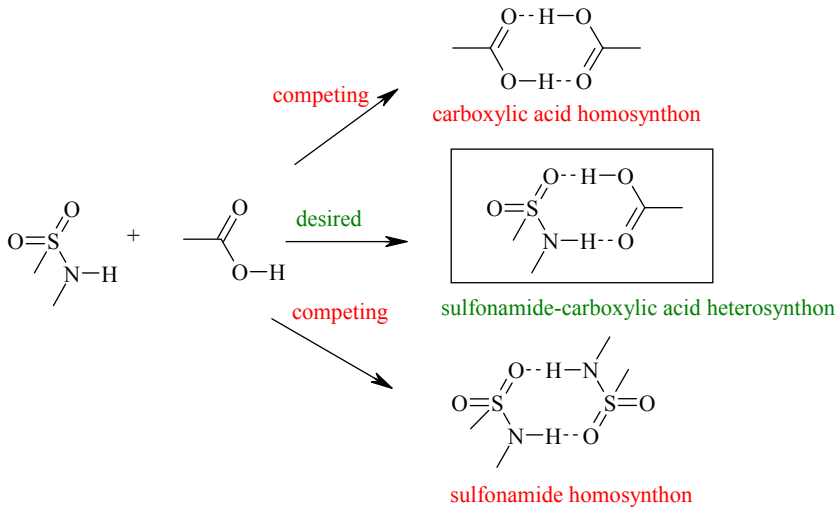

(a)

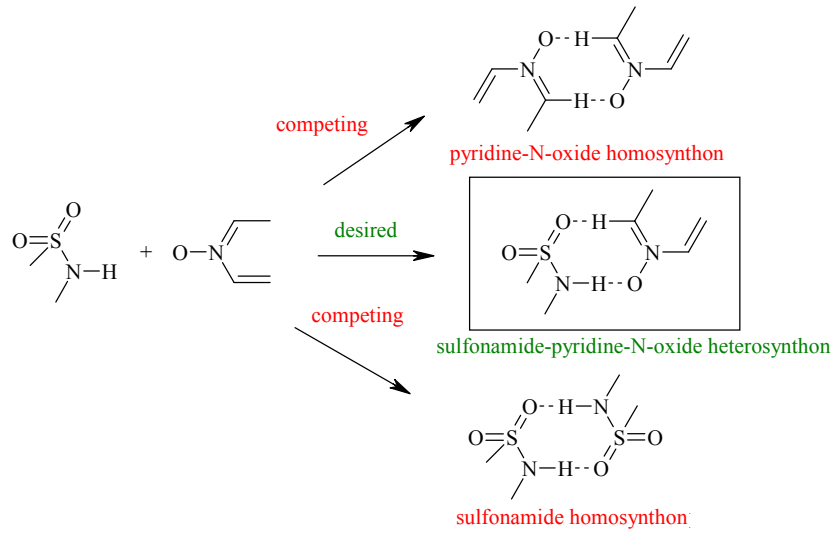

(b)

Scheme 2.2 Homo- vs. heterosynthon competition for the sulfonamide group. **a)** In sulfonamide–COOH (or $CONH_2$) the hydrogen bonds are of the strong O–H···O/ N–H···O type in the target heterosynthon and the competing homosynthons. **b)** In sulfonamide–pyridine-*N*-oxide, the target sulfonamide–pyridine-*N*-oxide has strongest donor–strongest acceptor pairing whereas the competing homosynthons are not so strong. This was reasoned to give higher success rate for the sulfonamide group to hydrogen bond with pyridine-*N*-oxide in co-crystallization experiments.

A stable heterosynthon assembly is based on the fact that the dissimilar functional groups will aggregate better compared to identical ones. Observations such as (1) the carboxamide–pyridine-*N*-oxide heterosynthon has hydrogen bond strength greater than the constituent homosynthons by about 3 kcal/mol[21], and (2) that pyridine-*N*-oxides are able to disrupt the strong urea α-network[22] suggested that the pyridine-*N*-oxide group will be a good complementary partner for the sulfonamide group to prepare heteromeric cocrystals.

2.3 Cambridge Structural Database Analysis

The Cambridge Structural Database[23] search (August 2010 update) for the sulfonamide group with the filters '3D coordinates determined, R-factor < 0.1, organic molecules only' gave 2090 hits, which included primary and secondary sulfonamide structures. This sulfonamide sub-database contained only 34 cocrystals (Table 2.1) without any solvent/ water inclusion, of which 5 are with primary sulfonamides (bold font in Table 2.1). There are 75 multi-component complexes such as salt hydrates and cocrystal solvates, 165 solvates, and 61 salt structures. These statistics show that the propensity of sulfonamide to form cocrystals is 1.63%, molecular complexes 3.59%, solvates 7.89%, and salts 2.91%. This means that the sulfonamide functional group is relatively less explored for cocrystal engineering. *Moreover, this version of the Cambridge database does not contain even a single hit of a primary sulfonamide and pyridine N-oxide functional group in the same crystal structure, suggesting that this class of heteromeric cocrystals is completely unexplored*. The anonymity of this group of cocrystals came as an additional drive to obtain

them in order to understand their hydrogen bonding interactions and explore the diverse synthons that build their crystal structures.

Table 2.1 Refcodes of sulfonamide cocrystals listed in CSD (Aug. 2010 update)

ADECIW	ATICIP	BCYTGA	GACCES	GEYSAE
GIYHUS	HORNEI	**JATMEW**	LIDVAW	LOMHUR
NETDIZ	RASSUZ	SACCAF	**SANAPY**	SMZTMP
SORWEB	**STHSAM**	SULTHE	UFERED	UNEZAO
VENLUV	**VIDGAR**	VIGFOH	VIGVOW	VUGMIT
VUGMOZ	VUZZIZ	VUZZUL	XEXCAE	XEXCEI
XOBCUN	XANNEH	YIZCAA	YOSMOI	

2.4 Crystallization of Sulfonamide-Pyridine-*N*-Oxide Cocrystals

Solution crystallization is the most common method of obtaining cocrystals where the individual components are dissolved in a suitable solvent and left for slow evaporation. Often, gentle warming is necessary to dissolve the solids, and an antisolvent is added to accelerate crystallization. Appearance of a new chemical complex is identified using DSC, IR, powder and single crystal X-ray diffraction. Precipitation of the individual components instead of the desired cocrystal due to incongruent solubilities and formation of undesired solvates/hydrates are common difficulties in the solution-based approach. Mechanochemical grinding[24] technique overcomes the problem of solubility differences of components to result in microcrystalline cocrystal product. On subjecting various sulfonamide and pyridine-*N*-oxide molecules to these techniques, we obtained six novel cocrystals of which two are with well known anti-diuretic drug Furosemide. Chemical structures of compounds successful in forming cocrystals are shown in Scheme 2.3.

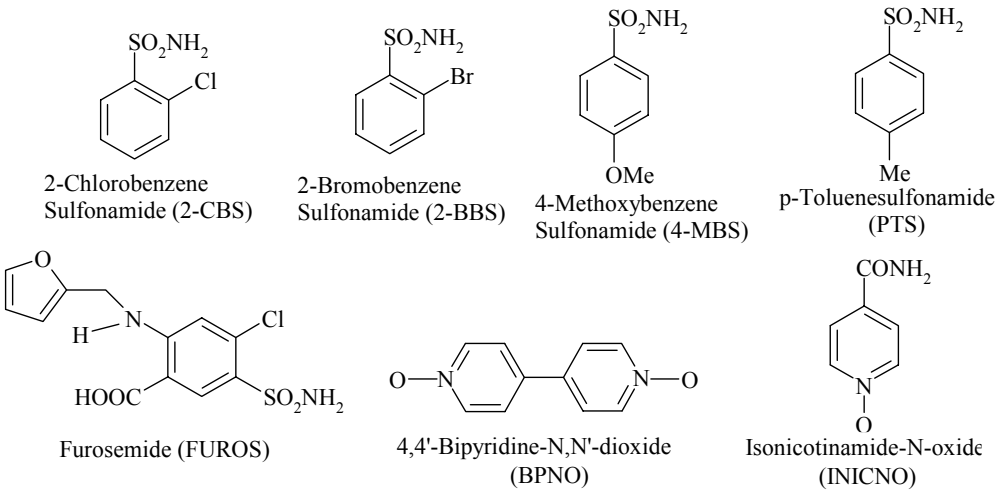

2-CBS–BPNO (1:1) **2-BBS–BPNO (1:0.5)** **4-MBS–BPNO (1:0.5)**

PTS–BPNO (2:1) **FUROS–BPNO–H_2O (1:1:0.25)** **FUROS–INICNO (1:1)**

Scheme 2.3 Chemical structures of Sulfonamide and Pyridine-*N*-oxide molecules successful in forming cocrystals. Abbreviations are used throughout the chapter.

Cocrystals of 2-CBS, 4-MBS, 2-BBS and PTS were obtained by the traditional solution crystallization method where 1:1 stoichiometric amounts of individual components were dissolved in a specific solvent and left for slow evaporation. However, this method was not successful with FUROS. For obtaining single crystals of FUROS with *N*-oxide coformers, firstly microcrystalline cocrystal product was obtained by grinding stoichiometric amounts of FUROS and *N*-oxide molecules using liquid assisted grinding approach[24b,c] with acetonitrile solvent. Only upon dissolution of this microcrystalline material in acetonitrile solvent and leaving it for slow evaporation did it result in single crystals of 0.25 hydrate with BPNO and a cocrystal with INICNO. (Cocrystallization details are mentioned in the experimental section). Bulk amounts of these cocrystals were also prepared using slurry grinding and fast evaporation under vacuum conditions[25]. Attempts with increasing the temperature of the solid-state reaction[26] or melt cocrystallization[27] did not yield any new adduct. Since both S=O and *N*-oxide acceptors are present in the system, the oxygen atom is subscripted to identify the functional group as $O_{sulfonamide}$ and O_{Noxide} whenever there is ambiguity. Crystallographic parameters of the cocrystals are listed in Table 2.2

Table 2.2 Crystallographic parameters of Sulfonamide-*N*-oxide Cocrystals

	2-CBS–BPNO (1:1)	2-BBS–BPNO (1:0.5)	4-MBS–BPNO (1:0.5)	PTS–BPNO (2:1)	FUROS–BPNO–H_2O (1:1:0.25)	FUROS–INICNO (1:1)
Empirical formula	$(C_6H_6O_2NSCl) \bullet (C_{10}H_8N_2O_2)$	$(C_6H_6O_2NSBr) \bullet 0.5(C_{10}H_8N_2O_2)$	$(C_7H_9O_3NS) \bullet 0.5(C_{10}H_8N_2O_2)$	$2(C_7H_9O_2NS) \bullet (C_{10}H_8N_2O_2)$	$(C_{12}H_{11}O_5N_2ClS) \bullet (C_{10}H_8N_2O_2) \bullet 0.5(O)$	$(C_{12}H_{11}O_5N_2ClS) \bullet (C_6H_6O_2N_2)$
Formula weight	379.81	660.36	562.61	530.61	526.92	468.87
Crystal system	Tetragonal	Triclinic	Monoclinic	Monoclinic	Triclinic	Triclinic
Space group	$P4_32_12$	$P\bar{1}$	$P2_1/c$	$P2_1/c$	$P\bar{1}$	$P\bar{1}$
T/K	100(2)	298(2)	100(2)	100(2)	100(2)	100(2)
a/Å	7.8871(5)	8.181(3)	8.7426(8)	10.3170(9)	8.0230(6)	5.2214(4)
b/Å	7.8871(5)	8.421(3)	5.2061(5)	12.3913(10)	8.3201(6)	9.5860(8)
c/Å	51.100(7)	10.250(4)	27.7269(19)	20.0553(17)	17.5479(12)	20.1540(17)
α/°	90.00	98.774(6)	90.00	90.00	77.7340(10)	85.2220(10)
β/°	90.00	95.521(6)	102.935(2)	103.7280(10)	77.5200(10)	88.7590(10)
γ/°	90.00	114.520(6)	90.00	90.00	81.2860(10)	74.8260(10)
Z	8	1	2	4	2	2
V/Å^3	3178.7(5)	624.9(4)	1229.96(18)	2490.6(4)	1110.71(14)	970.20(14)
D_{calc}/g cm^{-3}	1.587	1.755	1.519	1.415	1.576	1.605
Reflns collected	32933	6340	11917	25031	11547	10099
Obsd reflns	3142	2406	2422	4856	4339	3808
Unique reflns	3134	2207	2290	4493	4043	3566
R_1[I>2σ(I)]	0.0325	0.0299	0.0397	0.0335	0.0376	0.0317
wR_2[all]	0.0781	0.0764	0.1036	0.0900	0.0973	0.0849
No. of param.	234	163	173	343	341	338
GOF	1.150	1.110	1.082	1.017	1.059	1.038

2.5 Crystal Structure Analysis

2-Chlorobenzene sulfonamide–4,4′-bipyridine-*N, N*'-dioxide (2-CBS:BPNO, 1:1) This crystal structure in tetragonal space group $P4_32_12$ contains one molecule each of 2-CBS and BPNO in the asymmetric unit. The 2-CBS and BPNO molecules form a zigzag tape along the crystallographic [001] axis via a N–H···O_{Noxide} hydrogen bond (1.80Å, 173º). Hydrogen bonding interactions of all the crystal structures are listed in Table 2.3. The prominent N–H···$O_{sulfonamide}$ sulfonamide dimer in the parent molecule is absent in this cocrystal; one of the sulfonamide O is involved in intramolecular C–Cl···O contact of 3.06Å[28]. The cocrystal units are connected through C–H···O_{Noxide} interactions of BPNO (Figure 2.1).

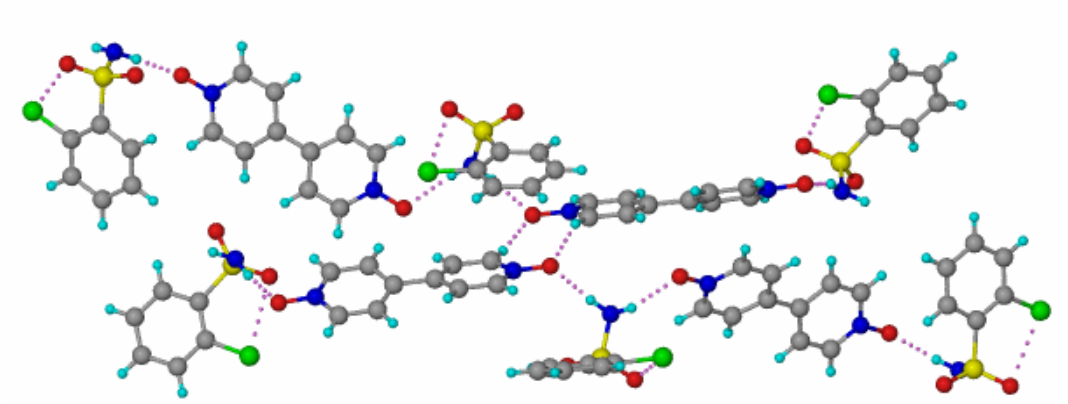

Figure 2.1 2-CBS and BPNO molecules are connected via a strong N–H···O_{Noxide} hydrogen bond and such binary units extend via a dimeric C–H···O_{Noxide} motif.

2-Bromobenzene sulfonamide–4,4′-bipyridine-*N,N*′-dioxide (2-BBS:BPNO 1:0.5) 2-BBS and BPNO molecules form a two-dimensional array of tetrameric $R^2_4(8)$ ring motifs[29] through N–H···O_{Noxide} hydrogen bonds. Auxiliary O···Br interactions resulting in a 10-membered ring between the adjacent 2BBS molecules lend additional stability to the crystal lattice. Unlike the 2CBS-BPNO structure where the sulfonamide and *N*-oxide components are connected through discrete N–H···O_{Noxide} hydrogen bond, dissimilar molecules in 2BBS-BPNO system are held through $R^2_4(8)$ ring motif, representing synthon diversity (Figure 2.2).

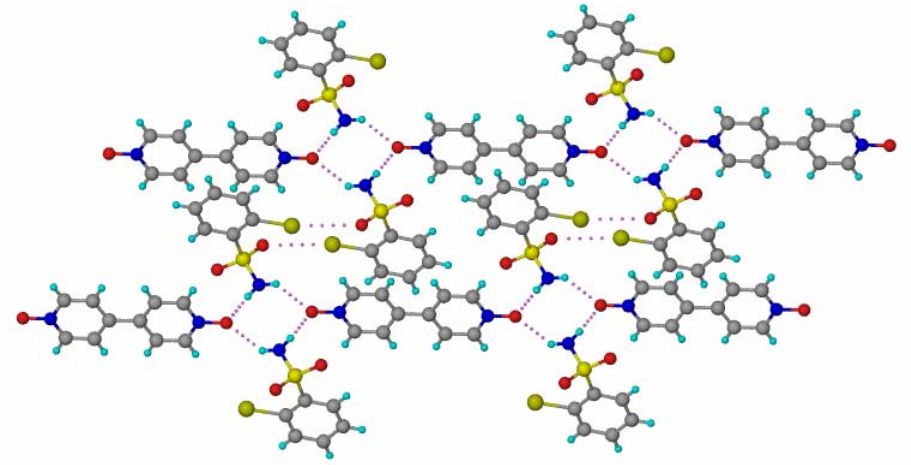

Figure 2.2 Tetrameric $R^2_4(8)$ of N–H···O_{Noxide} hydrogen bonds ring motifs assemble the binary adduct.

4-Methoxybenzene sulfonamide–4,4′-bipyridine-*N, N′*-dioxide (4-MBS:BPNO 1:0.5) 4-MBS molecules form a linear tape along the [010] axis through one point N–H···O_{Noxide} and N–H···$O_{sulfonamide}$ hydrogen bond (1.99Å, 166º; 1.74Å, 167º). Four 4-MBS and 2-BPNO molecules make large $R^6_6(34)$ rings with the p-anisyl groups projecting above and below the ring plane (Figure 2.3a). The commonly occurring sulfonamide dimer is absent in this structure. There is also an N–H···$O_{sulfonamide}$ $C(4)$ chain that can be discerned in the structure.

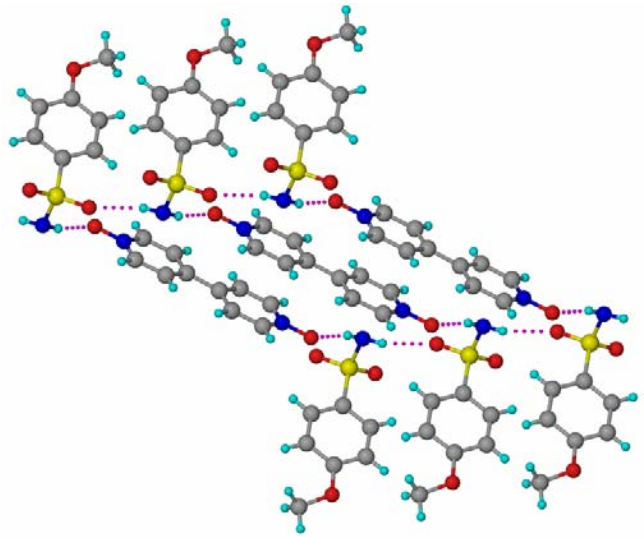

(a)

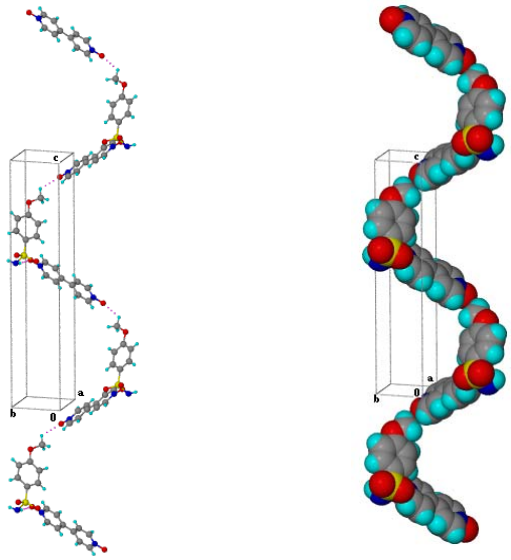

(b)

Figure 2.3a) Hydrogen bonded macrocyclic rings sustain the layer structure motif of 4-MBS–BPNO. **b)** Helical arrangement of alternating 4-MBS and BPNO molecules along the [001] axes are shown in ball-stick and space fill models.

4-Toluene sulfonamide–4,4′-bipyridine-*N,N′*-dioxide (PTS:BPNO 2:1) PTS and BPNO molecules form tetrameric ring motif $R^2_4(8)$ of N–H···O_{Noxide} hydrogen bonds through two symmetry independent TS molecules and two BPNO molecules(1.85Å, 173º, 1.97Å, 164º, 1.86Å, 164º, 1.80Å, 171º) as shown in Figure 2.4a. The sulfonamide O atoms are engaged in $R^2_2(9)$ ring motif through C–H···O interactions (Figure 2.4b).

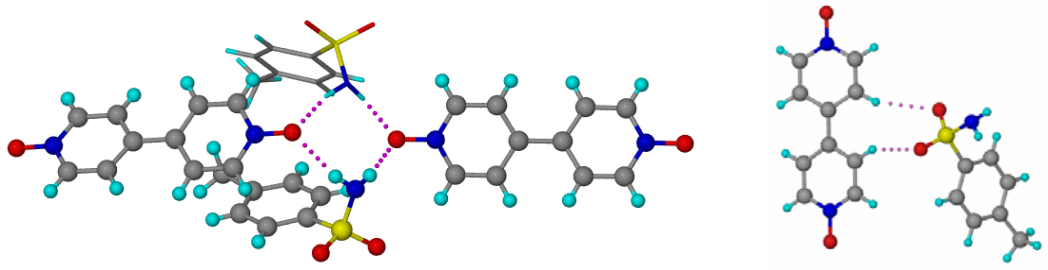

(a) (b)

Figure 2.4a) Tetrameric $R^2_4(8)$ rings of N–H···O hydrogen bonds between PTS and BPNO molecules. Symmetry-independent PTS molecules are shown as capped-stick and ball-stick models. **b)** C–H···O synthon of $R^2_2(9)$ motif in the crystal structure.

Furosemide–4,4′-bipyridine-*N,N′*-dioxide–0.25Hydrate (FUROS–BPNO–H_2O 1:1:0.25) This crystal structure contains one molecule each of FUROS, BPNO and a water molecule with 0.25 site occupancy factor. The crystal structure contains a prominent tetrameric ring motif of graph set $R^2_2(4)$ connected through strong N–H···O_{Noxide} hydrogen bond (2.04Å, 140.2°; Figure 2.5a). The molecular conformation of FUROS is frozen by an intramolecular N–H···O hydrogen bond (1.91Å, 132.3°) from the amine NH to the carboxylic acid C=O of $S(6)$ graph set notation[29]. *N*-oxide molecules are interconnected by two partial occupancy water molecules using non-covalent hydrogen bonding interactions. Further, the loss of water could also be detected in TGA (section 2.8, Figure 2.11). Incidentally, the cocrystal lattice retains the sulfonamide N–H···O dimer (1.95Å, 153.2°) from the parent furosemide molecule (Figure 2.5b). The $R^2_2(4)$ ring motifs are connected through O–H···O_{Noxide} (1.62Å, 157.9°) as shown in Figure 2.5c.

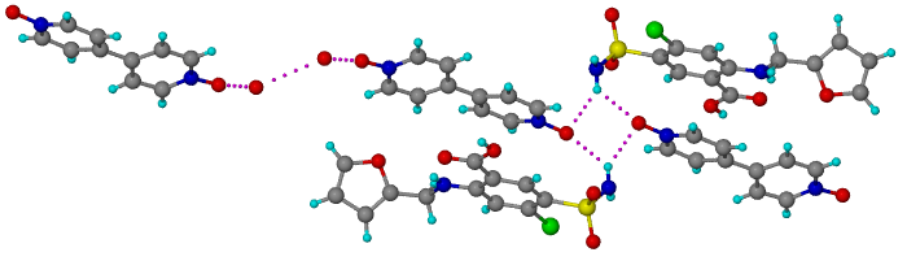

Figure 2.5a) BPNO molecules are connected to FUROS through tetrameric $R^2_2(4)$ ring motif on one side (right) and to another BPNO molecule through water bridges on the other side (left).

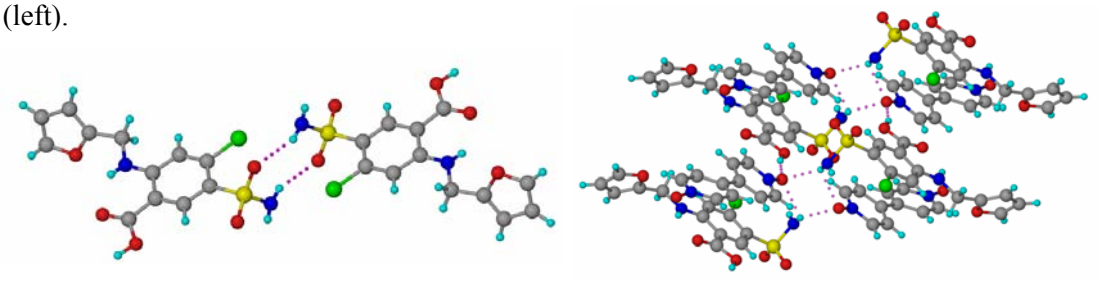

(b) (c)

Figure 2.5b) FUROS molecules connected through strong sulfonamide dimer $R^2_2(8)$ motif. **c)** Tetrameric $R^2_2(4)$ ring motifs are connected through O–H···O_{Noxide} hydrogen bond.

Furosemide–Isonicotinamide-*N*-oxide (FUROS–INICNO 1:1) The FUROS molecule in this crystal structure is disordered at the furan ring. The $R^2_2(8)$ ring motif between the carboxylic group of FUROS and the carboxamide group of INICNO is the primary heterosynthon (N–H···O 1.87Å, 167º; O–H···O 1.60Å, 168º) in this crystal lattice (Figure 2.6a). The sulfonamide group of FUROS connects the *N*-oxide moiety on INICNO through single point N–H···O_{Noxide} hydrogen bond (1.80Å, 162º). The FUROS and INICNO molecules extend to form large $R^4_4(32)$ [$R^2_2(8)$] ring motifs which in turn are connected through $R^2_2(8)$ C–H···O dimers (Figure 2.6b).

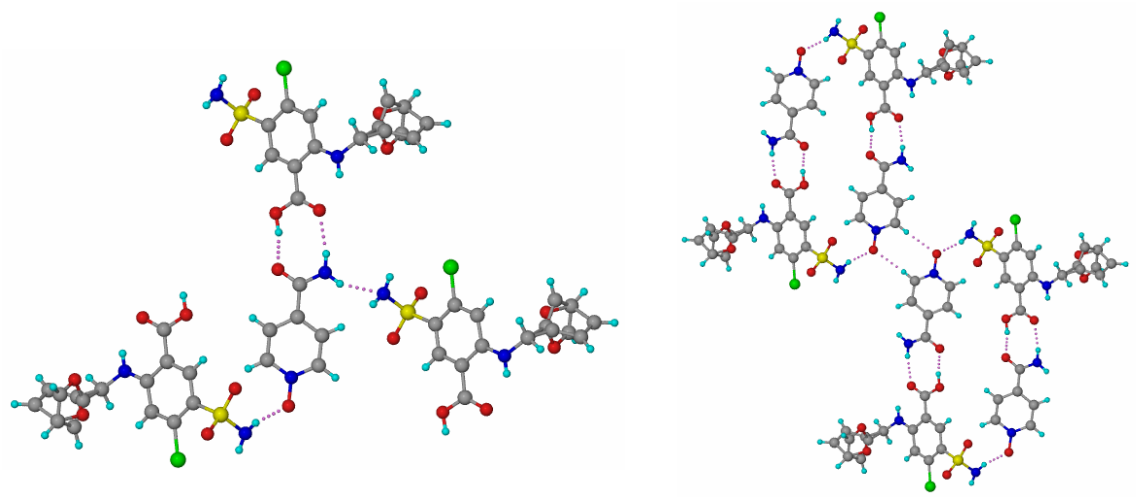

(a) (b)

Figure 2.6a) The INICNO coformer is connected to FUROS by amide–acid $R^2_2(8)$ motif and N–H···N hydrogen bond. **b)** $R^4_4(32)$ [$R^2_2(8)$] motif of N–H···O and O–H···O hydrogen bonds and C–H···O $R^2_2(8)$ dimer in FUROS–INICNO structure.

Table 2.3 Hydrogen bond parameters of Sulfonamide-*N*-oxide cocrystals. O–H, N–H and C–H distances are neutron-normalized to 0.983, 1.009 and 1.083Å respectively

D–H···A	D···A (Å)	H···A (Å)	D–H···A (°)	symmetry code
2-CBS–BPNO (1:1)				
N1–H1A···O4	2.806(3)	1.80	172.9	1/2+y,1/2–x,–3/4+z
N1–H1B···O3	2.839(3)	1.87	158.0	1+x, –1+y, –1+z
C3–H3···N1	3.388(3)	2.51	136.5	–1+x, y, z
C5–H5···O1	3.497(3)	2.42	168.4	–1/2+x,1/2–y,1/4–z
C6–H6···O1	2.825(3)	2.36	103.6	---[a]
C8–H8···O3	3.428(3)	2.35	173.0	y,1+x,2–z
C12–H12···O4	3.360(3)	2.29	169.2	3/2–x,1/2+y,7/4–z
C13–H13···O3	3.383(3)	2.40	149.1	y,1+x,2–z
C16–H16···O4	3.233(3)	2.23	153.1	3/2–x,–1/2+y,7/4–z
2-BBS–BPNO (1:0.5)				
N1–H1A···O3	2.812(3)	2.00	135.6	1–x,1–y, –z
N1–H1B···O3	2.806(3)	1.80	172.5	x, –1+y,z
C2–H2···O2	3.108(3)	2.40	121.3	–1–x,1–y,2–z
4-MBS–BPNO (1:0.5)				
N1–H1A···O3	2.737(2)	1.74	166.7	x, –1+y,z
N1–H2A···O2	2.988(2)	1.99	165.7	x,1+y,z
C12–H12···O1	3.321(2)	2.29	157.4	–1+x,1+y,z
PTS–BPNO (2:1)				
N2–H1A···O5	2.850(2)	1.86	164.0	–1+x,y,z
N2–H2A···O6	2.809(2)	1.80	170.7	x,3/2–y,1/2+z
N1–H3A···O6	2.858(2)	1.85	172.5	x, 3/2–y, 1/2+z
N1–H4A···O5	2.961(2)	1.97	164.1	–1+x,y,z
C2–H2···O1	2.893(2)	2.48	101.0	---[a]
C9–H9···O4	2.903(2)	2.49	101.0	---[a]
C21–H21···O1	3.180(2)	2.21	146.5	1+x, 3/2–y, –1/2+z
C23–H23···O4	3.324(2)	2.44	137.3	1+x,y,z
FUROS–BPNO-H_2O (1:1:0.25)				
N1–H1A···O6	2.897(2)	2.04	140.2	–2+x,y,1+z
N1–H1B···O2	2.886(2)	1.95	153.2	–1–x,1–y,2–z
N2–H2···O3	2.698(2)	1.91	132.3	---[a]
O4–H4···O6	2.564(2)	1.62	157.9	2–x,2–y,1–z
C3–H3···O1	2.819(2)	2.35	104.1	---[a]
C3–H3···O2	3.197(2)	2.46	124.0	–x,1–y,2–z
C11–H11···O3	3.239(2)	2.24	151.7	1–x,2–y,1–z
C12–H12···O7	3.239(3)	2.22	154.1	x,1+y,z
C16–H16···O1	3.178(2)	2.11	165.5	1+x,y, –1+z
C18–H18···Cl1	3.703(2)	2.66	160.7	–x,1–y,1–z

C19–H19···O1	3.330(2)	2.31	155.2	1+x,y, –1+z
C22–H22···O7	3.256(3)	2.23	156.7	1–x,1–y,1–z
FUROS–INICNO (1:1)				
N2–H2A···O3	2.866(2)	1.87	167.1	–2+x,y,z
N2–H2B···N4	3.074(2)	2.12	156.1	x, –1+y,z
N3–H3A···O3	2.694(2)	1.87	135.7	---[a]
N4–H4A···O1	2.784(2)	1.80	162.4	1–x,2–y, –z
O4–H4C···O2	2.569(2)	1.60	167.7	2+x, y, z
C4–H4···O5	3.277 (2)	2.35	142.0	x, –1+y,z
C5–H5···O1	3.414(2)	2.33	176.5	2–x,1–y,–z
C12–H12···O5	2.828(2)	2.36	103.8	---[a]

[a] = Intramolecular Hydrogen bond

2.6 Synthon Trends

The rationale behind studying crystalline molecular complexes like cocrystals is that a lot of information relating to synthon preferences is imbedded in its crystal structures since they represent minimum energy arrangements. Based on the synthons that build the supramolecular architectures of cocrystals, Zaworotko and coworkers[11d] classified the hydrogen bonding changes in going from single component to multi-component structures into two categories. Cocrystals belong to the first category when the inherent coformer simply acts as a spacer, retaining the original homosynthons of the starting components. On the other hand, when there is substantial change in hydrogen bonding because of the coformer functional groups, for example, acid or amide dimer homosynthon changing to acid–pyridine, amide–acid or amide–*N*-oxide heterosynthon, then the crystal structures belong to the second category. For example, cocrystals of well known anticonvulsant drug Carbamazepine (CBZ) with benzoquinone and terephthaldehyde retains the parent amide homodimer of CBZ, whereas the corresponding cocrystals with acetic acid and trimesic acid favor the heterodimer (Figure 2.7). Similarly, while the cocrystals of 4-hydroxybenzamide with 4,4'-bipyridine-*N,N'*-dioxide (BPNO) retains the parent amide homodimer, the corresponding cocrystal of BPNO with Temozolomide disrupts it[21b].

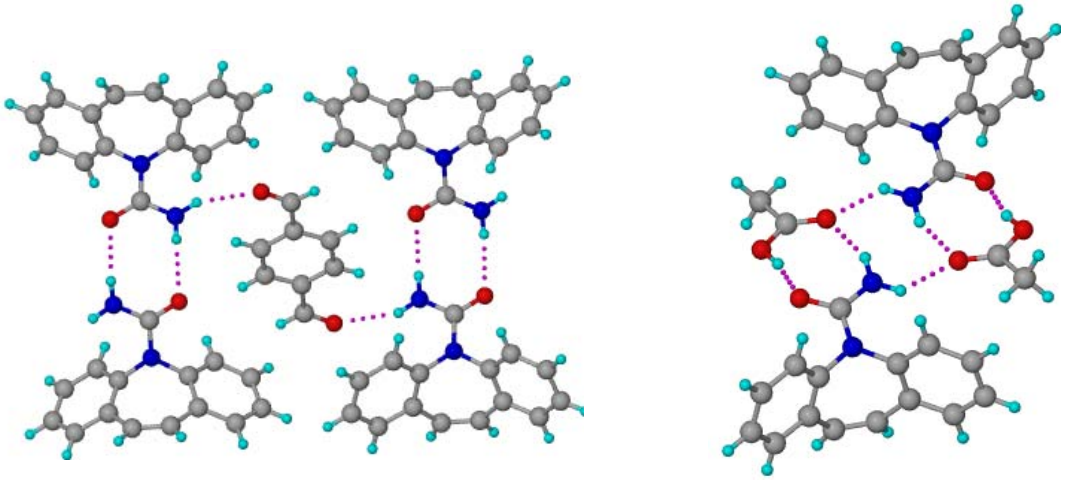

(a) (b)

Figure 2.7a) The prominent amide-amide homodimer of CBZ guest free form is retained in the CBZ-Terephthaldehyde cocrystal. **b)** While amide-Acid Heterosynthon is preferred in the CBZ-Acetic acid cocrystal. (Adapted from ref.11d)

A prominent feature of the sulfonamide crystal structures is their distinct amide homodimer synthon. During cocrystal formation, this robust homosynthon would compete with the probable heterosynthon resulting from the sulfonamide-coformer interactions. Various factors were found to determine the synthon outcome carboxamide-*N*-oxide cocrystals. In an attempt to form amide-*N*-oxide cocrystal between Barbital and Picolinamide-*N*-oxide[21b], presence of intramolecular hydrogen bonding in the coformer was shown to interrupt the formation of heterosynthon. It was noted in the dipolymorphic Nitronyl nitroxide uracil cocrystal[30], while the alpha and beta forms have strong amide–*N*-oxide synthon in their crystal structures, water molecule in its monohydrate crystal structure interrupts the formation of amide–*N*-oxide heterosynthon. Steric hindrance in Carbamazepine (CBZ)-Pyrazine *N,N'*- dioxide cocrystal[21b] was reasoned for the retention of parent amide homodimer. Therefore, intramolecular hydrogen bonding in the coformer molecules, presence of competing water molecules in the same crystal lattice and steric hindrance due to bulky components were shown to favor amide homodimer in amide-*N*-oxide cocrystals. In order to understand the synthon preferences among sulfonamide-*N*-oxide cocrystals, they were categorized based on the above classification. Interestingly, except the FUROS-BPNO-0.25H_2O, the parent sulfonamide homodimer was disrupted in all the other cocrystals.

Heteromeric interactions were favoured over parent homomeric interactions. Three reasons can be proposed for the synthon preferences among sulfonamide-*N*-oxide cocrystals. These conclusions are based on our previous reports on carboxamide-*N*-oxide cocrystals and a general understanding of the nature of *N*-oxide coformers. Firstly, the higher basicity of *N*-oxide molecules (pK_{HB} = 2.70) allows it to be in a better position to accept hydrogen bond donors for heterosynthon formation as compared to other coformer molecules. Secondly, the weak homosynthon of *N*-oxide molecules complements the first cause in favoring the heteromeric interactions. Thirdly, as shown in the case of amide-*N*-oxide cocrystals, the presence of competing water molecules retained the sulfonamide dimer in FUROS-BPNO-0.25H_2O. These observations sum up the synthon preferences observed in this class of cocrystals.

2.7 Spectroscopic Characterization

The nature of hydrogen bonding and extent of ionization can variably influence the vibrational energy levels of compounds on forming cocrystals or salts. IR and Raman instruments are sensitive to such changes, ably identifying and distinguishing novel solid forms from their starting components. All the sulfonamide-*N*-oxide cocrystals were characterized by IR and Raman Spectroscopy. Changes in the signature peaks associated with the transformation of the sulfonamide and the coformer to the new cocrystal structure were estimated. The N–H stretching vibrations of the sulfonamide group showed the expected red shift of 10-40 cm^{-1} due the formation of the stronger N–H···O_{Noxide} hydrogen bond in the cocrystal compared to N–H···$O_{sulfonamide}$, i.e. the N–H bond is weaker in the cocrystal. For example, in 2CBS-BPNO cocrystal while the parent N-H stretching frequency appeared at 3356.0cm^{-1} and 3254.0 cm^{-1}, the corresponding stretching frequencies in cocrystal appeared at 3332.7cm^{-1} and 3240.3cm^{-1} respectively. Similar differences were observed in the IR spectra of other compounds (Figure 2.8). Raman spectra of the cocrystals complemented the IR patterns in showing bathochromic shift in the N–H stretching peaks due to the weakening of the N–H bond. However, due to the weak intensities of the Raman peaks, the symmetric and asymmetric N–H peaks either merged together to give a single

broad band between 3400-3200 cm^{-1} in the cocrystals and the hydrate (Figure 2.9). Attempts to resolve the N–H peaks by increasing the laser intensity invariably resulted in the burning of sample. The changes in the N–H stretch, bend and S=O stretch vibrations in IR and Raman spectra of cocrystals are listed in Table 2.4.

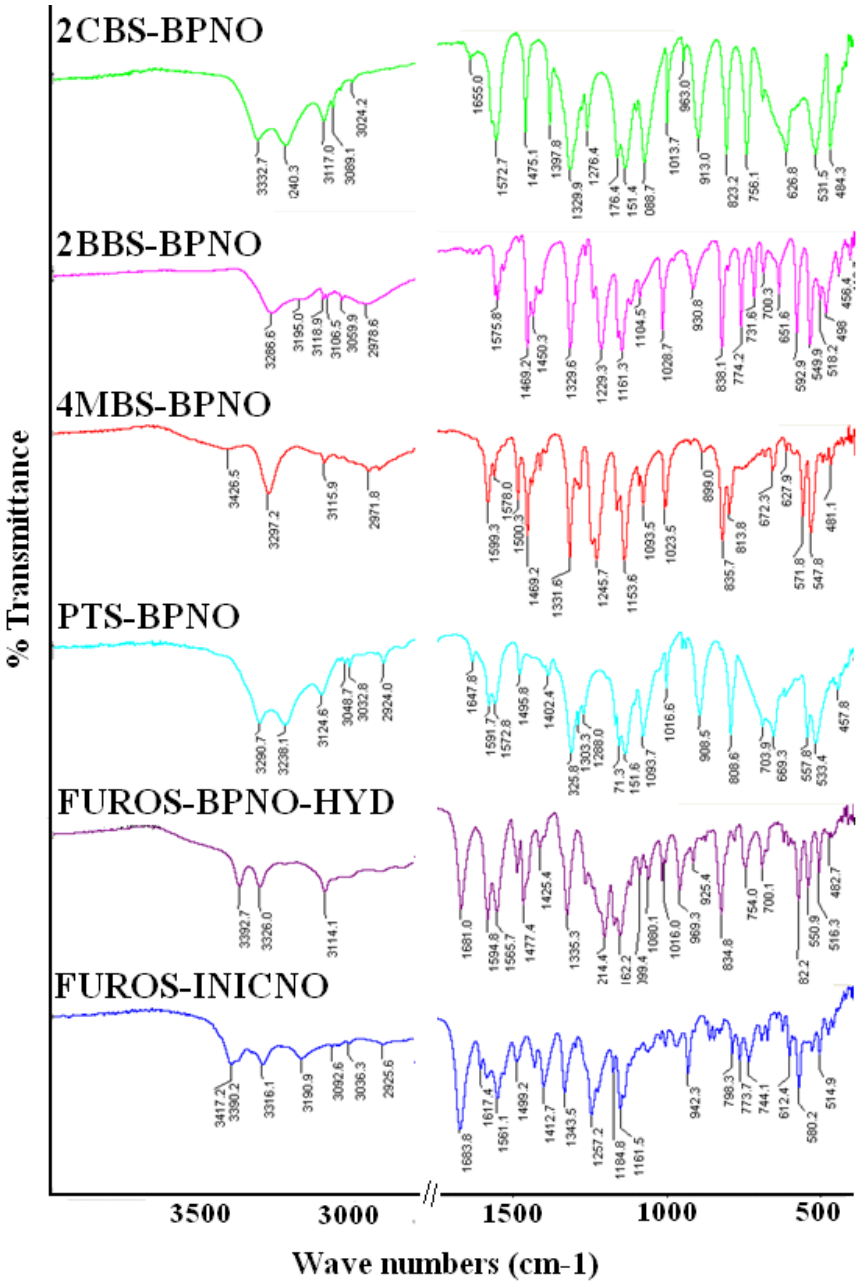

Figure 2.8 IR spectra of Sulfonamide-*N*-oxide cocrystals.

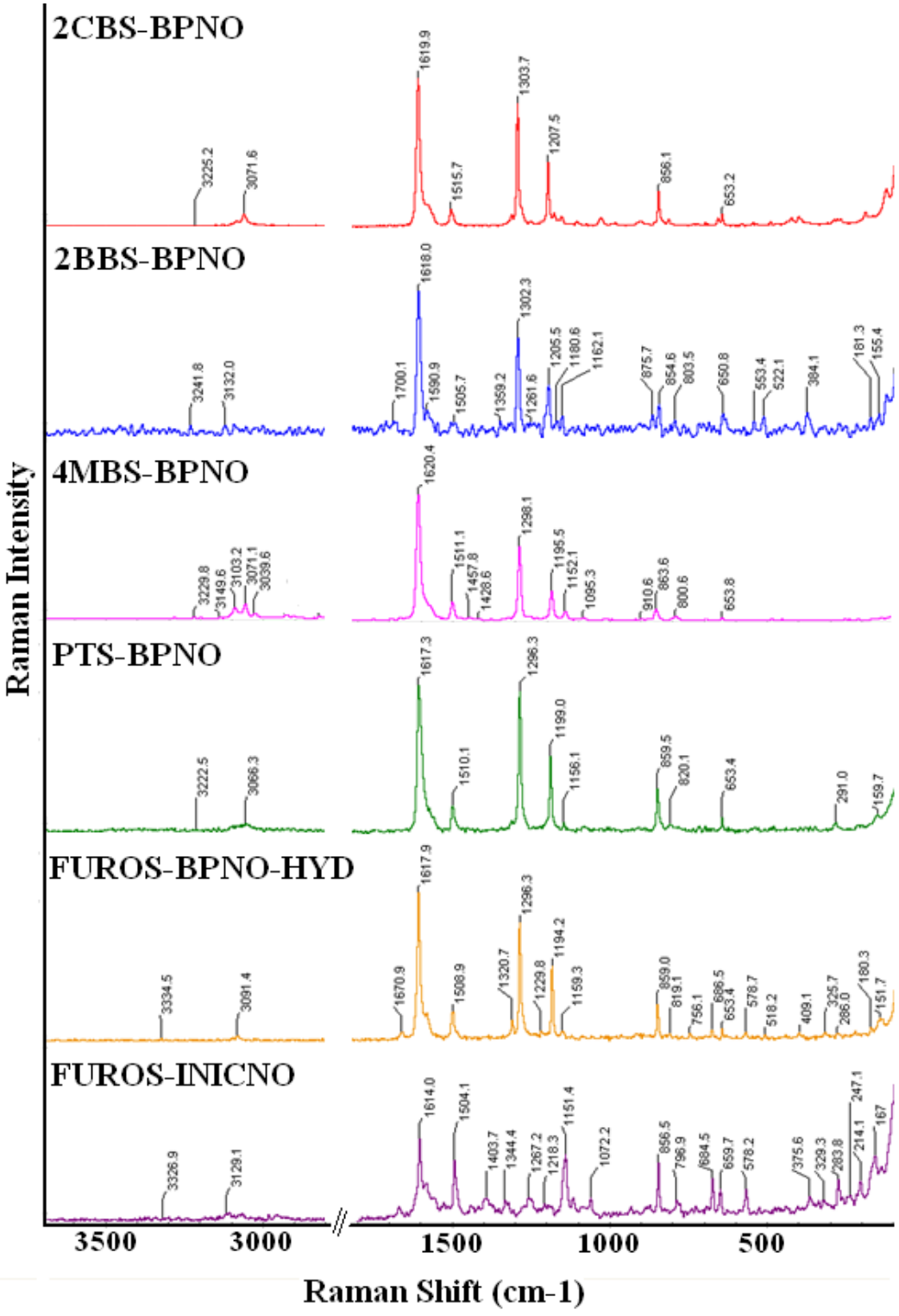

Figure 2.9 Raman spectra of Sulfonamide-*N*-oxide cocrystals.

Table 2.4 List of major IR and Raman stretching frequencies in the cocrystals and their individual components (in cm^{-1})

	Sulfonamide N–H stretch	N–H bending vibrations	S=O stretch
INFRARED			
CBS	3356.0, 3254.0	1572.8	1337.7, 1157.7
CBS–BPNO	3332.7, 3240.3	1572.7	1329.9, 1151.4
BBS	3364.3, 3261.0	1565.9	1335.8, 1173.9
BBS–BPNO	3286.6, 3194.2	1575.8	1331.7, 1161.3
MBS	3347.2, 3270.1	1598.5,1574.2	1309.7, 1157.2
MBS–BPNO	3297.2	1599.3,1578.0	1331.6, 1153.6
PTS	3325.7, 3243.0	1596.7, 1575.8	1325.8, 1151.6
PTS–BPNO	3290.0, 3238.1	1593.2	1327.3, 1152.4
FUROS	3400.0, 3351.0	1592.8,1565.3	1324.0,1143.2
FUROS–BPNO HYD	3392.7, 3326.0	1594.8,1565.7	1335.3,1162.2
INICNO	---	1547.8,1497.4	---
FUROS–INICNO	3390.2, 3316.1	1597.1, 1561.1	1343.5, 1161.5
RAMAN			
CBS	3256.9	1579.0	1330.6, 1163.9
CBS–BPNO	3225.2	1515.7	1303.7, 1163.1
BBS	3263.4	1575.5	1328.9, 1163.6
BBS–BPNO	3241.8	1505.7	1359.2, 1162.1
MBS	3251.8	1592.8	1303.4, 1137.8
MBS–BPNO	3228.3	1510.2	1322.3
PTS	3238.5	1596.3	1305.3, 1183.7
PTS–BPNO	3222.5	1510.2	1296.3, 1199.0
FUROS	3351.6	1597.5	1340.1, 1147.8
FUROS–BPNO HYD	3334.5	1508.9	1320.7, 1159.3
INICNO		1500.2	
FUROS–INICNO	3326.9	1504.1	1344.4, 1151.4

2.8 Thermal Analysis and Powder X-ray diffraction

Differential scanning calorimetry (DSC) and Thermo gravimetric analyses (TGA) were used to characterize the thermal behavior of sulfonamide-*N*-oxide cocrystals. DSC experiments showed a unique melting endotherm followed by decomposition (Figure 2.10). While the decomposition of BPNO coformer is responsible for the exotherm in its cocrystals with 2CBS, 2BBS, 4MBS and PTS molecules, the uncommon melting followed by

decomposition behavior of FUROS cocrystals is primarily due to the decomposition of furosemide to Chlorosulfamoylanthranilic acid and other by products[31] (Scheme 2.4). The endotherm due to the water loss in FUROS-BPNO-0.25 HYD could not be observed in DSC, nevertheless TGA analysis of this sample showed 0.85% water loss corresponding to the quarter water molecule (Figure 2.11). PXRD analysis of cocrystals overlayed with their calculated patterns showed excellent match indicating bulk phase purity (Figure 2.12)

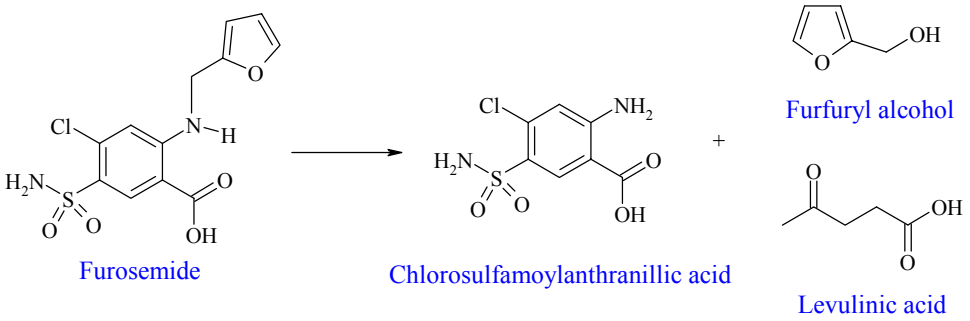

Scheme 2.4 Thermal degradation products of furosemide

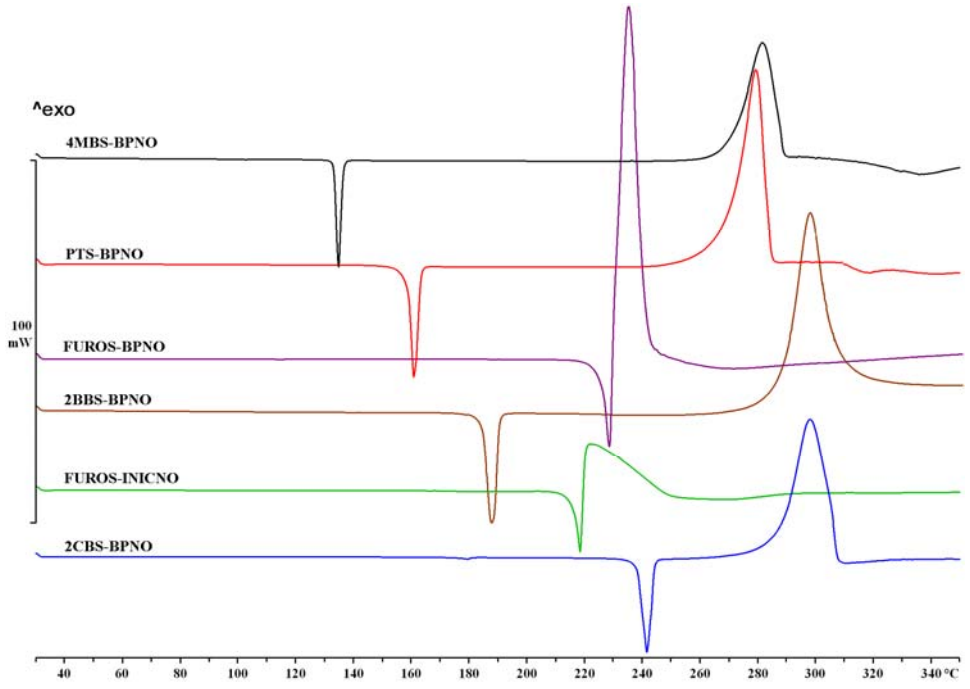

Figure 2.10 DSC heating curves of sulfonamide-*N*-oxide cocrystals

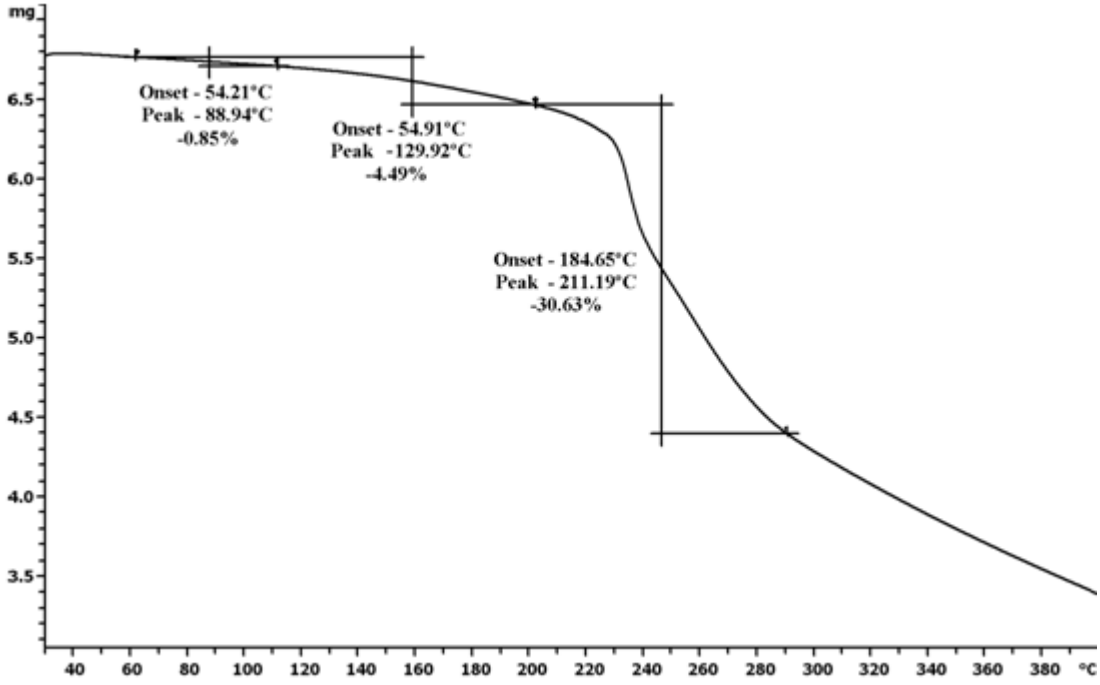

Figure 2.11 TGA curve of FUROS–BPNO–0.25H_2O. The weight loss of 0.85% between 60-90 °C accounts for the loss of ¼ water molecule. The major decomposition of cocrystal components occur between 120-300 °C.

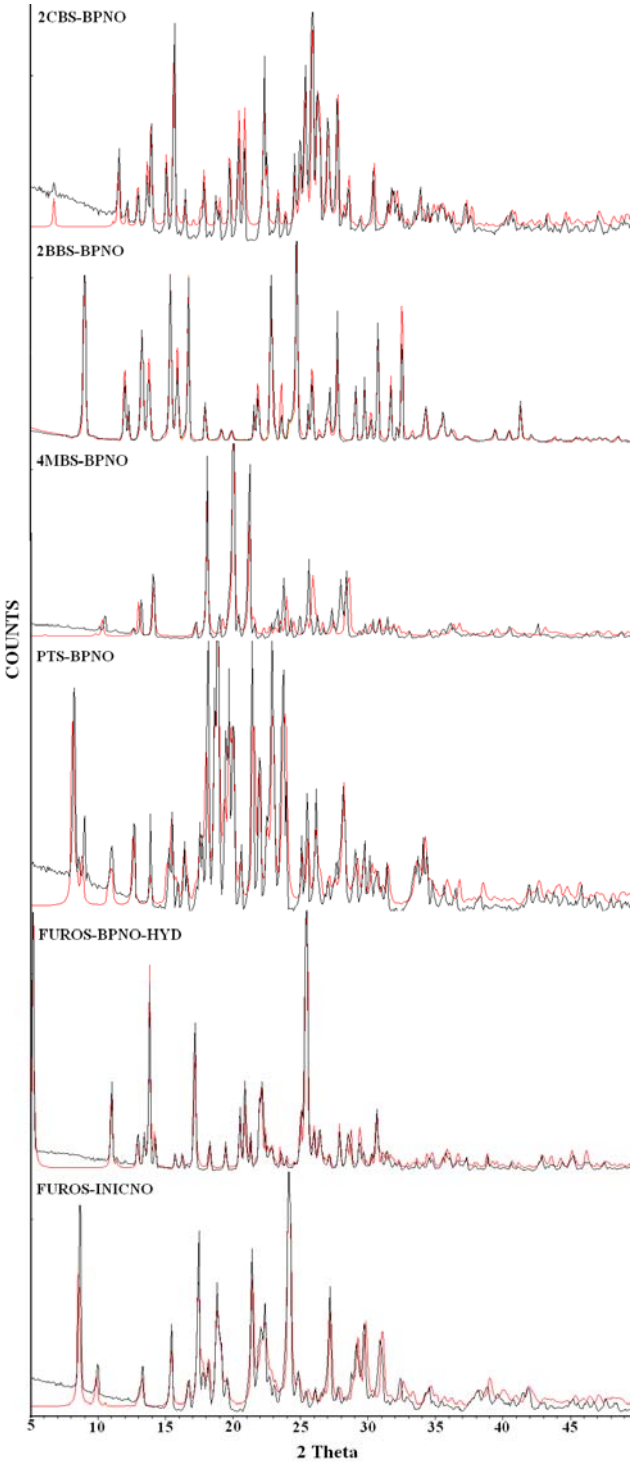

Figure 2.12 PXRD patterns of sulfonamide-pyridine-*N*-oxide cocrystals.

2.9 Discussion

The formation of the sulfonamide–pyridine-*N*-oxide heterosynthon appears to be very reliable due to the enhanced hydrogen bond donor and acceptor ability of the sulfonamide N-H and *N*-oxide, respectively. The formation of the dominant N–H···O_{Noxide} hydrogen bond in the crystal structure is based on the strongest donor (sulfonamide N-H) interacting with the strongest acceptor (*N*-oxide)[29]. The exact geometry of the sulfonamide motif, i.e. discrete N–H···O (D), cyclic motifs $R^2_4(8)$ or $R^2_2(4)$ (scheme 2.5) varies from one structure to another and it is difficult to anticipate their presence in a particular structure. Surprisingly, the two-point N–H···O + C–H···O heterosynthon of $R^2_2(8)$ geometry, similar to the carboxamide–pyridine-*N*-oxide heterosynthon was not observed in any structure. The non-planarity of the SO_2NH_2 group compared to the planar $CONH_2$ perhaps prevents the formation of two-point motif with an aromatic partner group. Whereas the six heavy atoms in the SO_2NH_2 dimer adopt various non planar arrangements resembling the chair conformation of cyclohexane, the arrangement is planar in the carboxamide amide dimer.

Even though a dominant sulfonamide–pyridine-*N*-oxide motif could not be identified in this subset of cocrystal structures, it is clear that bimolecular recognition can be reproducibly mediated between molecules (say drug and coformer) containing these two functional groups via a N–H···O_{Noxide} hydrogen bond or ring motif. A second preliminary observation is the lack of polymorphism in the cocrystals studied compared to relatively promiscuous multiple forms in some sulfonamides studied by us recently[32], and for sulfa drugs in general[20]. The newly identified sulfonamide–*N*-oxide heterosynthon is further illustrated with the cocrystals of loop diuretic Furosemide[33]. The recurring sulfonamide N–H···O $R^2_2(8)$ dimer in three polymorphs of this drug[34] is present in the hydrate with BPNO. The anti N-H makes an $R^2_2(4)$ ring motif with the *N*-oxide. The situation in FUROS–INICNO cocrystal is quite predictable; the strongest SO_2NH_2 donor bonds to the *N*-oxide acceptor and the COOH and $CONH_2$ groups of the drug and coformer make the acid–amide heterosynthon at the next level of hierarchy.

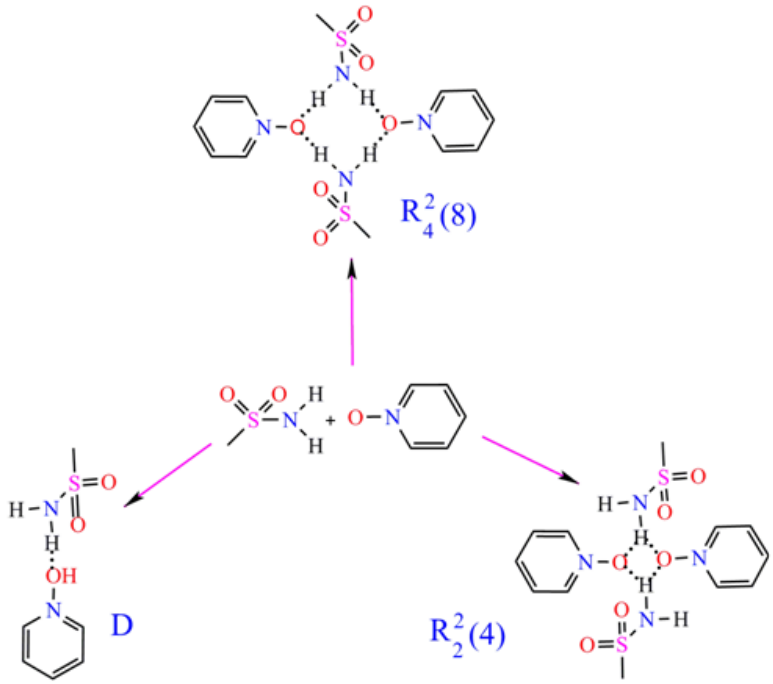

Scheme 2.5 Different motifs observed in the sulfonamide-*N*-oxide cocrystals.

2.10 Application of sulfonamide-*N*-oxide heterosynthon in preparing Drug-Drug Cocrystals

Discovering a novel heterosynthon for any functional group is highly essential since the resulting cocrystals may have wider applications ranging from pharmaceutical to materials chemistry. The novel heterosynthon described in this chapter may be used to form cocrystals of sulfonamide drugs with *N*-oxide containing coformers. Although GRAS listed *N*-oxide coformers are extremely rare, this heterosynthon finds important application in forming drug-drug cocrystals. Numerous literature reports highlight the importance of *N*-oxide compounds for anti-HIV and anti-cancer treatment[35]. For example, JPL-71 and its derivatives were shown to have significant growth inhibition effects on the cell lines of HIV strains. Likewise, Tirapazamine is an experimental anti-cancer *N*-oxide drug with promising activity against neck, head and gynecological cancer. *N*-oxides are also recognized as

important Phosphodiesterase IV inhibitors. Roflumilast *N*-oxide is a selective and long acting inhibitor of the enzyme Phosphodiesterase IV.

HIV and Cancer affected patients often suffer from additional health problems. These diseases invariably weaken the nervous, respiratory and immune systems. As a result different parts of the body become highly prone to bacterial, viral and fungal infections. This necessitates additional medication in the form of antibacterial, dermatological, antidiuretic, anticonvulsant drugs apart from the anti-HIV or anti-cancer drugs. Many of the sulfonamide drugs cater to these secondary infections. For example, Sulfadiazine acts as an antibacterial, Mafenide is a dermatological, Furosemide, a diuretic and Zonisamide an anticonvulsant. Using the heterosynthon highlighted in this chapter, drug cocrystals between *N*-oxide and sulfonamide drugs can be prepared. Just as insertion of a GRAS coformer into the crystal lattice of a drug molecule modulates its solubility and overcomes hydration problems[3, 12a, 36], cocrystallization of two drug molecules may result in 'Drug Synergy'[37]. It allows a therapeutic effect to be achieved with lower doses of component drugs. Alternatively, 'Promiscuous synergy' may arise when one of the component drugs non-specifically influence the physicochemical properties of other drug for example by increasing its bioavailability. These beneficial effects may positively influence the drug-patient compatibility and therapeutic efficacy of individual drug components (Scheme 2.6).

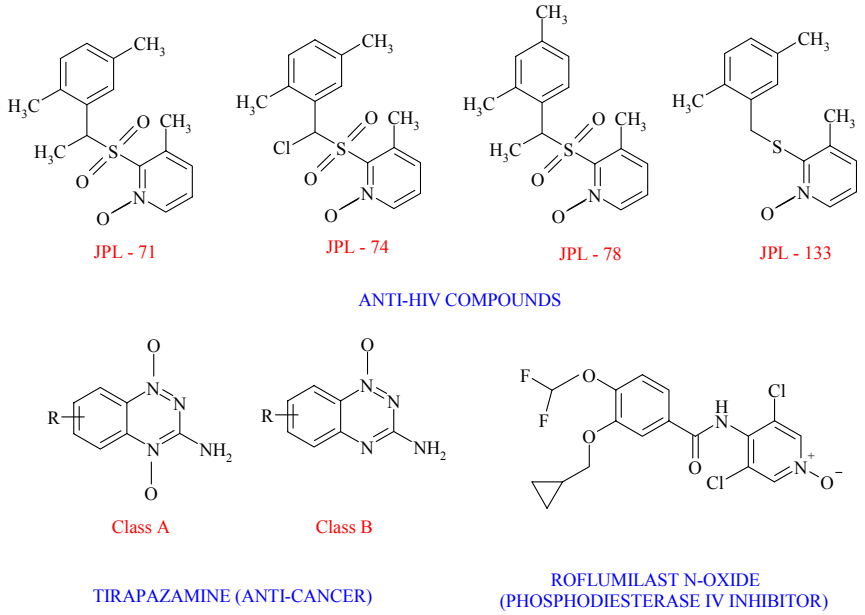

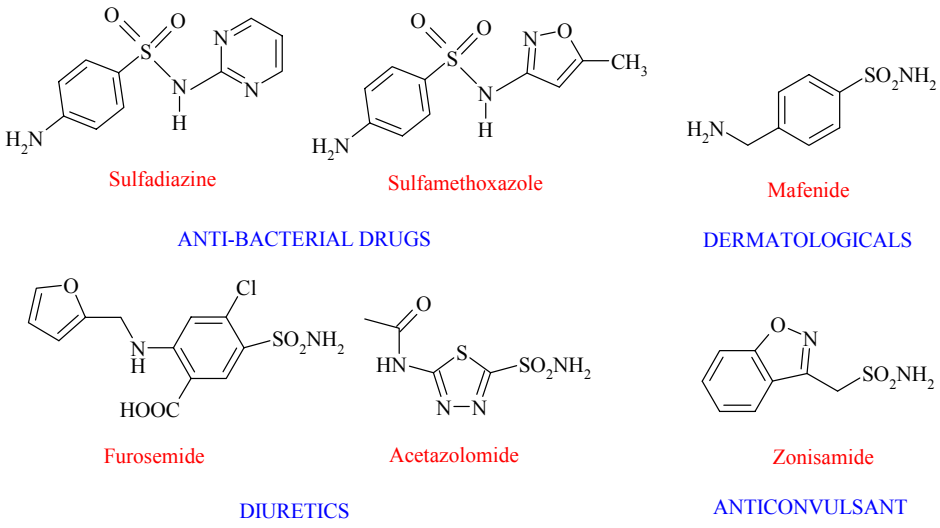

Scheme 2.6 List of *N*-oxide and sulfonamide drugs catering to various infections and diseases.

2.11 Conclusions

The ability of aromatic primary sulfonamides to make a strong hydrogen bond with pyridine-*N*-oxide molecules is demonstrated for the first time using various model compounds. The application of this synthon in preparing solid forms of APIs is demonstrated through cocrystals of a loop diuretic drug Furosemide. Inspite of the presence of variable synthon motifs in the cocrystals, the recurring N–H···O_{Noxide} motif is the stable binding interaction in all the cocrystals. The scope of this model study will be easily extendable to prepare pharmaceutical solids. The fact that pyridine-*N*-oxide functional group is present in some anti-HIV and anti-cancer drug molecules and discovery candidates, cocrystallizing them with sulfonamide drug molecules can form drug-drug cocrystals. They may synergistically influence each other in minimizing individual dose levels and enhance their therapeutic efficacy.

2.12 Experimental Section

Materials and methods Furosemide was extracted from commercial Lasix tablets using methanol solvent. NMR, IR and PXRD confirmed purity of the compound. Coformers (purity > 99.8%) were purchased from Sigma-Aldrich (Hyderabad, India). Solvents (purity > 99%) were purchased from Hychem Laboratories (Hyderabad, India).

Preparation of *N*-oxide 4,4′-bipyridine (1mmol, 156.19mg) was dissolved in Ethyl acetate solvent by stirring at room temperature. To this solution at room temperature m-chloroperoxybenzoicacid (2mmol, 345.14mg) solution in Ethyl acetate was added slowly and continued stirring. Pale white precipitate of 4,4′-bipyridine-*N,N'*-dioxide started appearing after about 20 mins. The whole reaction was complete in about 3hrs. Yield: > 95%. The precipitate was filtered, purity confirmed using NMR, IR and DSC and used for further experiments. Similar procedure was used to prepare Nicotinamide-*N*-oxide but only 1mmol of m-chloroperoxybenzoicacid was used in this case.

Cocrystal Preparation Broadly, three methods were adopted: (1) the components were dissolved in a suitable solvent and crystallization of new phases was examined (2) the components were manually ground with a few drops of solvent added, and then the material was dissolved in a solvent for single crystals to appear. (3) Stoichiometric amounts of the components were added to a minimum of appropriate solvent in a round bottom flask so as to make a supersaturated solution. This slurry was stirred for about 24 hrs to obtain cocrystal. A full list of experiments, various conditions employed and the results obtained for the cocrystals mentioned herein are shown in Table 2.5.

Table 2.5 Summary of Experimental conditions and Results

Experimental conditions	Product obtained
2-CBS-BPNO (1:1)	
MeOH, 4 mL, Room temp. (RT), Solution Crystallization (SC)	No cocrystal observed
EtOH, 4 mL, RT, SC	No cocrystal observed
i-PrOH, 4 mL, RT, SC	BPNO hydrate
n-PrOH, 4 mL, RT, SC	1:1 cocrystal after 4-5 d

1:1 Ratio, Slurry grinding (SG), CH3CN+n-ProH	powdery material of Cocrystal after 24hrs
2-BBS-BPNO (1:0.5)	
MeOH, RT, 3 mL, SC	No cocrystal observed
EtOH, RT, 4 mL, SC	1:0.5 cocrystal after 2-3 d
n-PrOH, RT, 4mL, SC	BPNO hydrate
DMF, RT, 3 mL, SC	No cocrystal observed
1:0.5 Ratio, SG, n-ProH	powdery material of Cocrystal after 24hrs
4-MBS-BPNO (1:0.5)	
MeOH, RT, 4mL, SC	BPNO hydrate
EtOH, RT, 4 mL, SC	4-MBS crystals
i-PrOH, RT, 5 mL, SC	4-MBS crystals
n-PrOH, RT, 4 mL, SC	1:0.5 cocrystal after 4-5 d
DMF, RT, 3ml,SC	No cocrystal observed
DMSO, RT, 3ml, SC	No cocrystal observed
1:0.5 Ratio, SG, i-BuOH	powdery material of Cocrystal after 24hrs
PTS-BPNO (2:1)	
MeOH, 5 mL, RT, SC	No cocrystal observed
EtOH, 5 mL, RT, SC	No cocrystal observed
n-PrOH, 4 mL, RT, SC	PTS
i-buOH, 7 mL, RT, SC	2:1 cocrystal after 4-5 d
1:0.5 Ratio, SG, i-BuOH	powdery material of Cocrystal after 24hrs
FUROS-BPNO-HYD(1:0.5:0.25)	
MeOH, 9 mL, RT, SC	FUROS Form 1
Abs. EtOH, 6mL, RT, SC	BPNO hydrate
4-5 drops CH_3CN, Liquid assisted grinding (LAG) MeOH, 9 mL, RT, SC	1:1:0.25 hydrate after 4 d
4-5 drops CH_3CN, LAG EtOH, 6 mL, SC, RT	FUROS Form 1
4-5 drops CH_3CN, LAG i-PrOH , 6 mL, RT, SC	No cocrystal observed
4-5 drops CH_3CN, LAG n-PrOH, 6 mL, RT, SC	FUROS Form 1
FUROS-INICNO (1:1)	
4-5 drops CH_3CN, LAG MeOH, 6 mL, RT, SC	No cocrystal observed
4-5 drops CH_3CN, LAG EtOH, 6 mL, RT, SC	1:1 cocrystal after 4 d
4-5drops CH_3CN, LAG n-PrOH, 5 mL, RT, SC	No cocrystal observed
4-5 drops CH_3CN, LAG i-PrOH, 6 mL, RT, SC	No cocrystal observed
4-5 drops CH_3CN, LAG i-BuOH, 6 mL, RT, SC	No cocrystal observed

X-ray Crystallography Reflections were collected on a Bruker SMART APEX-CCD diffractometer. Mo-Kα (λ = 0.71073Å) radiation was used to collect X-ray reflections on the single crystal. Data reduction was performed using Bruker SAINT software.[38] Intensities for absorption were corrected using SADABS.[39] RLATT3 and CELL_NOW programs[40] were used to generate a new reindexed cell for the structure MBS–BPNO, which was used during initialization and merging of raw data. Crystal structures were solved by direct methods and refined on F^2 with SHELXS-97 and SHELXL-97 programs[41] to give satisfactory *R* factor. Hydrogen atoms on O and N were experimentally located in difference electron density maps. All C–H atoms were fixed geometrically using HFIX command in SHELX-TL. In the modeled structure FUROS–INICNO the disorder was modeled for all the heavy atoms with isotropic displacement parameters using the PART command by assigning s.o.f. (site occupancy factor) of 0.5 and 0.5 for the two parts using the FVAR command. A check of the final CIF file using PLATON[42] did not show any missed symmetry. X-Seed[43] was used to prepare packing diagrams.

Powder X-ray Diffraction Powder X-ray diffraction of the samples were recorded on Bruker D8 Advance diffractometer using Cu-Kα X-radiation (λ = 1.5406Å) at 40 kV and 30 mA. Diffraction patterns were collected over 2θ range of 5-50° at scan rate of 1° min^{-1}. Powder Cell 2.4[44] was used for Rietveld refinement.

Vibrational Spectroscopy Nicolet 6700 FT-IR spectrometer with a NXR FT-Raman and NIR Module was used to record IR and Raman spectra. IR spectra were recorded on samples dispersed in KBr pellets. Raman spectra were recorded on samples contained in standard NMR diameter tubes or on compressed samples contained in a gold-coated sample holder.

Thermal Analysis DSC was performed on a Mettler Toledo DSC 822e module and TGA on a Mettler Toledo TGA/SDTA 851e module. The typical sample size is 3-5 mg for DSC and 8-12 mg for TGA. Samples were placed in sealed pin-pricked aluminum pans for DSC experiments and alumina pans for TGA experiments. A heating rate of 5 °C min^{-1} in the temperature range 30-400 °C was applied. Samples were purged by a stream of dry nitrogen flowing at 80 mL min^{-1} for DSC and 50 mL min^{-1} for TGA.

2.13 References

1. F. Wöhler, *Annalen Chemie Pharmacie,* 1844, **51**, 145-163.
2. (a) A. D. Bond, *CrystEngComm*, 2007, **9**, 833-834. (b) G. R. Desiraju, *CrystEngComm*, 2003, 5, 466-467. (c) A. parkin, C. J. Gilmore and C. C. Wilson, *Zeitschrift für Kristallographie,* 2008, **223**, 430.
3. (a) N. Shan and M. J. Zaworotko, *Drug Discov. Today,* 2008, **13**, 440-446. (b) N. Schultheiss and A. Newman, *Cryst. Growth Des*., 2009, **9**, 2950-2967. (c) N. J. Babu and A. Nangia, *Cryst. Growth Des*., 2011, **11**, 2662-2679.
4. (a) G. R. Desiraju, *Angew. Chem. Int. Ed. Engl.,* 1995, **34**, 2311-2327. (b) C. B. Aakeröy, *Acta Crystallogr. Sect. B,* 1997, **53**, 569-586. (c) B. Moulton and M. Zaworotko, *Chem. Rev*., 2001, **101**, 1629-1658.
5. (a) G. R. Desiraju, *Crystal Engineering: The Design of Organic Solids*, Elsevier, Amsterdam, 1989; (b) G. R. Desiraju, *J. Chem. Sci*., 2010, **122**, 667. (c) G. R. Desiraju, J. J. Vittal and A. Ramanan, *Crystal Engineering. A Textbook,* World Scientific Publishing, Singapore, 2011.
6. (a) M. C. Etter, *Acc. Chem. Res*., 1990, **23**, 120-126. (b) M. C. Etter, *J. Phys. Chem.*, 1990, **23**, 120-126.
7. T. Steiner, *Acta Crystallogr sect. B.,* 2001, **57**, 103.
8. (a) P. Vishweshwar, A. Nangia and V. M. Lynch, *J.Org. Chem*., 2002, **67**, 556-565. (b) T. R. Shattock, K. K. Arora, P. Vishweshwar and M. J. Zaworotko, *Cryst. Growth Des*., 2008, **8**, 4533-4545. (c) R. Santra, N. Ghosh and K. Biradha, *New J. Chem*., 2008, **32**, 1673-1676.
9. (a) B. R. Bhogala, S. Basavoju and A. Nangia, *CrystEngComm,* 2005, **7**, 551. (b) B. R. Bhogala, S. Basavoju and A. Nangia, *Cryst. Growth Des*., 2005, **5**, 1683. (c) B. R. Bhogala and A. Nangia, *Cryst. Growth Des.,* 2003, **3**, 547.
10. (a) C. B. Aakeröy and D. J. Salmon, *CrystEngComm,* 2005, **7**, 439. (b) C. B. Aakeröy, A. M. Beatty and B. A. Helfrich, *J. Am. Chem. Soc.,* 2002, **124**, 14425. (c) C. B. Aakeröy, A. M. Beatty and B. A. Helfrich, *Angew. Chem., Int. Ed.,* 2001, **40**, 3240.
11. (a) R. D. B. Walsh, M. W. Bradner, S. Fleishman, L. A. Morales, B. Moulton, N. Rodríguez-Hornedo and M. J. Zaworotko, *Chem. Commun.,* 2003, 186. (b) P.

Vishweshwar, J. A. McMahon and M. J. Zaworotko, in *Frontiers in Crystal Engineering*, E. R. T. Tiekink and J. J. Vittal, Eds., Wiley, Chichester, 2006, pp. 25-49. (c) Ö. Almarsson and M. J. Zaworotko, *Chem. Commun,* 2004, 1889. (d) S. G. Fleischman, S. S. Kuduva, J. A. McMahon, B. Moulton, R. D. B. Walsh, N. Rodríguez-Hornendo and M. J. Zaworotko, *Cryst. Growth Des.,* 2003, **3**, 909.

12. (a) A. V. Trask, W. D. S. Motherwell and W. Jones, *Cryst. Growth Des.,* 2005, **5**, 1013. (b) A. J. C Cabeza, G. M. Day, W. D. S. Motherwell and W. Jones, *J. Am. Chem. Soc.,* 2006, **128**, 14466. (c) A.V. Trask and W. Jones, *Top. Curr. Chem.,* 2005, **254**, 41. (d) A. Trask, W. D. S. Motherwell and W. Jones, *Int. J. Pharm*., 2006, **320**, 114. (e) A. Trask, W. D. S. Motherwell and W. Jones, *Cryst. Growth Des.,* 2005, **5**, 1013.
13. C. B. Aakeröy, S. Panikkattu, P. D. Chopade and J. Desper, *CrystEngComm*, 2013, **15**, 3125-3136.
14. J. N. Moorthy, R. Natarajan, P. Mal and P. Venugopalan, *J. Am. Chem. Soc.,* 2002, **124**, 6530-6531.
15. J. A. Bis, P. Vishweshwar, D. Weyna, and M. J. Zaworotko, *Mol. Pharmaceutics,* 2007, **4**, 401-416.
16. B. Sarma, N. K. Nath, B. R. Bhogala and A. Nangia, *Cryst. Growth Des*., 2009, **9**, 1546-1557.
17. S. J. Brooks, P A. Gale and M. E. Light, *CrystEngComm*, 2005, **7**, 586-591.
18. N. Brondel, E. J. A. Moynihan, K. N. Lehane, K. S. Eccles, C. J. Elcoate, S. J. Coles, S. E. Lawrence and A. R. Maguire, *CrystEngComm*, 2010, **12**, 2910-2927.
19. (a) S. S. Yang and J. K. Guillory, *J. Pharm. Sci.,* 1972, **61**, 26. (b) S. K. Ko, J. H. Jin, D. W. Jung, X. Tian and I. Shin, *Angew. Chem., Int. Ed.,* 2009, **48**, 7809. (c) M. R. Caira, *Mol. Pharmaceutics*, 2007, **4**, 310. (d) S. R Byrn, R. R Pfeiffer and J. G. Stowell, *Solid-State Chemistry of Drugs*; SSCI, Inc.: West Lafayette, IN, 1999, 160.
20. (a) T. Ishida, Y. In, M. Doi, M. Inoue and I. Yanagisawa, *Acta Crystallogr. Sect. B,* 1989, **45**, 505. (b) J. M. Leger, S. Alberola and A. Carpy, *Acta Crystallogr. Sect. B,* 1977, **33**, 3337. (c) M. R. Caira, *J. Chem. Crystallogr.* 1994, **24**, 695. (d) M. R. Caira, L. R. Nassimbeni, and A. F. Wilderwanck, *J. Chem. Soc. Perkin Trans.* 1995,

2, 2213. (e) S. Alberola, F. Sabon, J. Jaud, and J. Galy, *Acta Crystallogr. Sect. B,* 1977, **33**, 3337. (f) M. R. Caira, *J. Crystallogr. Spectrosc. Res.* 1992, **22**, 193.

21. (a) L. S. Reddy, N. J. Babu and A. Nangia, *Chem Commun*, 2006, 1369. (b) N. J. Babu, L. S. Reddy and A. Nangia, *Mol. Pharmaceutics*, 2007, **4**, 417. (c) N. J. Babu, L. S. Reddy, S. Aitipamula and A. Nangia, *Chem. – An Asian J.,* 2008, **3**, 1122.
22. (a) L. S. Reddy, S. Basavoju, V. R. Vangala, and A. Nangia, *Cryst. Growth Des*., 2006, **6**, 161. (b) V. Videnova-Adrabińska and E. Janeczko, *Chem. Commun*, 1999, 1527. (c) R. Custelcean, B. A. Moyer, V. S. Bryantsev and B. P. Hay, *Cryst. Growth Des.*, 2006*,* **6***,* 555. (d) R. Custelcean, *Chem. Commun*, 2008, 295.
23. Cambridge Crystallographic Data Center, Cambridge, UK, www.ccdc.cam.ac.uk.
24. (a) N. Shan, F. Toda and W. Jones, *Chem Commun,* 2002, 2372. (b) A. V. Trask, W. D. S. Motherwell and W. Jones, *Chem Commun,* 2004, 890. (c) T. Friščić, A. V. Trask, W. Jones and W. D. S. Motherwell, *Angew. Chem., Int. Ed*., 2006, **45**, 7546.
25. (a) P. P. Bag, M. Patni and C. M. Reddy, *CrystEngComm*, 2011, **13**, 5650.
26. L. S. Reddy, P. Bhatt, R. Banerjee, A. Nangia and G. J. Kruger, *Chem. Asian J.* 2007, **2**, 505.
27. (a) D. J. Berry, C. C. Seaton, W. Clegg, R. W. Harrington, S. J. Coles, P. N. Horton, M. B. Hursthouse, R. Storey, W. Jones, T. Friščić and N. Blagden, *Cryst. Growth Des.,* 2008, **8**, 1697. (b) G. Bettinetti, M. R. Caira, A. Callegari, M. Merli, M. Sorrenti and C. Tadini, *J. Pharm. Sci*., 2000, **89**, 478.
28. (a) B. K. Saha, A. Nangia and M. Jaskólski, *CrystEngComm,* 2005*,* **7***,* 355. (b) R. Thaimattam, C. V. K. Sharma, A. Clearfield and G. R. Desiraju, *Cryst. Growth Des.* 2001, **1**, 103.
29. (a) M. C. Etter, J. C. Macdonald and J. Bernstein, *Acta Crystallogr. Sect. B,* 1990, **46**, 256. (b) M. C. Etter and S. M. Reutzel, J. *Am. Chem. Soc*., 1991, **113**, 2586. (c) J. Bernstein, R. E. Davis, L. Shimoni and N. L. Chang, *Angew. Chem., Int. Ed. Engl*., 1995, **34**, 1555.
30. (a) R. Feher, K. Wurst, D. B. Amabilino and J. Veciana, *Inorg. Chimi. Acta*, 2008, **361**, 4094-4099. (b) R. Feher, K. Wurst, D. B. Amabilino and J. Veciana, *Mol. Cryst. Liq. Cryst.,* 1999, **334**, 333.

31. H. Beyers, S. F. Malan, J. G. Van der Watt and M. M. de Villiers, *Drug Dev. Ind. Pharm.*, 2000, **26**, 1077-1083.
32. P. Sanphui, B. Sarma and A. Nangia, *Cryst. Growth Des.,* 2010, **10**, 4550.
33. (a) P. A. Friedman, W. O. Berndt, In *Modern Pharmacology with Clinical Applications*; 5th ed., C. R Craig, R. E. Stitzel, Eds.; Little Brown & Company: Boston, 1997, pp 239-255. (b) M. G. Khan, *Encyclopedia of Heart Diseases*; Elsevier: New York, 2006.
34. N. J. Babu, S. Cherukuvada, R. Thakuria and A. Nangia, *Cryst. Growth Des.,* 2010, **10**, 1979.
35. (a) S. Feng, M. Yang, Z. Zhang, Z. Wang, D. Hong, H. Richter, G. M. Benson, B. Bleicher, U. Grether, R. E. Martin, J.-M. Plancher, B. Kuhn, M. G. Rudolph and L. Chen, *Biorg. Med. Chem. Lett.,* 2009, **19**, 2595. (b) S. R. McKeown, M. V. Hejmadi, I. A. McIntyre, J. J. McAleer and L. H. Patterson, *Br. J. Cancer*., 1995, **72**, 76. (c) C. R. Nishida, M. Lee, P. R. Ortiz de Montellano, *Mol. Pharmacol.*, 2010, **78**, 497.
36. S. Cherukuvada, N. J. Babu and A. Nangia, *J. Pharm. Sci.,* 2011, **100**, 3233.
37. (a) R. J. Thallarida, *J. Pharm. Exp. Ther.,* 2001, **298**, 865. (b) S. Ramón Garcia, C. Ng, H. Anderson, J. D. Chao, X. Zheng, T. Pfeifer, Y. Av-Gay, M. Roberge and C. J. Thompson, *Antimicrob. Agents Chemother.,* 2011, **55**, 3861.
38. *SAINT-Plus*, version 6.45; Bruker AXS Inc.: Madison, WI, 2003.
39. G. M. Sheldrick, *SADABS*, Program for Empirical Absorption Correction of Area Detector Data, University of Göttingen, Germany, 1997.
40. (a) *RLATT*, Reciprocal Lattice Viewer, Version 3.0, Bruker-AXS, 2000. (b) G. M. Sheldrick, *CELL_NOW*; University of Göttingen, Germany, 2004.
41. (a) *SMART (Version 5.625) and SHELX-TL (Version 6.12)*; Bruker-AXS Inc.: Madison, WI, 2000. (b) G. M. Sheldrick, *SHELXS-97and SHELXL-97*; University of Göttingen, Germany, 1997.
42. (a) A. L. Spek, PLATON, *A Multipurpose Crystallographic Tool*; Utrecht University: Utrecht, Netherland, 2002.
43. L. J. Barbour, *Supramol. Chem*., 2001, **1,** 189.
44. Powder Cell, a program for structure visualization, powder pattern calculation and profile fitting. http://www.ccp14.ac.uk/tutorial/powdcell/

CHAPTER THREE

SOLUBILITY AND STABILITY ADVANTAGE OF ACECLOFENAC SALTS

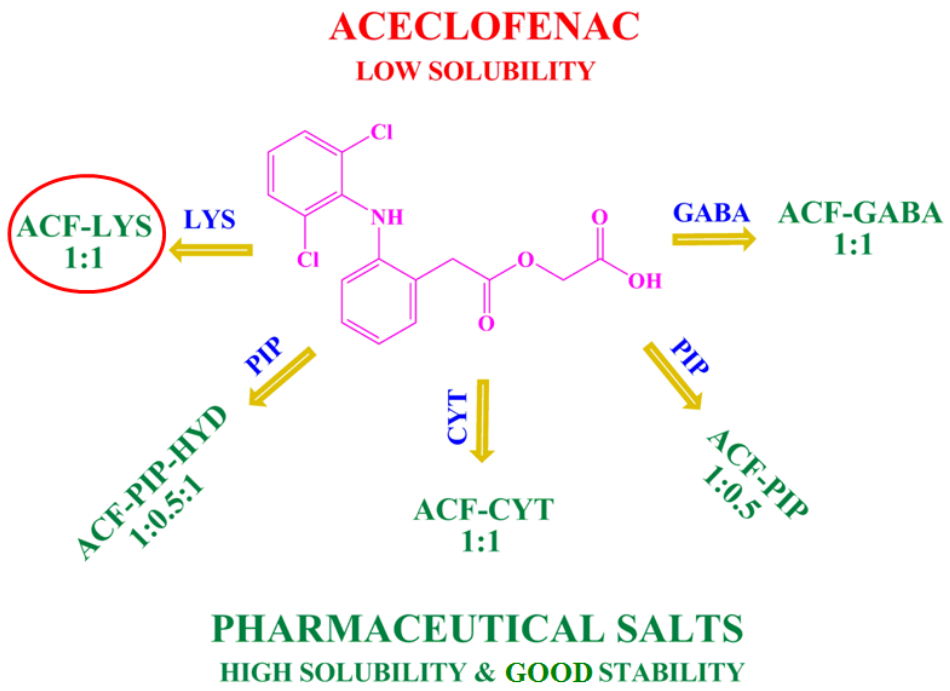

Solubility of Aceclofenac was improved by forming crystalline salts with mild basic coformers. The Aceclofenac-L-lysine salt is stable in accelerated ICH conditions of 40 °C, 75% RH for over 8 months and exhibited 156 times higher solubility, 135 fold faster dissolution rate compared to the parent drug.

3.1 Introduction

The discovery of biologically active molecules and their development as active pharmaceutical ingredients (API's) is a driver for the innovation of novel drugs and pharmaceuticals[1]. Even as high-throughput screening and combinatorial chemistry[2] has increased the number of new chemical entities (NCE's) many-fold, often poor bioavailability of these potential drug candidates poses a major hindrance in formulating them as API's. According to Serajuddin and coworkers[3], while NCE solubility of <20 μg/mL was practically unheard of until 1980s, the situation has changed completely in the current times with solubility of drug molecules lower than 1 μg/mL becoming commonplace. Therefore solid state modification of new chemical entities or existing drug molecules with an intention of developing marketable dosage forms has received greater attention in the current period than ever before. Since a better shelf life is intended, the marketable dosage form must strike a balance between high solubility and good stability[4]. Yet, development of the optimal oral dosage form should not affect the basic skeleton of the drug molecule since such a change will alter the molecular structure and the mode of binding at the site of drug action[5]. Hence, even as the discovery of lead molecules is an important step in drug development, optimization of their physicochemical parameters is a major bottleneck in developing them as active pharmaceutical ingredients, heightened in the era of patent cliffs[6].

Salt formation represents the traditional methodology for solid form development with diverse applications in pharmaceutical industry[3b,7]. Reddy et. al.[8] has reported the improvement in compaction properties of Acetaminophen by making a hydrochloride salt hydrate (A.HCl) of this molecule. They have noted that A.HCl has higher plasticity compared to the marketed form 1. This novel salt could be tableted at appreciable strength even and higher pressure. Salts have been successfully applied as additives to discover metastable polymorphs of drug molecules. For example, Byrn and coworkers[9] reported the generation of metastable form V of Flufenamic Acid (FA) by dissolving FA in ammonium chloride (NH_4Cl) solution. This novel polymorph was obtained by slow evaporation method with FA and NH_4Cl in 1:2 stoichiometric ratio. Similarly several reports highlight the importance of ionic liquids (salt in liquid form) as media for discovering novel

polymorphs[9b,c,d]. For instance, An et. al.[9b] reported a novel polymorph of Adefovir dipivoxil (AD) crystallized form 1-ally-3-ethylimidazolium tetrafluoroborate ($AEImBF_4$) ionic liquid. Apart from these notable applications, salt formation is primarily used in the pharmaceutical industry for solubility modulation of drug molecules. The widespread use of salt formation for solubility enhancement of drug molecules is evidenced by about 50% of drug molecules marketed as salts. It is the most preferred approach for aqueous solubility enhancement of a liquid formulation for parenteral administration[10]. Numerous literature reports highlight this ability of salts through various criteria comprising solubility and stoichiometry of the counter ion, polymorphism etc. Nangia and coworkers[11] reported the improvement in the solubility of antipsychotic drug Olanzapine through mono and dimaleate salts. They have highlighted the importance of counter ion stoichiometry in varying the solubility of drug molecule. Galcera et. al.[12] noted the effect of counter ion on the solubility of isostructural pharmaceutical salts of anticonvulsant drug Lamotrigine. They showed that the solubility of the salts varied linearly with the solubility of corresponding counterions. The research group of Desiraju[13] reported the saccharinate salts of various Active pharmaceutical ingredients (API's) with improved solubility. They have highlighted the importance of saccharinate counter ion as an able salt former. Puigjaner and coworkers[14] documented the importance of screening for polymorphs of pharmaceutical salts and their effect on the solubility of parent molecule. They have reported three polymorphs of Ziprasidone maleate and showed that "form C" exhibited the highest solubility ever reported for Ziprasidone salts.

Zaworotko and coworkers[15] went a step further in studying the pharmacokinetic behavior of salts apart from their solubility. They have obtained various solid forms of anticonvulsant drug Lamotrigine (LT). Dissolution studies on these solid forms showed that LT-saccharinate salt (**5**) showed highest solubility in aqueous media at 0.45mg/mL followed by LT-nicotinamide cocrystal (**3**, 0.30mg/mL), pure LT (0.28mg/mL), LT-nicotinamide cocrystal hydrate (**4**, 0.23mg/mL) and LT-methyl paraben cocrystal form II (**2**, 0.21mg/mL) (Figure 3.1a). Pharmacokinetic studies were performed on **3, 4, 5** and pure LT in Sprague-Dawley rats over 24h time period to estimate their serum concentrations. Two hours after dosing the serum concentration of **5** was shown to be 3.5μg/mL which is 1.5 times higher than pure LT. The $AUC_{0\text{-}24h}$ for **3, 4, 5** and pure LT was found to be 37, 26, 66 and 60 μg

h/mL respectively (Figure 3.1b). Thus LT-saccharinate salt was shown to exhibit the highest initial serum concentration, the lowest T_{max} (time to reach maximum serum concentration) and highest $AUC_{0\text{-}24h}$. In Short the ability of salts in replicating the solubility advantage conferred by them during in vitro studies into improving the bioavailability of the parent drug during in vivo studies is highlighted here. Numerous other reports highlight this solubility modulating ability of salts[16] for solid form development and better therapeutic efficacy.

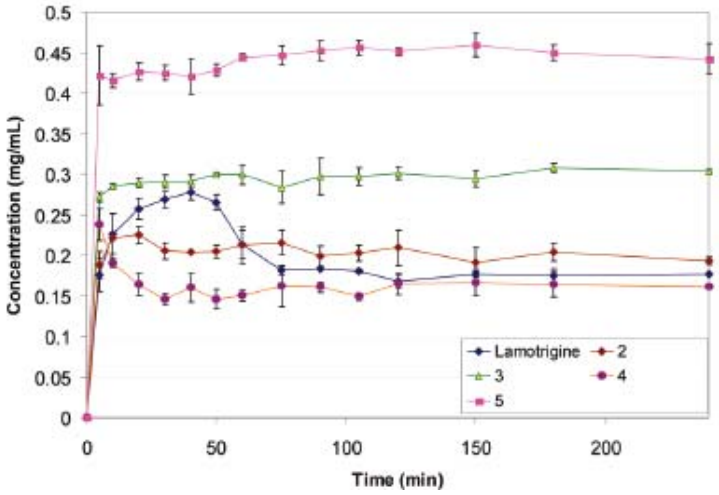

(a)

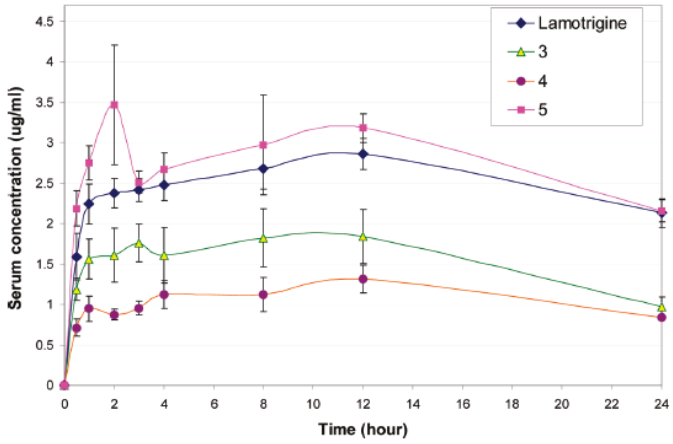

(b)

Figure 3.1a) Aqueous Dissolution profiles for LT and crystal forms 2-5. **b)** Rat serum concentrations of LT, **3, 4,** and **5.** (Adapted from ref.15).

3.2 Literature Reports on Aceclofenac

Aceclofenac (2-(2,6-dichlorophenylamine)phenylacetoxyacetic acid, ACF hereafter) is an orally effective non-steroidal anti-inflammatory drug (NSAID) with remarkable anti-inflammatory, analgesic and antipyretic properties[17]. It belongs to the class of phenyl acetic acid and was found to be the most tolerated drug among NSAIDs with a lower incidence of adverse gastrointestinal effects. It is a BCS class II drug with poor aqueous solubility of 58 μg/mL[18]. In literature attempts towards improving the solubility of ACF were made through the formation of triethanolamine salt[19] and arginate salt[20] in addition to solid dispersion techniques[21]. Although a pharmaceutical cocrystal of ACF with nicotinamide was reported[22] and characterized by FT-IR and DSC, no solubility studies were performed to ascertain the dissolution advantage of the cocrystal. Other reports[23] divulge various derivatives of ACF and its stability improvement in water through salts. The major challenge with ACF salt formation is that it undergoes degradation in strongly acidic or basic conditions to give the inactive indolinone by-product[23b, 24] (Scheme 3.1).

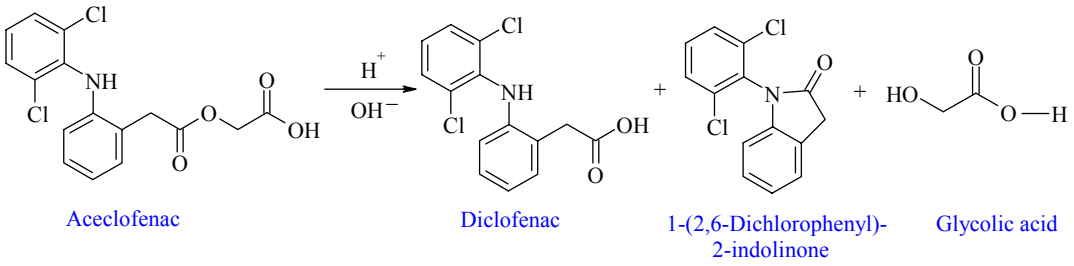

Scheme 3.1 Transformation of ACF under strongly acidic or basic conditions to the inactive Indolinone derivative.

The cyclized product (indolinone) was also isolated during our attempts to form sodium or potassium salt of ACF with bases such as Na_2CO_3, NaOH, KOH, K_2CO_3, etc. Therefore, unlike the other members of its class, such as indomethacin and diclofenac, which are marketed as their sodium salt trihydrate and potassium salt respectively, ACF is marketed as a neutral molecule. Since salt formation is not a straight forward strategy for ACF due to its

inherent cyclization, cautious selection of coformers which can improve its solubility without affecting this transformation is important.

3.3 Design and Preparation of Aceclofenac solid forms

We noted that a systematic crystal engineering[25] of ACF to improve solubility within the above boundary parameters is not reported. Although solubility enhancement of certain drug molecules through metastable polymorphs[26] is documented, uncertainty about accidental phase transformation to the stable crystalline modification during dissolution or on storage makes this strategy less attractive for drug development. Hence we set out to address the poor solubility of ACF through cocrystals[27], a currently popular supramolecular approach to tune the solubility and pharmacokinetic properties of drug substances and salt formation, a long know strategy for solubility enhancement. Since the major functional moiety of ACF, the carboxylic acid group has been well studied and shown to form robust heterosynthons[28] through O–H···O and O–H···N hydrogen bonds with various complementary functional groups like amide, pyridine, amine, acid etc. Our idea was to use this functional group, which through molecular recognition and self assembly can form solid forms with various coformers, resulting in solubility enhancement of the parent molecule. In order to obtain novel solid forms, we have subjected ACF and several GRAS[29] coformers through various solid forms screening techniques[30]. In the process we obtained novel salts of ACF with piperazine (PIP), cytosine (CYT), L-lysine (LYS) and γ-aminobutyric acid (GABA) (Scheme 3.2). In addition, a salt hydrate with piperazine and a cocrystal hydrate with 4,4′-bipyridine (BIP) are also discovered. These solid forms were characterized by X-ray diffraction, spectroscopic, and thermal techniques, and all of them except ACF-PIP were found to be stable at accelerated humidity conditions. We were unable to obtain single crystals of ACF-LYS and ACF-GABA for X-ray diffraction. Nevertheless, they were characterized by their unique powder X-ray diffraction pattern and the stoichiometry was determined by ^{1}H NMR. ACF-LYS crystalline salt is thermodynamically stable compared to the reported amorphous form. All the salts exhibited higher solubility and dissolution rate compared to the pure drug.

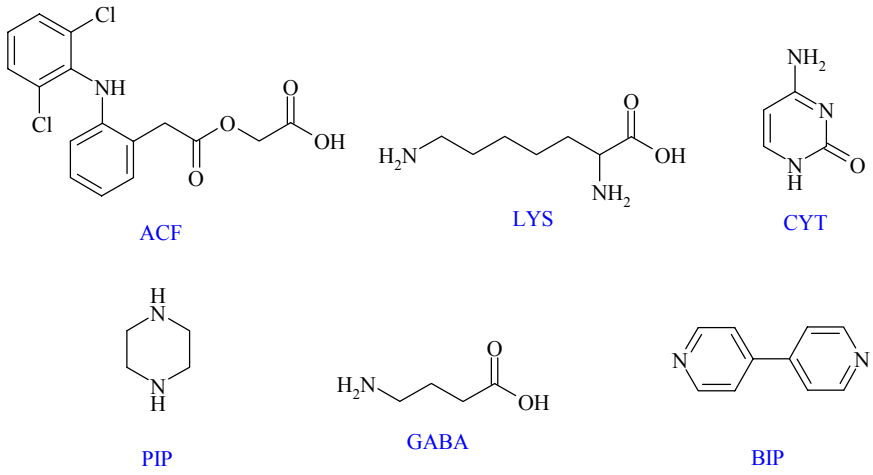

Scheme 3.2 Aceclofenac and coformers discussed in this study. Compound abbreviations are used throughout the chapter.

3.4 Results and Discussion

Salt formation is an acid-base reaction involving transfer of proton from acid to base: A–H + B → (A^-) (B^+–H). The "rule of three"[31] is a useful guide to predict salt formation between organic acids and bases. Thus salt formation requires a difference of at least three pK_a units between the acid (A–H) and the conjugate base (B^+–H), i.e. if (Δ pK_a < 0) then it would most certainly result in a cocrystal and if the (Δ pK_a > 3) then it would result in a salt and the intermediate range of 0-3 is an unpredictable zone with multiple proton states being observed to result in a salt, cocrystal or salt-cocrystal[31c]. ACF is a moderately strong acid (pK_a = 3.46). Hence salt formation is expected with coformers of sufficient basicity. With the parent compound being labile to strongly acidic or basic conditions, the coformers selected should be such that they can form a salt/cocrystal but not too strong for cyclization to the inactive indolinone. The pK_a values of ACF, salt/cocrystal formers and ΔpK_a values are listed in Table 3.1. In this study the ΔpK_a "rule of three" was observed in all cases to give salts with CYT, PIP, LYS and GABA and a cocrystal with BIP.

Table 3.1 Coformers resulting in salts/cocrystals with ACF and their ΔpK_a values[a]

	pK_a in water	ΔpK_a	Cocrystal/salt
ACF	3.46	---	---
BIP	4.61	1.15	1:0.5 Cocrystal Hydrate
CYT	5.93	2.47	1:0.5 Salt
PIP	9.72	6.26	1:0.5 Salt
PIP	9.72	6.26	1:0.5 Salt Hydrate
LYS	10.29	6.76	1:1 Salt
GABA	10.22	6.83	1:1 Salt

[a]pK_a's were calculated using Marvin 5.10.1, 2012, ChemAxon (http://www.chemaxon.com)

The X-ray crystal structure of a guest free form of ACF is reported but with incomplete proton location in the structure[32]. For a better understanding of the hydrogen bonding motifs, reflections on a crystal of the guest free form were collected at 100 K to obtain the complete crystal structure The crystallographic parameters of ACF and its salt forms are shown in Table 3.2.

Table 3.2 Crystallographic parameters of ACF salts.

	ACF	ACF-BIP-H_2O (1:0.5:0.5)	ACF-CYT (1:1)	ACF-PIP (1:0.5)	ACF-PIP-H_2O (1:0.5:1)
Form wt	354.17	882.55	465.28	397.24	415.26
Cryst syst	Monoclinic	Monoclinic	Monoclinic	Monoclinic	Monoclinic
Sp gr	$P2_1/n$	$P2_1/c$	$P2_1/n$	$P2_1/n$	$P2_1/c$
T (K)	100(2)	100(2)	100(2)	100(2)	100(2)
a/Å	12.284(3)	7.5085(5)	11.2960(10)	9.1898(11)	14.555(4)
b/Å	8.198(2)	11.9908(8)	8.7429(8)	5.5983(7)	14.950(4)
c/Å	15.484(4)	22.2488(15)	20.8507(19)	34.890(4)	8.557(3)
α/°	90	90	90	90	90
β/°	96.174(4)	91.5690(10)	98.0120(10)	94.038(2)	92.473(4)
γ/°	90	90	90	90	90
Z	4	2	4	4	4
V (Å^3)	1550.3(7)	2002.4(2)	2039.1(3)	1790.5(4)	1860.1(9)
Rflns collect	15306	18720	20400	17574	18911
Unique rflns	3030	3520	4019	3515	3674
Obsd rflns	2305	3315	3791	3143	3504
Parameters	216	288	300	247	264
R_1	0.0535	0.0293	0.0361	0.0499	0.0335
wR_2	0.1288	0.0770	0.0880	0.1112	0.0825
GOF	1.047	1.056	1.102	1.130	1.103

3.4.1 Crystal Structure Description

Aceclofenac (ACF) ACF consists of 2 aryl moieties, the N-2,6-dichlorophenyl group and the N-phenylacetyloxyacetic acid group. The aryl rings are inclined at a dihedral angle of 67º. This twist in the ortho-substituted phenyl rings at the secondary amine relieves steric hindrance. Dissolution of ACF in toluene and leaving the solution for slow evaporation afforded diffraction quality single crystals which solved and refined in the space group $P2_1/n$. In contrast to the other members of its class, such as diclofenac[33] and indomethacin[34], where the carboxylic acid forms a centrosymmetric O–H···O dimer, ACF extends through catemeric O–H···O hydrogen bond along the *b*-axis (O1···O2, 1.90Å, 135º) resulting in a tape motif (Figure 3.2a). Hydrogen bond parameters are listed in Table 3.3

Normally the rare catemer motif is favored over the dimer synthon only when auxiliary C–H···O interactions from an acidic or activated carbon donor nearby the acid moiety invariably stabilize the crystal structure[35]. Similar stabilizing interactions were observed in ACF through the activated CH group and Cl···O interactions. While the CH_2 group between the phenyl ring and the ester moiety form a weak C–H···O interaction (C4···O2, 2.29Å, 174º) between the molecules connected via the *C*(4) chain (Figure 3.2a), the CH_2 group between the ester and acid functional moieties connect the interlayer catemer tapes through centrosymmetric C2–H2A···O4 (2.32Å, 171º) interaction forming a $R^2_2(10)$ ring motif[36] (Figure 3.2b and 3.2c). An intermolecular Cl···O interaction (3.12Å) between adjacent molecules fortifies the catemer motif. The detailed role of C–H···O interactions in the catemer structure is possible to elucidate now with complete location of hydrogen atoms. Acemetacin, a molecule with similar acetyloxyacetic acid group was recently reported to have a catemer chain polymorph[37]. An intramolecular N–H···O hydrogen bond (N1···O4, 2.13Å, 147º) of *S*(7) type makes the molecule rigid. We have not found a dimer structure for ACF so far.

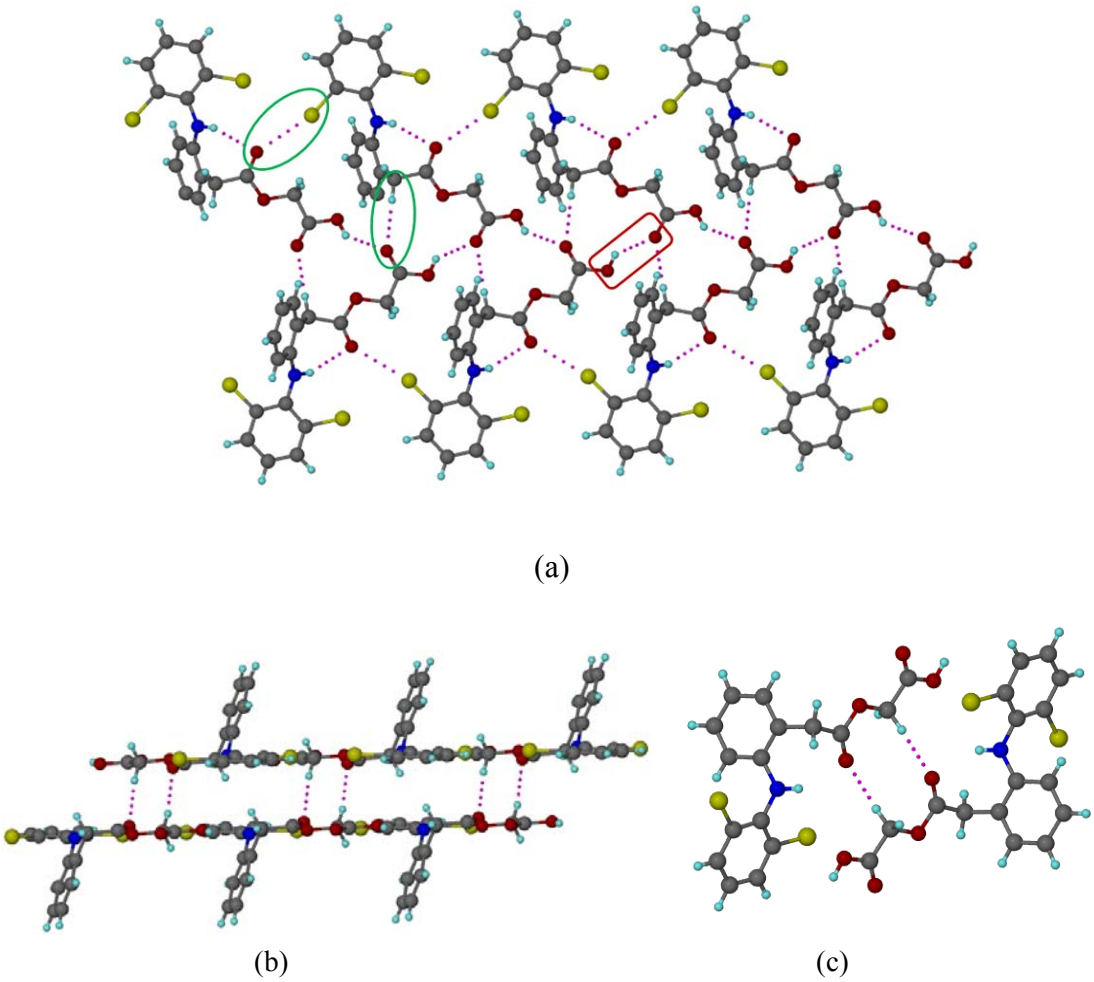

(a)

(b) (c)

Figure 3.2a) Catemeric O–H···O hydrogen bonds extend the ACF molecules in a tape motif supported by auxiliary C–H···O and Cl···O interactions. The strong O–H···O H bond is marked by a rectangle (red) and the weak C–H···O and Cl···O interactions by a circle (green). **b)** Weak C–H···O interactions connecting the adjacent catemer tapes**. c)** Molecules in adjacent layers are connected through centrosymmetric C–H···O $R^2_2(10)$ motif.

Aceclofenac-4,4′-bipyridine-hydrate (ACF-BIP-HYD) Crystallization of a 1:0.5 stoichiometric amount of ACF and BIP in MeOH-CH_3CN solvent mixture afforded single crystals of ACF-BIP hydrate which solved and refined in the monoclinic space group $P2_1/c$ in 1:0.5:0.5 ratio. The water O atom was refined with s.o.f 0.5. The most acidic COOH donor of ACF hydrogen bonds with the most basic pyridine N acceptor of BIP through an

O–H···N hydrogen bond (O1···N2, 1.62Å, 172º) (Figure 3.3a), consistent with Etter's hydrogen bond pairing rules[38]. ACF molecules in adjacent layers are connected through water molecules acting as bridges (O5–H5A···O2, 1.81Å, 181°, and O5–H5B···O2, 1.88Å, 151°) (Figure 3.3b). Auxiliary O···Cl interactions provide support to stabilize the crystal lattice.

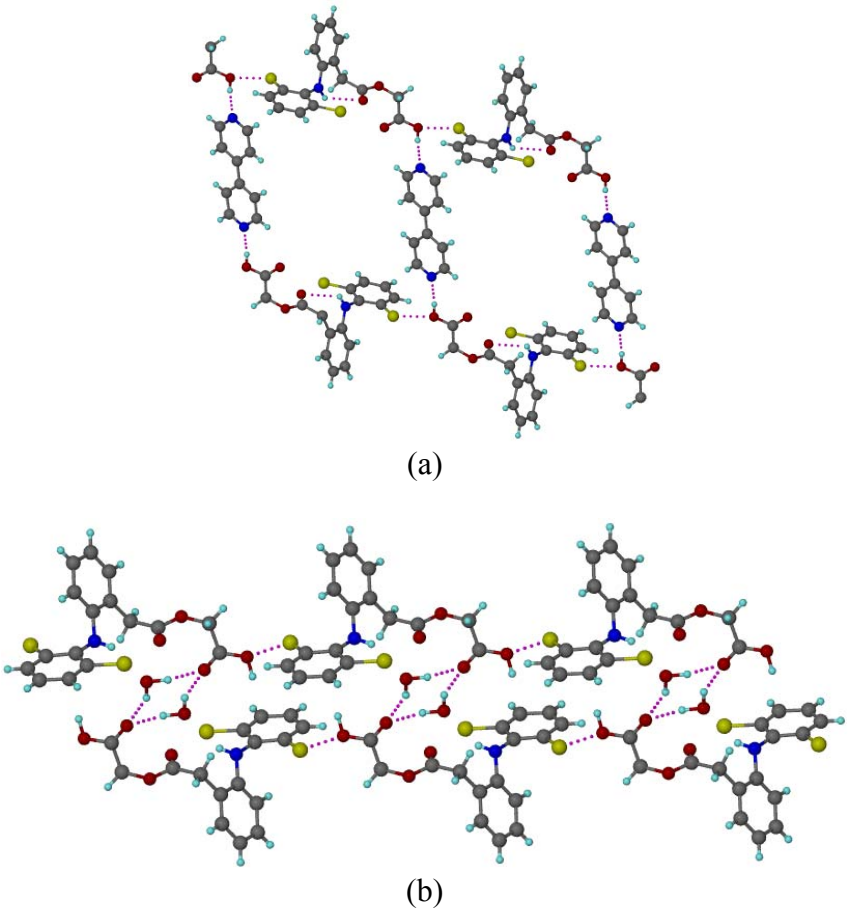

(a)

(b)

Figure 3.3a) ACF and BIP molecules are connected through O–H···N hydrogen bond.
b) Adjacent ACF layers are connected through water bridges in a tetramer O–H···O motif.

Cytosinium-aceclofenate salt (ACF-CYT) Single crystals of 1:1 cytosinium-aceclofenate salt were obtained from EtOH-CH_3CN. The X-ray crystal structure of ACF-CYT was solved and refined in the monoclinic space group $P2_1/n$. The major difference between this crystal

structure and that of ACF-BIP-HYD is that the proton is transferred from the COOH group of ACF to the basic N2 nitrogen of CYT to form an ionic N2−H1A^{+}···O1^{-} hydrogen bond (1.71Å, 180º) resulting in a salt. The protonation state of the carboxylic acid and the basic nitrogen in acid−base structures can be difficult to predict in multi-component structures. There are several cases of borderline proton location and a continuum of O···H···N hydrogen bond states was also noted[39]. The electron density maps of X-ray diffraction showed that the acidic H atom is transferred and covalently bonded to the cytosine N, making a hydrogen bond with the COO^{-} acceptor. The two C−O distances are near equal (1.246(2)Å, 1.267(2) Å) in the carboxylate group. Hydrogen bonding is mediated by the two-point carboxylate···aminopyrimidine synthon of $R^2_2(8)$ geometry. Two ACF molecules are hydrogen-bonded to two CYT molecules via the carboxylate···amine $R^2_4(8)$ motif. The N3 nitrogen of CYT forms a N3–H3A···O1 hydrogen bond with the O1 carboxylate oxygen (1.74Å, 173º) of ACF (Figure 3.4).

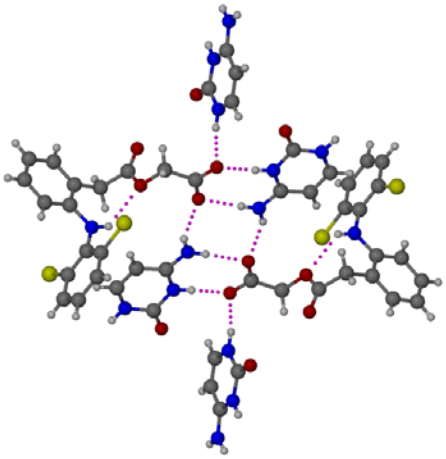

Figure 3.4 $R^2_2(8)$ and $R^2_4(8)$ N−H···O hydrogen bond ring motifs in the crystal structure of ACF-CYT salt.

Piperazinium-aceclofenate salt (ACF-PIP) This molecular salt crystallized in space group $P2_1/n$ with one molecule of aceclofenate anion and a half molecule of piperazinium cation in the asymmetric unit. The piperazinium cation forms two N^{+}–H···O^{-} ionic hydrogen bonds, N2^{+}–H1A···O1^{-} (1.68Å, 169º) and N2^{+}–H1A···O2^{-} (2.46Å, 124º). C–O bond distances and CNC bond angles are consistent with those for a salt species[31] (Figure 3.5). Piperazine is a pharmaceutically acceptable cyclic diamine with anthelminthic activity. Given its high

basicity (pK_a = 9.72) it can act both as a neutral and a cationic coformer to give a cocrystal or a salt depending on the acidity of the parent API. Nangia and coworkers[40] reported three monocationic forms of piperazine with anti-inflammatory drug meclofenamic acid were reported from our group. Through this work two dicationic forms of piperazine, ACF-PIP and ACF-PIP-HYD, are added.

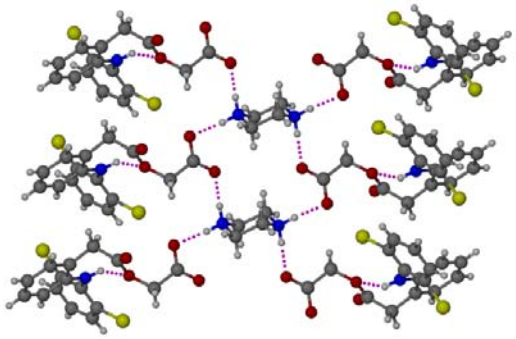

Figure 3.5 ACF and PIP molecules are connected through N–H···O^- hydrogen bond.

Piperazinium-aceclofenate monohydrate salt (ACF-PIP-HYD) This 1:0.5:1 salt hydrate crystal from EtOH-CH_3CN was solved in space group $P2_1/c$. One side the dicationic piperazinium molecule is connected to aceclofenate anion through N^+–H···O^- ionic hydrogen bond, $N2^+$–H1A···$O1^-$ (1.67Å, 175º), and on the other side ACF and water molecules bridge through $N2^+$–H2C···O5 (1.84Å, 144º) and O5–H5B···$O1^-$ (1.83Å, 171º) hydrogen bonds respectively, resulting in a $R^4_6(12)$ ring motif (Figure 3.6).

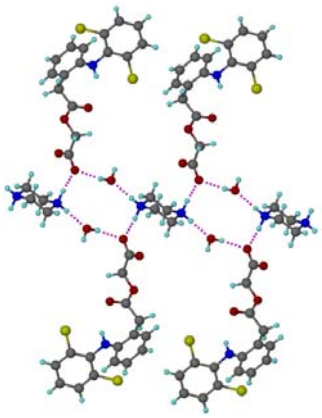

Figure 3.6 $R^4_6(12)$ hydrogen bond ring motif in the crystal structure of ACF-PIP-HYD salt hydrate.

Structural analysis revealed deeper insights into the packing efficiency and bond strength of ACF salt forms in comparison to the parent molecule. As discussed earlier, ACF can form major bonding interactions through its ester, amine and acid functional groups. Structural analysis showed that the N-H and ester functional groups are held together by an intramolecular hydrogen bond in ACF and its solid forms. Therefore the homomeric and heteromeric interactions in ACF and its solid forms are primarily due to the hydrogen bonding interactions at –COOH functional group. In ACF, the acid protons formed catemeric O1–H1A···O2 chain (1.90Å) with neighboring molecules stabilized by auxiliary C–H···O interactions. In ACF-BIP-HYD, a heteromeric O1–H1A···N2 (1.62Å) hydrogen bond with BIP molecules is present. In ACF-BIP-HYD, the ACF molecules in adjacent planes are further stabilized by water bridges. In all the salt structures, a complete proton transfer to the basic nitrogen of coformer resulted in short and ionic hydrogen bonds. Apart from the bifurcated N–H···O^- interactions (1.68Å in ACF-PIP and 1.67Å in ACF-PIP-HYD), a two point $R^2_2(8)$ ring motif between carboxylate and aminopyrimidine moieties strengthens the crystal lattice in ACF-CYT. Therefore all the solid forms of ACF are better stabilized by stronger and shorter ionic interactions which can have beneficial effects on their physicochemical properties. This was observed in our solubility and solid form stability studies of ACF solid forms (discussion later), where all the salts except ACF-PIP were found to be stable in accelerated ICH conditions and positively modulated the solubility of parent drug.

Table 3.3 Hydrogen bond parameters of ACF solid forms. O–H, N–H and C–H distances are neutron-normalized to 0.983, 1.009 and 1.083Å respectively

D–H···A	D···A (Å)	H···A (Å)	D–H···A (°)	symmetry code
ACF				
O1–H1A···O2	2.690(3)	1.90	135	3/2–x,–1/2+y,1/2–z
N1–H1B···Cl1	2.968(3)	2.63	100	---[a]
N1–H1B···O4	3.025(3)	2.13	147	---[a]
C2–H2A···O4	3.397(4)	2.32	171	1–x,–y,–z
C4–H4B···O2	3.366(3)	2.29	174	3/2–x,1/2+y,1/2–z
ACF–BIP–H_2O (1:0.5:0.5)				
O1–H1A···N2	2.5970(16)	1.63	173	2–x, –1/2+y,1/2–z
N1–H1B···Cl1	2.9726(12)	2.55	113	---[a]

N1–H1B···O4	3.0095(16)	2.28	148	---[a]
O5–H5A···O2	2.794(3)	1.81	168	1–x,1/2+y, 1/2–z
O5–H5B···O2	2.786(3)	1.88	151	–1+x,1/2–y, –1/2+z
C4–H4A···O5	3.097(3)	2.48	121	1–x, –1/2+y, 1/2–z
		ACF–CYT (1:1)		
N2–H1A···O1	2.7150(19)	1.71	180	1–x,2–y, –z
N1–H1B···Cl1	3.0163(15)	2.63	103	---[a]
N1–H1B···O3	2.9175(19)	2.04	144	---[a]
N3–H3A···O1	2.7420(18)	1.74	173	1/2+x,3/2–y,1/2+z
N4–H4C···O2	2.857(2)	1.85	178	1–x,2–y, –z
N4–H4D···O2	2.7902(19)	1.93	141	---[a]
C4–H4B···O2	3.521(2)	2.44	174	1–x,2–y, –z
C14–H14···O5	3.213(2)	2.43	128	–1+x,y,z
		ACF–PIP (1:0.5)		
N2–H1A···O1	2.673(3)	1.68	169	x,1+y,z
N2–H1A···O2	3.142(3)	2.46	124	x,1+y,z
N1–H1B···Cl1	3.013(2)	2.62	103	---[a]
N1–H1B···O3	2.924(3)	2.04	145	---[a]
N2–H2C···O2	2.653(3)	1.65	173	x,1+y,z
C2–H2A···O1	3.497(3)	2.44	164	x,–1+y,z
C4–H4A···Cl1	3.510(3)	2.64	137	x,1+y,z
		ACF–PIP–H_2O (1:0.5:1)		
N2–H1A···O1	2.6792(19)	1.67	175	–x,-y,1–z
N1–H1B···Cl2	2.9949(17)	2.60	103	---[a]
N1–H1B···O4	2.970(2)	2.12	141	---[a]
N2–H2C···O5	2.724(2)	1.84	144	---[a]
O5–H5A···O2	2.7106(19)	1.73	178	x,1/2–y,1/2+z
O5–H5B···O1	2.8090(19)	1.83	171	x,1+y,1+z
C2–H2B···O4	2.693(2)	2.26	102	---[a]
C2–H2B···O3	3.446(2)	2.47	150	x, –1/2-y, –1/2+z
C4–H4A···O1	3.561(2)	2.51	163	x, –1/2-y,1/2+z
C17–H17B···O2	3.231(2)	2.32	140	x,1+y,z
C18–H18A···O4	3.222(2)	2.38	134	x,1/2–y,1/2+z

[a] = Intramolecular hydrogen bond

3.4.2 Conformational Flexibility

The chemical diagram of ACF (Scheme 3.2) suggests that this conformationally flexible molecule can adopt different conformations in the solid-state. Significant differences were observed in the conformations of ACF in its guest free form and salt/cocrystal structures

(Figure 3.7). In ACF conformational differences arise because of free rotation around single bonds[41], mainly about the acetoxyacetic acid group. Selected torsional angles are listed in Table 3.4.

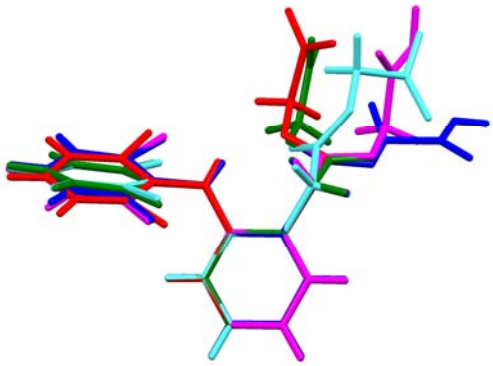

Figure 3.7 An overlay diagram of the ACF molecule extracted from the guest free form and salts. Color codes: Violet – ACF, Magenta – ACF-BIP-HYD, Green – ACF-CYT, Red-ACF-PIP, and Blue – ACF-PIP-HYD.

Table 3.4 Torsion angles in ACF crystal structures

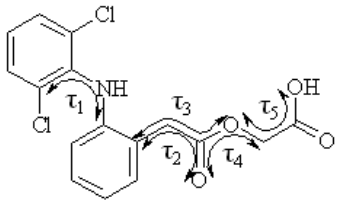

	τ_1	τ_2	τ_3	τ_4	τ_5
ACF	67.3(3)	69.6(3)	–108.5(2)	3.5(4)	178.4(2)
ACF-BIP-HYD	66.6(2)	64.1(2)	–115.2(1)	5.9(2)	168.4(1)
ACF-CYT	75.9(2)	–109.4(2)	68.8(2)	6.4(2)	–176.5(1)
ACF-PIP	61.8(3)	–105.4(3)	73.5(2)	–8.4(3)	35.2(3)
ACF-PIP-HYD	78.8(2)	13.8(2)	–169.2(1)	–0.8(2)	–161.7(1)

τ_1 – C10-N1-C11-C16, τ_2 – O4-C3-C4-C5, τ_3 – O3-C3-C4-C5, τ_4 – C2-O3-C3-O4
τ_5 – O1-C1-C2-O3

3.4.3 Powder X-ray diffraction

Powder X-ray diffraction is a reliable characterization tool to establish the formation of novel solid forms[42]. It can unambiguously distinguish the resulting product phases from its

starting materials through the unique diffraction line pattern. The PXRD of the novel solid forms prepared in this work (Figure 3.8) confirm the bulk solid phase purity and homogeneity of each crystalline phase which showed an excellent overlay of the experimental powder pattern with the calculated lines from the crystal structure. ACF-LYS and ACF-GABA were compared with the starting components to establish novel product phases because their single crystal X-ray structures are not available for comparison.

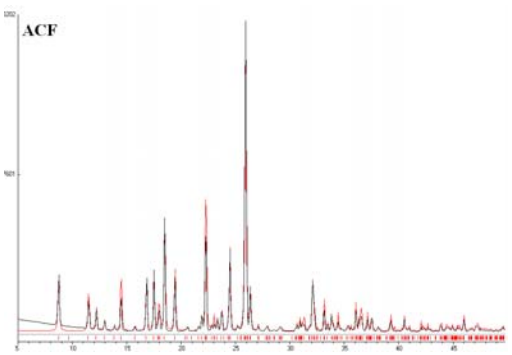

(a)

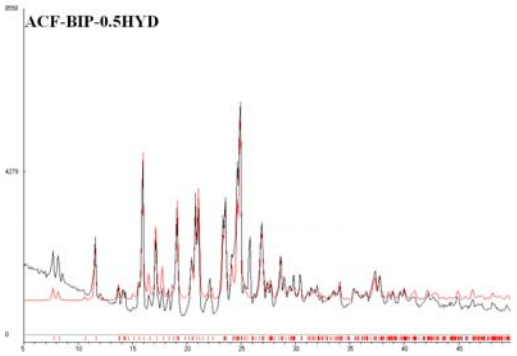

(b)

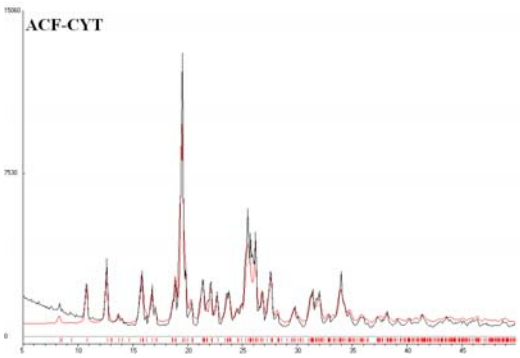

(c)

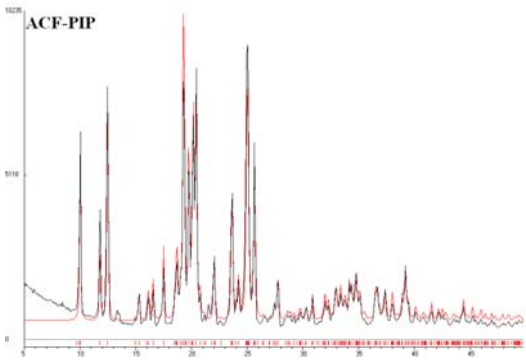

(d)

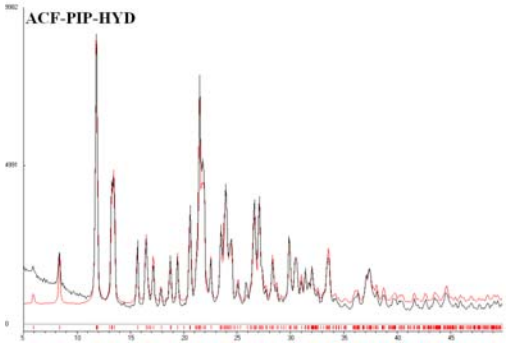

(e)

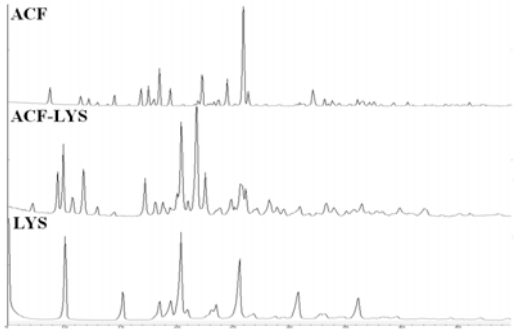

(f)

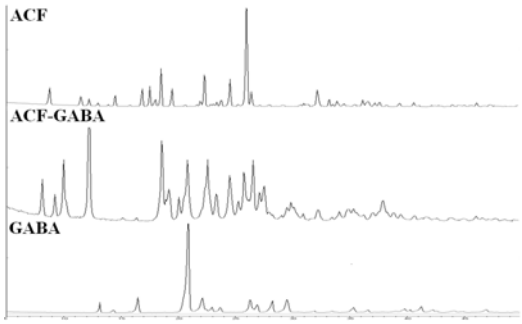

(g)

Figure 3.8 Overlay of experimental PXRD patterns of ACF solid forms showed good match with their calculated line patterns from the X-ray crystal structures indicating bulk purity and homogeneity. In case of ACF-LYS and ACF-GABA where there are no single crystal structures, comparison is made with the starting components.

3.4.4 Thermal Analysis

Whereas the DSC of cocrystal/salt shows a unique melting point compared to that of the starting components, a TGA trace establishes the stoichiometry of water or solvent molecules in case of hydrates and solvates. This way apart from acting as purity indicator, thermal measurements complement the XRD technique in confirming the formation of novel crystalline forms. The characteristic melting/decomposition profiles are shown as endo/exotherm in DSC heating curve. The DSC trace of the novel solid forms prepared in this work (Figure 3.9) showed unique melting behavior distinguishing them from the starting materials. We did not notice any correlation between the melting point of the coformer and its corresponding salt as observed for certain cocrystal systems[27] (Table 3.5). The water content in ACF-BIP-0.5HYD could not be detected through DSC. Nevertheless, water stoichiometry in ACF-BIP-0.5HYD and ACF-PIP-HYD bulk phases was confirmed by TGA and HSM experiments (Figure 3.10) which showed an excellent match with the calculated amount of water in the crystal structure.

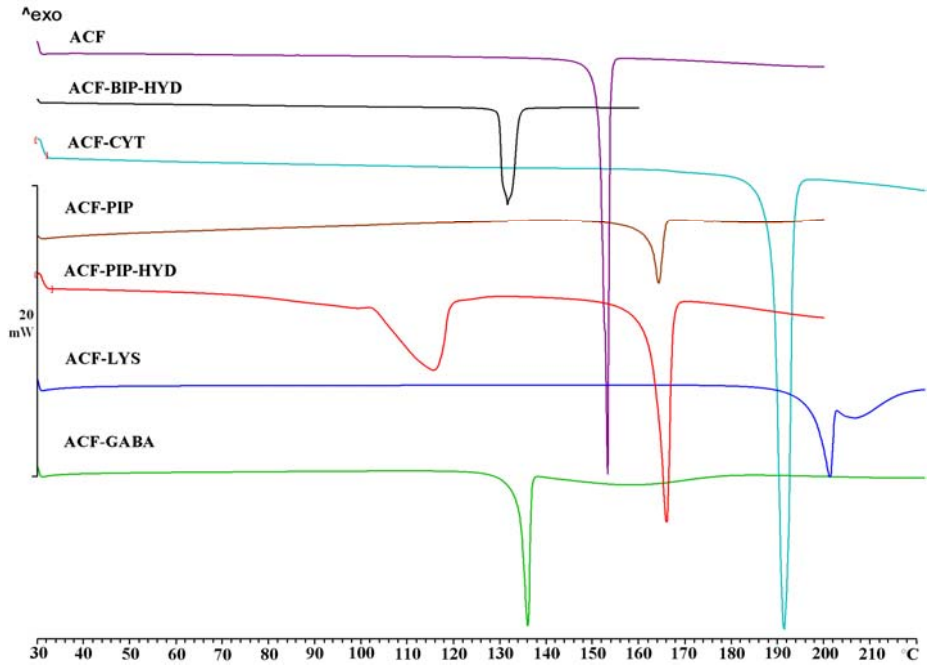

Figure 3.9 DSC heating curves show a sharp melting endotherm for each solid form.

Table 3.5 Melting point of ACF salts/cocrystals and the coformers.

S.No	ACF salts/cocrystal	Melting Point(°C)	Coformer	Melting Point (°C)
1	ACF-BIP-HYD	132.4	4,4'-Bipyridine	110-114
2	ACF-CYT	185.2	Cytosine	320-325
3	ACF-PIP	164.2	Piperazine	106
4	ACF-PIP-HYD	166.2	Piperazine	106
5	ACF-LYS	201.0	L-Lysine	196
6	ACF-GABA	135.5	γ-Aminobutyric acid	203

Melting point of ACF – 151.4°C

3.4.5 Vibrational Spectroscopy

Changes in the hydrogen bonding patterns of the starting materials on forming cocrystals/salts are expected to influence the energies of vibrational modes associated with the functional groups[43]. Differences in the bonding patterns hint at the functional groups

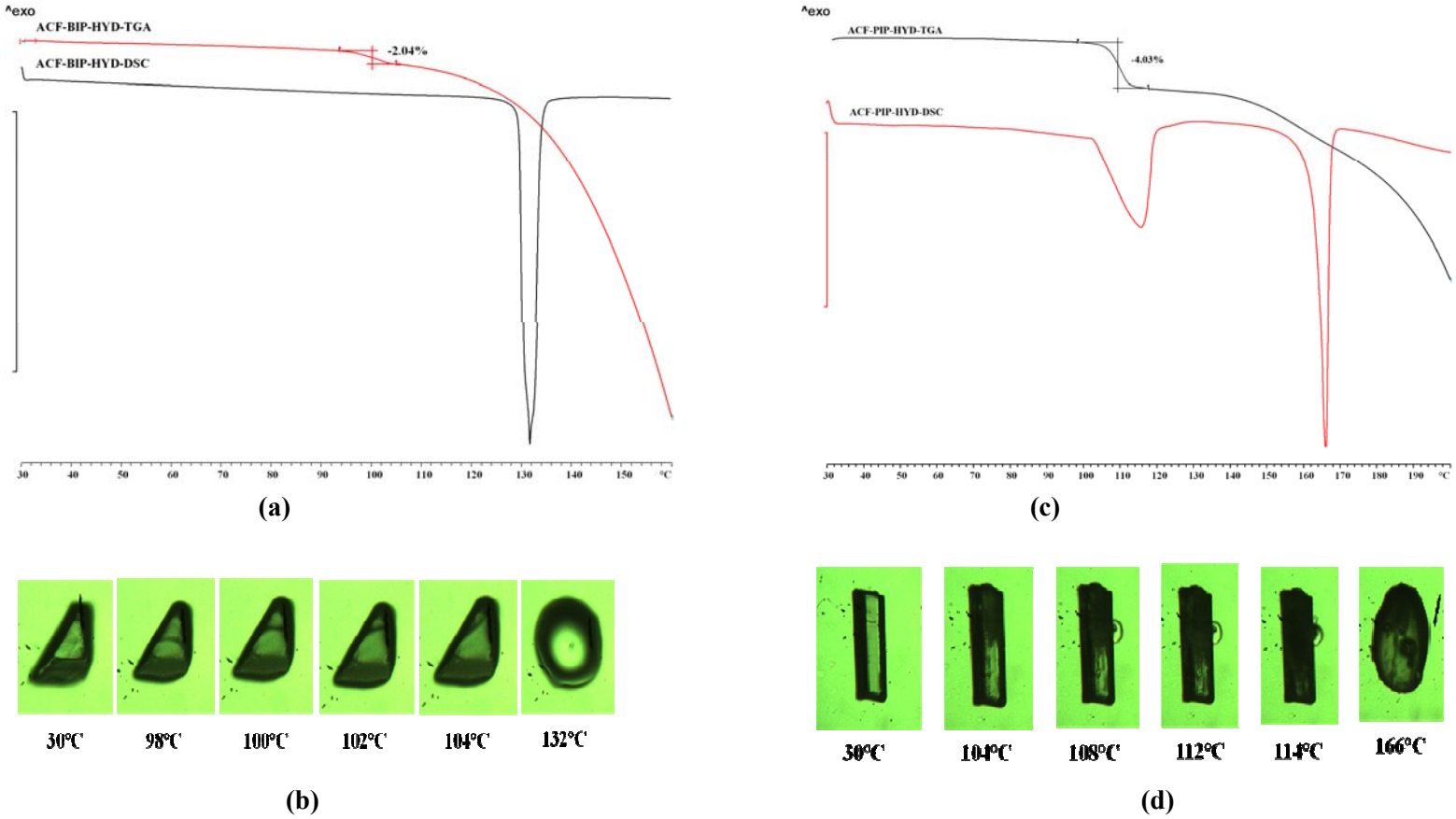

Figure 3.10 a) Overlay of DSC and TGA thermograms of ACF–BIP–HYD. TGA measurements showed water loss of 2.04% which matches with the calculated amount of stoichiometric water in the crystal lattice. **b)** HSM snapshot of ACF–BIP–HYD showed water loss between 98–104 °C. **c)** Overlay of DSC and TGA thermograms of ACF–PIP–HYD. The stoichiometric water loss of 4.03% matches with the calculated amount of stoichiometric water in the crystal lattice. The endotherm for water loss in ACF–PIP–HYD matches with the melting endotherm of the hydrate. **d)** HSM snapshot of ACF–PIP–HYD showed water loss between 104–114 °C.

involved thereby efficiently complementing the diffraction methods in the characterization of solid forms. In the IR spectrum of ACF, the COOH functional group is present as a monomer and hence the carbonyl group appears as a sharp peak at 1771.4 cm^{-1}. The ester and amine functional moieties are connected to each other through intramolecular hydrogen bond and appear at 1716.6 cm^{-1} and 3318.9 cm^{-1}. The bands due to C–O stretch and O–H bend appear at 1256.4 cm^{-1} and 1400.0 cm^{-1}. These hydrogen bonding functional groups showed significant changes in their vibrational patterns on salt/cocrystal formation (Figure 3.11). In ACF-BIP-HYD significant changes were observed in the N-H frequencies of ACF indicative of differences in the hydrogen bond pattern. While the N-H stretching frequency shifted to 3296.2 cm^{-1}, its bending frequency appeared at 1602.2 cm^{-1}. Due to its hydrogen bonding to the acid moiety of ACF, the C=N stretch in BIP shifted from 1408.5 cm^{-1} to 1416.9 cm^{-1} in the cocrystal. In all the salts, the acid moiety exists as carboxylate ion which is characterized by a strong asymmetric stretch at 1650-1450 cm^{-1}, and a weaker symmetric stretch near 1350-1250 cm^{-1} in their IR spectra. Asymmetric and symmetric stretching frequencies of carboxylate ion indicative of salt formation appeared at 1492.2cm^{-1} and 1232.4 cm^{-1} in ACF-CYT, 1450.8 cm^{-1} and 1245.6 cm^{-1} in ACF-PIP, 1453.7cm^{-1} 1292.5 cm^{-1} in ACF-PIP-HYD, 1453.3 cm^{-1} and 1242.1 cm^{-1} in ACF-LYS, 1452.1 cm^{-1} and 1241.1 cm^{-1} in ACF-GABA as compared to 1771.4 cm^{-1} stretching peak of monomeric carboxylic acid of ACF molecule.

The complementary Raman spectra also showed similar changes in the product phases compared to the starting components (Figure 3.12). In ACF-BIP-HYD, the Raman shift for N-H stretching frequency was observed at 3299.7 cm^{-1}, and it's bending frequency at 1611.5 cm^{-1} indicating changes in the hydrogen bond pattern of ACF in the cocrystal. Similar to the IR spectra, significant changes in the Raman spectra of salts were observed due to the formation of carboxylate ion. The raman shift due to asymmetric and symmetric stretching frequencies of carboxylate ion appeared at 1414.2 cm^{-1}, 1254.9 cm^{-1} in ACF-CYT, 1450.8 cm^{-1}, 1237.0 cm^{-1} in ACF-PIP, 1451.7 cm^{-1}, 1237.0 cm^{-1} in ACF-PIP-HYD, 1425.2 cm^{-1}, 1234.7 cm^{-1} in ACF-LYS 1420.9 cm^{-1}, 1234.2 cm^{-1} in ACF-GABA as compared to the monomeric carboxylic acid shift of ACF at 1726.4 cm^{-1}. Thus both IR and Raman spectra of cocrystal and salts with significant changes in their stretching and bending frequencies

proved invaluable in establishing their unique bonding pattern. They ably complemented the diffraction techniques in highlighting their novelty. Significant FT-IR and FT-Raman frequencies are summarized in Table 3.6.

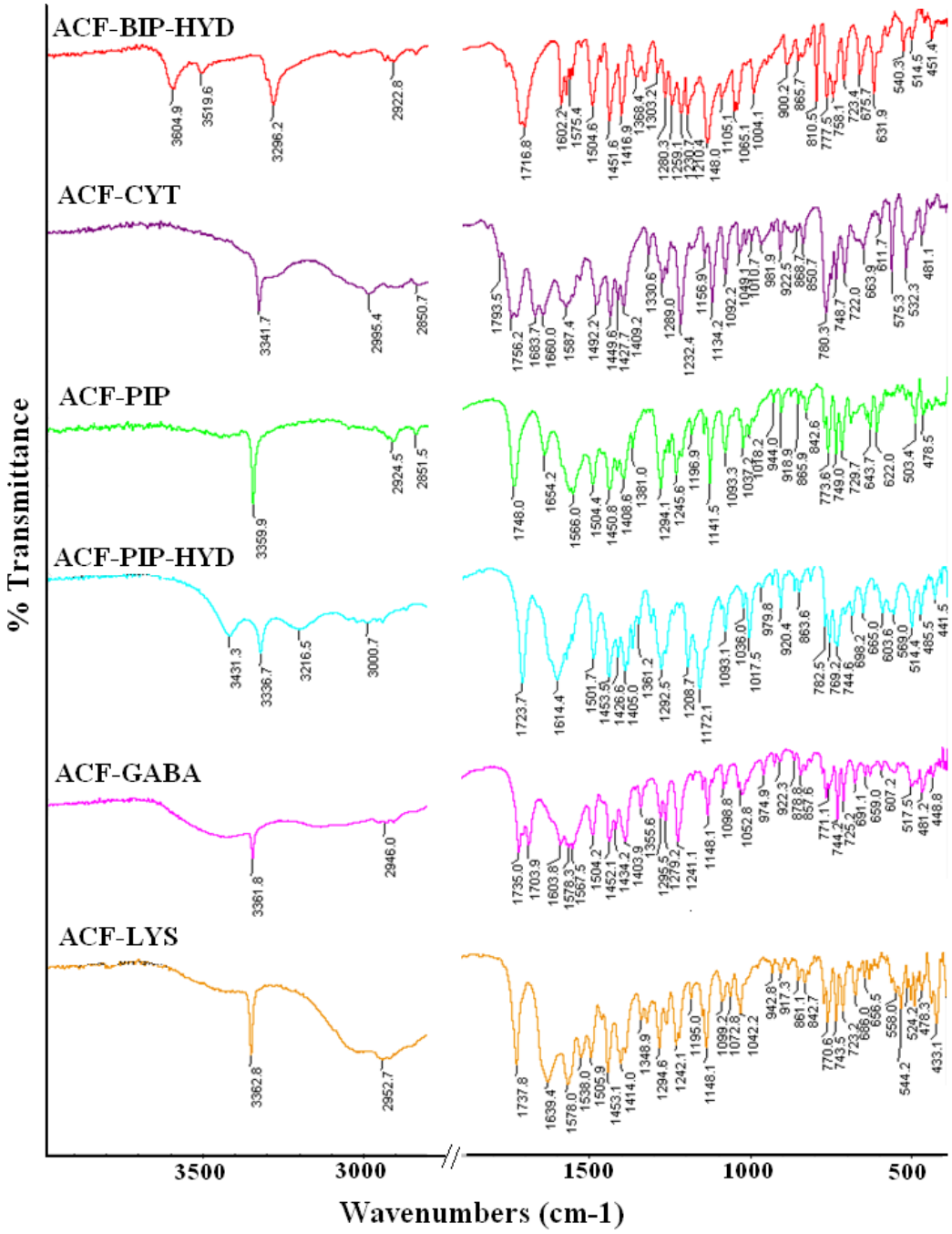

Figure 3.11 Overlay of IR spectra of ACF solid forms.

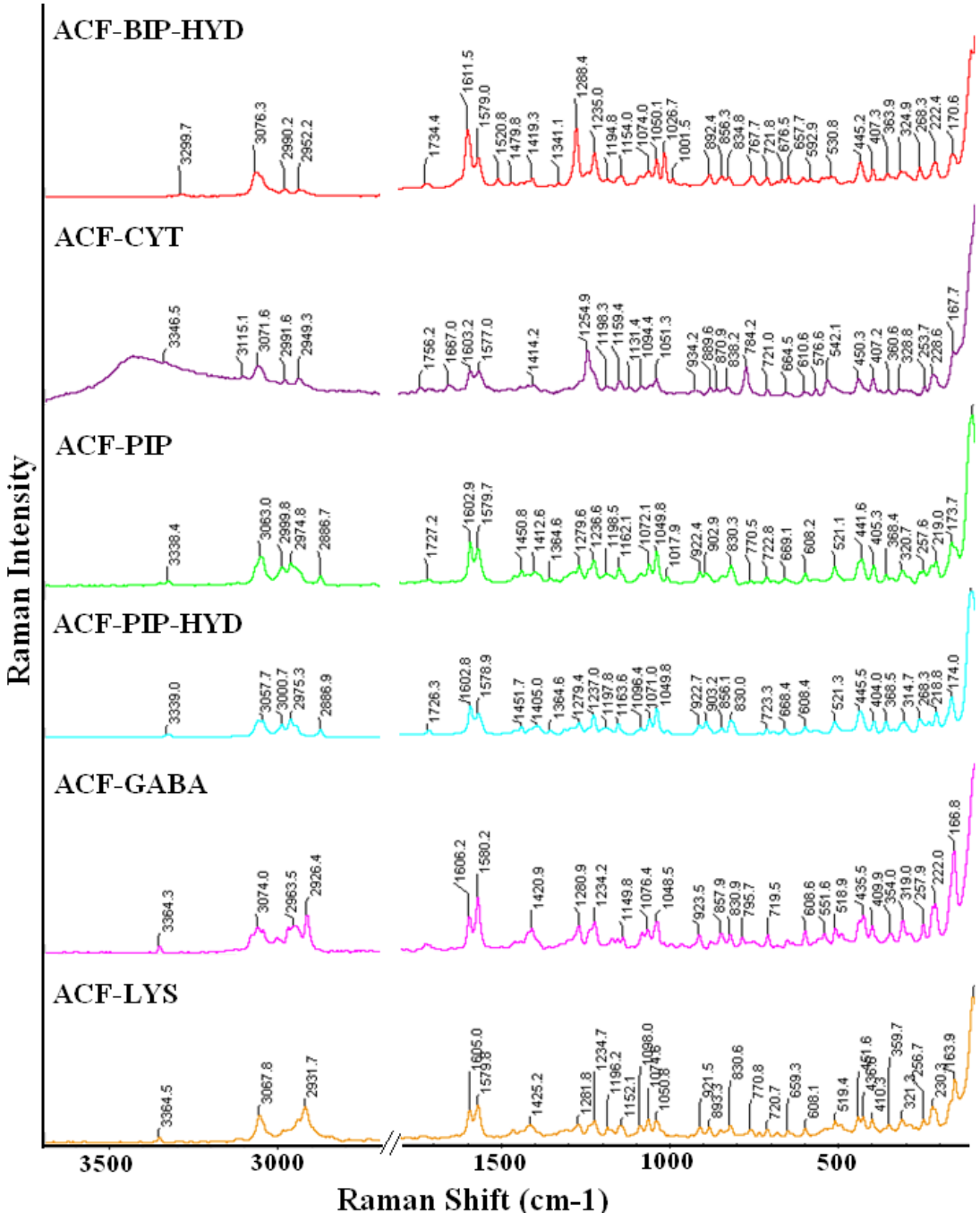

Figure 3.12 Overlay of Raman spectra of ACF solid forms.

Table 3.6 IR and Raman frequencies of ACF solid forms and starting components (in $cm^{-1)}$

	INFRARED				
	N-H stretch	C=O stretch	Carboxylate asym. stretch	Carboxylate sym. stretch	N-H bend
ACF	3318.9	1716.6, 1771.4	--	--	1589.4
ACF-BIP-HYD	3296.2	1716.8	--	--	1602.2
ACF-CYT	3341.7	1683.7, 1756.2	1492.2	1232.4	1587.4
CYT	3381.4	1661.9	--	--	1537.4
ACF-PIP	3359.9	1748.0	1450.8	1245.6	1566.0
PIP	3207.9	--	--	--	--
ACF-PIP-HYD	3336.7	1723.7	1453.7	1292.5	1614.4
ACF-GABA	3361.8	1735.0, 1703.9	1452.1	1241.1	1603.8
GABA	--	--	--	--	1640.7
ACF-LYS	3362.8	1737.8	1453.3	1242.1	1639.4
LYS	3422.9	--	1500.1	1286.4	1625.9
	RAMAN				
ACF	3321.0	1726.4	--	--	1605.0
ACF-BIP-HYD	3299.7	1734.4	--	--	1611.5
ACF-CYT	3346.5	1756.2, 1667.0	1414.2	1254.9	1603.2
CYT		1650.5			1529.6
ACF-PIP	3338.4	1727.2	1450.8	1237.0	1602.9
PIP	3288.2				1449.9
ACF-PIP-HYD	3339.0	1726.3	1451.7	1237.0	1602.8
ACF-GABA	3364.3	1720.2	1420.9	1234.2	1606.2
GABA	3253.6	--	--	--	1636.6
ACF-LYS	3364.5	1744.0	1425.2	1234.7	1605.0
LYS	3363.5	--	1456.9	1168.9	1609.1

3.4.6 ss-NMR Spectroscopy

ss-NMR spectroscopy can nondestructively provide detailed information about the differences in hydrogen bonding, molecular environment, and short range order in crystalline and amorphous solids[44]. ^{13}C ss-NMR analysis of the novel solid forms of ACF showed clear

differences in the product phases when compared with the starting components. Based on the extent of proton transfer the position of the COOH carbon atom differed in ss-NMR spectra. Whereas the neutral COOH peak appeared at 174.1 ppm in the parent drug, it showed a clear downfield shift in salts where it exists as a carboxylate anion (Figure 3.13). In ACF−BIP−HYD there is no proton transfer from ACF to the coformer. Hydrogen bonding of the COOH donor to the pyridyl nitrogen of BIP showed a downfield shift to 174.8 ppm. In salts, larger downfield shifts were observed due to complete proton transfer. The chemical shift of COO^- carbon in salts was shifted downfield to 176.5 ppm in ACF−CYT, 174.4 in ACF−PIP, 174.8 in ACF−PIP−HYD, 175.1 ppm in ACF−LYS, and 174.9 ppm in ACF−GABA (Table 3.7).

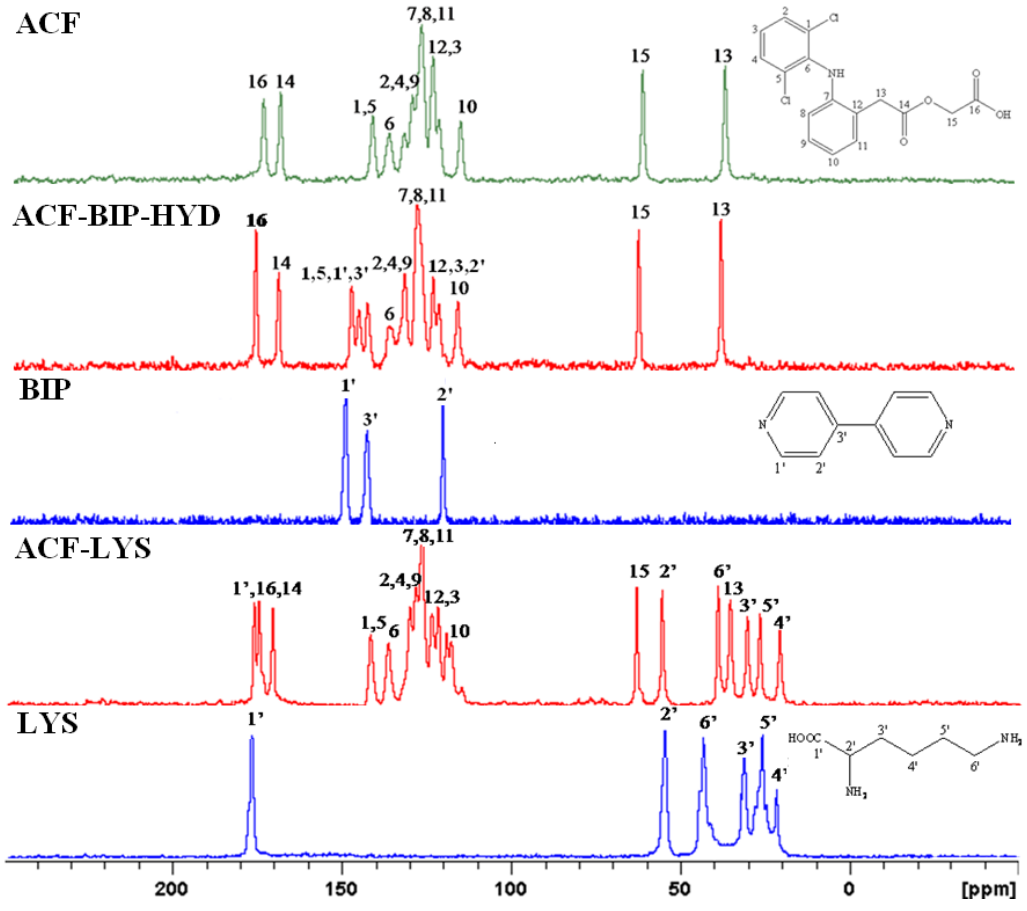

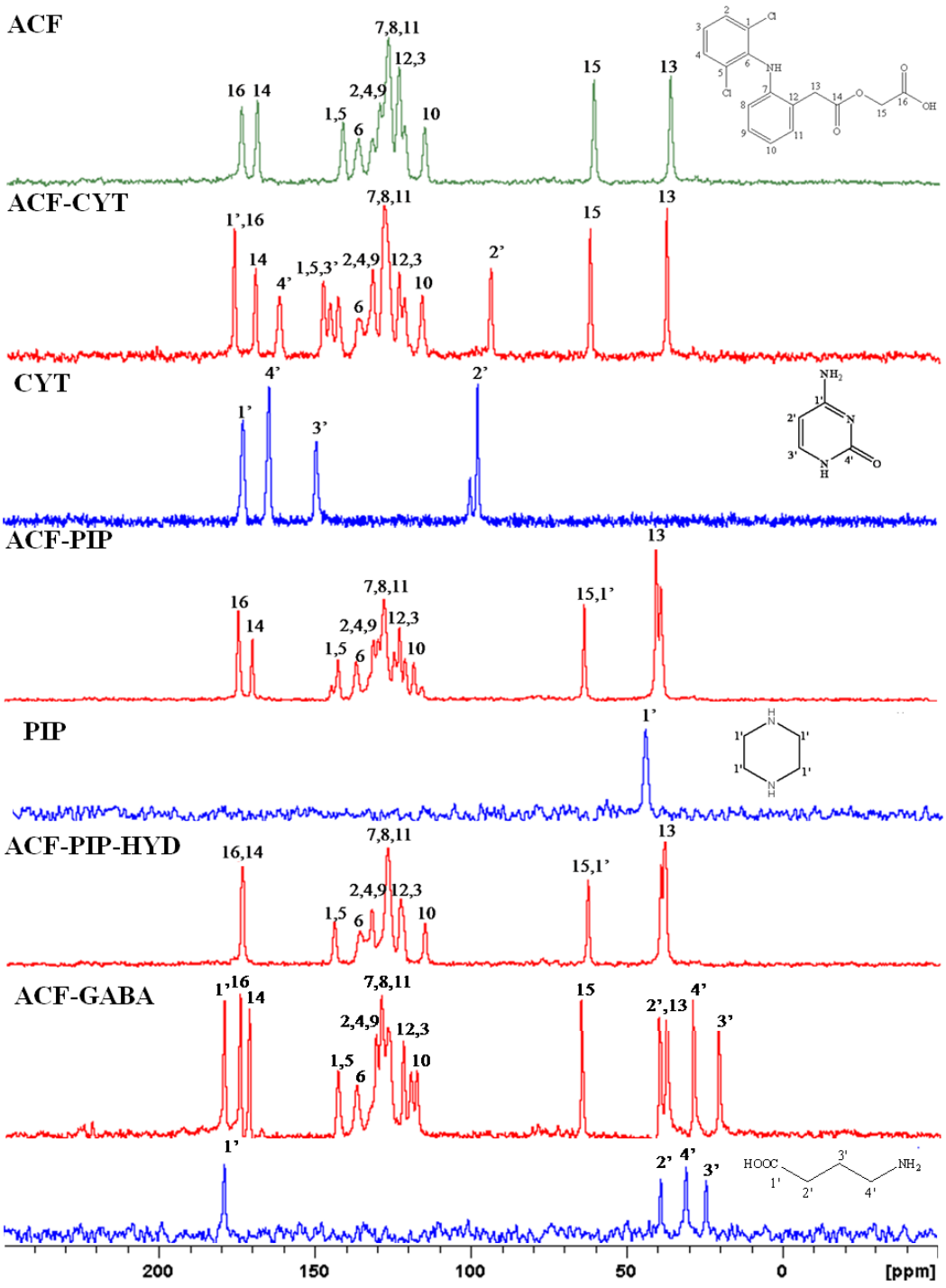

Figure 3.13 Overlay of ss-NMR spectra of ACF solid forms with the starting components.

Table 3.7 ss-NMR ^{13}C chemical shifts (δ, ppm) of ACF salts.

Carbon No.	ACF	BIP	ACF-BIP	CYT	ACF-CYT	PIP	ACF-PIP	ACF-PIP-HYD	LYS	ACF-LYS	GABA	ACF-GABA
1,5	141.7		142.9		145.7, 143.2		144.4, 142.4	144.3		142.2		143.0
2,4	132.2		132.8		132.2		132.2	133.5		130.6		130.7
3	121.7		122.4		121.9		122.6	123.2		119.8		122.1
6	136.6		137.8		136.8		136.5	136.1		136.9		136.9
7,8,11	127.0		127.9		128.4		127.5	127.3		127.1		127.1
9	129.8		128.7		132.2		129.5	132.3		128.8		129.1
10	115.4		116.8		116.2		139.6	115.2		118.4		117.8
12	123.6		123.6		123.7		124.3	123.2		122.3		122.1
13	36.4		37.2		37.7		38.7	38.3		36.0		38.0
14	169.1		170.2		169.7		169.8	173.9		171.0		171.3
15	61.0		62.3		62.2		63.4	63.0		63.7		65.0
16	174.1		174.8		176.5		174.4	174.8		175.1		174.9
1’		149.4	149.9	172.4	176.5	45.4	63.4	63.0	176.5	176.5	177.8	179.3
2’		144.1	144.4	97.2	94.1				54.6	56.1	39.2	40.2
3’		121.2	121.7	148.9	147.9				31.3	31.0	24.3	21.3
4’				164.1	161.9				21.6	21.4	30.5	29.4
5’									24.7	27.3		
6’									43.3	39.7		

3.4.7 Crystalline and Amorphous ACF-LYS salt

Amorphous forms, due to their excess thermodynamic functions tend to be less stable compared to their crystalline counterparts[11,45]. Hence, they transform to the thermodynamic crystalline phase during slurry grinding, storage and at times even at ambient conditions. The amorphous form of ACF−LYS salt was prepared by lyophilization[20]. The amorphous nature of the product was characterized by PXRD and DSC (Figure 3.14a, 3.14b). PXRD of the amorphous solid kept in accelerated ICH conditions[46] (40 °C, 75% RH) for 24 h matched with the crystalline salt (Figure 3.14c) prepared in this work. The same result was observed on slurry grinding of amorphous material in water for 24 h. Stabilization of the amorphous phase confers additional benefits like higher solubility and dissolution. In literature stable amorphous forms have been marketed targeting various infections and diseases. For example, Anti-fungal drug Itraconazole[47] (ITZ) is marketed by Janssen Pharmaceutica as Sporanox capsules where the amorphous ITZ is coated on 0.4-0.5 mm diameter sucrose spheres and stabilized by inactive excipients and binders which include hydroxypropyl methylcellulose, poly(ethylene glycol) (PEG) 20000 and starch. The conversion of amorphous ACF-LYS to the crystalline phase obtained in this work establishes its thermodynamic nature. Supporting evidence for its phase stability was also obtained through stability studies in accelerated ICH conditions (discussion next).

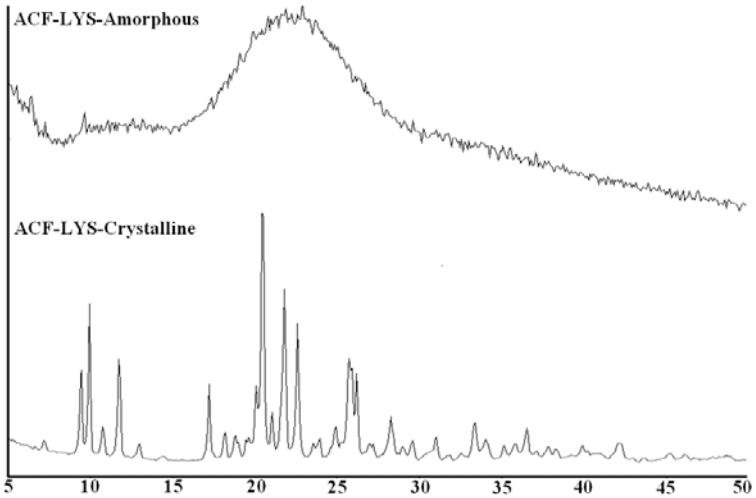

(a)

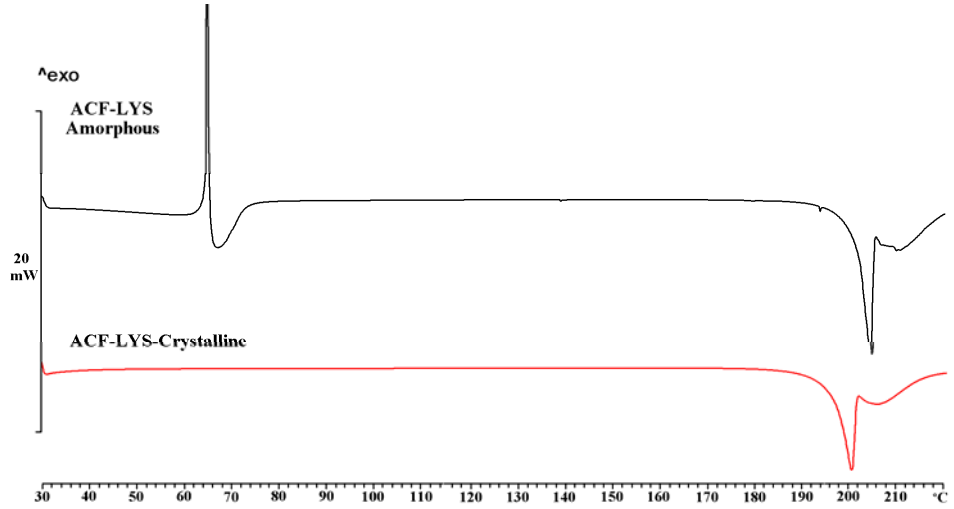

(b)

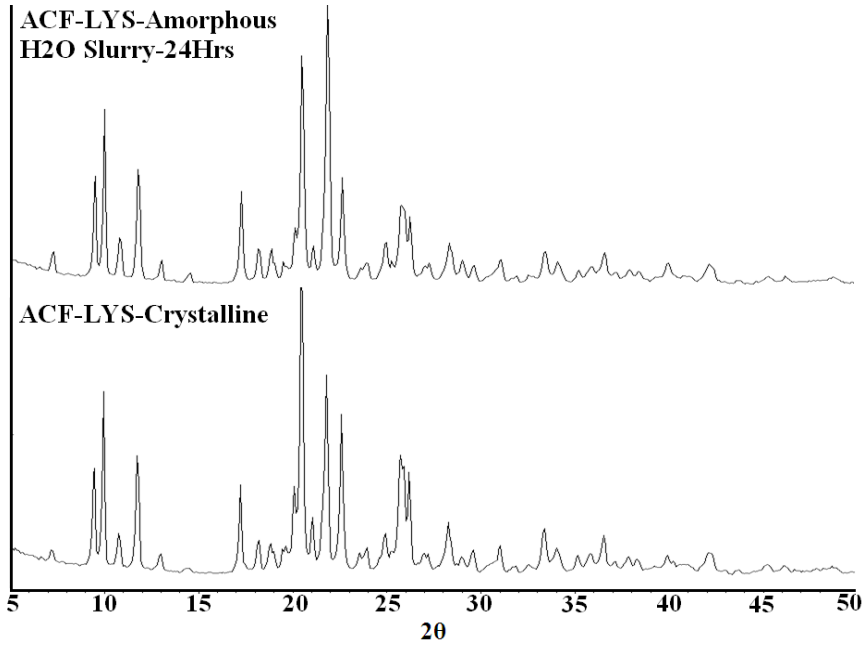

(c)

Figure 3.14 a-b) PXRD and DSC comparison of ACF-LYS amorphous and crystalline forms. **c)** Conversion of ACF-LYS amorphous phase to the crystalline form after 24hrs aqueous slurry experiment. Similar transformation to the crystalline salt was observed on keeping amorphous phase in accelerated ICH conditions for 24 hrs.

3.4.8 Solid Form Stability

Stability studies on ACF and its salts were carried out in accelerated stability ICH (International conference on Harmonization) conditions of 40°C temperature and 75% relative humidity. Powder XRD was recorded on all the solid forms at regular intervals upto 8 months. Based on the characteristic peak positions, stability of the samples to the set humidity conditions was assessed. ACF-CYT, ACF-PIP-HYD, ACF-LYS and ACF-GABA were found to be equally stable as that of the reference ACF drug throughout the 8 months period by PXRD analysis (Figure 3.15a-e). Based on the changes in powder XRD pattern, ACF-PIP was found to convert to ACF-PIP-HYD within 3 days (Figure 3.15f). From the stability studies we established that ACF-CYT, ACF-PIP-HYD, ACF-LYS and ACF-GABA have similar stability as that of the reference drug but with the added advantage of higher solubility (discussed later) compared to ACF. We did not observe any peaks for by-products such as diclofenac and indolinone of Scheme 3.1 (Figure 3.15g) in the long terms stability experiments.

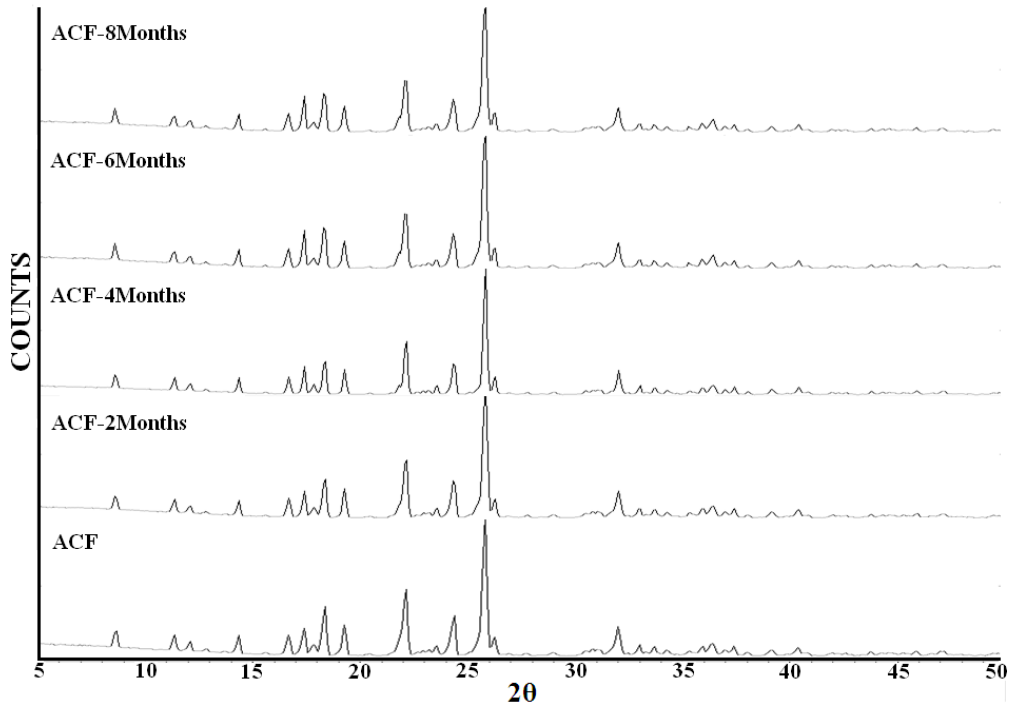

(a)

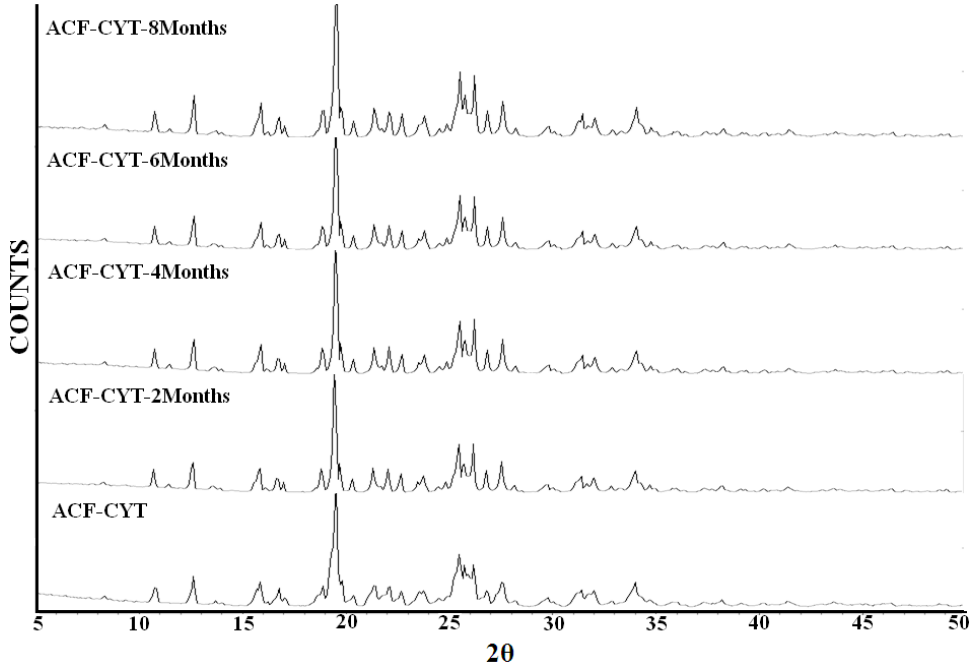
ACF-CYT-8Months
ACF-CYT-6Months
ACF-CYT-4Months
ACF-CYT-2Months
ACF-CYT
COUNTS
5
10
15
20
25
30
35
40
45
50
2θ

(b)

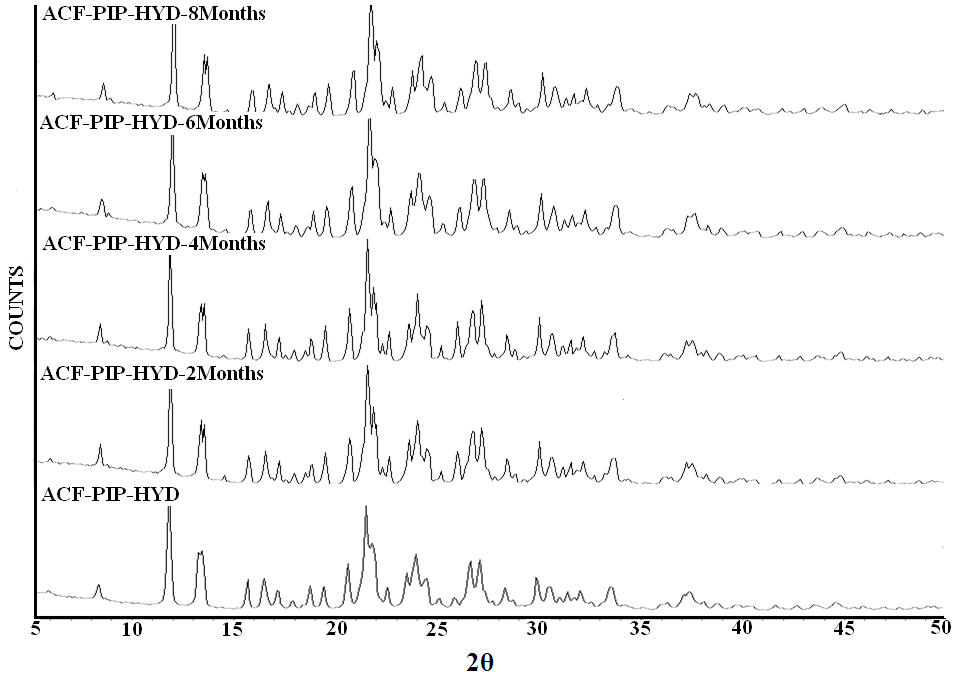
ACF-PIP-HYD-8Months
ACF-PIP-HYD-6Months
ACF-PIP-HYD-4Months
ACF-PIP-HYD-2Months
ACF-PIP-HYD
COUNTS
5
10
15
20
25
30
35
40
45
50
2θ

(c)

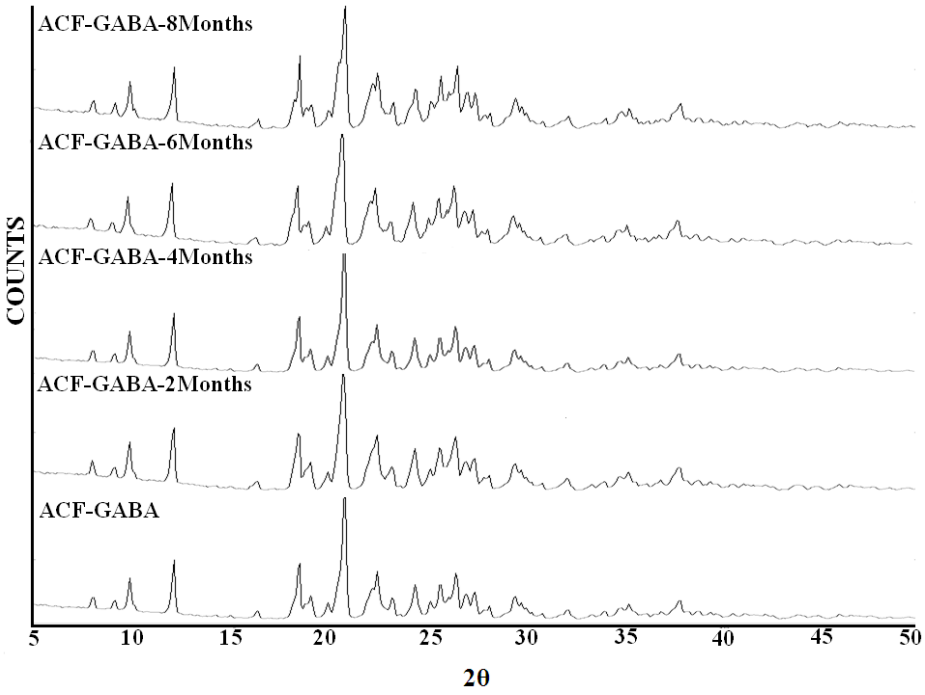
ACF-GABA-8Months
ACF-GABA-6Months
ACF-GABA-4Months
ACF-GABA-2Months
ACF-GABA
COUNTS
5
10
15
20
25
30
35
40
45
50
2θ

(d)

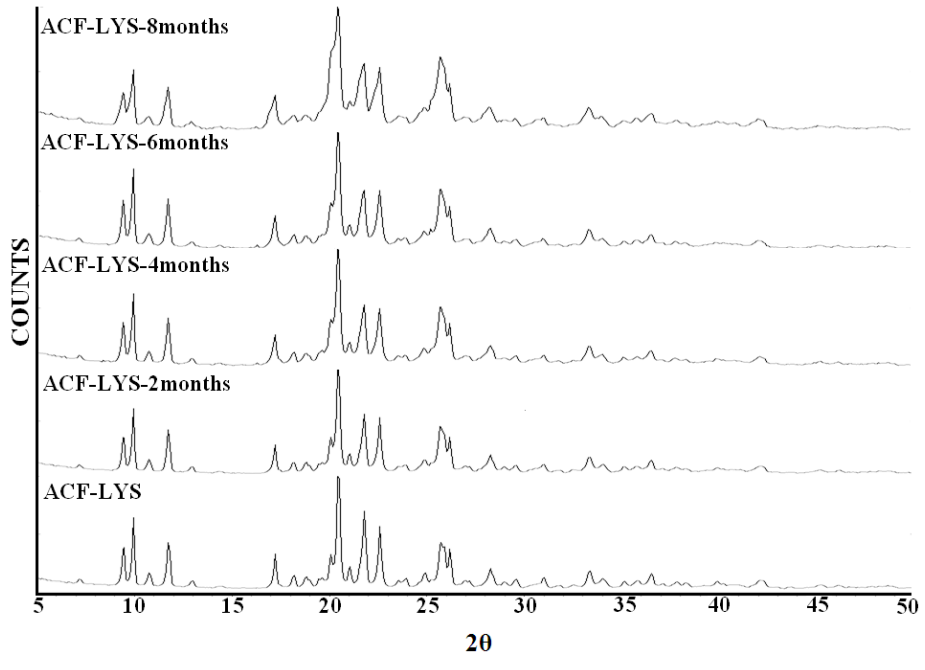
ACF-LYS-8months
ACF-LYS-6months
ACF-LYS-4months
ACF-LYS-2months
ACF-LYS
COUNTS
5
10
15
20
25
30
35
40
45
50
2θ

(e)

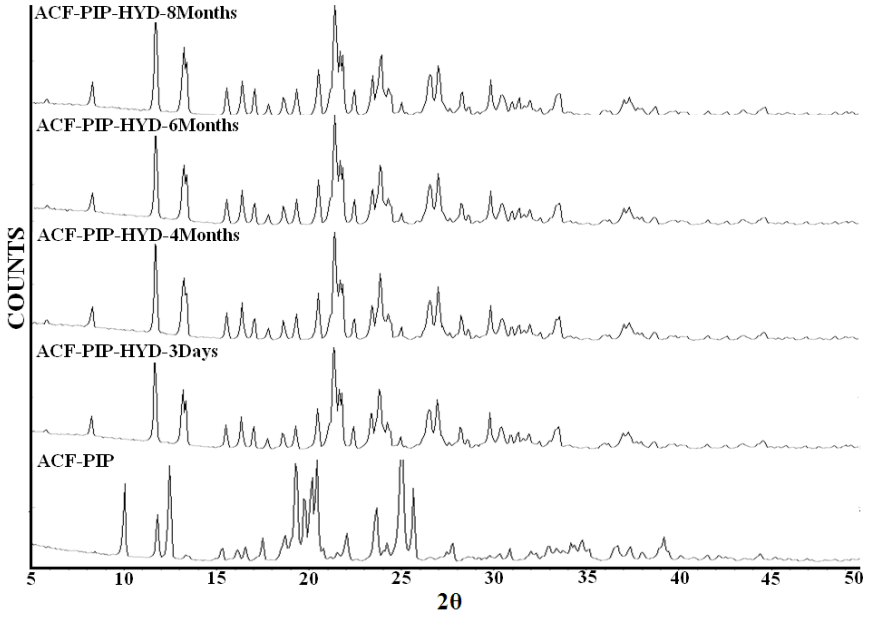

(f)

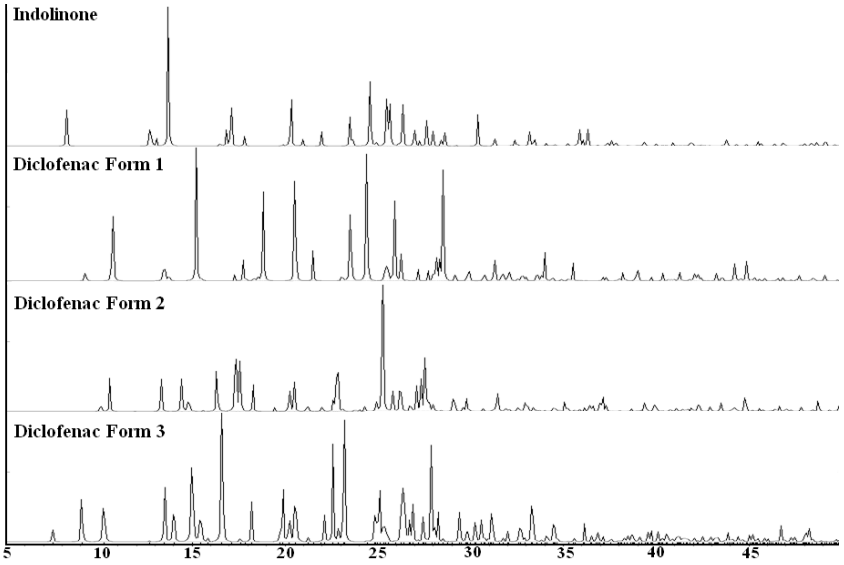

(g)

Figure 3.15a-e) PXRD patterns of ACF and its stable solid forms in accelerated stability conditions of 40 °C and 75% RH at regular intervals. **f)** ACF-PIP converted to ACF–PIP–HYD in 3 days, which in turn was stable for up to 8 months. **g)** Calculated PXRD line plots form the crystal structures of indolinone by-product of Scheme 3.1 and diclofenac polymorphs to confirm their absence during extended stability testing.

3.4.9 Solubility and Dissolution

An important goal of drug development is to maintain optimum physicochemical parameters which have a major impact on its efficacy. Solubility and permeability of a drug molecule determine its mode of administration into the body. Solubility remains a major concern for BCS class II drugs since it largely limits bioavailability[48]. Hence, physical or chemical modifications are necessary for such drugs in order to modulate solubility and improve therapeutic efficacy. Solubility and dissolution studies were carried out on ACF (a BCS class II drug) salts to evaluate the solubility advantage. Equilibrium solubility of ACF, ACF−CYT, ACF−PIP-HYD and ACF−LYS was determined in 25% EtOH−water medium because the concentration of ACF in pure water is very low. The equilibrium solubility experiment was performed for 48 h. Solubility of ACF−PIP and ACF−GABA could not be determined since the former converted to its more stable hydrate and the latter dissociated into the starting components due to the incongruent solubilities of ACF and GABA[49]. The stable ACF−CYT, ACF−PIP−HYD and ACF−LYS salts exhibited 16.3, 3.5 and 156.5 times higher solubility than the reference drug ACF.

Dissolution rate is a time dependant phenomenon and this method is preferable for those drugs which undergo phase transformation during the equilibrium solubility experiment. Intrinsic dissolution rate (IDR) gives an idea of the peak concentration and the amount of the drug dissolved in a short time period (30 min to 2 h) before it undergoes any phase transformation/dissociation[50]. IDR experiments on ACF salts were performed in 25% EtOH−water for 1.5 h by the rotating disk intrinsic dissolution rate (DIDR) method[51] at 37 °C. ACF−LYS showed 135 fold higher IDR than ACF followed by ACF−GABA (x112.7), ACF−CYT (x11.6), ACF−PIP (x3.4), and ACF−PIP−HYD (x2.6). As expected, while ACF−PIP converted to its hydrate and ACF−GABA dissociated into the starting components at the end of IDR experiment, the other salts were stable. We did not observe any trend between the melting point of the salt and its dissolution rate, i.e. lower the melting point higher the IDR, similar to those reported for certain cocrystals[27a,c,d,52a]. The dissolution rates are better correlated to the coformer solubility (a kinetic parameter) rather than the melting point (thermodynamic). ACF−CYT did not follow this order. Intrinsic dissolution rate curves

are displayed in Figure 3.16, and dissolution rates, melting points, and coformer solubility are listed in Table 3.8. The amount of dissolved ACF after 1.5 h ($AUC_{0\text{-}1.5}$) is 105.33 mg h/L for ACF, 218.5 mg h/L for ACF−PIP−HYD, 836.5 mg h/L for ACF−CYT, and 13451.1 mg h/L for ACF−LYS. The AUC value, which indicates the total dissolved ACF in a given time period, is the highest for ACF−LYS (x127.7 times greater than ACF). PXRD plots of the residue at the end of the equilibrium solubility and dissolution experiments are shown in Figure 3.17. ACF-LYS salt having the highest dissolution rate and good solid form stability in solubility and humidity experiments is a promising candidate as a soluble ACF salt. Moreover, the salt former L-lysine is completely safe. For example, ibuprofen lysinate salt is marketed under the brand name Neoprofen[53].

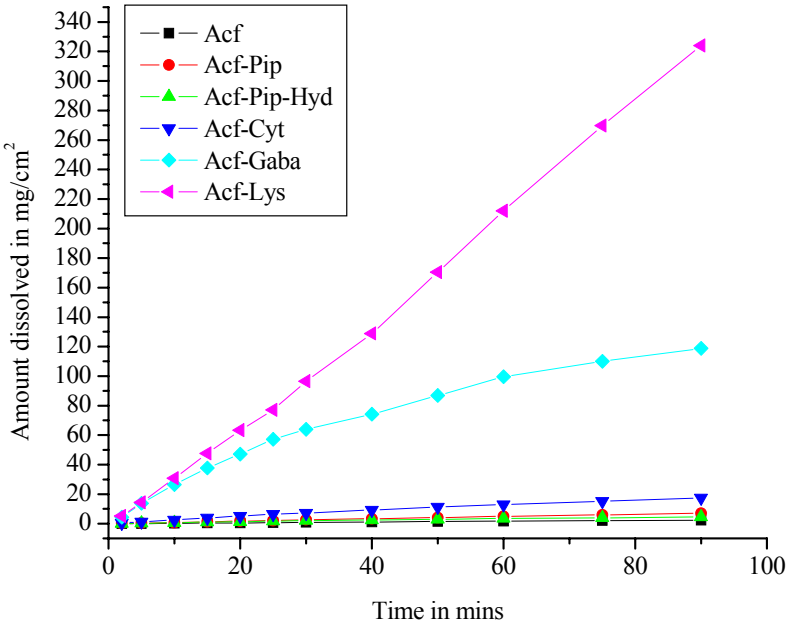

Figure 3.16 Intrinsic dissolution rate curves of ACF salts in 25% EtOH−water.

Table 3.8 Intrinsic dissolution rates of ACF salts. The number of times enhancement of IDR and AUC with respect to ACF is given in parentheses.

Compound	Molar extinction coefficient, ε /mM cm	Equilibrium Solubility (g/L)	IDR (mg/cm^2)/ min ($x10^{-3}$)	M.P. (°C)	$AUC_{0-1.5h}$ (mg h)/L	Coformer solubility in water (g/L)
ACF	9.41	0.174	0.022	151.4	105.3	0.058
ACF−CYT	11.61	2.85 (x 16.37)	0.256 (x11.64)	185.2	836.5 (x7.9)	7.7
ACF−PIP	8.33	---	0.076 (x3.46)	164.2	316.3 (x3.0)	1000
ACF−PIP−HYD	9.57	1.01 (x 3.56)	0.057 (x2.59)	162.4	218.5 (x2.1)	1000
ACF−LYS	9.26	27.23 (x 156.51)	2.97 (x135.0)	201.0	13451.1 (x127.7)	1500
ACF−GABA	10.28	---	2.48 (x 112.7)	135.5	6431.1 (x61.1)	1300

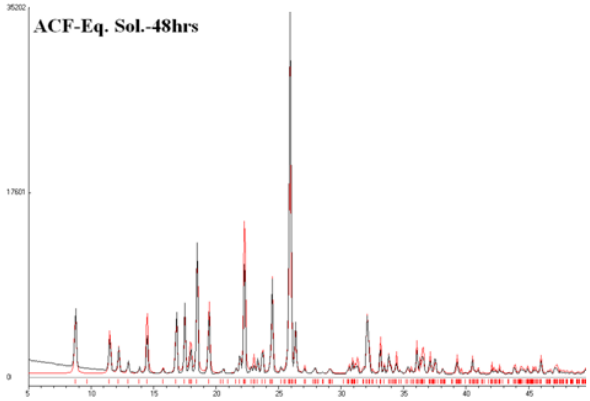

(a)

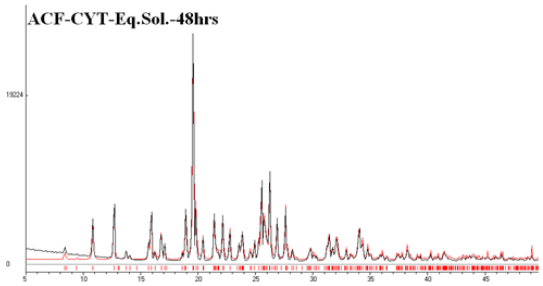

(b)

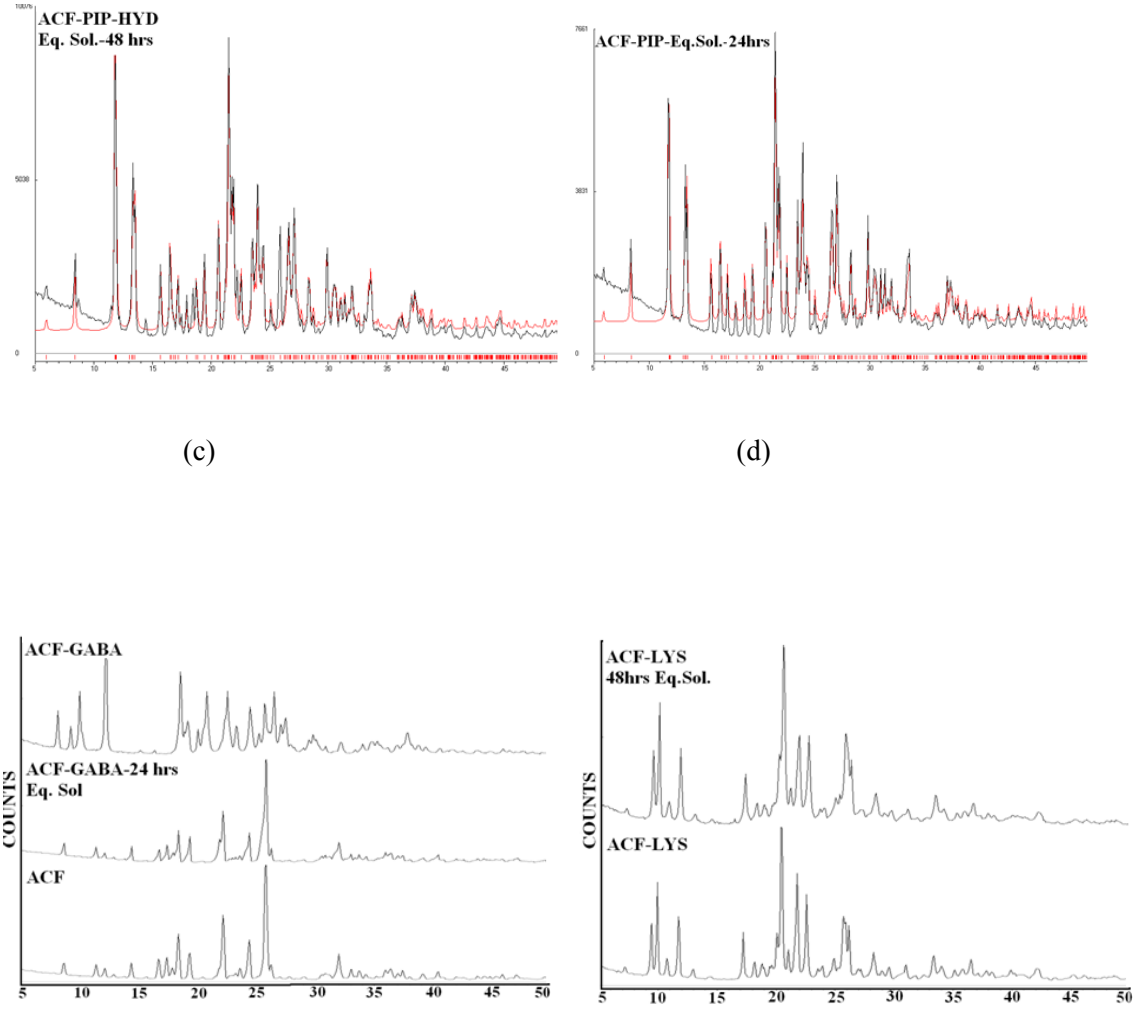

Figure 3.17 PXRD plots of ACF and its salts at the end of the equilibrium solubility experiment in 25% EtOH-Water medium. All the salts were found to be stable except ACF-PIP and ACF-GABA which converted to ACF-PIP-HYD and individual components respectively after 24hrs. Similar stability outcome was observed even at the end of dissolution experiments.

3.5 Conclusions

Slurry grinding of ACF with carefully selected GRAS coformers resulted in novel salts of higher solubility, dissolution and comparable solid form stability. The chemical transformation of ACF to the indolinone derivative under extreme acidic and basic pH was avoided by the use of weak organic bases. A large ΔpK_a of >6 resulted in salts with piperazine, lysine and GABA and moreover even a small ΔpK_a of 2.5 for cytosine also gave a salt. A reason for favorable salt formation with cytosine could be the two-point synthon between 2-aminopyrimidine and COOH group, which facilitates proton transfer. All the salts were characterized by thermal, spectroscopic and diffraction techniques. The stoichiometry of ACF-LYS and ACF−GABA for which single X-ray crystal data could not be obtained was established by ^{1}H NMR. The intrinsic dissolution rate of ACF−lysine is 135 times, solubility is 156 times, and AUC value 127 times higher than that of the reference crystalline drug. Solid form stability at accelerated ICH conditions of 40 ºC and 75% RH showed that ACF−LYS is stable for over 8 months. The ultimate aim of this work was to improve the solubility of ACF without affecting its solid form stability or cause chemical transformation and this was achieved through salt formation using mild basic coformers.

3.6 Experimental Section

ACF was obtained from Dalian HongRiDongSheng Import & Export Co. Ltd. (China). Coformers (purity > 99.8%) were purchased from Sigma-Aldrich (Hyderabad, India). Solvents (purity > 99%) were purchased from Hychem Laboratories (Hyderabad, India). Water filtered through a double deionized purification system (Aqua DM, Bhanu, Hyderabad, India) was used for all experiments.

Preparation of ACF solid forms ACF (212.4 mg) and 4,4'-BIP (46.8 mg) in 1:0.5 molar ratio were slurry ground in 5 mL of EtOH for 3 h. The formation of cocrystal hydrate was confirmed by PXRD, DSC and TGA. 30 mg of this material was dissolved in 5 mL EtOH

and left for slow evaporation at ambient conditions. Single crystals suitable for X-ray diffraction were obtained after 4-5 days.

ACF (212.4 mg) and CYT (66.6 mg) in 1:1 molar ratio were slurry ground in 5 mL EtOH for 3 h. Salt formation was confirmed by PXRD. 30 mg of this material was dissolved in 5 mL EtOH-CH_3CN 1:1 solvent mixture and left for slow evaporation at ambient conditions. Single crystals suitable for X-ray diffraction were obtained after 4-5 days.

ACF (70.8 mg) and PIP (8.6 mg) in 1:0.5 molar ratio was dissolved in 5 mL acetone and left for slow evaporation at ambient conditions. Single crystals suitable for X-ray diffraction were obtained after 4 h. The starting materials were crystallized in above conditions repeatedly to obtain the bulk material.

ACF (70.8 mg) and PIP (8.6 mg) in 1:0.5 molar ratio were slurry ground in 5mL EtOH for 3 h. The salt hydrate was formed based on PXRD, DSC and TGA. 30 mg of this material was dissolved in 5 mL EtOH-CH_3CN 1:1 solvent mixture and left for slow evaporation at ambient conditions. Single crystals suitable for X-ray diffraction were obtained after 4-5 days.

ACF (212.4 mg) and LYS (87.6 mg) in 1:1 molar ratio were slurry ground in 5 mL EtOH for 3 h. Salt formation was confirmed by PXRD and ^{1}H NMR.

ACF (212.4 mg) and GABA (61.8 mg) in 1:1 molar ratio were slurry ground in 5 mL EtOH for 3 h. Salt formation was confirmed by PXRD and ^{1}H NMR.

To a solution of 292 mg of LYS in 20 mL water, 708 mg of ACF was added with stirring. The solution was filtered through Whatmann filter paper and lyophilized. The ACF-LYS salt residue was obtained as an amorphous powder.

^{1}H NMR spectroscopy All ground products were characterized by ^{1}H NMR to confirm their stoichiometry. Proton NMR spectra were recorded on Bruker Avance 400 MHz spectrometer (Bruker-Biospin, Karlsruhe, Germany). Chemical shifts are quoted in δ scale and J coupling in Hz.

ACF-LYS (1:1) ^{1}H NMR (D_2O): 1.28 (2H, quintet, J 7.5), 1.51 (2H, quintet, J 7.5), 1.68 (2H, q, J 7.5), 2.78 (2H, t, J 7.5), 3.79 (2H, s), 4.28 (2H, s), 6.21 (1H, d, J 8), 6.83 (1H, t, J 8), 7.0 (1H, t, J 8), 7.11 (1H, t, J 8), 7.19 (1H, d, J 8), 7.39 (2H, d, J 8). COOHs and NHs of ACF and LYS exchange in solvent.

ACF-GABA (1:1) ^{1}H NMR (DMSO-d_6): 1.70 (2H, quintet, J 7.5), 2.27 (2H, t, J 7.5), 2.74 (2H, t, J 7.5), 3.81 (2H, s), 4.33 (2H, s), 6.22 (1H, d, J 8), 6.83 (1H, t, J 8), 7.0 (1H, t, J 8), 7.18 (1H, t, J 8), 7.20 (1H, d, J 8), 7.49 (2H, d, J 8). COOHs and NHs of ACF and GABA exchange in solvent.

Solid-state NMR spectroscopy Solid-state ^{13}C NMR spectra were recorded on Bruker Avance 400 MHz spectrometer (Bruker-Biospin, Karlsruhe, Germany, operating at 100 MHz for ^{13}C nucleus). ss-NMR measurements were carried out on Bruker 4-mm double resonance CP-MAS probe in zirconia rotors with a Kel-F cap at 5.0 kHz spinning rate with a cross-polarization contact time of 2.5 ms and a delay of 8 s. ^{13}C NMR spectra were recorded at 100 MHz and referenced to the methylene carbon of glycine, and then recalibrated to the TMS scale ($\delta_{glycine}$ = 43.3 ppm).

Solid form stability About 200 mg of each solid compounds was placed in an open petri dish and stored without a lid in a Thermolab T-908 stability chamber (Thermolab Instruments, Mumbai, India) pre-maintained at 40 °C and 75% RH (as per the WHO/ICH guidelines) for 8 months. Solid form stability and integrity of the samples was assessed periodically for every one week by PXRD.

Dissolution and solubility measurements The solubility curves of ACF salts were measured using the Higuchi and Connor method[54] in 25% ethanol-water medium at 30 °C. First, the absorbance of a known concentration of the salt was measured at the given λ_{max} (ACF 274 nm, ACF-CYT 270 nm, ACF-PIP 273 nm, ACF-PIP-HYD 273 nm, ACF-LYS 275 nm, ACF-GABA 274 nm) in 25% ethanol-water on Thermo Scientific Evolution 300 UV-vis spectrometer (Thermo Scientific, Waltham, MA). These absorbance values were plotted against several known concentrations to prepare the concentration vs. intensity

calibration curve. From the slope of the calibration curves, molar extinction coefficients for ACF salts were calculated. An excess amount of the sample was added to 6 mL of 25% ethanol-water. The supersaturated solution was stirred at 300 rpm using a magnetic stirrer at 30 °C. After 24 h, the suspension was filtered through Whatman's 0.45 µm syringe filter. The filtered aliquots were diluted sufficiently, and the absorbance was measured at the given λ_{max}. IDR experiments were carried out on USP-certified Electrolab TDT-08L dissolution tester (Mumbai, India). Dissolution experiments were performed for 1.5 h in 25% ethanol–water at 37 °C. Prior to IDR estimation, standard curves for all the compounds were obtained spectrophotometrically at their respective λ_{max}. The calculated molar extinction coefficients were used to determine the IDR values. For IDR measurements, 200 mg of the compound was taken in the intrinsic attachment and compressed to 0.5-cm^2 disk using a hydraulic press 4.0 ton/ in^2 pressure for 5 min. The intrinsic attachment was placed in a jar of 500 mL medium preheated to 37 °C and rotated at 150 rpm. 5 mL of the aliquot was collected at specific time intervals, and the concentration of the aliquots was determined with appropriate dilutions from the predetermined standard curves of the respective compounds. The IDR of the compound was calculated in the linear region of the dissolution curve (which is the slope of the curve or amount of drug dissolved/surface area of the disk) per unit time. The identity of the undissolved material after the dissolution experiment was ascertained by PXRD. The nature of the solid samples after disk compression and solubility/dissolution measurements were verified by PXRD.

3.7 References

1. (a) S. R. Byrn, R. R. Pfeiffer and G. G. Stowell, *Solid-State Chemistry of Drugs*, SSCI, West Lafayette, IN, 1999 (b) H. G. Brittain, *Physical Characterization of Pharmaceutical Solids*, Marcel Dekker Inc. NY, 1995.
2. (a) C. G. Smith and J. J. O'Donnell, *The Process of New Drug Discovery and Development. Informa*, Newyork, 2006 (b) J. Aaltonen, M. Allesø, S. Mirza, V. Koradia, K. C. Gordon and J. Rantanen, *Eur. J. Pharm. Biopharm.,* 2009, **71**, 23-37.

3. (a) S. Li, H. He, L. Parthiban, H. Yin and A. T. M. Serajuddin, *J. Pharm. Sci.,* 2005, **94**, 1396 (b) A. T. M. Serajuddin, *Adv. Drug Delivery Rev*., 2007, **59**, 603.
4. (a) D. Hörter and J. B. Dressman, *Adv. Drug Delivery Rev*., 1997, **25**, 3 (b) A. J. Aguiar, J. Krc, A. W. Kinkel and J. C. Samyn, *J. Pharm. Sci.,* 1967, **56**, 847-853.
5. C. R. Gardner, C. T. Walsh and Ö. Almarsson, *Nat. Rev. Drug Disc*., 2004, **3**, 926.
6. (a) R. Mullin, *Chem. Eng. News,* 2012, **90**, 15 (b) M. May, *Nature Med*., 2009, **15**, 1243 (c) L. F. Joseph and J. M. Hale, *Pharm. Times,* 2012, **78**, 124.
7. (a) S. M. Berge, L. D. Bighley and D. C. Monkhouse, *J. Pharm. Sci.,* 1977, **66**, 1 (b) B. Sarma, R. Thakuria, N. K. Nath and A. Nangia, *CrystEngComm*, 2011, **13**, 3232-3240 (c) J. B. Nanubolu, B. Sridhar, K. Ravikumar and S. Cherukuvada, *CrystEngComm*, DOI: 10.1039/C3CE00022B (d) W. Ong, E. Y. Cheung, K. A. Schultz, C. Smith, J. Bourassa and M. B. Hickey, *CrystEngComm*, 2012, **14**, 2428.
8. S. R. Perumalla, L. Shi and C. C. Sun, *CrystEngComm*, 2012, **14**, 2389.
9. (a) E. H. Lee, S. X. M. Boerrigter, A. F. C. Rumondor, S. P. Chamarthy and S. R. Byrn, *Cryst. Growth Des.,* 2008, **8**, 91-97. (b) J. An, J. Kim, S. Chang and W. Kim, *Cryst. Growth Des.,* 2010*,* **10***,* 3044 (c) X. X. Li, X. D. Xu, Y. Y. Den, J. Feng, L. Ge, L. M. Zhang, *Cryst. Res. Technol.,* 2008, **43**, 1062 (c) M. L. Pusey, M. S. Paley, M. B. Turner and R. D. Rogers, *Cryst. Growth Des.,* 2007, **7**, 787.
10. S. Sweetana and M. J. Akers, *J. Pharm. Sci. Tech*., 1996, **50**, 330.
11. R. Thakuria and A. Nangia, *CrystEngComm*, 2011, **13**, 1759-1764.
12. J. Galcera and E. Molins, *Cryst. Growth Des.,* 2009, **9**, 327-334.
13. (a) R. Banerjee, P. M. Bhatt, N. V. Ravindra and G. R. Desiraju, *Cryst. Growth Des.,* 2005, **5**, 2299-2309 (b) P. M. Bhatt, N. V. Ravindra, R. Banerjee and G. R. Desiraju, *Chem Commun*, 2005, **8**, 1073-1075.
14. A. Portell, R. Barbas, M. Font-Bardia, P. Dalmases, R. Prohens and C. Puigjaner, *CrystEngComm*, 2009, **11**, 791-795.
15. M. L. Cheney, N. Shan, E. R. Healey, M. Hanna, L. Wojtas, M. J. Zaworotko, V. Sava, S. Song and J. R. Sanchez-Ramos, *Cryst. Growth Des*., 2010, **10**, 395-405.
16. (a) N. R. Goud, S. Gangavaram, K. Suresh, S. Pal, S. G. Manjunatha, S. Nambiar and A. Nangia, *J. Pharm. Sci.,* 2012, **101**, 664 (b) G. Bolla and A. Nangia, *Cryst.*

Growth Des., 2012, **12**, 6250-6259 (c) S. Basavoju, D. Bostrom and S. P. Velaga, *Cryst. Growth Des.*, 2006, **6**, 2699-2708.

17. (a) British Pharmacopoeia, The Stationary Office, MHRA, British Pharmacopoeial Commission Office, London, 2005 (b) J. E. F. Reynolds, *Martindale: The Complete Drug Reference*, Massachusetts, 1999.
18. (a) B. Lee and H. Jung, *Pharm. Sci. Suppl.,* 1999, **4**, 14 (b) T. Kim, J. Shin and B. Lee, *AAPS Annual Meeting*, Denver, Colorado, 2001.
19. M. Sevukarajan, S. S. Parveen, R. Nair and T. M. Badivaddin, *J. Pharm. Sci. Res*. 2011, **3**, 1280.
20. N. W. Kim and J. Il, *Novel Amino acid Salt of Aceclofenac having high bioavailability and Pharmaceutical preparation comprising the same as Active Ingredient*. Patent No. 1020050005894A, Korean Industrial Property Office, Korea, 2003.
21. F. A. Maulvi, S. J. Dalwadi, V. T. Thakkar, T. G. Soni, M. C. Gohel and T. R. Gandhi *Powder Technol*., 2011, **207**, 47 (b) S. S. Shinde, S. S. Patil, F. I. Mevekari and A. S. Satpute, *Int. J. Adv. Pharm. Sci.,* 2010, **1**, 299.
22. M. Sevukarajan, B. Thanuja, S. Riyaz and N. Rahul, *J. Pharm. Sci. Res*., 2011, **3**, 1288.
23. (a) A. V. Casas, R. Rue du, *New 2-((2,6-dichlorophenyl)amine)phenylacetoxyacetyl derivatives, the process for preparing the same and their use in therapeutics.* Patent No. EP0119932A1, European Patent Office, Barcelona, 1984 (b) A. Sallmann, *New Salts of 2-[(2,6-dichlorophenyl)amine]phenylacetoxyacetic acid with organic basic cations*. Patent No. US005708024A, United States patent office, 1998.
24. S. Azhlawar and T. K. Ravi, *Int. J. Pharm. Pharm. Sci*., 2011, **3**, 245.
25. (a) G. R. Desiraju, J. J. Vittal and A. Ramanan, *Crystal Engineering. A Textbook,* World Scientific Publishing, Singapore, 2011 (b) G. R. Desiraju, *Crystal Engineering. The Design of Organic Solids*. Elsevier, 1989.
26. (a) P. Sanphui, N. R. Goud, U. B. R. khandavilli, S. Bhanoth and A. Nangia, *Chem Commun*, 2011, **47**, 5013-5015 (b) S. Aitipamula, P. S. Chow and R. B. H. Tan, *CrystEngComm*, 2009, **11**, 1823-1827.

27. (a) N. Schultheiss, and A. Newman, *Cryst. Growth Des.,* 2009, **9**, 2950. (b) W, Jones W. D. S. Motherwell and A. V. Trask, *MRS Bull.,* 2006, **31**, 875. (c) M. K. Stanton and A. Bak, *Cryst. Growth Des*., 2008, **8**, 3856. (d) M. K. Stanton, S. Tufekcic, C. Morgan and A. Bak, *Cryst. Growth Des*., 2009, **9**, 1344.
28. (a) G. R. Desiraju, *Angew. Chem. Int. Ed. Engl.,* 1995, **34**, 2311-2327. (b) Ö. Almarsson and M. J. Zaworotko, *Chem Commun,* 2004, **17**, 1889. (c) R. D. B. Walsh, M. W. Bradner, S. Fleischman, L. A. Morales, B. Moulton, N. Rodríguez-Hornedo and M. J. Zaworotko, *Chem Commun*, 2003, 186.
29. GRAS chemicals list may be accessed at www.fda.gov/Food/FoodIngredientsPackaging/GenerallyRecognizedasSafeGRAS/GRASSubstancesSCOGSDatabase/default.htm
30. (a) A. V. Trask and W. Jones, *Top. Curr. Chem*., 2005, **254**, 41. (b) N. Shan, F. Toda, and W. Jones, *Chem Commun*, 2002, **20**, 2372.
31. (a) C. B. Aakeroy, M. E. Fasulo and J. Desper, *Mol. Pharmaceutics*, 2007, **4**, 317. (b) B. Sarma, N. K. Nath, B. R. Bhogala and A. Nangia, *Cryst. Growth Des*., 2009, **9**, 1546. (c) S. L. Childs, G. P. Stahly and A Park, *Mol. Pharmaceutics,* 2007, **4**, 323. (d) A. J. Cruz-Cabeza, *CrystEngComm,* 2012, **14**, 6362.
32. A. Alvarez-Larena, J. F. Piniella, E. Carrasco, A. Ginebreda, S. Julia and G. Germain, *J. Crystallogr. Spec. Res*., 1992, **22**, 323.
33. G. L. Perlovich, A, O. Surov, L.K. Hansen and A. Bauer-Brandl, *J. Pharm. Sci*., 2007, **96**, 1031.
34. (a) X. Chen, K. R. Morris, U. J. Griesser, S. R. Byrn and J. G. Stowell, *J. Am. Chem. Soc*., 2002, **124**, 15012. (b) P. J. Cox and P. L. Manson, *Acta Crystallogr. Sect. E,* 2003, **59**, 986.
35. (a) S. S. Kuduva, D. C. Craig, A. Nangia and G. R. Desiraju, *J. Am. Chem. Soc*., 1999, **121**, 1936. (b) D. Das, R. K. R. Jetti, R. Boese and G. R. Desiraju, *Cryst. Growth Des*., 2003, **3**, 675. (c) D. Das, G. R. Desiraju, *Chem. – Asian J*., 2006, **1**, 231.
36. a) J. Bernstein, R. E. Davis, L. Shimoni and N. L. Chang, *Angew. Chem., Int. Ed. Engl*., 1995, **34**, 1555. (b) M. C. Etter, *Acc. Chem. Res*., 1990, **23**, 120. (c) M. C. Etter, *J. Phys. Chem*., 1991, **95**, 4601.

37. P. Sanphui, G. Bolla, U. Das, A. K. Mukherjee and A. Nangia, *CrystEngComm,* 2013*,* **15***,* 34.
38. (a) M. C. Etter, J. C. Macdonald and J. Bernstein, *Acta Crystallogr. Sect. B, 1990*, **46**, 256 (b) M. C. Etter and S. M. Reutzel, *J. Am. Chem. Soc*., 1991, **113**, 2586.
39. a) J. S. Stevens, S. J. Byard and S. L. M. Schroeder, *J. Pharm. Sci*., 2010, **99**, 4453 (b) Z. J. Li, Y. Abramov, J. Bordner, J. Leonard, A. Medek and A. V. Trask, *J. Am. Chem. Soc*., 2006, **128**, 8199.
40. P. Sanphui, G. Bolla and A. Nangia, *Cryst. Growth Des*., 2012, **12**, 2023.
41. (a) A. Nangia, *Acc. Chem. Res*., 2008, **41**, 595 (b) N. J. Babu, S. Cherukuvada, R. Thakuria and A. Nangia, *Cryst. Growth Des*., 2010, **10**, 1979.
42. (a) J. F. Remenar, M. L. Peterson, P. W. Stephens, Z. Zhang, Y. Zimekov and M. B. Hickey, *Mol. Pharmaceutics,* 2007, **4***,* 386. (b) S. Karki, T. Friščić, L. Fábián, and W. Jones, *CrystEngComm,* 2010, **12**, 4038.
43. (a) R. M. Silverstein, *Spectrometric Identification of Organic Compounds*. 6th Ed.; John Wiley & Sons, Inc.: New York, 2002. (b) E. Smith and G. Dent, *Modern Raman Spectroscopy, A Practical Approach*, John Wiley: New York, 2005.
44. (a) F. G. Vogt, J. S. Clawson, M. Strohmeier, A. J. Edwards, T. N. Pham and S. A. Watson, *Cryst. Growth Des.,* 2009, **9**, 921. (b) D. Braga, L. Maini, G. de Sanctis, K. Rubini, F. Grepioni, M. R. Chierotti and R. Gobetto, *Chem – Eur. J*., 2003, **9**, 5538.
45. (a) S. Strydom, W. Liebenberg, L.Yu, and M. de Villiers, *Int. J. Pharm*., 2009, **379**, 72-81 (b) T. Miyazaki, S. Yoshioka, Y. Aso and T. Kawanishi, *Int. J. Pharm*., 2007, **336**, 191-195.
46. Stability testing of Active Pharmaceutical Ingredients and Finished Pharmaceutical Products, WHO Technical Report Series, No. 953, http://www.ich.org/fileadmin/Public_Web_Site/ICH_Products/Guidelines/Quality/Q1F/Stability_Guideline_WHO.pdf
47. J. F. Remenar, S. L. Morissette, M. L. Peterson, B. Moulton, J. M. MacPhee, H. R. Guzmán and Ö Almarsson, *J. Am. Chem. Soc.,* 2003, **125**, 8456-8457.
48. (a) T. Takagi, C. Ramachandran, M. Bermejo, S. Yamashita, L. X. Yu and G. L. Amidon, *Mol. Pharmaceutics,* 2006, **3**, 631 (b) C. A. Lipinski, Solubility in Water and DMSO: issues and potential Solutions. *In Pharmaceutical Profiling in Drug*

Discovery for Lead Selection: R. T. Borchardt, E. H. Kerns, C. A. Lipinski, D. R. Thakker and B. Wang, Eds.; AAPS Press: Arlington, VA, 2004, pp. 93-125.

49. S. L. Childs, N. Rodríguez-Hornedo, L. S. Reddy, A. Jayasankar, C. Maheshwari, L. McCausland, R. Shipplett and B. C. Stahly, *CrystEngComm*, 2008, **10**, 856.
50. J. B. Dressman, G. L. Amidon, C. Reppas and V. P. Shah, *Pharm. Res*., 1998, **15**, 11.
51. L. X. Yu, A. S. Carlin, G. L. Amidon and A. S. Hussain, *Int. J. Pharm*., 2004, **270**, 221.
52. (a) R. Abramowitz and S. H. Yalkowsky, *Pharm. Res*., 1990, **7**, 942 (b) D. J. Good and N. Rodríguez-Hornedo, *Cryst. Growth Des*., 2009, **9**, 2252.
53. (a) P. H. Su, J. Y. Chen, C. M. Su, T. C. Huang and H. S. Lee, *Pediatr. Int*., 2003, **45**, 665 (b) G. Geisslinger, K. Dietzel, H. Bezler, B. Nuernberg and K. Brune, *Int. J. Clin. Pharmacol. Ther. Toxicol.,* 1989, **27**, 324.
54. T. Higuchi, K. A. Connors, *Adv. Anal. Chem. Instrum*., 1965, **4**, 117.

CHAPTER FOUR

POLYMORPHISM IN SULFACETAMIDE-ACETAMIDE COCRYSTAL

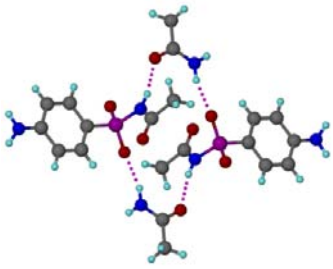

Form 1

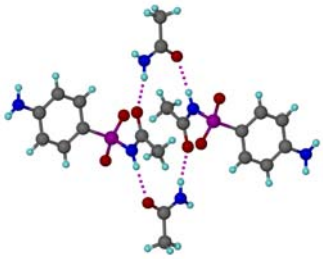

Form 2

Synthon and Packing Polymorphs

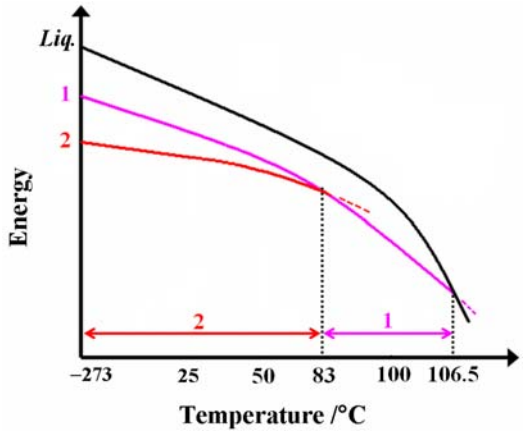

Semi-quantitative free energy vs. temperature diagram to show the polymorphic transformations and relative stability of Sulfacetamide-Acetamide cocrystal polymorphs. Form 2 is the stable polymorph at –273°C. It has the lowest free energy between 25-83°C; Form 1 is the stable polymorph above 83°C until it melts at 106 °C.

4.1 Introduction

The phenomenon of polymorphism continues to play a pivotal role in pharmaceutical solid-state industry with its ability to modulate the physicochemical properties of Active Pharmaceutical Ingredients (APIs)[1]. Polymorphs of a drug molecule offer diversity in terms of solubility, dissolution, flowability etc. in addition to a provision for patent protection[1c,2]. While numerous literature reports highlight the importance of polymorphism in single component API's and organic compounds[1,3], similar studies on the multicomponent cocrystals are relatively less[4]. Of late, there has been a renewed interest in the polymorphism of multi-component cocrystals since it offers a viable option to expand the structural landscape of a molecule for application in the fields of optical[5], material[6], pharmaceutical[7] and organic synthesis[8]. MacGillivray and coworkers[9] obtained three polymorphs of *all-trans*-2,5-bis(4-ethenylpyridyl)thiophene (DVPT) and 4-hexylresorcinol (4HR) cocrystal, which exhibited reversible and concerted reorganizations upon heating and cooling. The reorganizations are postulated to proceed through three motions comprising alkyl translations, olefin rotations and rotational tilts. The movements were shown to be collective, being propagated in close packed repeating units. This discovery was shown as a major step in understanding how organic solids can support the development of crystalline molecular machines and devices.

Apart from this notable application of cocrystal polymorphs, both polymorphism and cocrystallization have been identified as 'good cobuilders' in pharmaceutical industry since both are favored by an affinity to form various hydrogen bonds with implications in modulating physicochemical properties and solid form optimization of API's[10]. Srinivasulu et.al.[11] reported the first trimorphic cocrystal of API's including Ethenzamide (EA), and Gentisic Acid, (GA) where significant differences were observed in the packing and conformation of polymorphs. The cocrystal polymorphs showed good dissolution profile in comparison to EA. The dissolution advantage in combination with simple and convenient preparation methods was shown to favor these multi API cocrystals as potential solids for delivery of combination drugs (Figure 4.1).

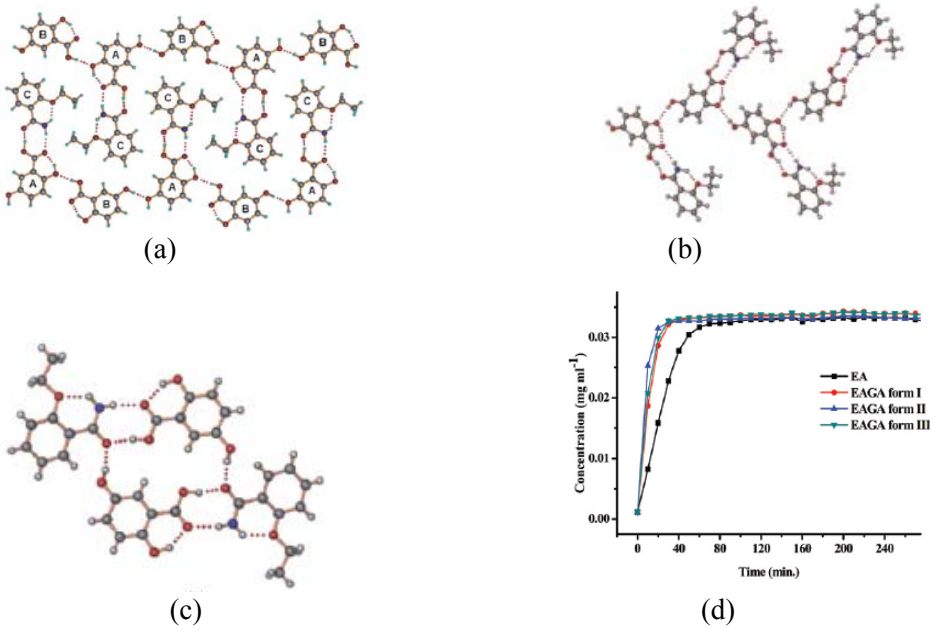

Figure 4.1a) Zipper like structure of EA-GA form 1. **b)** Hydrogen bonded linear tape in the crystal structure of form II. **c)** A hydrogen bonded tetrameric motif in the crystal structure of form III. **d)** Dissolution profile of cocrystal polymorphs in comparison to EA showed ~2 times increment in dissolution rate (Adapted from ref. 11).

On the downside, these crystalline modifications may pose problems for controlled production, stability, formulation and storage[2]. Consequently, apart from the traditional methods like powder X-ray diffraction (PXRD) and Infrared spectroscopy, much of the research effort is now placed on novel methods[12] of characterizing polymorphs for reliable identification of the optimum solid form. Different groups identified various methods for discovering, stabilizing and optimizing cocrystal polymorphs. Ter Horst et. al.[13] prepared two polymorphs of Carbamazepine-nicotinamide cocrystal through solvent mediated transformation process by suspending dry mixture of the pure crystalline components in ethanol. In accordance with the Ostwald's 'rule of steps'[14] metastable polymorph appeared first followed by the stable polymorph which grew at the expense of metastable phase. Jones and coworkers[4a] developed a novel approach to preparing pharmaceutical cocrystals involving crystallization at solvent-solvent interface which was employed to produce a thermodynamically stable polymorph of phenazine: mesaconic acid system. Tan and

colleagues[15] identified two new polymorphs of Ethenzamide-Ethyl malonic acid cocrystal where the polymorphic outcome of the grinding experiments was remarkably dependent on the polarity of the solvent used to assist grinding. Various other research groups[16] highlighted the importance of thermal, slurry and grinding methods as stability indicators for classifying polymorphs into kinetic and thermodynamic phases. Poor screening of polymorphism in cocrystals could be an impending factor since it may lead to accidental phase transformation which might significantly affect their solubility, stability and bioavailability. These literature reports highlight the importance of applying diverse screening methods for obtaining polymorphs of cocrystals and establishing their stability relationships in order to develop the stable pharmaceutical cocrystal.

4.2 CSD analysis of –SO_2NHCO- group and literature reports on Sulfacetamide

The –SO_2NHCO- group occupies a place of prominence in drug molecules, being a common functional moiety of Tolbutamide, Glimepiride, Torasemide, Chlorpropamide etc. A CSD search for molecules with –SO_2NHCO– skeleton showed 1528 hits. Among them only five single component (refcodes: BEDMIG, TOHBUN, TORSEM, ZZZPUS, MAZTAJ) and two multi-component systems (refcodes: UNEZAO, VUHFIO) showed polymorphism. Therefore there are few cases of polymorphism in –SO_2NHCO– containing compounds. Exploring the structural outcome in this group of molecules through polymorphs is highly essential to understand the diversity in their packing and synthons patterns. This would enable us to have a better understanding of the hydrogen bonding interactions which would be helpful in discovering novel solid forms for pharmaceutical applications. Therefore we have set out to discover novel polymorphs of single and multicomponent systems of a representative drug molecule belonging to this group and determine the stability relationship between them. For this purpose we have chosen an antibacterial drug, Sulfacetamide (Scheme 4.1, SACT hereafter). SACT belongs to the class of sulfonamide antibacterial drugs and has been extensively documented for its usage in treating ophthalmic injuries and dermatitis[17]. It has been investigated as a therapeutic agent for the treatment of pityriasis versicolor and rosacea[18]. Recent reports indicate that it may act as antifungal drug by a

CYP51A1-independent mechanism[19]. The sodium salt of SACT is used as a topical treatment for ophthalmic infections. SACT is active against both Gram-positive and Gram-negative bacteria. It competitively inhibits the generation of Para-aminobenzoic acid causing interference of bacterial DNA synthesis[20]. In literature, crystal structures of SACT guest free form, sodium salt monohydrate, silver salt, and a cocrystal with caffeine are reported[21]. SACT do not have a reported history of polymorphism either as a single component or through its multicomponent cocrystals. Our idea was to explore polymorphism in cocrystals of SACT in addition to the parent compound itself. This would enable us to have a better understanding of the synthon and packing diversity in $–SO_2NHCO–$ containing molecules which would have implications in developing solid forms of related molecules for pharmaceutical applications.

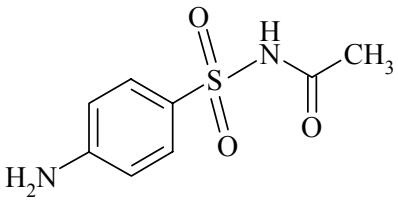

Scheme 4.1 Molecular structure of SACT

4.3 Preparation of cocrystal polymorphs

In order to discover novel polymorphs of SACT, we have used common polymorph screening techniques like solution crystallization from various solvents and solvent mixtures at different temperatures, melt crystallization and seeding with structurally similar molecules. Inspite of numerous attempts using above techniques, we could not obtain polymorphs of SACT. Then we have focused our attention on preparing multicomponent solid forms of SACT and discover their polymorphs. Various solid form screening methods like mechanochemical grinding, slurry grinding and fast evaporation under controlled vacuum (rotary evaporator) conditions were used to prepare cocrystals[7c,23]. On subjecting SACT and different GRAS[24] coformers to above methods in various stoichiometric ratios we

obtained novel cocrystals with theophylline, isonicotinamide, 4,4′-bipyridine, acetamide and a salt with 4-aminopyridine. We adopted solution crystallization method from various solvents and solvent mixtures to discover polymorphs of these cocrystals. After several crystallization experiments, we obtained two polymorphs of a 1:1 SACT-Acetamide (ACT) cocrystal. The other cocrystals which did not result in polymorphs are discussed in chapter 6.

4.4 CSD analysis of polymorphic cocrystals

Although popularly used as a coformer for solubility enhancement of poorly soluble drugs and by itself a polymorphic[25] molecule, ACT did not show even a single hit under the category of cocrystal polymorphs when a CSD analysis (Aug. 2012 update) revealed 78 pairs of polymorphic cocrystals till date (Table 4.1). Hence, this will be the first cocrystal polymorph pair with acetamide as one of the component. Based on the recent literature, although a polymorphic compound is shown to have higher probability of forming cocrystals[26], but it remains unclear whether a compound needs to be polymorphic in order to obtain polymorphs of its cocrystals. To resolve the ambiguity we have analyzed the individual components of the cocrystal polymorphs for polymorphism. The analysis revealed that of the 78 pairs of cocrystal polymorphs, 37 pairs have at least one of their components being polymorphic, 6 of them have both and 35 pairs have none of the components showing polymorphism (Table 4.1). Therefore although 43 (55.1%) pairs of cocrystal polymorphs have either one or more of the components showing polymorphism, it is not significantly higher compared to the 35 (44.9%) cocrystals where none of the components have polymorphic nature. Although this classification comes with a caution since the extent of search for polymorphs of a compound could differ, but as such these statistics show that more than the polymorphic ability of the individual compounds it is the molecular flexibility, intermolecular functional group complementarity, synthon robustness, and structural fit that determines polymorphism in cocrystals[26b,27]. Both the SACT-ACT polymorphs were characterized by single and powder X-ray diffraction, Differential scanning calorimetry (DSC), IR, Raman, Solid state NMR, Variable temperature PXRD and Hot stage microscopy

(HSM). Solubility advantage of these polymorphic cocrystals was ascertained by performing solubility and dissolution experiments.

Table 4.1 List of 78 Polymorphic cocrystals (Aug 2012 update) *

ABEKUN	ABUNIU	ACOYOG	**AJAJEA**	***AWIHOE***
ANTCYB	**ANUMEC**	**BIVSIJ01**	**BONTON**	CAZLAR
COHWIF	**DINPAR**	DOKGUG	**DURZAR**	EFOZAB
ELEGUY	**ENAZOI**	**EPUPUB**	EXUQUJ	**FAHLEF**
FIHYEA	**HADKUT**	**HORXOB**	IJETOG	**IJIBEJ**
KIBQOC	**KIHYOQ**	**LOCVOO**	***LOFKIB***	**MIYKOU**
MOXVIF	MUROXA	**NAPYMA**	***NARSOP***	NITRIR
NOVSIA	**NUGZEV**	**NUJVUJ**	**NUKWEW**	**NUKXEX**
ODOBIT	PTZTCQ	QUIDON	QULLUF	***RIFQAY***
RIWWEA	RURROM	**SAYMUB**	**SEOTCR**	**TAMBUE**
TECCAF01	**TEHNAW**	TIPWIY	**TONDUV**	TUPRBN01
ULAWAF	UNEZAO	**VAKTOS**	VEJXAJ	**VUHFIO**
VUJSOJ	WANNUV	**WATREP**	WOBQEK	**WOTZAG**
WUZHOP	**XETZIG**	XOLHUC	YABHAM	ZODWIY
ZZZGMW01	EWAPAU	**EXAPID**	**POTREV**	UBUJIM
PANQUS	YASGOQ	WOQBAF		

*Refcodes in normal font represent the set of cocrystal polymorphs were one of the component is polymorphic, those in bold italics stand for the cocrystal polymorphs where both the components exhibit polymorphism and the rest of them in bold font come under the category of cocrystal polymorphs where none of the individual components have reported polymorphic nature.

4.5 Results and Discussion

Experimentally tested facts like the compounds with high Z′ polymorphs have higher probability of forming cocrystals than those with low Z′ structures[26c,d], and certain CSD based statistics like polymorphic compounds as such are better suited for forming cocrystals than non-polymorphic compounds[26a,b], are useful criteria in selecting a compound for cocrystallization study. Nevertheless, numerous exceptions to these criteria warrant a better strategy for cocrystal formation. Moreover, SACT do not qualify the above criteria for cocrystallization since it is not polymorphic, yet it has a reported cocrystal with caffeine[21c].

In such cases, supramolecular synthon strategy is by far the better yard stick for forming cocrystals where crystal engineering principles[28] and hydrogen bonding rules[29] form the design elements for their preparation. The principle functional moieties in SACT molecule are sulfonamide, carboxamide and amine. Among these, carboxamide is shown to form heterosynthons with diverse functional groups like acid, amide, amine, pyridine etc. Ranking in terms of their probability of occurrence, amide-acid heterosynthon scores very high with its robustness[30].

Based on our CSD analysis of cocrystal polymorphs we made an interesting observation in terms of the acid-amide synthon robustness. We found that of the 78 cocrystal polymorph sets reported in the CSD, 25 of them contain amide (carboxamide and sulfonamide) functional group (Table 4.2). In this subgroup of cocrystal polymorphs, 13 cocrystals were formed by hydrogen bonding with –COOH containing coformers (52%, refcodes in normal font in Table 4.2), 5 with amide coformers (20%, refcodes in bold font in Table 4.2) and 7 with other functional groups (28%) (refcodes in bold italics in Table 4.2). This analysis would not only strengthen the empirically proved fact that acid-amide functional groups form a reliable heterosynthon but also hint at the diversity in the hydrogen bonding patterns and packing arrangements offered by this synthon, resulting in polymorphism in cocrystals.

Table 4.2 Refcodes of Cocrystal polymorphs containing sulfonamide or carboxamide functional groups in one of their components (25 pairs)

TUPRBN	EXUQUJ	IJIBEJ	MOXVIF	MUROXA
NUKXEX	QULLUF	TIPWIY	ULAWAF	VAKTOS
VEJXAJ	WUZHOP	ZODWIY	YASGOQ	***XETZIG***
EFOZAB	**LOFKIB**	**UNEZAO**	**VUHFIO**	**EXAPID**
AJAJEA	***WOBQEK***	***YABHAM***	***ANUMEC***	***HADKUT***

With this backdrop we performed mechanochemical grinding[23a,d] and solution crystallization of SACT with various GRAS coformers. Inspite of the carboxamide group affinity for –COOH functional moieties, we did not obtain any cocrystals with acid coformers. Instead, on liquid assisted grinding[23a,d] of SACT with amide coformers we obtained novel solid forms with acetamide, theophylline, isonicotinamide, 4,4′-bipyridine, caffeine and 4-amino

pyridine. In order to obtain single crystals of these solid forms we used solution crystallization technique. Although a commonly used technique for cocrystal preparation, solution crystallization carries the disadvantage of having incongruent solubilities of the starting materials in a particular solvent resulting in the crystallization of the components separately. A recent article highlighted the use of solvent-solvent interface approach for the preparation of cocrystals[4a]. Inspite of several solution crystallization experiments of SACT cocrystals in different solvents, the crystals obtained did not indicate polymorphic diversity based on their cell parameters. But on crystallizing from toluene-ethyl acetate solvent mixture and ethyl acetate-methyl ethyl ketone solvent mixture we obtained the two polymorphs of SACT-ACT 1:1 cocrystal. In accord with the aim of this chapter i.e. to discover novel polymorphs of -SO_2NHCO- containing molecule, analyze their synthon and packing differences and determine the stability relationship between them, we have restricted our discussion in this chapter to SACT-ACT cocrystal polymorphs. The other non-polymorphic cocrystals are discussed in chapter 6.

Bulk scale production of SACT-ACT form 1 for further analysis was done by dissolving stoichiometric amounts of individual components in acetone and evaporating the solution under vacuum using a rotary evaporator. Form 2 was obtained by ball mill grinding of the stoichiometric amounts of individual components. PXRD patterns of both the forms obtained in bulk scale matched very well with their calculated patterns (Figure 4.2). The crystallographic parameters of the polymorphs are listed in Table 4.3 and their neutron-normalized hydrogen bonding distances in Table 4.4.

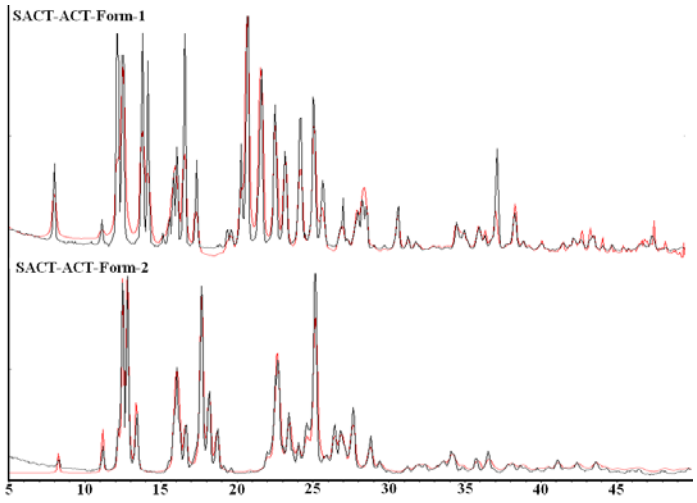

Figure 4.2 PXRD patterns of SACT-ACT polymorphs match very well with their calculated patterns indicating bulk scale purity.

Table 4.3 Crystallographic parameters of SACT-ACT cocrystal polymorphs

	SACT-ACT Form 1	SACT-ACT Form 2
Emp form.	$C_{10}H_{15}N_3O_4S$	$C_{10}H_{15}N_3O_4S$
Form wt	273.31	273.31
Cryst syst	Monoclinic	Monoclinic
Sp gr	$P2_1/c$	$C2/c$
T/K	298(2)	298(2)
a/Å	11.2134(6)	22.2392(16)
b/Å	7.7976(4)	8.4705(4)
c/Å	16.1280(7)	14.7710(11)
α/°	90.00	90.00
β/°	103.260(5)	107.056(8)
γ/°	90.00	90.00
Z	4	8
V/Å^3	1372.59(12)	2660.1(3)
Rflns collect	5157	4513
Unique rflns	2334	2256
Obsd rflns	1606	1741
Parameters	185	185
R_1	0.0511	0.0462
wR_2	0.1287	0.1203
GOF	1.017	1.048

Table 4.4 Hydrogen bond parameters of SACT-ACT cocrystal polymorphs. O–H, N–H and C–H distances are neutron-normalized to 0.983, 1.009 and 1.083Å respectively

D–H···A	D···A (Å)	H···A (Å)	D–H···A (°)	symmetry code
SACT-ACT-FORM-1				
N1–H1A···O2	3.107(4)	2.18	153	x, 1/2–y,1/2+z
N1–H1B···O4	3.011(4)	2.02	166	x, 1/2–y,1/2+z
N2–H2A···O4	2.762(4)	1.76	172	1–x, 1–y, –z
N3–H3A···O1	2.918(4)	1.92	169	1+x, y, z
N3–H3B···O3	3.134(5)	2.23	148	1–x, –1/2+y,1/2–z
C8–H8C···O1	3.361(5)	2.42	144	–x, 1–y, –z
SACT-ACT-FORM-2				
N1–H1A···O2	3.178(4)	2.19	164	x, –1+y, z
N1–H1B···O4	2.986(4)	1.98	178	1/2+x, –1/2+y, z
N2–H2A···O4	2.777(3)	1.77	177	1/2–x, 3/2–y, –z
N3–H3A···O3	3.033(3)	2.29	129	1/2–x, 1/2–y, –z
N3–H3B···O3	3.013(4)	2.01	174	1/2–x, 1/2–y, –z

4.5.1 Crystal Structure Analysis

Sact-Act-Form-1 Cocrystallization of SACT and ACT in 1:1 ratio in ethyl acetate-methyl ethyl ketone solvent mixture afforded block shaped crystals of form 1 which solved and refined in monoclinic $P2_1/c$ space group. A tetrameric ring formed by the interaction of 2 molecules each of SACT and ACT is the prominent motif in this polymorph. This motif is sustained by four N–H···O hydrogen bonds where the syn N–H of ACT interacts with sulfonamide oxygen (N3···O1, 1.92Å, 169°) and amide N–H of SACT is bound to ACT carbonyl oxygen (N2···O4, 1.76Å, 172°). As a result two each of N–H···$O_{sulfonamide}$ and N–H···$O_{carbonyl}$ units bind the tetrameric motif (Figure 4.3a). Apart from this, the bifurcated acetamide $O_{carbonyl}$ forms an N–H···O hydrogen bond (N1···O4, 2.02Å, 166°) with the aniline N–H of neighboring SACT extending the tetrameric units into the 2D lattice (Figure 4.3b). Other primary N–H···O hydrogen bonds between the aniline N–H with the neighboring SACT $O_{sulfonamide}$ (N1···O2, 2.18Å, 153°) and those between ACT N–H and SACT $O_{carbonyl}$ (N3···O3, 2.23Å, 148°) along with the auxiliary C–H···O hydrogen bonds (C8···O1, 2.42Å, 144°) stabilize the crystal lattice (Figure 4.3c).

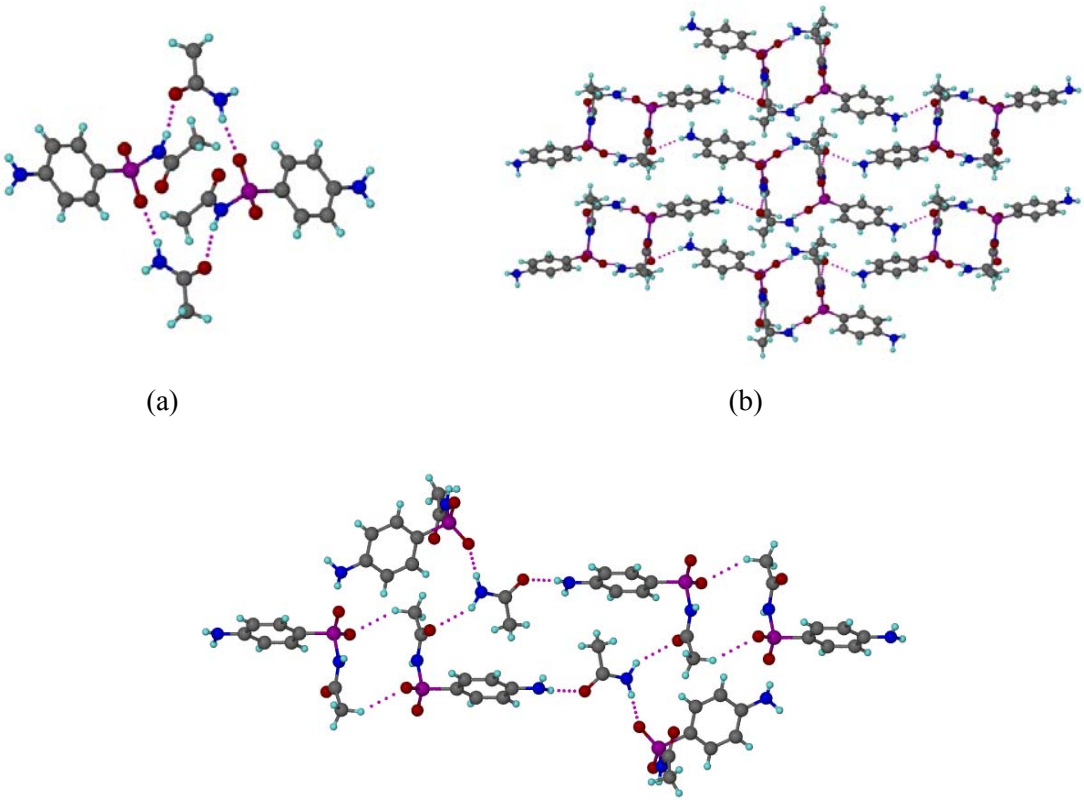

(a) (b)

(c)

Figure 4.3a) Tetrameric ring motif connected through two each of one point N–H···$O_{sulfonamide}$ and N–H···$O_{carbonyl}$ hydrogen bonds. **b)** The one point N2–H2A···O4 hydrogen bond extends the tetrameric motifs into the 2D and 3D lattice. **c)** One point N–H···O and C–H···O hydrogen bonds stabilize the crystal lattice.

Sact-Act-Form-2 Cocrystallization of SACT and ACT in 1:1 ratio in ethyl acetate-toluene solvent mixture afforded plate shaped crystals of form 2 which solved and refined in monoclinic *C*2/*c* space group. Similar to form 1, the tetrameric ring is the prominent motif here. But unlike form 1, all the four hydrogen bonding interactions in this tetrameric motif are sustained by N–H···$O_{carbonyl}$ hydrogen bonds where the syn N–H of ACT interact with SACT carboxamide oxygen (N3···O3, 2.29Å, 129°) and amide N–H of SACT is bound to ACT carbonyl oxygen (N2···O4, 1.77Å, 177°), contributing two each to the tetrameric unit (Figure 4.4a). The anti N–H of ACT connect these discrete tetrameric units through centrosymmetric N–H···$O_{carbonyl}$ hydrogen bond (N3–H3B···O3, 2.01Å, 174°), forming an

$R^2_4(8)$ ring motif[31] which extend them along 1D plane (Figure 4.4b). The ACT $O_{carbonyl}$ forms a bifurcated hydrogen bond with aniline N–H of neighboring SACT (N1–H1B···O4, 1.98Å, 178°) extending these 1D sheets into the 2D lattice. In addition, the aniline proton forms an N–H···$O_{sulfonamide}$ bond (N1–H1A···O2, 2.19Å, 164°) with the adjacent SACT molecule strengthening the crystal lattice (Figure 4.4c).

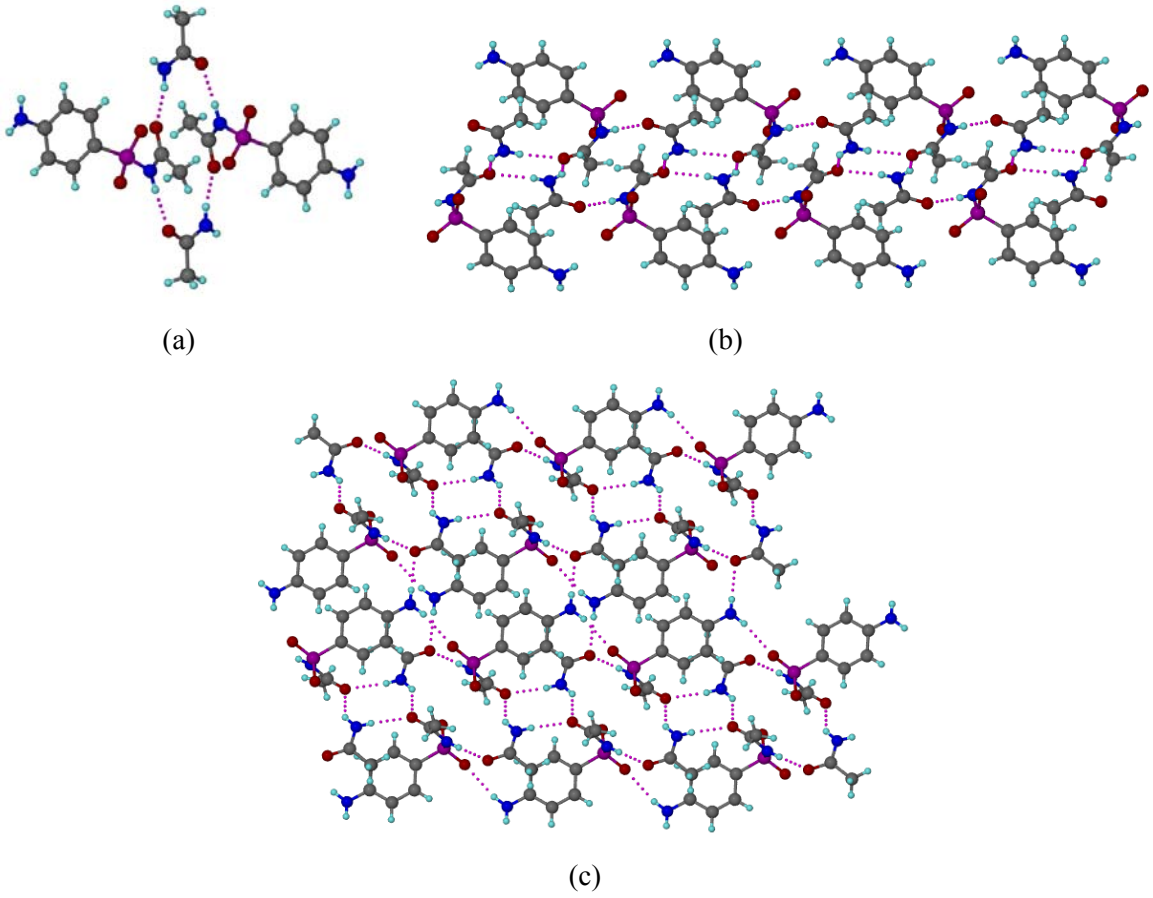

Figure 4.4a) Tetrameric ring motif connected through four one point N–H···$O_{carbonyl}$ hydrogen bonds. **b)** $R^2_4(8)$ ring motifs extend the discrete tetrameric units along 1D plane. **c)** One point N1–H1B···O4 hydrogen bonds extend the 1D sheet into the 2D lattice.

In order to understand the structural diversity in SACT-ACT cocrystal sysytem, we compared the synthon patterns exhibited by the polymorphs of reported two component systems i.e. Carbamazepine-Saccharin, Refcode – UNEZAO and Ethenzamide-Saccharin, Refcode - VUHFIO belonging to –SO_2NHCO– group with those observed in our cocrystal polymorphs. We found that, while an amide homodimer and a heterodimer distinguishes the polymorphs in Carbamazepine-Saccharin cocrystal[16e], a dimer and a catemer synthon differentiates the polymorphs of Ethenzamide-Saccharin cocrystal[16d]. Unlike these known synthon patterns, a prominent tetrameric ring motif comprising two molecules each of drug and coformer was observed in the SACT-ACT polymorphs. Variation in these synthon patterns is reasoned to the differences in planarity of SO_2NH group. Sulfonamide moiety was part of a ring in the reported cocrystal polymorphic structures which adopted a favorable planar geometry for dimer formation. Whereas in SACT-ACT polymorphic system, sulfonamide group is part of an open chain where the –SO_2 and –NH groups are not in the same plane for forming a homo or heterodimer. Similar distinguishing synthon patterns were observed in carboxamide-*N*-oxide and sulfonamide-*N*-oxide cocrystals. The latter group of cocrystals was discussed in chapter 2[32]. The tetrameric ring motif observed in SACT-ACT cocrystal polymorphs adds variation to the synthon patterns observed in rarely polymorphic –SO_2NHCO– class of molecules.

4.5.2 Molecular Geometry

The molecular structure of SACT (Scheme 4.1) suggests the possibility of conformational flexibility around sulfonyl acetamide group. Nevertheless, significant torsional angle differences are essential to consider these SACT-ACT modifications under the category of conformational polymorphs[33]. An overlay of the SACT and ACT molecules of both the polymorphs (Figure 4.5) showed that both the forms adopt virtually the same conformation with minimum differences in their torsion angles (Table 4.5). Therefore, although the torsion angles are not significantly different to classify then under the category of conformational polymorphs, yet they are good enough to cause major differences in their packing arrangements resulting in polymorphism. Therefore, with clear differences in their

hydrogen bonding patterns, this polymorphic system can be considered as a prominent case of synthon and packing polymorphism[34].

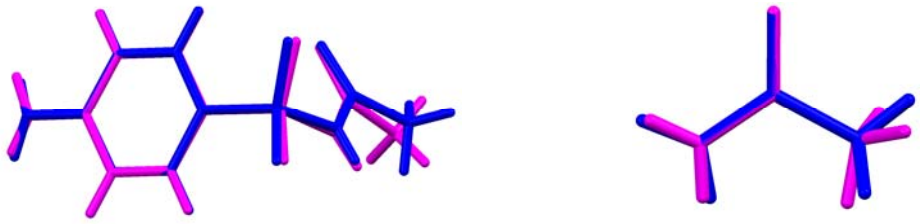

Figure 4.5 overlay of conformers of SACT and ACT molecules in Form 1 and 2. Color codes: Form 1 – Blue, Form 2 – Magenta.

Table 4.5 Torsion angles of SACT-ACT polymorphs

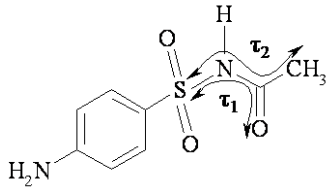

	τ_1	τ_2
Form 1	–1.4(5)	179.6(2)
Form 2	2.4(4)	–175.2(2)

τ_1 – S1-N2-C7-O3, τ_2 – S1-N2-C7-C8

4.5.3 Spectroscopic Characterization of Cocrystal Polymorphs

Infrared and Raman analysis of polymorphs can be invaluable in terms of complementing the diffraction techniques in establishing their unique nature. Both the polymorphs of SACT-ACT cocrystal were characterized through IR and Raman, which showed minor but significant differences between them. Minor changes in the infrared spectra of the polymorphs hint at the absence of significant intramolecular changes on transforming from one form to the other[35]. This was supported by the torsion angle analysis which showed minimum intramolecular changes in terms of conformation (above). While the N-H stretching of the SACT molecule appears at 3465.7 cm^{-1} and 3437.0 cm^{-1} in form 1, the

corresponding peaks appear at 3470.5 cm^{-1} and 3435.2 cm^{-1} in form 2 (Figure 4.6a). Similarly, the N-H Raman shift for SACT molecule was observed at 3463.2 cm^{-1} and 3471.3 cm^{-1} in form 1 and form 2 respectively (Figure 4.6 b). Even the other stretching and bending modes showed such minor but significant differences between form 1 and form 2, effectively distinguishing them. Major IR and Raman peak values are shown in Table 4.6.

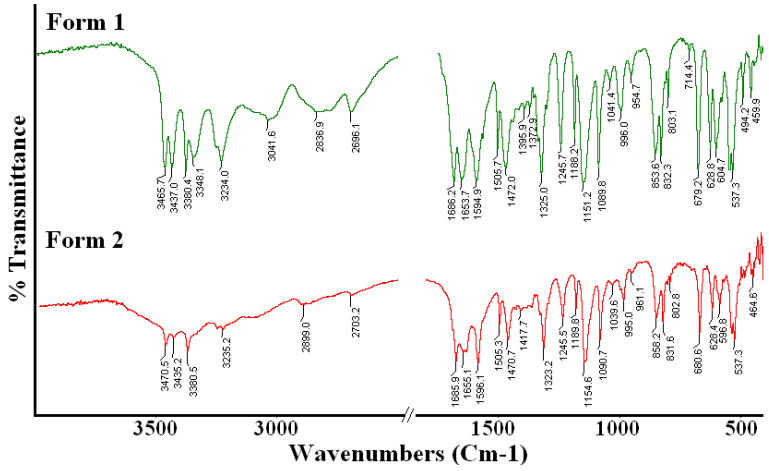

(a)

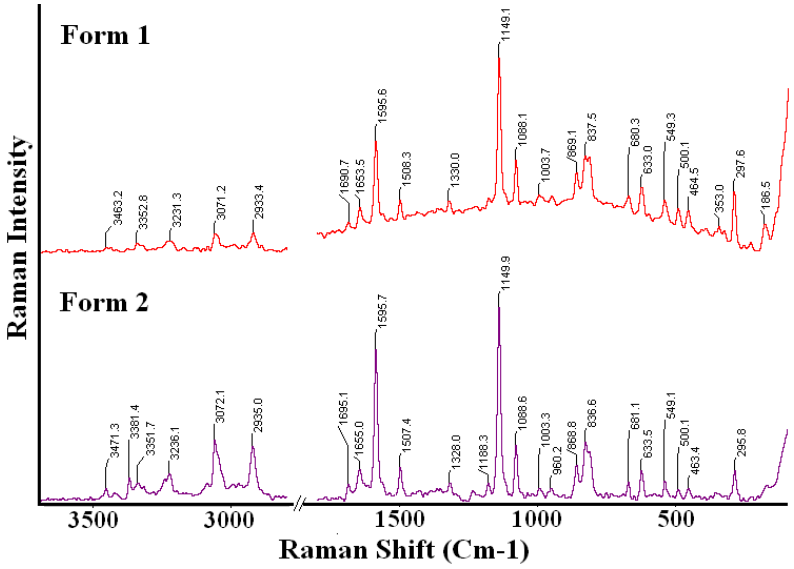

(b)

Figure 4.6 IR and Raman spectra of SACT-ACT cocrystal polymorphs.

Table 4.6 Major IR and Raman Peak values of SACT-ACT polymorphs

	C-H Stretch (cm^{-1})	N-H Stretch (cm^{-1})	C=O Stretch (cm^{-1})	N-H bend (cm^{-1})
		IR		
Form 1	3041.6, 2836.9	3465.7, 3437.0 3380.4,3348.1, 3234.0	1686.2, 1653.2	1594.1
Form 2	2899.0	3470.5, 3435.2 3380.5, 3235.2	1685.9, 1655.1	1596.1
		RAMAN		
Form 1	3071.2, 2933.4	3463.2, 3352.8, 3231.3	1690.0, 1653.5	1595.6
Form 2	3072.1, 2935.0	3471.3, 3381.4, 3351.7, 3236.1	1695.1, 1655.0	1595.7

^{13}C ssNMR analysis of SACT-ACT cocrystal polymorphs showed significant differences in the chemical shifts of the relative carbon atoms. While the chemical shift due to carbonyl carbon of SACT and ACT appeared at 175.3 ppm and 172.8 ppm in form 1, they showed significant downfield shift in form 2 at 175.8 ppm and 173.5 ppm. More importantly, the carbon atoms ortho to the $–NH_2$ attached carbon of aniline ring (carbons named 5 and 7) showed up as single peak in form 1 where as they bifurcated in form 2 (Figure 4.7). Even the remaining carbon atoms showed significant chemical shift differences, essentially distinguishing both the forms (Table 4.7).

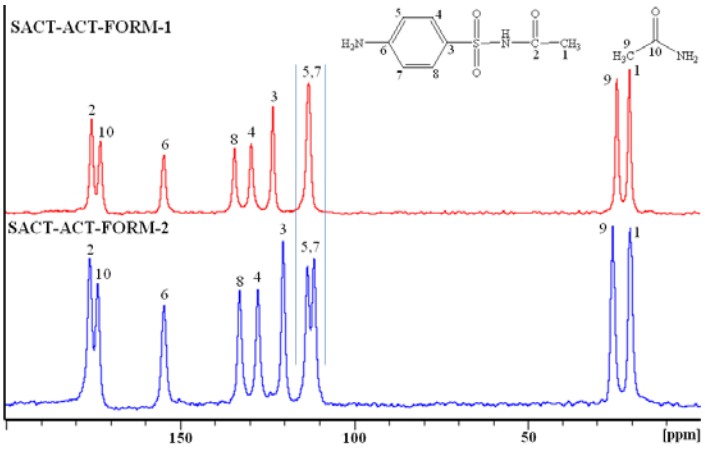

Figure 4.7 ssNMR analyses of SACT-ACT cocrystal polymorphs. Carbon atoms 5 and 7 appeared as single peak in form 1 whereas they bifurcated into two peaks in form 2. (Highlighted between the blue lines).

Table 4.7 ^{13}C ss-NMR chemical shift values (δ, ppm) of SACT-ACT Cocrystal Polymorphs.

Carbon No.	SACT-ACT-FORM-1	SACT-ACT-FORM-2
1	20.8	20.3
9	24.4	25.4
5,7	112.9	111.4, 113.2
3	123.1	120.2
4	129.3	127.5
8	134.3	132.7
6	154.6	154.5
10	172.8	173.5
2	175.3	175.8

4.6 Relative Stability of SACT-ACT Cocrystal Polymorphs

Fulfilling the hydrogen bonding interactions between donors and acceptors with better packing efficiency would determine the stability of crystal lattice. The polymorph which manages to strike a better balance between these factors will be the stable of the lot. Crystal density and packing fraction analysis of SACT-ACT cocrystal polymorphs showed that the calculated density (Form 1, – 1.323 g cm^{-3}, form 2, – 1.365 g cm^{-3}) and packing fraction (form 1, – 63.8%, form 2, – 66%) of form 2 is higher than form 1. According to the density rule[36] proposed by Burger and Ramberger, the form with higher density is the stable modification and the one with lower density is the metastable phase. Application of this rule to the SACT-ACT cocrystal polymorphs shows that form 2 is more stable compared to form 1. Stability relationship between the polymorphs was also investigated using thermal methods like DSC, Hot stage microscopy and VT-PXRD. In the DSC experiments both the polymorphs were heated from 30°C to 150°C in order to determine the possible phase transitions and melting point. Form 1 heating curve did not show any phase transition before melting at 106.5°C. In case of form 2 we observed a transition point between 79-83°C which was ascribed to the phase transformation of form 2 to form 1 (Figure 4.8). This form conversion was also supported by VT-PXRD experiments (discussion later). Based on the Burger and Ramberger's heat of transition rule[36], thermal behavior of polymorphs can be classified into enantiotropic or monotropic systems. According to the heat of transition rule, if there is an endothermic phase transition, and if the transition point lies below that, then the

polymorphs are classified as enantiotropic, and in case of an exothermic phase transition polymorphs are meant to have a monotropic relationship. Application of the heat of transition rule to the SACT-ACT cocrystal polymorphs suggests enantiotropic relationship. Due to phase transition, it was not possible to obtain the melting point of form 2. It was calculated using the equation proposed by J. O Henck[37a] which was successfully used by various groups[37] to calculate the melting point of polymorphs undergoing phase transformation. Application of this equation to SACT-ACT cocrystal system revealed the melting point of form 2 as 103.4°C (Scheme 4.2). In accordance with the heat of fusion rule[36] the lower melting point and higher ΔH_{fus} of form 2 compared to form 1 indicates enantiotropic relationship, supporting the conclusion inferred from the heat of transition rule (Table 4.8). DSC measurements suggest that as form 2 undergoes endothermic phase transition to form 1, it is the stable phase below the transition point and form 1 is the stable modification above the transition point.

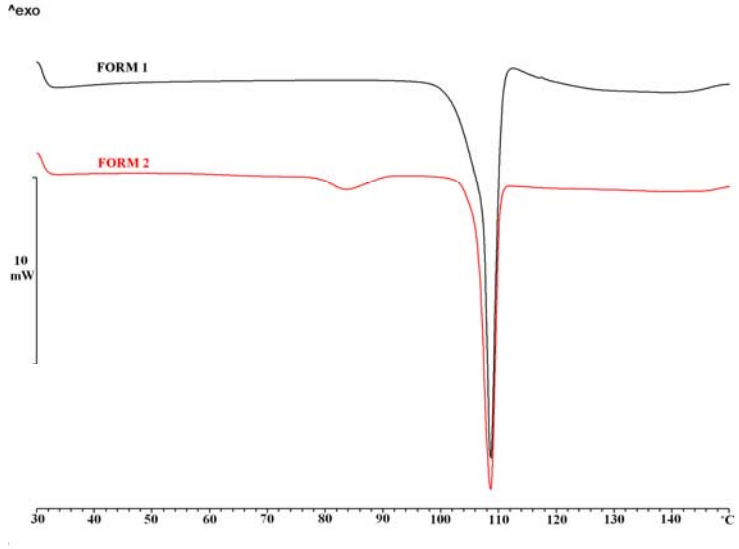

Figure 4.8 DSC heating curves of SACT-ACT cocrystal polymorphs form 1 (Black), Form 2 (Red) performed at 10°C/min.

$$T_{fus(form\ 2)} = \frac{\Delta H_{fus(form\ 2)} \times T_{fus(form\ 1)} \times T_{trs}}{(\Delta H_{fus(form\ 2)} \times T_{fus(form\ 1)}) + (T_{trs} \times \Delta H_{fus(form\ 1)}) - (T_{fus(form\ 1)} \times \Delta H_{fus(form\ 1)})}$$

$$T_{fus(form\ 2)} = \frac{32.3 \times 106.5 \times 79}{(106.5 \times 32.3) + (79 \times 29.5) - (106.5 \times 29.5)} = 103.4^{\circ} C$$

$\Delta H_{fus(form\ 2)}$ = Enthalpy of fusion of form 2 (Enthalpy of fusion of form 1 + Enthalpy of Transition) = 32.3 kJ/mol
$T_{fus(form\ 1)}$ = Temperature of fusion of form 1 = 106.5°C
T_{trs} = Temperature of transition from form 2 to form 1 = 79°C
$\Delta H_{fus(form\ 1)}$ = Enthalpy of fusion of form 1 = 29.5 kJ/mol
$T_{fus(form\ 2)}$ = Temperature of fusion of form 1 (calculated) = 103.4°C

Scheme 4.2 Calculation of melting point of SACT-ACT form 2.

Table 4.8 Enthalpy values of the cocrystal polymorphs at a heating rate of 10°C/min.

Form	T_{trs} /°C	ΔH_{trs} (KJ/mol)	T_m/°C	ΔH_{fus} (KJ/mol)
1	--	--	106.5	29.5
2	79	2.8	103.4*	32.3#

* Calculation showed in Scheme 4.2.

$\Delta H_{fus\ (form\ 2)} = \Delta H_{fus\ (form\ 1)} + \Delta H_{trs}$ (ref. 37b)

Hot stage microscopy was used to get a visual evidence of the morphological and thermal events that occurred during the DSC analysis. Single crystals of both form 1 and 2 grown from suitable solvents were mounted on the HSM slides and heated from 30°C to 110°C. As observed in DSC experiments, there were no morphological changes indicating phase transition on heating Form 1 crystal on heating before it melted at 105°C (Figure 4.9a). Whereas form 2 transformed into small crystallites around 81-83°C indicating phase transition as observed in its DSC thermogram which went on to melt again at 105°C (Figure

4.9b). A slight change in the melting temperature of the crystals in HSM experiments is not unusual because in DSC, experiments are performed in a closed environment whereas in HSM the crystals are exposed to ambient conditions where the influence of external environmental may cause a slight variation in the melting point. HSM results suggest that form 2 to form 1 conversion is not a single crystal-single crystal phase transformation[15] but a solid-solid phase transition with significant morphological changes.

a) Form 1

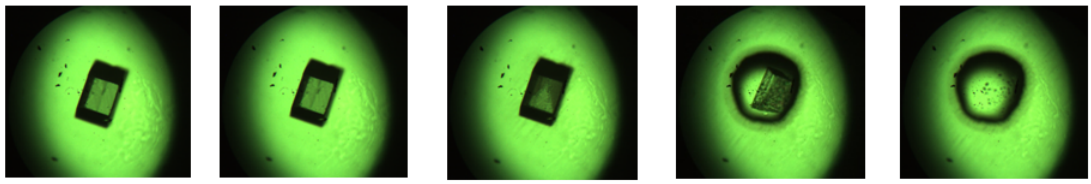

30°C 60°C 90°C 103°C 105°C

b) Form 2

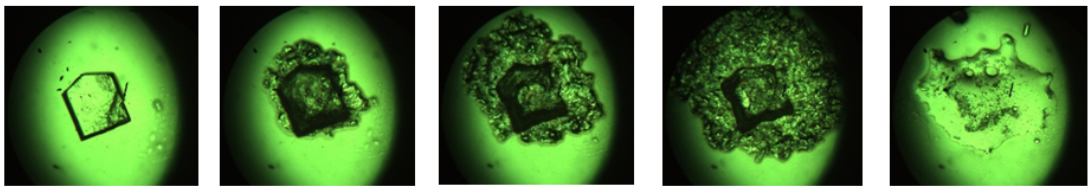

30°C 81°C 82°C 83°C 105°C

Figure 4.9 HSM snapshots of SACT: ACT cocrystal polymorphs. **a)** No morphological changes were observed in form 1. **b)** Significant morphological changes in form 2 can be seen between 81-83°C.

Variable temperature X-ray diffraction experiments were performed on SACT-ACT cocrystal polymorphs to confirm the phase transformation of form 2 to form 1 as suggested by DSC and HSM experiments and thermal stability of form 1 which did not show any phase transition upon heating. Pure polymorphs of form 1 and form 2 were obtained through bulk preparation methods and the purity of these phase were confirmed by overlaying their

experimental patterns with the respective calculated patterns which showed an excellent match. Upon phase purity analysis, these forms were subjected to VT-PXRD experiments. PXRD were recorded at regular intervals from 30°C to 90°C. While Pure form 1 did not show any phase change during this temperature range (Figure 4.10a), form 2 converted to form 1 which can be seen from the powder patterns at 80°C and 83°C suggesting phase transition (Figure 4.10b). VT-PXRD experiments act as excellent evidence to the DSC measurements that indeed the endothermic phase transition observed during form 2 heating curve is due to its phase transformation to form 1.

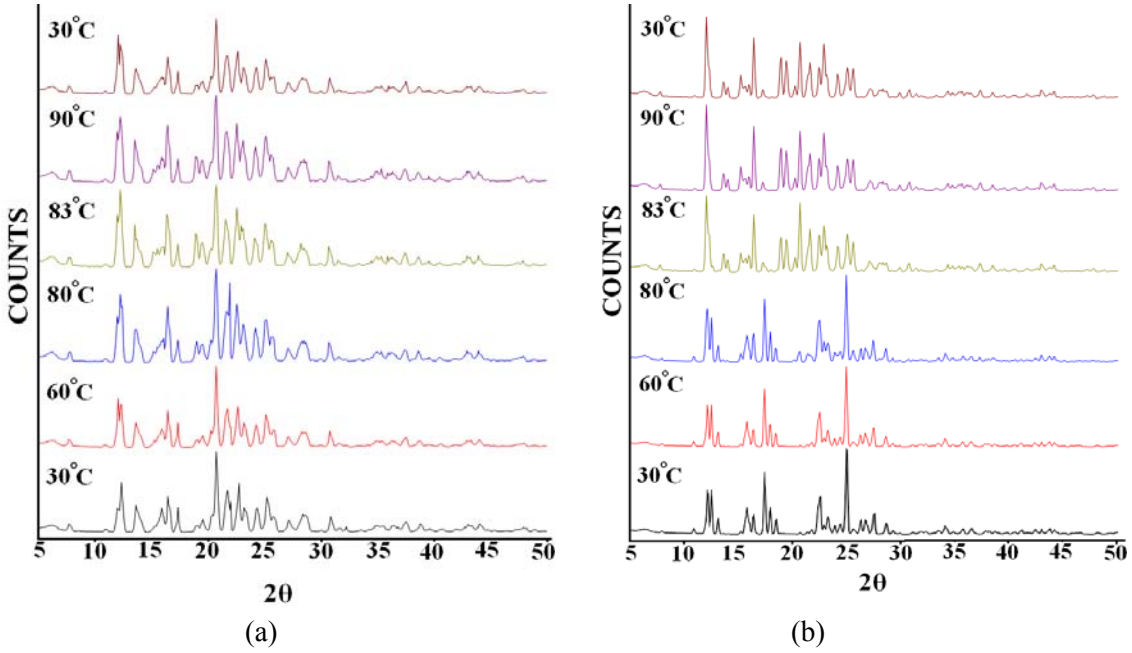

Figure 4.10a) VT-PXRD characterization of Form 1. **b)** VT-PXRD analysis of form 2 showing phase transformation to form 1 between 80-83°C.

From the thermal analysis of SACT-ACT cocrystal polymorphs through DSC, HSM and VT-PXRD experiments we were able to conclude that form 2 is the most stable phase below the transition point and vice-versa. Yet phase stability studies at ambient conditions are very important in order to establish the thermodynamic modification of the two forms at room temperature. The stable phase at room temperature was determined by subjecting both the forms to slurry and grinding experiments[23a,b,d].

4.7 Solvent Mediated Stability Experiments

Very often slurry grinding of cocrystals in a particular solvent results in the precipitation of the less soluble component due to the incongruent solubilities of the constituent solids. Similar problem was encountered during slurry grinding of SACT-ACT cocrystal polymorphs in water, EtOH, i-PrOH, CH_3CN etc. Unless the cocrystal is stable in the chosen solvent, phase stability studies of its polymorphs cannot be determined. Therefore on examining the cocrystal stability in various polar and non-polar solvents we found that the cocrystal is stable in toluene. Hence this solvent was used for all the solvent mediated stability experiments. Slurry grinding experiments were performed on both form 1 and form 2 separately along with a competitive slurry experiment, where both the forms are taken together in 1:1 stoichiometric ratio. Upon slurry grinding, pure form 1 converted to form 2 in 2 days (Figure 4.11a), the competitive slurry experiment resulted in pure form 2 within 12 hr (Figure 4.11b) whereas pure form 2 was found to be stable upto 72 hr (Figure 4.11c). Based on the solvent mediated stability experiments we could demonstrate that form 2 is the thermodynamic phase at room temperature. This stability relationship was cross checked by performing mechanochemical grinding experiments.

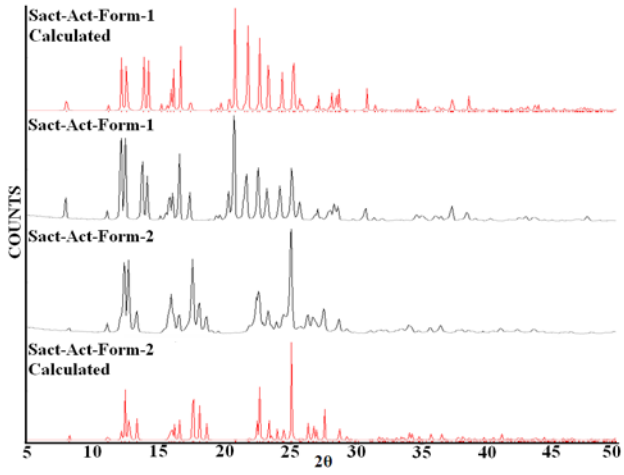

Figure 4.11a) Overlay of experimental PXRD pattern of SACT-ACT form 1(2^{nd} from top) with the experimental PXRD matching with form 2, obtained after slurry grinding in toluene for 2 days (3^{rd} from top). The respective calculated patterns of form1 and 2 (top and bottom) are shown for comparison.

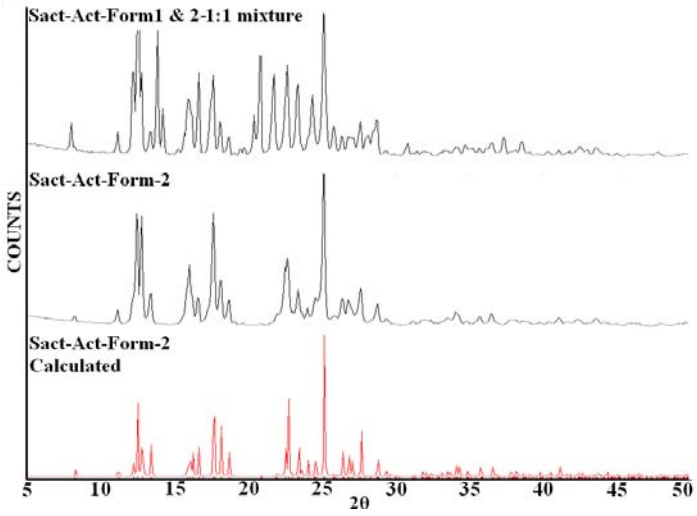

Figure 4.11b) Overlay of experimental PXRD pattern of 1:1 mixture of SACT-ACT form 1 and 2(top) with the experimental PXRD matching with form 2, obtained after slurry grinding in toluene for 12 Hr (middle). The calculated pattern of form 2 is shown for comparison (below).

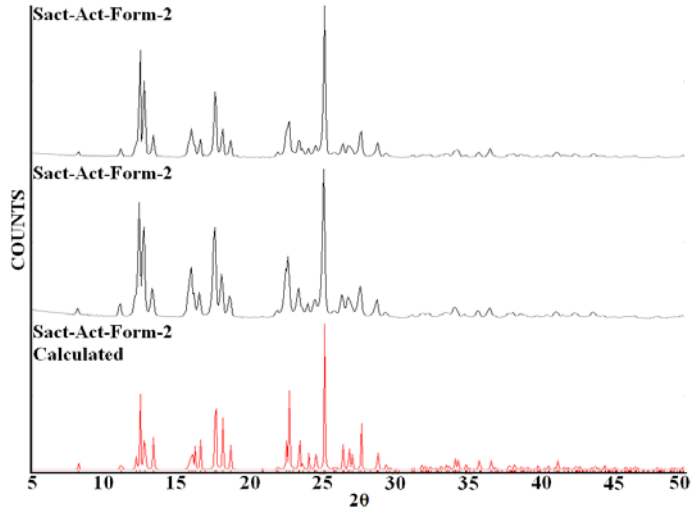

Figure 4.11c) Overlay of experimental PXRD pattern of SACT-ACT form 2(Top) with the experimental PXRD matching with form 2 obtained after slurry grinding in toluene for 3 days (middle). The calculated pattern of form 2 is shown for comparison (below)**.**

4.8 Solid State Grinding Experiments

Neat grinding of SACT and ACT in a mixer-mill in 1:1 stoichiometric ratio resulted in the metastable form 1 within 10 min as observed in certain polymorphic cocrystal systems[16d]. This is in accordance with the Ostwald's law of stages[14] which state that always the metastable form appears first followed by the more stable thermodynamic form. As expected further grinding of form 1 in the mixer-mill grinder resulted in complete conversion to form 2 in 30 min (Figure 4.12a). While competitive grinding of both the forms together in 1:1 stoichiometric ratio resulted in complete transformation to form 2 in 10 min (Figure 4.12b), grinding pure form 2 in similar experimental conditions did not show any phase change upto 3hr (Figure 4.12c). Nevertheless, the grinding experiments ably complement the solvent mediated stability experiments in establishing form 2 as the thermodynamic phase at room temperature.

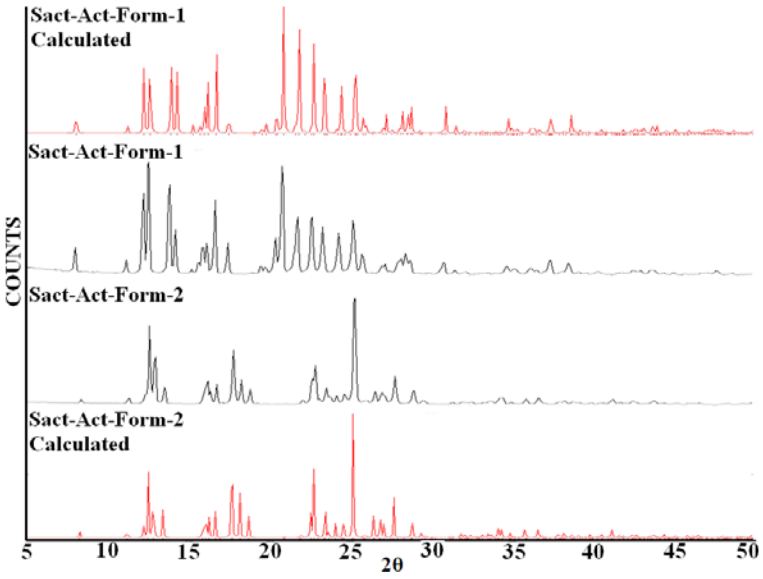

Figure 4.12a) Overlay of experimental PXRD pattern of SACT-ACT form 1(2nd from top) with the experimental PXRD matching with form 2, obtained after neat grinding in ball mill for 30 min (3rd from top). The respective calculated patterns of form 1 and 2 (top and bottom) are shown for comparison.

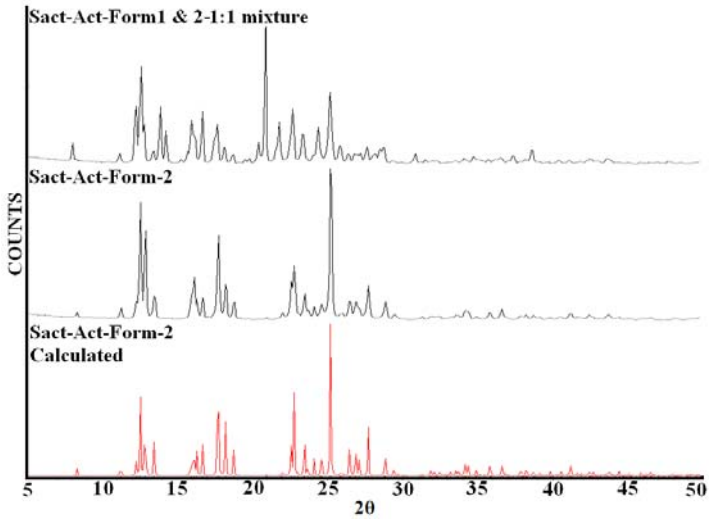

Figure 4.12b) Overlay of experimental PXRD pattern of 1:1 mixture of SACT-ACT form 1 and 2(top) with the experimental PXRD matching with form 2, obtained after neat grinding in ball mill for 10 min (middle). The calculated pattern of form 2 is shown for comparison.

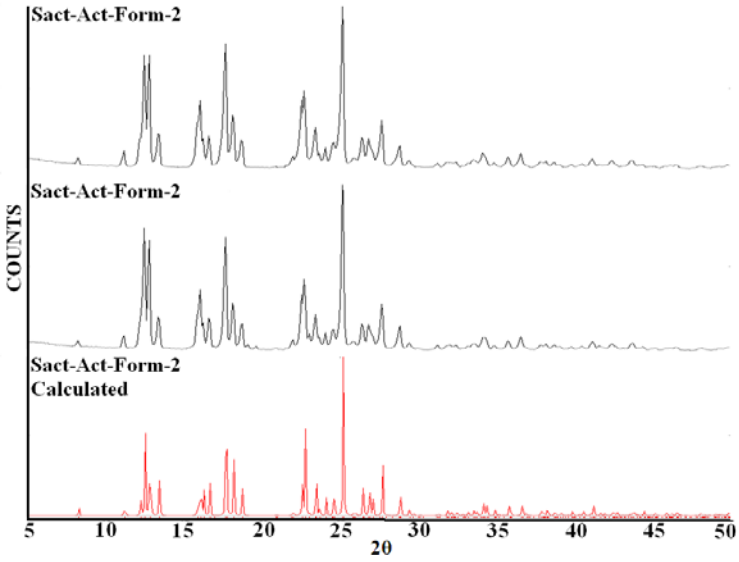

Figure 4.12c) Overlay of experimental PXRD pattern of SACT-ACT form 2(Top) with the experimental PXRD matching with form 2 obtained after neat grinding in ball mill for 3 hours (middle). The calculated pattern of form 2 is shown for comparison.

A semi-schematic Energy vs Temperature (E-T) diagram consistent with the results obtained through DSC, HSM, VT-PXTD, slurry and grinding experiments is shown in Figure 4.13. The E-T diagram establishes form 2 as the most stable phase at absolute zero based on the density rule[36]. The conversion of form 1 to form 2 at ambient conditions is rationalized by the low free energy of the latter polymorph between 25-83°C. The phase transition of form 2 to form 1 and the melting point of form 1 are represented through a crossover at 83°C (transition point) and 106.5°C (melting point) respectively.

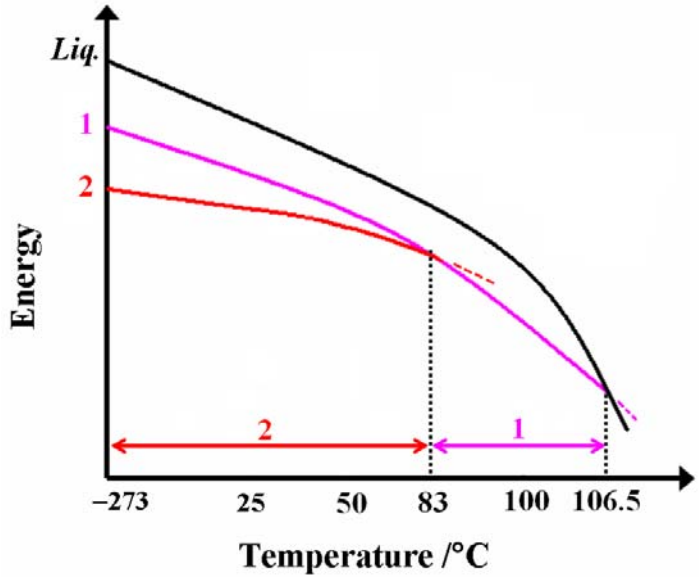

Figure 4.13 Semischematic energy vs temperature diagram to show the relative stability and phase transformation of SACT-ACT cocrystal polymorphs. At -273°C form 2 is the stable phase. Between 25-83°C form 2 is the stable modification since form 1 converted to form 2 in slurry and grinding experiments. The transition point at 83°C is due to the conversion of form 2 to form 1 on heating. Form 1 is stable above 83°C before it melts at about 106.5°C. The dashed line indicates that the polymorph has transformed to another phase at that temperature, T_{trs}.

4.9 Solubility and Dissolution Experiments

In the past decade, Pharmaceutical cocrystals have attracted the attention of both the academic and the pharmaceutical industries equally with their ability to address the poor physicochemical properties of API's[7]. In certain cases cocrystals have been used to decrease the solubility of certain high solubility bioactive molecules and drugs in order to improve bioavailability[38]. Normally, a metastable polymorph has higher solubility compared to the stable form due to higher free energy. Hence, in order to assess the trend in the solubility of cocrystal polymorphs and to ascertain the ability of ACT coformer in modulating the solubility parameters of SACT, we performed solubility and dissolution studies. SACT has good solubility in water (12.5 mg/mL)[39]. Therefore, equilibrium solubility of SACT and its cocrystal polymorphs were performed in pH 7 buffer medium for 24 hr. Apart from SACT, the solubility of cocrystal polymorphs could not be determined due to the incongruent solubilities of the components. In both the cases less soluble SACT was precipitated at the end of the solubility experiment.

Dissolution, a time dependant phenomenon proves beneficial for those cocrystals/salts which undergo hydration or phase transformation during solubility experiments[40]. Dissolution experiments for SACT and its cocrystal polymorphs were performed for 4hr in pH 7 buffer by the rotating disc intrinsic dissolution rate method[41]. SACT-ACT form 1 showed 1.57 times and SACT-ACT form 2 showed 1.27 times more solubility than SACT (Figure 4.14). The amount of drug dissolved at the end of dissolution experiment ($AUC_{0\text{-}4hr}$) is 64763.6 mg h/L for SACT, 105679.4 mg h/L for SACT-ACT form 1 and 80853.0 mg h/L for SACT-ACT form 2 (Table 4.9). The AUC value which is an indication of the total amount of dissolved drug in the given time is highest for SACT-ACT form 1 (1.63 times more compared to SACT). From the solubility experiments we could infer that the cocrystal polymorphs followed the generally observed trend of metastable polymorphs being more soluble than their stable counterparts. PXRD plots of the residue at the end of the equilibrium solubility and dissolution experiment are shown in Figure 4.15.

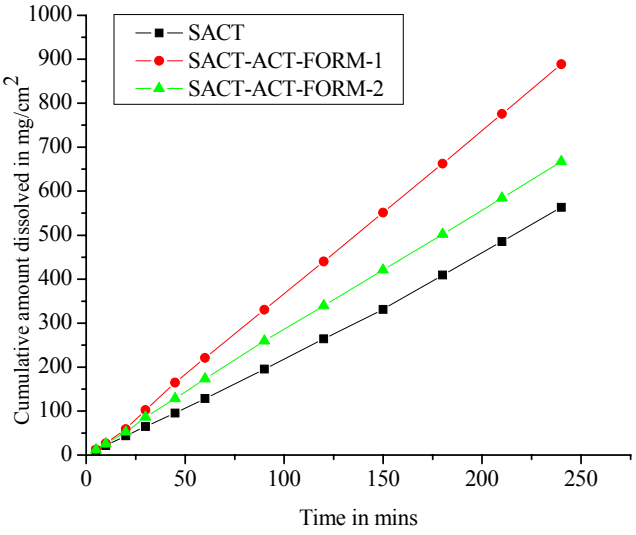

Figure 4.14 Intrinsic dissolution rate curves of SACT and its cocrystal polymorphs in pH 7 Buffer.

Table 4.9 Intrinsic dissolution rates of SACT polymorphs along with their molar extinction coefficient (ε), and AUC values. The number of times enhancement of IDR and AUC with respect to SACT is given in parentheses.

Compound	Molar Extinction coefficient (mM^{-1} cm^{-1})	Eq. Sol (g/L)	IDR in (mg/cm^2/min)	$AUC_{0\text{-}4h}$ (mgh/L)
SACT	22.8	14.5	2.18	64763.6
FORM 1	17.9	--	3.4 (x 1.57)	105679.4 (x1.63)
FORM 2	19.9	--	2.8 (x 1.27)	80853.0 (x1.25)

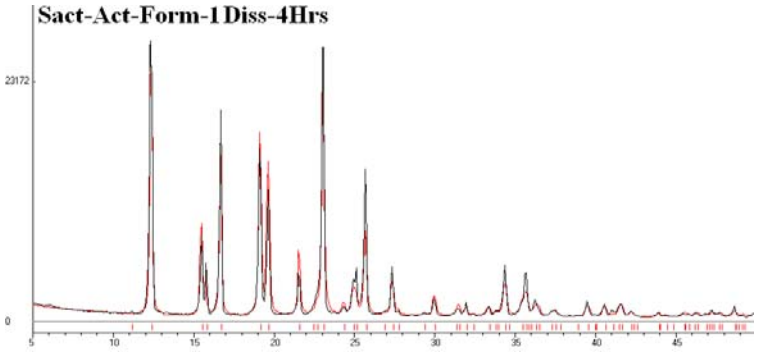

(a)

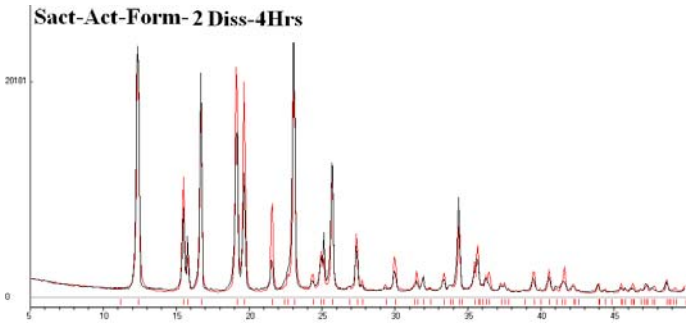

(b)

Figure 4.15 PXRD plots of SACT cocrystal polymorphs at the end of dissolution experiment matches with the calculated XRD pattern of SACT indicating form conversion. Similar phase transformation was observed at the end of solubility experiment on cocrystal polymorphs.

4.10 Conclusions

The primary aim of this work was to obtain polymorphs of compounds belonging to rarely polymorphic group of $–SO_2NHCO–$ skeleton containing molecules, explore the diversity in their packing and synthon patterns and determine their stability relationship. This would enable us to have a better understanding of hydrogen bonding interactions in this group of molecules which would have implications in developing novel solid forms of related drug molecules for better therapeutic efficacy. This was achieved by discovering two polymorphs of a cocrystal involving SACT and acetamide. Both the forms have been very well characterized using spectroscopic, thermal and diffraction methods. Structural analysis revealed significant differences in the hydrogen bonding patterns and packing modes of both the forms. With minor conformational differences, this system is shown to be a prominent example of synthon and packing polymorphism. Application of thermal methods like DSC, HSM and VT-PXRD showed that both the forms are enantiotropically related to each other. In combination with slurry and grinding techniques, we have established SACT-ACT form 2 as the thermodynamic phase and the form 1 as the metastable kinetic modification. Dissolution studies showed that both the forms followed the generally observed trend of metastable forms being more soluble compared to their stable counterparts. The metastable

SACT-ACT Form 1 showed 1.57 times and the stable form 2 showed 1.27 times more IDR compared to SACT. With significant increase in polymorphic cocrystals in the past decade and the diverse applications that come with them, we have also highlighted the importance of thorough characterization of cocrystal polymorphs. Establishing their stability relationships would not only prove to be extremely beneficial in overcoming accidental phase transformations but also help in an informed selection of the optimal solid form for pharmaceutical development.

4.11 Experimental Section

SACT and ACT were obtained from Sigma-Aldrich (Hyderabad, India). Solvents (purity > 99%) were purchased from Hychem Laboratories (Hyderabad, India). Water filtered through a double deionized purification system (Aqua DM, Bhanu, Hyderabad, India) was used for all experiments.

Preparation of cocrystal polymorphs SACT (42.8 mg) and ACT (11.8 mg) in 1:1 molar ratio were dissolved in 6 mL of Ethyl acetate-Methyl ethyl ketone solvent mixture and left for slow evaporation. Single crystals of form 1 suitable for X-ray diffraction were obtained after 3 days. Bulk amount of this polymorph for further characterization was prepared by dissolving SACT and ACT (321 mg and 88.5 mg, 1:1 molar ratio) in 5 mL of acetone and evaporating the solution in a rotary evaporator. The bulk material matched very well with the calculated pattern of form 1 crystal structure.

SACT (42.8 mg) and ACT (11.8 mg) in 1:1 molar ratio were dissolved in 8:3 ratio of Ethyl acetate-Toluene solvent mixture and left for slow evaporation. Single crystals of form 2 suitable for X-ray diffraction were obtained after 4 days. Bulk preparation of this polymorph for further characterization was done by mechanochemical grinding of SACT and ACT (321 mg and 88.5 mg, 1:1 molar ratio) in a mixer-mill (Retsch, Germany) for 1 hr. The bulk material matched very well with the calculated pattern of form 2 crystal structure.

Phase Transformation Experiments Grinding experiments were done on 100 mg scale. Competitive grinding experiments were carried out on 1:1 stoichiometric ratio of the

polymorphs (100 mg each). A Retsch mixer-mill equipped with a 5 mL stainless steel grinding jar and SS balls of 4 mm diameter was used for mechanical grinding. Slurry experiments were also done on 100mg scale. Competitive slurry experiments were carried out on 1:1 stoichiometric ratio of the polymorphs (100 mg each). Toluene (5 mL in each experiment) was used as solvent in slurry experiments.

Powder X-ray diffraction VT-PXRD was performed on the same instrument equipped with a variable temperature stage -TTK450 module. PXRD patterns for both the forms were collected at 30, 60, 80, 86 and 92ºC. All the powder patterns were plotted using Origin 7.0 software.

Hot-Stage microscopy (HSM) HSM was performed on a Wagner & Munz PolythermA Hot Stage and Heiztisch microscope. A Moticam 1000 (1.3 MP) camera supported by software Motic Image Plus 2.0ML is used to record images.

Cambridge Structural Database The CSD (version 5.29, November 2007, ConQuest 1.10, August 2012 update) was searched for cocrystal polymorphs. The parameters "all polymorphic structures with 3D coordinates determined", "no errors", "no polymeric", and "no ions" were searched to give 9468 hits. Crystal structures were visualized with Mercury 2.0, and 78 sets of cocrystal polymorphs were manually retrieved (3D coordinates reported for all polymorph sets). Crystal structures with any degree of disorder were excluded.

Dissolution and solubility measurements The solubility and dissolution experiments (500 mg of compound was taken in the intrinsic attachment) on cocrystal polymorphs were performed in pH 7 buffer medium at λ_{max} (SACT at 256 nm and SACT-ACT form 1 and 2 at 257 nm). The procedure is similar to that mentioned in chapter 3.

4.12 References

1. (a).W. C. McCrone, *Polymorphism in Physics and Chemistry of the Organic Solid-state*, Eds. D. Fox, M. M. Labes, A. Weissberger, Wiley Interscience, Newyork, 1965 (b) J. Haleblian and W. C. McCrone, *J. Pharm. Sci*, 1969, **58**, 911 (c) J.

Bernstein, *Polymorphism in Molecular Crystals*, Clarendon, Oxford, 2002 (d) H. G. Brittan, *Polymorphism in Pharmaceutical Solids*, Marcel Dekker, Newyork, 1999 (e) J. Bernstein, *Cryst. Growth Des*., 2011, **11**, 632 (f) J. Chen, B. Sarma, J. M. B. Evans and A. Myerson, *Cryst. Growth Des*., 2011, **11**, 887.

2. (a) R. J. Davey, *Chem Commun*, 2003, 1463 (b) A. Panagopoulou-Kaplani and S. Malamataris, *Int. J. Pharm*., 2000, **195**, 239 (c) S. R. Chemburkar, J. Bauer, K. Deming, H. Spiwek, K. Patel, J. Morris, R. Henry, S. Spanton, W. Dziki, W. Porter, J. Quick, P. Bauer, J. Donaubauer, B. A. Narayanan, M. Soldani, D. Riley and K. McFarland, *Org. Process Res. Dev*., 2000, **4**, 413.
3. (a) S. Cherukuvada, R. Thakuria and A. Nangia, *Cryst. Growth Des.,* 2010, **10**, 3931-3941 (b) N. J. Babu, S. Cherukuvada, R. Thakuria and A. Nangia, *Cryst. Growth Des.,* 2010, **10**, 1979-1989 (c) B. Sarma, P. Sanphui and A. Nangia, *Cryst. Growth Des.,* 2010, **10**, 2388-2399 (d) N. Zencirci, T. Gelbrich, D. C. Apperley, R. K. Harris, V. Kahlenberg and U. J. Griesser, *Cryst. Growth Des.,* 2010, **10**, 302-313.
4. (a) M. D. Eddleston, S. Sivachelvam and W. Jones, *CrystEngComm,* 2013, **15**, 175 (b) D. Braga, G. Palladino, M. Polito, K. Rubini, F. Grepioni, M. R. Chierotti and R. Gobetto, *Chem. Eur. J*., 2008, **14**, 10149.
5. (a) M. C. Etter, G. M. Frankenbach and D. A. Adsmond, *Mol. Cryst. Liq. Cryst.* 1990, **187**, 285-299 (b) M. Morimoto, S. Kobatake and M. Irie, *Chem Commun*, 2008, 335-337.
6. A. N. Sokolov, T. Friščić and L. R. MacGillivray, *J. Am. Chem. Soc.* 2006, **128**, 2806-2807.
7. (a) N. Schultheiss and A. Newman, *Cryst. Growth Des*., 2009, **9**, 2950 (b) N. J. Babu and A. Nangia, *Cryst. Growth Des*., 2011, **11**, 2662 (c) N. R. Goud, S. Gangavaram, K. Suresh, S. Pal, S. G. Manjunatha, S. Nambiar and A. Nangia, *J. Pharm. Sci*., 2012, **101**, 664 (c) W. Jones, W. D. S. Motherwell and A. V. Trask, *M. R. S. Bull.,* 2006, **31**, 875-879.
8. (a) L. R. MacGillivray, G. S. Papaefstathiou, T. Friščić, T. D. Hamilton, D.-K. Bučar, Q. Chu, D. B. Varshney and I. G. Georgiev, *Acc. Chem. Res.,* 2008, **41**, 280-291 (b) L. R. MacGillivray, G. S. Papaefstathiou, T. Friščić, D. B. Varshney and T. D. Hamilton, *Top. Curr. Chem.*, 2004, **248**, 201-221.

9. A. N. Sokolov, D. C. Swenson and L. R. MacGillivray, *Proc. Natl. Acad. Sci*., 2008, **105**, 1794-1797.
10. C. B. Aakeröy, A. M. Beatty, B. A. Helfrich and M. Nieuwenhuyzen, *Cryst. Growth Des*., 2003, **3**, 159-165.
11. S. Aitipamula, P. S. Chow and R. B. H. Tan, *CrystEngComm,* 2009, **11**, 1823.
12. (a) M. L. Peterson, S. L. Morissette, C. McNulty, A. Goldsweig, P. Shaw, M. LeQuesne, L. Monagle, N. Encina, J. Marchionna and A. Johnson, *J. Am. Chem. Soc*., 2002, **124**, 10958 (b) S. L. Morissette, S. Soukasene, D. Levinson, M. J. Cima and Ö. Almarsson, *Proc. Nat. Acad. Sci*., 2003, **100**, 2180.
13. J. H. ter Horst and P. W. Cains, *Cryst. Growth Des.*, 2008, **8**, 2537-2542.
14. W. Ostwald, *Z. Phys. Chem.,* 1987, **22**, 289.
15. S. Aitipamula, P. S. Chow and R. B. H. Tan, *CrystEngComm,* 2010, **12**, 3691-3697.
16. (a) S. Aitipamula, P. S. Chow and R. B. H. Tan, *Cryst. Growth Des*., 2010, **10**, 2229. (b) B. R. Srikanth, P. Vishweshwar and P. Vyas, *Chem Commun*, 2007, 2375 (c) N. J. Babu, L. S. Reddy, S. Aitipamula, and A. Nangia, *Chem-Asian J*., 2008, **3**, 1122. (d) S. Aitipamula, P. S. Chow and R. B. H. Tan, *CrystEngComm,* 2009, **11**, 889 (e) S. G. Fleischman, S. S. Kuduva, J. A. McMahon, B. Moulton, R. D. B. Walsh, N. Rodríguez-Hornedo and M. J. Zaworotko, *Cryst. Growth Des*., 2003, **3**, 909.
17. (a) D. Sensoy, E. Cevher, A. Sarici, M. Yilmaz, A. Özdamar and N. Bergisadi, *Eur. J. Pharm. Biopharm.,* 2009, **72**, 487 (b) http://www.drugs.com/mtm/klaron.html
18. (a) C. A. Hull and S. M. Johnson, *Cutis*, 2004, **73**, 425 (b) J. Q. Del Rosso, *Cutis,* 2004, **73**, 29 (c) I. Meghan, B. S. Dubina, B. Alan and M. D. Fleischer Jr., *Arch. Dermatol.,* 2009, **145**, 1027.
19. A. Mastrolorenzo and C. T. Supuran *Met. Based Drugs*, 2000, **7**, 49.
20. G. L. Mandell, J. E. Bennett, R. Dolin, Eds., *Mandell, Douglas, and Bennett's Principles of Infectious Diseases,* NewYork, Churchill Livingstone Inc; 2000.
21. (a) A. K. Basak and S. K. Mazumdar, *Cryst.Struc.Commun*., 1982, **11**, 1609 (b) M Ghosh, A K. Basak and S. K. Mazumdar, *J. Cryst. Spec. Res*., 1987, **17**, 739 (c) P. A. M. Leger, S. Alberola and E. A. Carpy, *Acta Crystallogr. Sect. B*, 1977, **33**, 1455.

22. (a) A. Mukherjee, P. Grobelny, T. S. Thakur and G. R. Desiraju, *Cryst. Growth Des*., 2011, **11**, 2637 (b) R. Dubey, M. S. Pavan and G. R. Desiraju, *Chem. Commun.,* 2012, **48**, 9020.
23. (a) A. V. Trask and W. Jones, *Top Cur. Chem*., 2005, **254**, 41 (b) N. Shan, F. Toda and W. Jones, *Chem Commun,* 2002, **20**, 2372 (c) P. P. Bag, M. Patni and C. M. Reddy, *CrystEngComm*, 2011, **13**, 5650 (d) S. Karki, T. Friščić, W. Jones and S. D. Motherwell, *Mol. Pharmaceutics,* 2007, **4**, 347.
24. GRAS Chemical List. Accessed at www.fda.gov/Food/FoodIngredientsPackaging/GenerallyRecognizedasSafeGRAS/GRASSubstancesSCOGSDatabase/default.htm
25. (a) G. A. Jeffrey, J. R. Ruble, R. K. McMullan, D. J. Defrees, J. S. Binkley and J. A. Pople, *Acta Crystallogr. Sect. B*, 1980, **36**, 2292 (b) J. W. Bats, M. C. Haberecht and M Wagner, *Acta Crystallogr. Sect. E*, 2003, **59**, 1483.
26. (a) C. B. Aakeroy, A.M. Beatty and B. A. Helfrich, *Angew Chem Int. Ed.,* 2001, **40**, 3240 (b) Ö Almarsson and M. J. Zaworotko, *Chem Commun*, 2004, 1889 (c) K.M. Anderson, M. R. Probert, C. N. whitely, A. M. Rowland, A. E. Goeta and J. W. Steed. *Cryst. Growth Des*., 2009, **9**, 1082 (d) H. J. Lehmler, L. W. Robertson, S. Parkin and C. P. Brock, *Acta Crystallogr. Sect. B*, 2002, **58**, 140.
27. (a) N. J. Babu and A. Nangia, *CrystEngComm*, 2007, **9**, 980 (b) D. Das, R. Banerjee, R. Mondal, J. A. K. Howard, R. Boese and G. R. Desiraju, *Chem Commun*, 2006, 555 (c) J. W. Steed, *CrystEngComm*, 2003, 169 (d) K. M. Anderson, A. E. Goeta, K. S. B. Hancock and J. W. Steed, *Chem Commun*, 2006, 2138.
28. (a) G. R. Desiraju, J. J. Vittal, A. Ramanan, *Crystal Engineering. A Textbook,* World Scientific Publishing, Singapore, 2011 (b) G. R. Desiraju, *Crystal Engineering. The Design of Organic Solids*. Elsevier, 1989 (c) G. R. Desiraju, *Angew. Chem., Int. Ed. Engl*., 1995, **34**, 2311 (b) R. D. B. Walsh, M. W. Bradner, S. Fleischman, L. A. Morales, B. Moulton, N. Rodríguez-Hornedo and M. J. Zaworotko, *Chem Commun*, 2003, 186.
29. (a) M. C. Etter, J. C. Macdonald and J. Bernstein, *Acta Crystallogr. Sect. B,* 1990, **46**, 256 (b) M. C. Etter and S. M. Reutzel, J. *Am. Chem. Soc*., 1991, **113**, 2586.

30. (a) A. Nangia and G. R. Desiraju, *Top Curr. Chem*., 1998, **198**, 57 (b) P. Vishweshwar, A. Nangia and V. M. Lynch, *Cryst. Growth Des*., 2003, **3**, 783 (c) P. Vishweshwar, J. A. McMahon, M. L. Peterson, M. B. Hickey, T. R. Shattock and M. J. Zaworotko, *Chem Commun,* 2005, 4601.
31. (a) J. Bernstein, R. E. Davis, L. Shimoni and N. L. Chang, Angew. *Chem., Int. Ed. Engl*., 1995, **34**, 1555 (b) M. C. Etter, *Acc. Chem. Res*., 1990, **23**, 120 (c) M. C. Etter, *J. Phys. Chem*., 1991, **95**, 4601.
32. (a) N. J. Babu, L. S. Reddy and A. Nangia, *Mol. Pharmaceutics*, 2007, **4**, 417 (b) L. S. Reddy, N. J. Babu, A. Nangia, *Chem Commun*, 2006, 1369 (c) N.R. Goud, N. J. Babu, A. Nangia, *Cryst. Growth Des*., 2011, **11**, 1930.
33. A. Nangia, *Acc Chem Res*, 2008, **41**, 595-604.
34. (a) Babu, N. J and A. Nangia, *CrystEngComm*, 2007, **9**, 980 (b) J. Thun, L. Seyfarth, C. Butterhof, J. Senker, R. E. Dinnebier and J. Breu, *Cryst. Growth Des*., 2009, **9**, 2435 (c) D. E. Braun, T. Gelbrich, V. Kahlenberg, G. Laus, J. Wieser and U. J. Griesser, *New J Chem*., 2008, **32**, 1677.
35. A. A. Ebert Jr and H. B. Gottlieb, *J. Am. Chem. Soc*., 1952, **74**, 2806.
36. A. Burger and R. Ramberger, *Microchim. Acta II*, 1979, 273.
37. (a) J. O. Henck, Konformationspolymorphie n-butylsubstituierter Arzneistoffe. Innsbruck: Thesis, p 41 (b) D. E. Braun, T. Gelbrich, V. Kahlenberg, R. Tessadri, J. Weiser and U. J. Griesser, *J. Pharm. Sci*., 2009, **98**, 2010 (c) L. Yu, *J. Pharm. Sci*., 1995, **84**, 966 (c) U. J. Griesser, D. Weigand, J. M. Rollinger, M. Haddow and E. Gstrein, *J. Therm. Anal. Calorim*., 2004, **77**, 511.
38. (a) C. B. Aakeroy, S. Forbes and J. Desper, *J. Am Chem. Soc*., 2009, **131**, 17048 (b) K Arora, P. Kavuru, S. Kesani, A. Smith, L. Wojtas, R. Shytle and M. Zaworotko, http://www.aapsj.org/abstracts/AM_2011/W5049.pdf
39. http://www.drugbank.ca/drugs/DB00634
40. J. B. Dressman, G. L. Amidon, C. Reppas and V. P. Shah, *Pharm. Res*., 1998, **15**, 11.
41. L. X. Yu, A. S. Carlin, G. L. Amidon and A. S. Hussain, *Int. J. Pharm*., 2004, **270**, 221.

CHAPTER FIVE

FAST DISSOLVING EUTECTIC COMPOSITIONS OF CURCUMIN

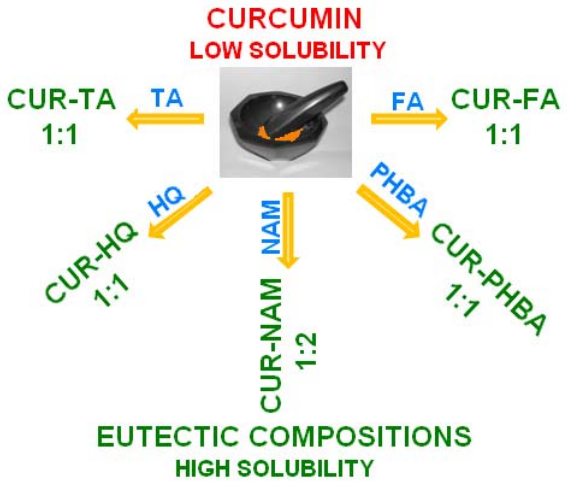

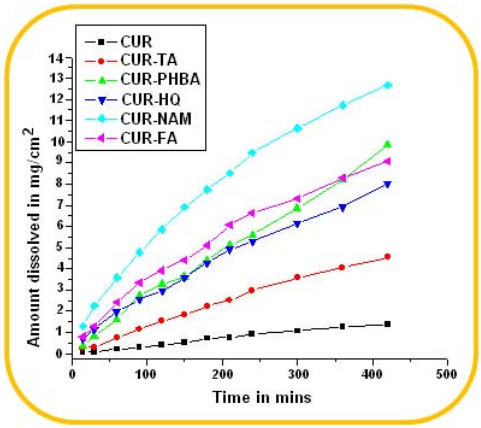

The bioactive agent Curcumin was screened with pharmaceutically acceptable coformers to discover solid forms of high solubility. Mechanochemical grinding of Curcumin with coformers in a fixed stoichiometric ratio resulted in binary eutectic compositions with Nicotinamide (1:2), Ferulic acid (1:1), Hydroquinone (1:1), p-Hydroxybenzoic acid (1:1), and L-tartaric acid (1:1). The eutectic nature of these crystalline solids was established by differential scanning calorimetry. The best case of CUR−NAM eutectic exhibits 10-fold faster IDR and 6-times higher AUC compared to Curcumin.

5.1 Introduction

The optimization of physico-chemical properties of a drug molecule has fundamental and commercial significance in the development of solid oral dosage forms.[1] The physical state of a low water-soluble drug or bioactive compound will significantly influence its bioavailability.[2] Therefore, identification of the best crystalline form by solid form screening has become a mandatory step in drug discovery and pharmaceutical development.[3] Even as salt formation is the most preferred strategy to improve the solubility, dissolution, and stability of drug substances, the approach is limited to those molecules which contain an ionizable functional group, such as an acid or a base. On the down side, salts tend to be more hygroscopic[4] than neutral substances. Physical solid form modification by altering the hydrogen bonding motifs of a compound by non-covalently binding it with a second component is now popularized as cocrystals, a new composition of matter exhibiting improved solubility and stability[5]. The other methods for solubility enhancement of drug molecules include Eutectics,[6] Solid dispersions,[7] Solubilization by surfactants,[8] and supersaturating drug delivery systems[9] etc.

Among the less often used methods, eutectic mixtures are one of the most promising alternate strategies for solubility modulation and bioavailability improvement of drug molecules and bioactive compounds[10]. As a consequence of their random molecular arrangement, excess thermodynamic functions and lower melting point compared to the starting components, eutectics confer higher solubility and dissolution to the parent molecule[11]. Unlike solid dispersions where the composition is mainly amorphous in nature[12], eutectic compositions are crystalline with minimum possibility of undue phase transformations. From the classic sodium chloride–water eutectic mixture[13a] used for refrigeration to the more recent energy storage purposes[13b], eutectics presence is felt in daily life and more importantly in pharmaceuticals. A 1:1 mixture of pharmaceutically active compounds Lidocaine (melting point: 68°C) and Prilocaine (melting point: 38°C) form a eutectic composition[14] which is an oil at ambient conditions with melting point of 18°C. It is popularly used as a dermal anaesthetic. The excess thermodynamic functions of eutectics confer higher solubility to the parent molecule. Nangia and coworkers[10a] reported the first of

a kind binary eutectic composition between cocrystals. Their idea was to develop a ternary cocrystal between Pyrazinamide, Succinic acid and Isoniazid which resulted in a eutectic mixture of binary cocrystals. They showed through dissolution experiments that this binary eutectic qualifies the WHO biowaiver dissolution criteria while the starting components do not clear the bar. Hence it was proposed to be useful in preparing an Immediate Release (IR) solid oral dosage formulation. Chiou and colleagues[10d] have reported that a eutectic composition of antifungal drug Griseofulvin with succinic acid (55% w/w of Griseofulvin) have shown 6-7 times faster dissolution rate compared to pure Griseofulvin. Apart from solubility enhancement, eutectics have been highly promising in improving the bioavailability of drug molecules. Sekiguchi et. al.[10e] reported that a eutectic mixture of sulfathiazole (STZ)-urea (52%:48%) improved the blood levels of the parent drug in humans as compared to the ordinary STZ. Peak concentration of the drug was achieved faster in the case of eutectic composition. As a control experiment they have compared the blood levels of physical mixtures of STZ-urea with ordinary STZ, which did not show any difference in the blood level concentration. Therefore they have concluded that the eutectic nature of the STZ-urea mixture resulted in improved blood levels of STZ (Figure 5.1).

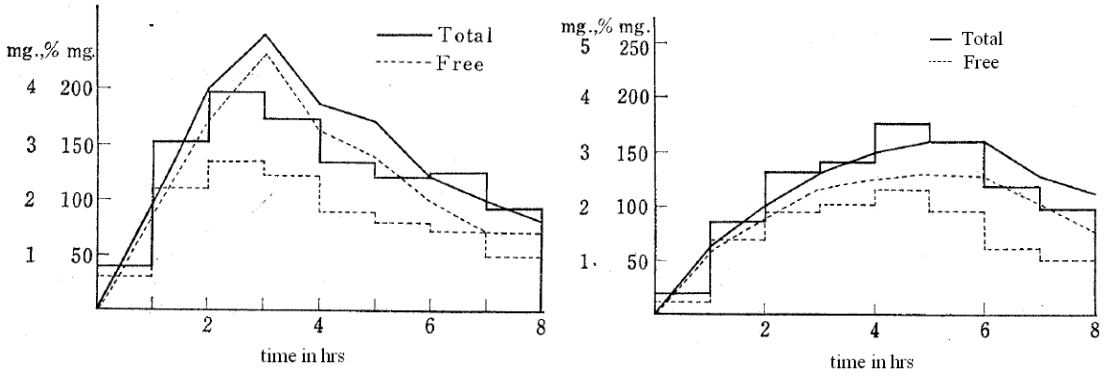

(a) (b)

Figure 5.1 Concentration in blood (curve) and amount excreted in urine (histogram) after ingestion of **a)** Sulfathiazole-Urea eutectic **b)** ordinary sulfathiazole. Above graphs clearly indicate that the amount of sulfathiazole dissolved is higher and peak concentration was achieved faster in the case of sulfathiazole-urea eutectic as compared to pure sulfathiazole (Adapted from ref. 10e).

Eutectic mixtures have been shown to improve the permeability of drug molecules. Itraconazole is an effective antifungal drug for topical treatment of fungal infections. Since Itraconazole is neither hydrophilic nor lipophilic, appropriate vehicle for its topical skin delivery is essential. Park and coworkers[10f] showed that a 2% (w/w) eutectic mixture of Itraconazole and phenol along with other constituents significantly enhanced the skin permeation profiles of Itraconazole when tested on hairless mouse skin. Similarly, Stott and coworkers[10g] prepared Ibuprofen eutectic compositions with terpene compounds. They have shown that Ibuprofen: Thymol 40:60 (% w/w) eutectic improved the permeability of Ibuprofen by 12.7 times compared to the pure drug. In essence, eutectics were shown to confer both solubility and bioavailability advantage to the parent molecules.

5.2 Curcumin - Literature Reports

Curcumin (diferuloylmethane) is the active ingredient of the dietary Indian spice turmeric. It is a hydrophobic polyphenol derived from the rhizome of the herb curcuma longa[15]. Apart from its application as an amyloid specific dye in *E.Coli,* curcumin has diverse pharmacological activities such as anti-inflammatory, antioxidant, anticancer[16a,b] and as a potential drug for the treatment of Alzheimer's disease.[16c] Curcumin was reported to be safe at high doses of 12g/day[17] in humans. Lao and colleagues[18] studied the safety of curcumin in healthy volunteers. These volunteers were enrolled for a single oral administration of curcumin with doses escalating from 500 mg to 12000 mg. Among the 24 enrolled patients, 7 developed grade 1 toxicity symptoms (mild, do not usually require treatment) like headache, rashes, yellowish stool etc. which are not dose related. These Phase I clinical trials performed for 4 months confirmed the safety of curcumin in humans at high doses. Taking advantage of these high safety dose levels, several groups all over the world performed clinical trials on curcumin in order to test its pharmacological activity against various diseases. Sharma and colleagues[19,18b] performed phase I clinical trials to evaluate the effect of curcumin in patients with advanced colorectal cancer. Doses ranging from 36-500mg were administered daily for 4 months. Five out of the 15 patients had radiologically stable disease for 4 months and one of the patient showed significant reduction of the

carcinoembryonic antigen (CEA). In a Phase I study conducted by cheng and coworkers[20], patients with premature lesions were enrolled. Indicative lesions before and after curcumin treatment were compared histologically. Histological improvement was seen in one of the two patients with bladder cancer, two of the seven patients with oral Leukoplakia and two of the six patients with Bowen's disease. These data are suggestive of a chemopreventive effect of curcumin. A brief list of ongoing clinical trials with curcumin in patients with different diseases is shown below (Table 5.1).

Table 5.1 Examples of ongoing clinical trials with curcumin

DISEASE	INSTITUTION	STUDY DESIGN	STARTING DATE
Multiple Myeloma	M. D. Anderson Cancer Center, USA	Pilot study with two arms: Curcumin vs. Curcumin + bioperine	Nov. 2004
Pancreatic Cancer	M. D. Anderson Cancer Center, USA	Phase II single arm: Curcumin	Nov. 2004
Pancreatic Cancer	Rambam Medical Center, Israel	Phase II single arm: Curcumin + Gemcitabine	July 2004
Familial Adenomatous polyposis	John Hopkins University, USA	Phase II: Curcumin	Nov. 2005
Sporadic Adenomatous polyps	University of Pensylvania, USA	Phase II: Placebo controlled: curcuminoids	July 2005
Aberrant crypt foci in colon	University of medicine and dentistry, New Jersey, USA	Phase II: Curcuminoids vs. Sulindac	Apr 2004
Alzheimer's disease	University of Pensylvania, USA	Phase II, Placebo controlled: curcumin C3 complex	July 2003
Alzheimer's disease	Chinese university of Hong kong, Hong kong	Phase I/II, placebo controlled: curcumin+ ginkgo extract	Oct 2004

(Data taken from ref. 18b)

Inspite of such promising pharmacological activity, the therapeutic effectiveness of curcumin is limited by very low solubility (7.8 mg/L) and poor bioavailability[18a]. Low absorption, rapid metabolism, and fast systemic elimination from the biological system are the main reasons for poor bioavailability. The oral bioavailability of curcumin was found to

be about 1% in rats. In a phase I study conducted in healthy human volunteers by Lao and colleagues[18a], serum taken prior to and 1, 2, and 4h after application of curcumin were analyzed by HPLC. Curcumin was not detectable in any of the samples except in two patients who were given 10000 and 12000 mg dose levels respectively. The serum curcumin levels of these patients were 29.7-30.4 ng/mL and 50.5-51.2 ng/mL at 1h and 4h of taking curcumin respectively. These data indicate an extremely low bioavailability of curcumin following oral application. Only at higher doses of 3600 – 12000 mg could a detectable level of curcumin be observed in plasma and urine. Curcumin was also reported to decompose rapidly in neutral and alkaline medium, with >90% decomposition occurring within 30 min in pH 7.4 buffer.[21] Therefore even though curcumin has excellent efficacy and good safety, it is not yet approved as a therapeutic agent or a drug for clinical use due to its poor solubility and bioavailability. The stability and bioavailability of curcumin has been enhanced through adjuvants such as piperine to block metabolic pathways. Novel drug delivery platforms such as nanoparticles and micelles and through concomitant administration of curcumin with lecithin, quercetin, genistein, eugenol, terpinol, etc. are also reported.[22] Other strategies adopted for bioavailability enhancement are complexation with 1–10% of rubusoside[23a] and combining curcumin with phosphatidyl choline in equimolar quantities.[23b] Inspite of these strategies, curcumin is not yet approved as a drug molecule.

5.3 Preparation of Binary Eutectic compositions of Curcumin

Solid form modification through polymorphs[24] and cocrystals[5] is an attractive strategy for optimizing the physicochemical properties of drug molecules and bioactive compounds. Recently, while examining the structural landscape of curcumin through common solid form screening methods like solution crystallization and mechanochemical grinding, we obtained novel polymorphs[25a] and cocrystals[25b] with resorcinol and pyrogallol. Even as the polymorphs and cocrystals with pyrogallol and resorcinol exhibited solubility advantage, polymorphs are prone to phase transformation, the faster dissolving curcumin-pyrogallol cocrystal is paired with a non-GRAS[26] partner molecule and the solubility enhancement was modest with the GRAS molecule resorcinol (4.7 fold). Of course, curcumin–pyrogallol has

potential as a drug–drug cocrystal given the recent anticancer activity of pyrogallol in lung tissue[27]. Nevertheless, encouraged by these preliminary results, we performed co-crystallization of curcumin with several GRAS[26] coformers in order to obtain novel solid forms with improved physicochemical properties. Mechanochemical grinding[28] of curcumin and the coformer in stoichiometric ratio gave binary eutectic compositions with nicotinamide (NAM), ferulic acid (FA), hydroquinone (HQ), *p*-hydroxybenzoic acid (PHBA), and L-tartaric acid (TA) instead of the expected cocrystals. These novel eutectic compositions were characterized by various thermal diffraction and spectroscopic techniques. All the eutectic compositions showed better dissolution profiles in comparison to curcumin.

5.4 Results and Discussion

Eutectic composition of bioactive molecules with pharmaceutically acceptable coformers in order to improve their physicochemical properties has not been studied. Whereas eutectic formation through coprecipitation[29a] and melt crystallization[29b] are reported, the use of mechanochemical grinding for eutectic formation is rare and attempted only in a few cases.[10a,30] Compaction of drug tablets is known to induce eutectic formation of acetaminophen–caffeine and acetaminophen-propylphenazone systems.[31] The five binary eutectic compositions in this study comprising CUR–NAM, CUR–FA, CUR–HQ, CUR–PHBA, and CUR–TA were obtained by grinding the components in stoichiometric ratio (Scheme 5.1). Unlike solid solutions which form by the ‘dissolution’ of a minor second component into the lattice of the major crystallite, eutectic mixtures result form a supersaturation of the minor component in the lattice of the major component.[10b,32] In the present case, the distinction between major and minor is superficial since they are mixed in stoichiometric amount. This supersaturation results in multiple phases (solid solutions) wherein the components retain their individual lattice structures and their interfaces comprise imperfect atomic arrangements, weaker non-covalent interactions, and unfulfilled bonds. Therefore eutectic compositions do not show any significant changes in their diffraction patterns or spectroscopic signature peaks. Such incoherent boundaries between the solid solution phases result in a eutectic microstructure which generally adopts a lamellar

arrangement. The non-uniform microstructure leads to increase in internal energy resulting in lowering of melting point and conferring higher solubility due to the higher free energy of the solid.[29a, 33] The stoichiometry of all the eutectics studied here is 1:1 except CUR–NAM which was found to be 1:2 by proton NMR peak integration. A DSC of 1:1 product of CUR-NAM showed an additional endotherm at higher temperature (about 145°C) for the unreacted solidus component along with the eutectic endotherm (of 1:2) at about 110 °C. The lower melting endotherm and the lack of changes in IR and PXRD (discussion next) suggested that mechanochemical grinding of curcumin with various coformers produced binary eutectic compositions instead of cocrystals.

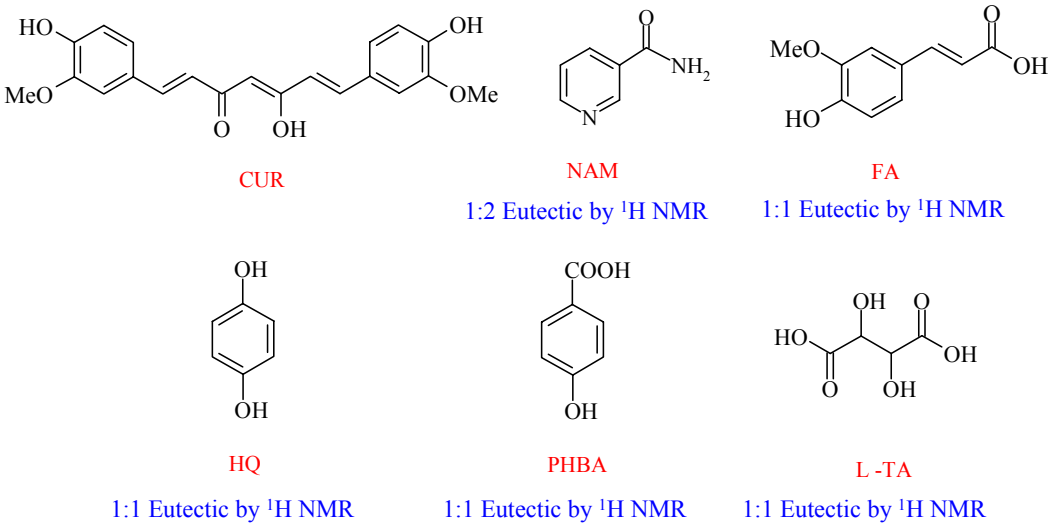

Scheme 5.1 Curcumin and coformers discussed in this study. The stoichiometry of curcumin–coformer was determined by ^{1}H NMR and eutectic nature established by DSC.

5.4.1 Powder X-ray Diffraction

Single crystal X-ray diffraction is a reliable technique to analyze the solid-state structure.[34] However, good quality single crystals is a basic requirement. Numerous failed attempts were made to grow single crystals of CUR–NAM, CUR–FA, CUR–HQ, CUR–PHBA and CUR–TA by solution crystallization and Kofler method.[35] A possible reason for not obtaining single crystals could be the mismatched or incongruent solubility of the two components in the solvents used for crystallization or large differences in the melting point of the components which made the Kofler method unsuitable for preparing single crystals. Powder XRD of the ground mixture of all the binary phases exhibited diffraction peaks that matched with the individual components (Figure 5.2), and there was no evidence of new or unique lines. Nevertheless, a lower melting endotherm in all cases suggested a eutectic composition (discussed next). Therefore, weak intermolecular interactions and unfulfilled bonds in the eutectic composition could be a reason for not obtaining single crystals.

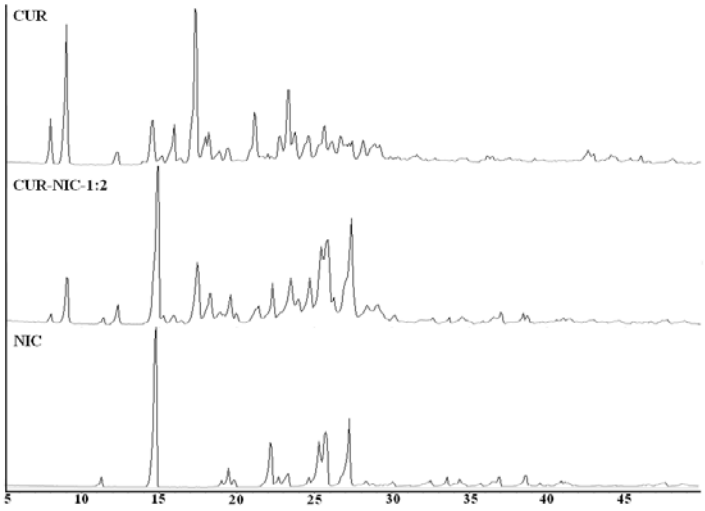

(a)

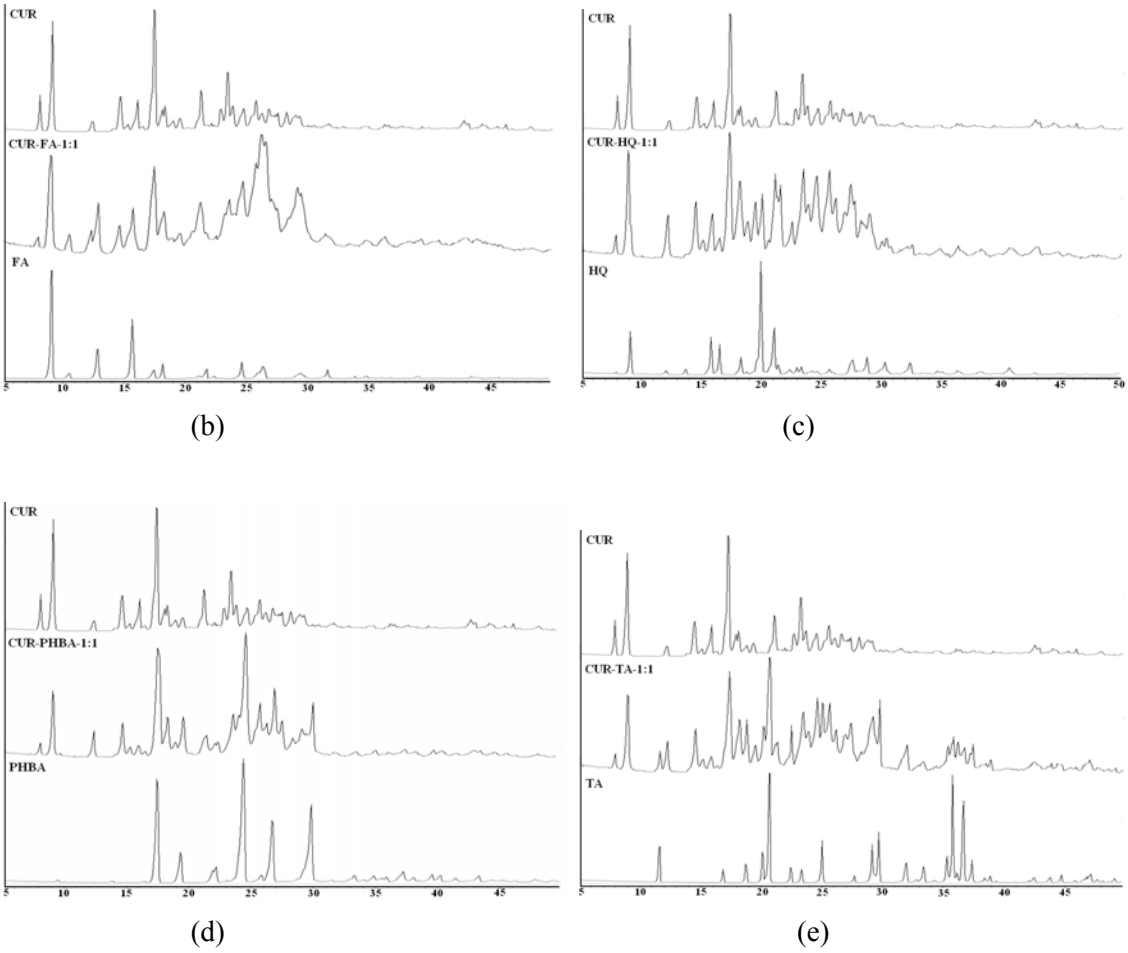

Figure 5.2 PXRD patterns of curcumin binary eutectic compositions overlayed with their starting components. There is no shift in the 2θ value of the eutectics compared to the individual components. This confirms that they are not cocrystals

5.4.2 Thermal Analysis

DSC is the most informative technique (and perhaps the only one) to establish eutectic nature of a composition. DSC analysis at a heating rate of 5°C/min showed that the product obtained by grinding curcumin and nicotinamide in 1:2 ratio has a lower melting point (CUR–NAM 110.5 °C) than that of the starting materials (CUR 181.4°C, NAM 128.3 °C).

Similar lowering of melting point for eutectic (Figure 5.3) was observed for CUR–FA (145.1 °C, FA 168–172 °C), CUR–HQ (137.5 °C, HQ 172 °C), CUR–PHBA (153.9 °C, PHBA 214–217°C) and CUR–TA (164.0 °C, TA 171–174°C). The lower melting point of the eutectic is due to weak interactions in the non-random organized product and higher entropy.[11] While the lower melting NAM formed the lowest melting eutectic in the group, the other eutectic compositions did not show any direct correlation with the melting point of the coformer. In contrast, cocrystal systems can display more regular trends[10a,5,36]. The formation of eutectic phases upon grinding was reproduced by heating of the physical mixtures in the DSC pan at a heating rate of 5°C/min. Similar to polymorphs wherein temperature causes breaking, reorganization, and making of bonds in enantiotropic systems, random unorganized molecules in the physical mixture could become non-random, organized upon heating, resulting in a eutectic with its characteristic lower melting point. The thermal profiles of ground and heated physical mixtures were similar (Table 5.2). A slightly higher T_{onset} in DSC for the physical mixture compared to the ground material (by about 3–4°C but lower temperature than the melting points of the pure components) indicate that eutectic formation is accelerated by grinding. Higher T_{onset} temperatures of the physical mixtures compared to the grinded mixtures are depicted in the overlay thermograms (Figure 5.3). The increased contact surface area between the components after grinding induces weaker eutectic interactions (a preformed eutectic), which requires lower activation energy to reach the melting temperature. In the physical mixture, however, the contact area between the components is less and so larger activation energy is required to bring the components together for inducing weak interactions (eutectic on heating). The excess activation energy required for the physical mixture gives it a slightly higher T_{onset} value compared to that of the ground mixture.[31] DSC thermograms of the ground components at room temperature and heating of the physical mixtures show that both processes resulted in a binary eutectic. In order to minimize phase transformation during heating the behavior of curcumin eutectics and physical mixtures were analyzed at higher heating rate of 200 °C/min in DSC. Except for a slight shift in the melting points, the eutectics and physical mixtures showed a similar melting behavior (Figure 5.4) to those at 5 °C/min (Table 5.2). This experiment supports the fact that irrespective of the heating rate the grinded mixture has a lower melting point (a preformed eutectic) compared to the physical mixture (eutectic on heating) and that grinding

curcumin with the coformer resulted in a eutectic. The pressure of grinding often induces cocrystal formation[28,37] by breaking and making hydrogen bonds, but when there is misfit/ mismatch or lack of secondary interactions to give a stable lattice structure,[38] the product is a eutectic composition. When the components are not entropically driven to accommodate in the lattice structure, the ground material behaves like a physical mixture, for example, as for curcumin–L-malic acid 1:1 ground product (Figure 5.5), whose melting point matches with that of the individual components. The onward crystallization of cocrystals from eutectic mixtures is monitored by DSC and HSM techniques.[39] When two endotherms are observed in DSC (different from the melting points of the starting components), the first one is due to melting of the eutectic and the second one for melting of the cocrystal grown from the eutectic.[40] Such two endotherm DSCs were not observed in our cases, meaning that cocrystals were not formed upon heating.

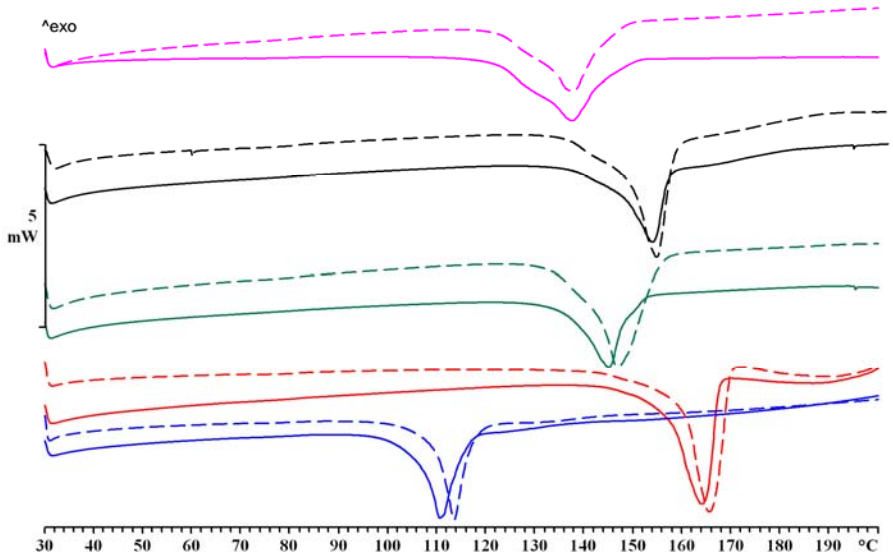

Figure 5.3 Overlay of DSC thermograms of eutectic compositions obtained by mechano-chemical grinding of curcumin and coformer (solid line) and the physical mixtures (dash line) at heating rate of 5°C/min. The ground mixtures of curcumin eutectics CUR–NAM (blue), CUR–TA (red), CUR–FA (green), CUR–PHBA (black), and CUR–HQ (violet) showed lower T_{onset} compared to the physical mixtures.

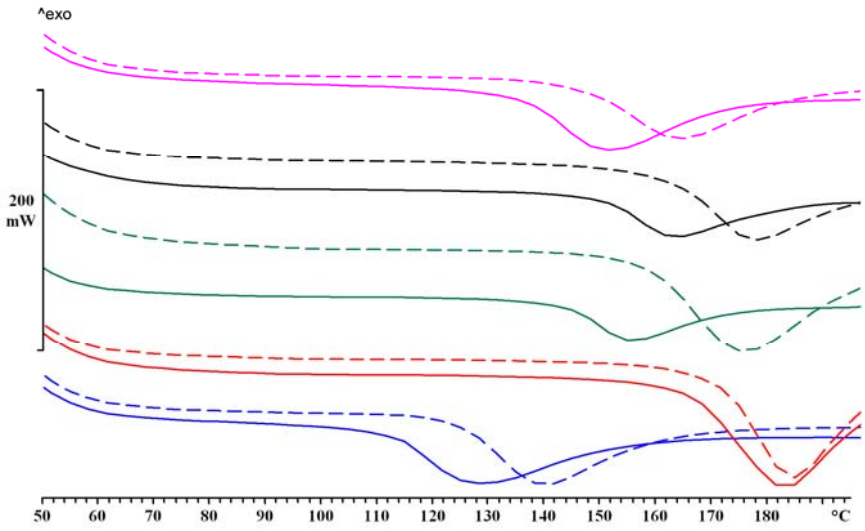

Figure 5.4 Overlay of the DSC thermograms of eutectic compositions obtained by mechanochemical grinding of curcumin and coformer (solid line) and the physical mixture (dash line) at a heating rate of 200°C/min. The ground mixtures of curcumin eutectics CUR-NAM (blue), CUR-TA (red), CUR-FA(green), CUR-PHBA(black) and CUR-HQ(violet) showed lower T_{onset} compared to the physical mixtures.

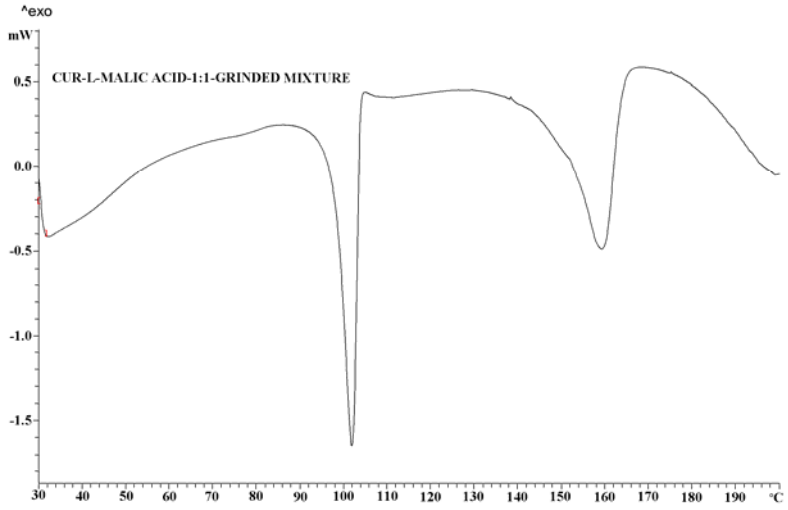

Figure 5.5 DSC of CUR-L-malic acid ground mixture. The melting points match with those of the pure components. M. point of L-malic acid 101-104 °C, CUR 181.4 °C.

Table 5.2 Melting point of binary curcumin eutectics obtained by DSC analysis of grinded mixture and physical mixture

S. No.	Eutectic phase	Coformer m.p. (°C)	Melting point of ground product at 5 °C/min (°C, T_{onset}, T_{peak})	Melting point of physical mixture at 5 °C/min (°C, T_{onset}, T_{peak})	Melting point of ground product at 200°C/min (°C, T_{onset}, T_{peak})	Melting point of physical mixture at 200°C/min (°C, T_{onset}, T_{peak})
1	Curcumin–TA (1:1)	168–170	156.9, 164.0	159.3, 165.4	162, 182	166, 184
2	Curcumin–PHBA (1:1)	214–217	146.5, 153.9	148.7, 154.7	148, 162	156, 176
3	Curcumin–HQ (1:1)	172.0	126.7, 137.5	129.6, 137.6	133, 147	145, 165
4	Curcumin NAM (1:2)	128.3	106.6, 110.5	109.5, 113.9	111, 127	122, 140
5	Curcumin-FA (1:1)	168–172	137.4, 145.1	141.1, 146.9	142, 156	156, 174

Melting point of curcumin is 181.4°C (ref. 25a).

5.4.3 Spectroscopic Analysis

IR and Raman spectroscopy respond to changes in vibrational modes of covalent bonds as a result of changes in intermolecular interactions.[41a,b] ss-NMR is sensitive to changes in short-range near-neighbor environment of the molecule.[41c] They complement diffraction techniques in understanding the nature and strength of interactions in the crystal lattice. Spectroscopic techniques have certain threshold limits below which they are not sensitive enough to quantify the strength of interactions and differences in structures for chemical interpretation. IR-Raman analysis of CUR–NAM eutectic showed vibrational frequencies which matched with those of the individual components, for example, the phenolic OH

stretch at 3510.9 cm^{-1} for curcumin was shifted just slightly to 3508.7 cm^{-1} in the product, a difference too small to conclude any structural changes. Similar minor shifts were observed for other IR frequencies in CUR–NAM (Figure 5.6).

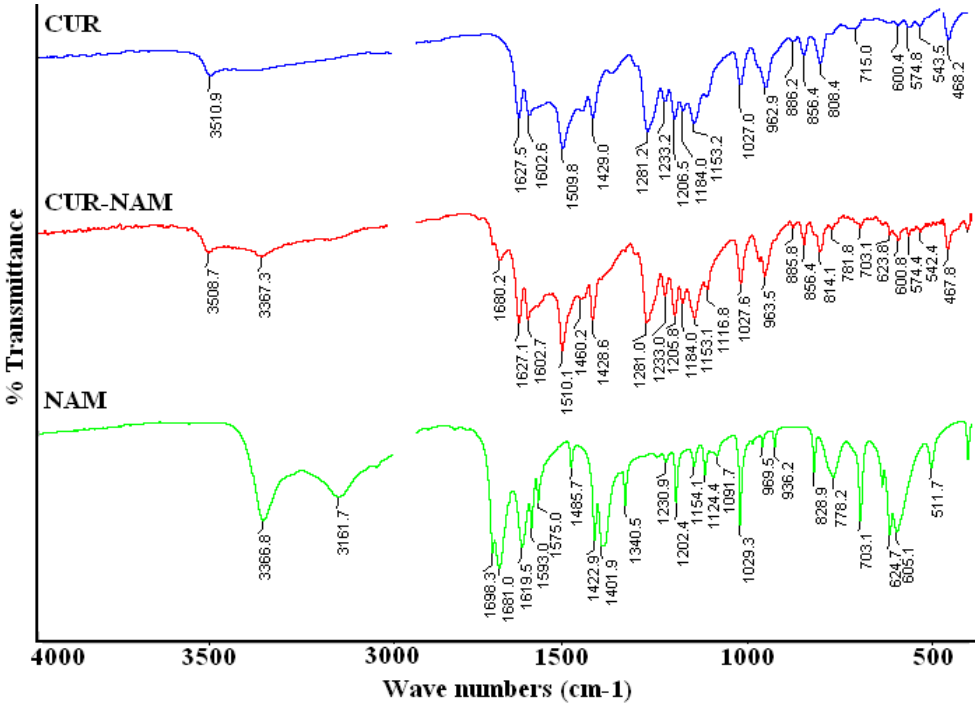

Figure 5.6 IR spectra of CUR-NAM eutectic composition compared with its starting components.

The other eutectic compositions followed the same trend with insignificant differences in the IR spectra of eutectics compared to those of the individual components (Figure 5.7, Table 5.3). Similar observations were made during Raman analysis of curcumin eutectic compositions and their starting materials. The α, β – unsaturated carbonyl peak in the raman spectra of curcumin appeared at 1626.0 cm^{-1}. On forming eutectic with nicotinamide, the raman spectra of CUR-NAM showed up at 1629.2 cm^{-1} which is not significantly different

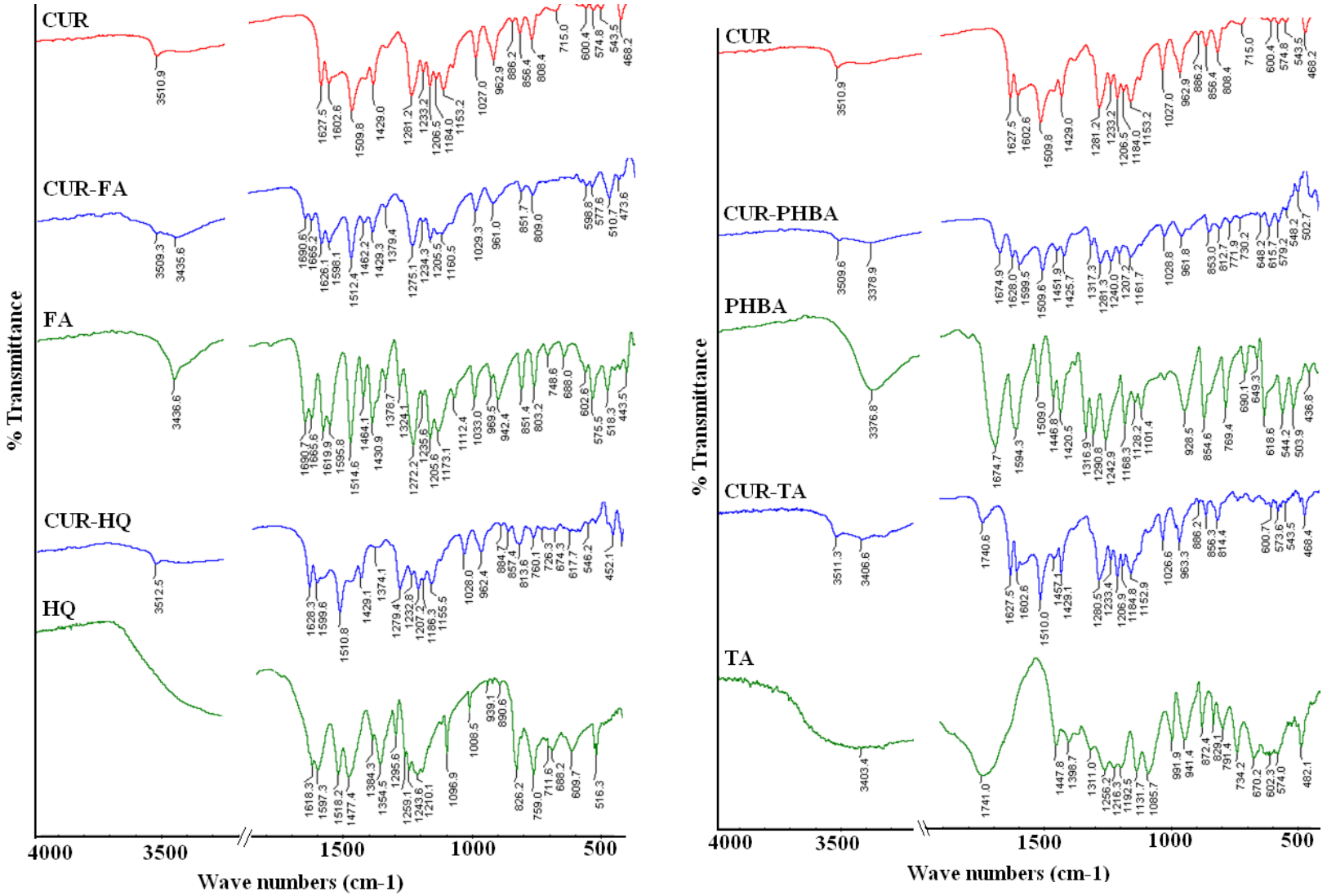

Figure 5.7 IR spectra of curcumin binary eutectic compositions compared with their starting components.

to be interpreted as a change in the hydrogen bonding patterns of the starting materials on forming eutectic compositions. The raman spectra of CUR-NAM eutectic overlayed with its starting components is shown below (Figure 5.8, Table 5.4) and that of the other eutectics in Figure 5.9.

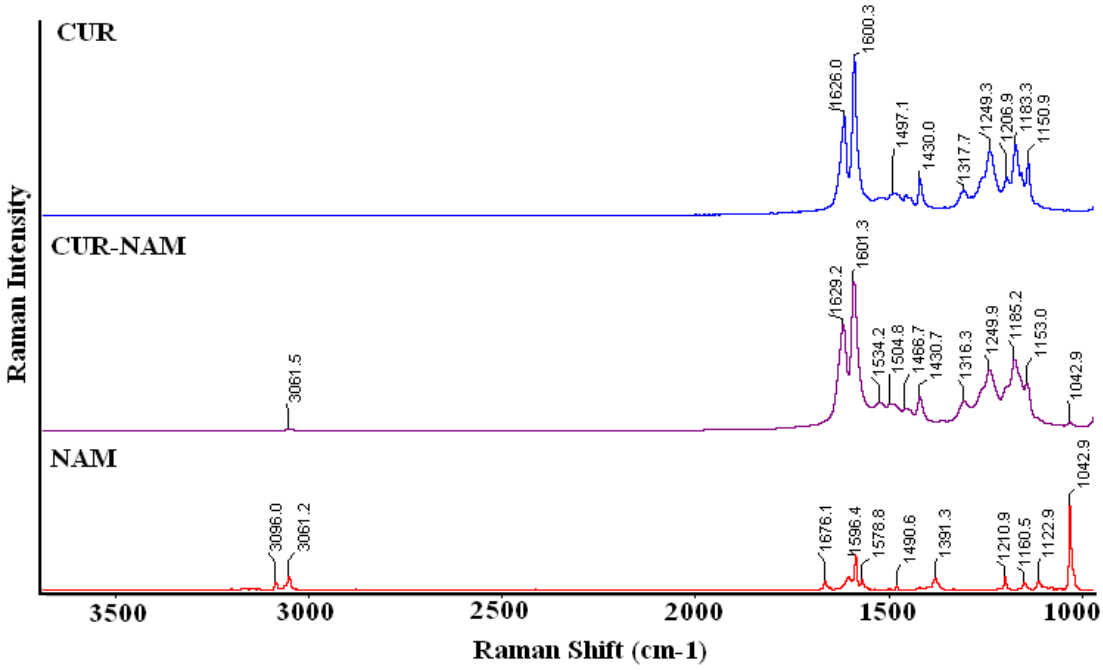

Figure 5.8 Raman spectra of CUR-NAM eutectic in comparison with their starting components.

Solid-state ^{13}C NMR spectroscopy provides information about differences in bonding patterns, molecular conformations, and molecular mobility. Whereas we noted significant changes in the chemical shifts for curcumin cocrystals,[25a] δ value differences of a similar magnitude were not observed for curcumin eutectics, possibly due to weak interactions in their solid state assembly. The phenol carbon of curcumin at δ 157.6 ppm was shifted slightly downfield to δ 158.4 ppm in the eutectic CUR–NAM, but again this change is too small to make conclusions about a crystalline phase with different molecular

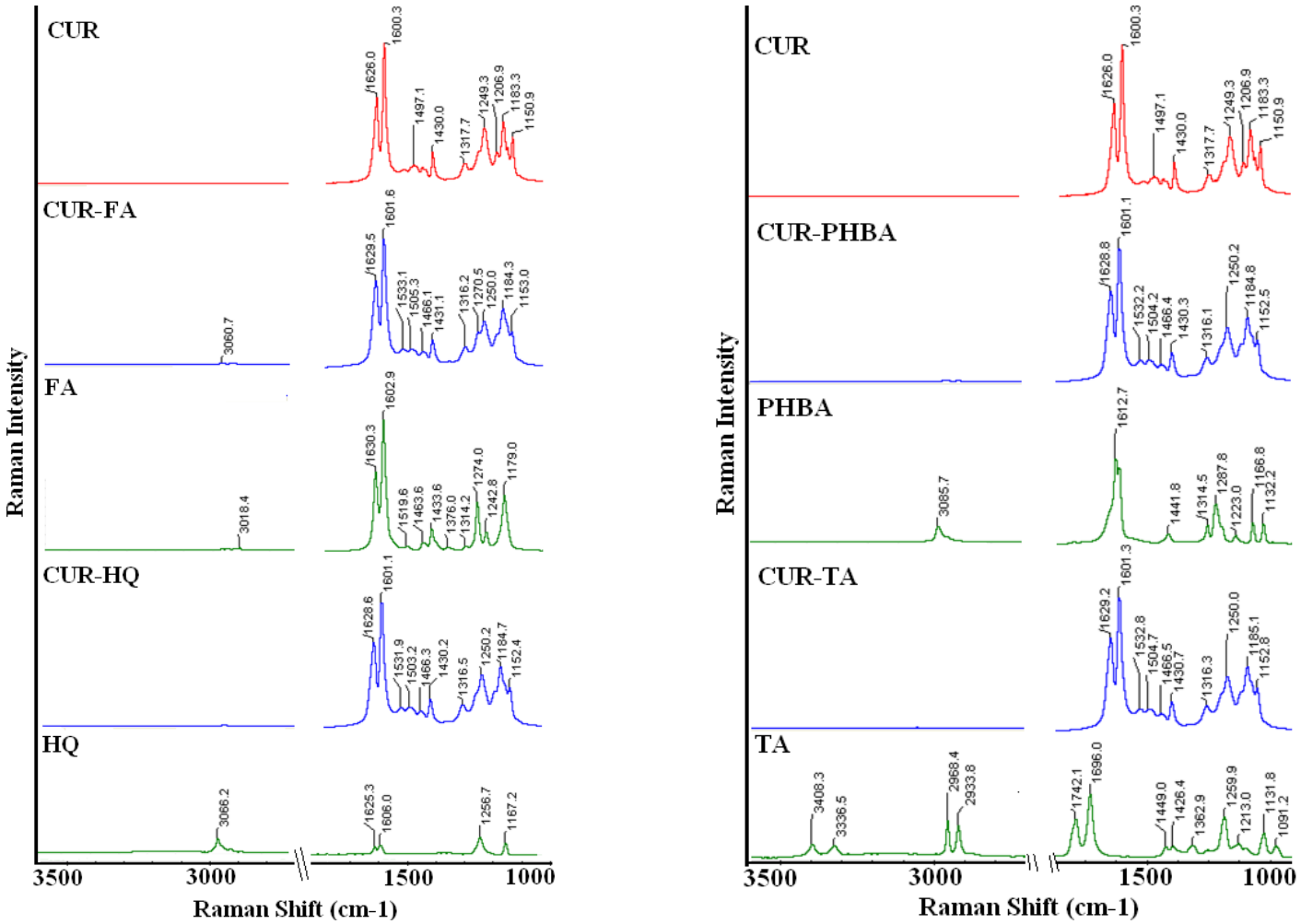

Figure 5.9 Raman spectra of curcumin eutectic compositions overlayed with their starting components.

arrangement in the crystal lattice (Figure 5.10). Even the ss-NMR spectra of other eutectic compositions indicated the absence of cocrystal with insignificant differences in the chemical shift peak positions as compared to the starting materials. (Figure 5.11, Table 5.5) nevertheless, the lower melting temperature is strongly indicative of eutectic phase. Further experiments are necessary such as pair distribution function PXRD[42] to assign the small drifts in the spectra to the eutectic phases.

Table 5.3 FT-IR vibrational stretching frequencies (ν_s, cm^{-1}) of curcumin eutectic compositions compared to the individual components.

	Phenolic/ Aliphatic OH	C=O stretch	Aromatic C=C	Enol C–O	Phenol/ Aliphatic C–O	Carboxamide N-H
CUR	3510.9	1627.5	1602.6	1429.0	1281.2	–
NAM		1681.0	1619.5			3366.8, 3161.7
CUR-NAM	3508.7	1680.2, 1627.1	1602.6	1428.6	1281.0	3367.3
FA	3436.6	1690.7	1595.8	–	1272.2	–
CUR-FA	3509.3, 3435.6	1690.6, 1626.1	1598.1	1429.3	1275.1	–
HQ	3267.4	–	1597.3	–	1295.6	–
CUR-HQ	3512.5	1628.3	1599.6	1429.1	1279.4	–
PHBA	3376.8	1674.7	1594.3	–	1290.8	–
CUR-PHBA	3509.6, 3378.9	1674.9. 1628.0	1599.5	1425.7	1281.3	–
TA	3403.4	1741.0	–	–	1256.2	–
CUR-TA	3511.3, 3406.6	1740.6	1602.6	1429.1	1280.5	–

Table 5.4 Diagnostic FT-Raman wave numbers (ν_s, cm^{-1}) of curcumin eutectic compositions compared to the individual components

	C=O	Aromatic C=C	Enol C–O	Phenol C–O/ Aliphatic C–O	N-H bending vibrations
CUR	1626.0	1600.3	1430.0	1249.3	–
NAM	1676.1	1596.4	–	–	1578.8
CUR-NAM	1629.2	1601.3	1430.7	1249.9	–
FA	1630.3	1602.9	–	1274.0	–
CUR-FA	1629.5	1601.6	1431.1	1250.0, 1270.5	–
HQ		1606.0		1256.7	–
CUR-HQ	1628.6	1601.1	1430.2	1250.2	–
PHBA	1612.7	1601.6	–	1223.0	–
CUR-PHBA	1628.8	1601.1	1430.3	1250.2	–
TA	1696.0	–	–	1251.9	–
CUR-TA	1629.2	1601.3	1430.7	1250.0	–

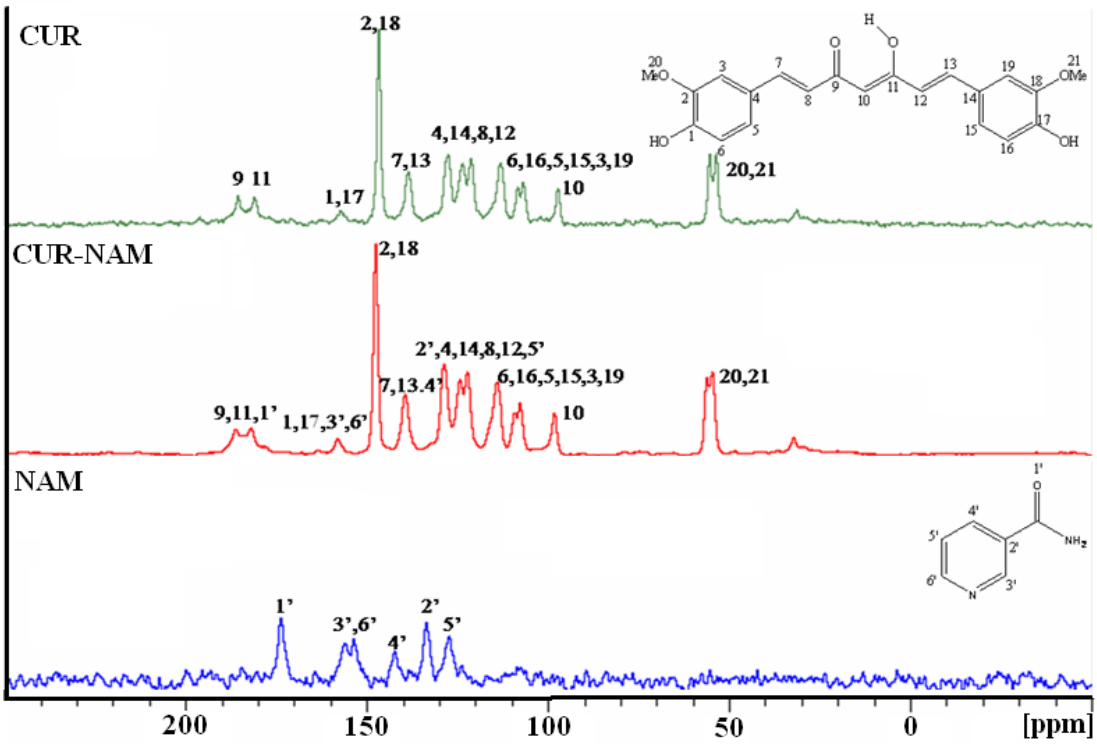

Figure 5.10 ss-NMR spectra of CUR-NAM eutectic compared with its starting components.

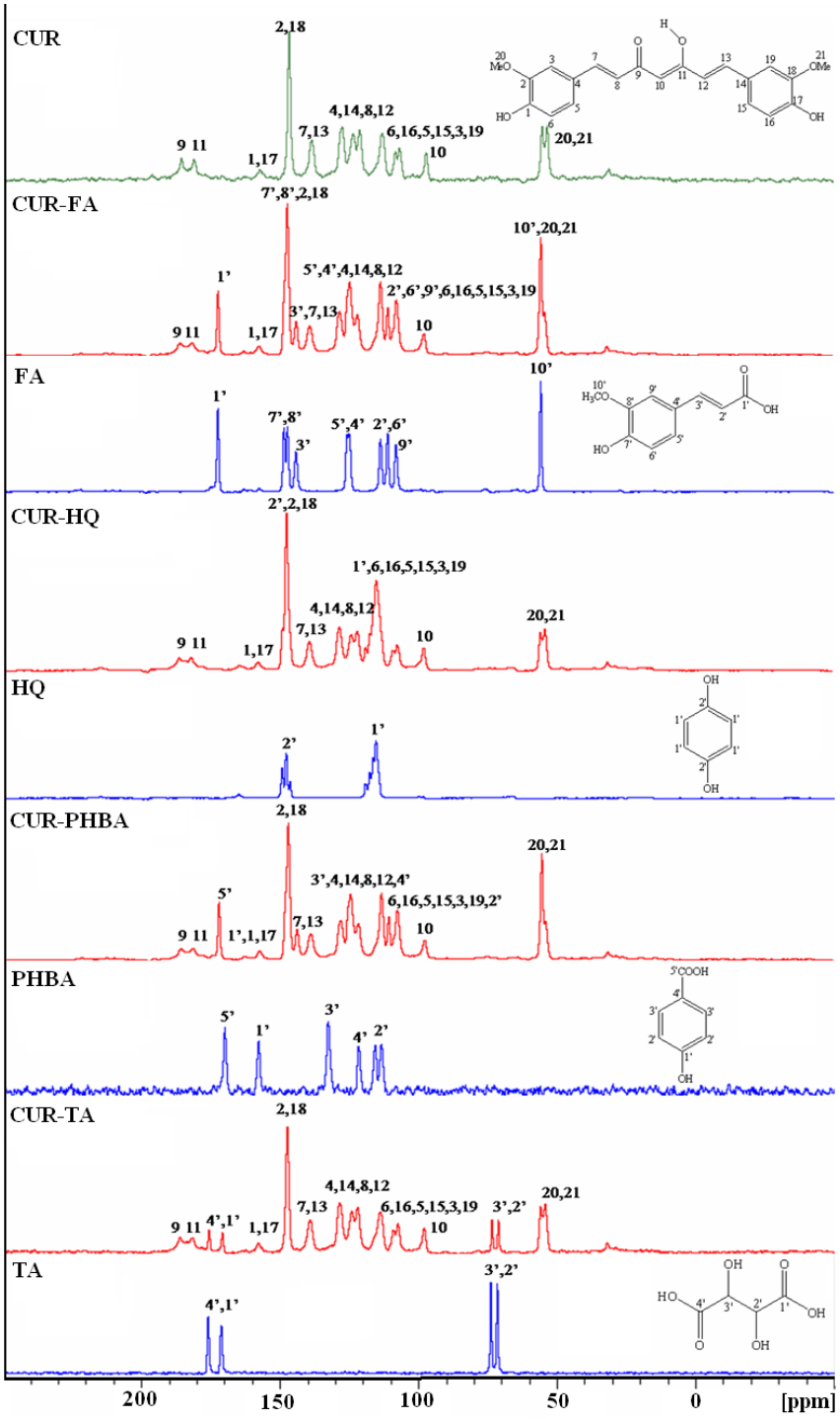

Figure 5.11 ss-NMR spectra of curcumin eutectic compositions compared with the corresponding spectra of their starting components.

Table 5.5 ^{13}C ss-NMR chemical shifts (δ, ppm) of curcumin eutectic compositions and the pure components.

Carbon No.	CUR	NAM	CUR–NAM	FA	CUR–FA	HQ	CUR–HQ	PHBA	CUR–PHBA	TA	CUR–TA
1,17	157.6	–	158.4	–	158.0	–	158.1	–	158.4	–	158.1
2,18	146.9	–	147.7	–	147.5	–	147.7	–	147.6	–	147.7
3,19	106.9	–	107.8	–	108.2	–	107.8	–	107.7	–	107.7
4,14	127.7	–	128.8	–	128.6	–	128.6	–	128.6	–	128.7
5,15	108.5	–	109.4	–	111.3	–	109.3	–	109.3	–	109.4
6,16	113.4	–	114.2	–	113.9	–	115.4	–	114.2	–	114.3
7,13	138.7	–	139.6	–	139.5	–	139.5	–	139.6	–	139.6
8,12	123.7, 121.3	–	124.5, 122.4	–	125.1, 122.3	–	124.4, 122.3	–	124.4, 122.2	–	124.5, 122.3
9,11	185.7, 183.7	–	186.5, 182.2	–	186.4, 182.1	–	186.3, 184.0	–	186.4, 184.4	–	186.5, 183.7
10	97.4	–	98.3	–	98.2	–	98.3	–	98.2	–	98.3
20,21	55.5,53.7	–	56.3,54.7	–	56.0,54.6	–	56.3,54.5	–	56.3,54.6	–	56.3,54.6
1',	–	174.3	174.7	172.6	172.6	116.5	117.7	158.3	158.4	175.9	175.9
2'	–	133.1	128.8	113.9	113.9	147.7	149.1	115.9, 113.9	114.2	73.9	73.9
3'	–	155.9	158.4	144.4	144.4	–	–	133.2	133.9	71.6	71.6
4'	–	142.6	139.6	125.2	125.1	–	–	122.1	122.4	171.2	171.1
5'	–	127.8	128.8	126.0	125.1	–	–	170.5	171.1	–	–
6'	–	152.9	158.4	111.3	111.3	–	–	–	–	–	–
7'	–	–	–	148.8	147.5	–	–	–	–	–	–
8'	–	–	–	147.5	147.5	–	–	–	–	–	–
9'	–	–	–	108.3	108.2	–	–	–	–	–	–
10'	–	–	–	56.0	56.0	–	–	–	–	–	–

5.4.4 Solubility and Dissolution

The bioavailability and efficacy of a drug largely depends upon its solubility and dissolution rate in the aqueous medium. Eutectics are known to confer high solubility and faster dissolution to the parent drug molecules because of their excess thermodynamic functions such as high free energy, greater molecular mobility, and weaker intermolecular interactions.[29a,43] The solubility and dissolution rates of eutectics CUR–NAM, CUR–FA, CUR–HQ, CUR–PHBA and CUR–TA were determined in 40% EtOH–water medium because the concentration of curcumin in pure water is very low. It was not possible to obtain equilibrium solubility (at 24, 48 h) because the eutectic components dissociated after some time due to incongruent solubilities; curcumin is completely insoluble and the coformers are highly soluble in the medium. The more soluble component of an incongruent composition dissolves faster into solution, precipitating the less soluble species.[44] Due to the very high solubility of the coformer in 40% EtOH–water, the coformers dissolved quickly leaving behind a precipitate of curcumin. Dissolution rate, be it of tablet or powder, is a kinetic or time-dependent phenomenon. IDR is the method of choice for those drugs that undergo phase transformation (e.g. polymorph, hydrate) or dissociation (cocrystal, eutectic) during slurry solubility measurements. IDR gives an idea of the time required for drug onset (typically 30 min or less), peak concentration of the drug (C_{max}), the amount of drug dissolved (AUC), and the time taken for dissolution before phase transformation/ drug cocrystal dissociation occurs (say 4–6–8 h). Faster dissolution rate and high oral drug delivery[45] are the goal in pharmaceutical development.

IDR experiments on curcumin eutectics were performed in 40% EtOH–water for 7 h by the rotating disk intrinsic dissolution rate (DIDR) method[46] at 37 °C. CUR–NAM showed 10.6 fold higher IDR than curcumin but the other eutectics CUR–FA, CUR–HQ, CUR–PHBA, and CUR–TA showed less dramatic accelerations of 6.8, 5.6, 4.4, and 2.1 times. PXRD of the residue remaining at the end of dissolution experiment matched with that of curcumin form 1, indicating dissociation to the components due to incongruent solubility of curcumin and coformers. We observed a semi-quantitative trend between the melting point of the eutectic and its dissolution rate, i.e. lower the melting point higher the IDR, similar to the

trend for cocrystals[5,36]. The only exception to this trend is CUR–FA. Interestingly, the eutectic melting points were much better correlated to dissolution rates[47a] than coformer solubility.[47b] Nevertheless, these correlations are quite system dependent and not universal[31,33,43] in nature. Intrinsic dissolution rate curves are displayed in Figure 5.12, and dissolution rates, melting points, and coformer solubility are listed in Table 5.6. The amount of dissolved curcumin after 5 h ($AUC_{0\text{-}5h}$) is 315.1 mg h/L for CUR, 530.7 mg h/L for CUR–TA, 1059.7 mg h/L for CUR–PHBA, 1016.5 for CUR–HQ, 1842.6 for CUR–NAM, and 1256.0 for CUR–FA. The AUC value, which indicates the total dissolved curcumin in a given time period, is the highest for CUR–NAM (5.85 times greater than curcumin), followed by CUR–FA, and then CUR–PHBA. To compare with cocrystals, $AUC_{0\text{-}5h}$ values for curcumin–resorcinol and curcumin–pyrogallol cocrystals are 888.8 mg h/L and 3141.3 mg h/L respectively.[25b] To summarize, the solubility of curcumin is increased between 3–11 times and total dissolved curcumin 2–6 times through binary eutectic compositions. Curcumin–pyrogallol cocrystal exhibited the highest dissolution rate but pyrogallol is not a GRAS molecule and has its own pharmacological profile.[27] Therefore novel curcumin eutectics appear to be promising candidates for solubility enhancement of the herbal active ingredient with safe additives whereas the pyrogallol cocrystal could be developed as a multi-drug polypill.

In addition to IDR, powder dissolution (PD) was measured. Unlike IDR wherein the effect of particle size is overcome by making a pellet, particle size distribution is very important in PD since drug particles are directly exposed to the aqueous solvent. Smaller particles with larger surface area have higher solubility. For a set of compounds solubility order can be different when measured and compared through IDR and PD methods. This variation is due to non-uniform particle size distribution in PD measurements.[48] Particles of a near-uniform size distribution (25–75 μm) were obtained by sieving the powders through 75 μm mesh and then the sieved powder again through 25 μm mesh. Even after taking PSD in a narrow range, the solubility numbers did not match any better with the IDR numbers (Figure 5.13). While CUR–NAM eutectic exhibited the highest solubility and higher AUC in IDR experiments, The PD rates for 120 min (peak solubility) are CUR–FA 244 mg/L > CUR–TA 226 mg/L > CUR–HQ 219 mg/L > CUR–PHBA 214 mg/L > CUR–NAM 197 mg/L > CUR 99 mg/L

indicate a difference in the solubility order. We observed that eutectics with smaller particles, for example, CUR–FA and CUR–TA, exhibited higher solubility than larger PSD eutectic CUR–NAM. Powder Dissolution rates and $AUC_{0\text{-}5h}$ of binary eutectics are listed in Table 5.7. Physical effects play a greater role in eutectic compositions which have weak interactions and so the role of coformer, or chemical effects, is less.[46b] Despite these subtle effects and differences in physical behavior, the main objective of enhancing curcumin solubility was successfully achieved in binary eutectic compositions. Moreover, nicotinamide, ferulic acid, and tartaric acid are safe chemicals and used as additives in nutraceuticals and drugs. Representative PXRD pattern at the end of solubility and dissolution experiments is shown in Figure 5.14.

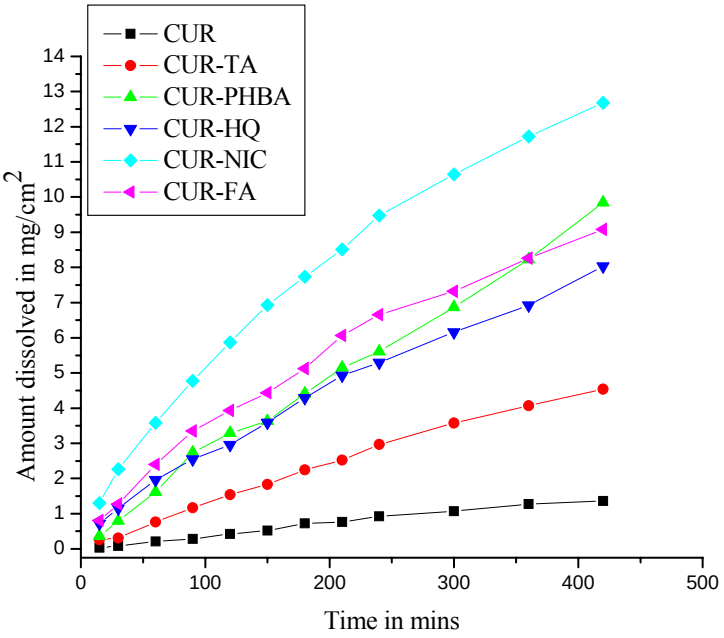

Figure 5.12 Intrinsic dissolution rate curves of curcumin binary eutectic compositions in 40% EtOH–water.

Table 5.6 Intrinsic dissolution rates of curcumin eutectic compositions along with their molar extinction coefficient (ε), and melting point. The number of times enhancement of IDR and AUC with respect to curcumin is given in parentheses.

Compound	Molar extinction coefficient, ε /mM cm	Intrinsic dissolution rate, $(mg/cm^2)/min$ $(x10^{-3})$	M.P.(°C)	Solubility of coformer in water g/L	Area under the curve, $AUC_{0\text{-}5h}$ (mg h)/L
CUR	46.21	6.1	181.4	0.008	315.1
CUR–TA	33.77	13.2 (x 2.16)	164.0	1333	530.7 (x 1.68)
CUR–PHBA	40.97	27.0 (x 4.43)	153.9	5	1059.7 (x3.36)
CUR–HQ	36.51	34.4 (x5.64)	137.5	70	1016.5 (x3.26)
CUR–NAM	42.82	64.7 (x 10.6)	110.5	1000	1842.6 (x5.85)
CUR–FA	38.68	41.2 (x 6.75)	145.1	0.78	1256.0 (x3.99)

The dissolution rate of curcumin–resorcinol and curcumin–pyrogallol cocrystals is 4.72 and 11.76 times faster than curcumin (ref. 25b).

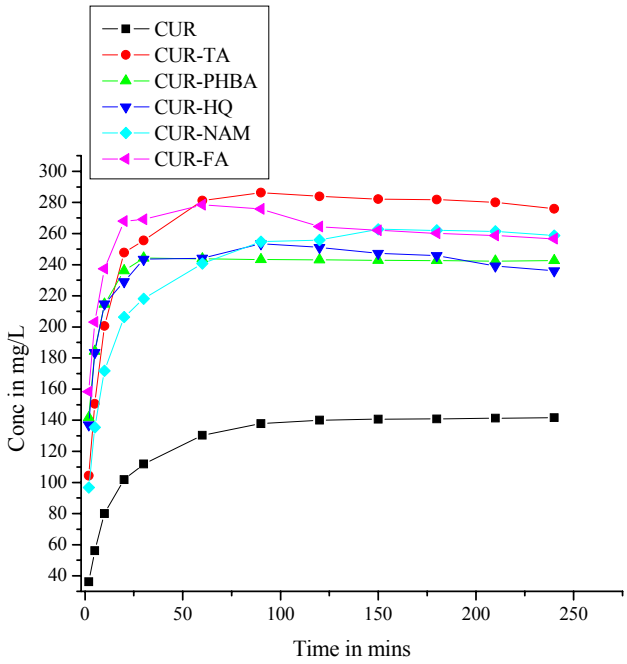

Figure 5.13 Powder dissolution rates of curcumin binary eutectic compositions in 40% EtOH–water.

Table 5.7 Powder dissolution rate of curcumin eutectic compositions and their AUC values.

Compound	Solution concentration in mg/L (120 min)	AUC for 120 min (mg h)/L	Solubility of coformer in water g/L
CUR	99	1428.2	0.008
CUR–TA	226	3113.2	1333
CUR–PHBA	214	2806.2	5
CUR–HQ	219	2840.4	70
CUR–NAM	197	2709.7	1000
CUR–FA	244	3148.4	0.78

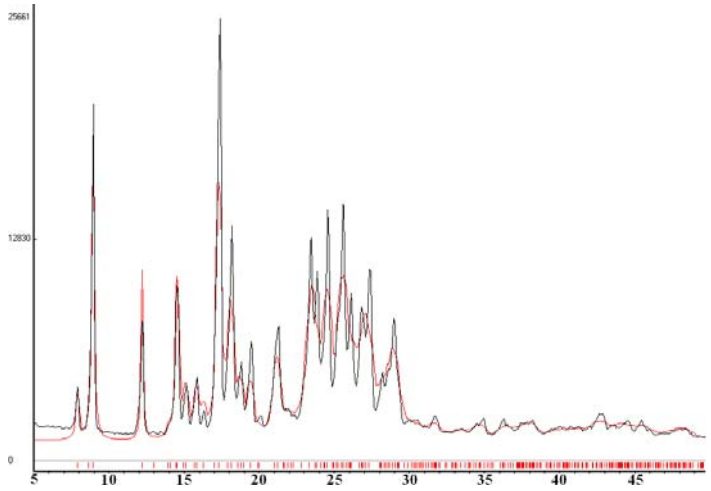

Figure 5.14 Representative PXRD pattern of curcumin and all the eutectics at the end of solubility and dissolution experiments matches very well with the calculated pattern of curcumin.

5.4.5 Towards Understanding Design Aspect in Eutectics

The ultimate aim of developing solid forms of curcumin was to optimize its physicochemical properties like solubility, dissolution etc. In order to realize this we have used crystal engineering principles[49] and hydrogen bonding rules[50] as design elements to form cocrystals of curcumin. Mechanochemical grinding of curcumin with various GRAS coformers resulted in binary eutectics instead of cocrystals. Although the sole purpose of addressing the

solubility issue of curcumin was served through binary eutectics of which CUR-NAM, CUR-FA and CUR-TA showed better solubility compared to the previously reported pharmaceutical cocrystal of curcumin with resorcinol, yet the accidental discovery of the eutectics raise concerns at the lack of design aspect in preparing them. The lack of proper characterization tools to analyze the solid state assembly of a eutectic composition would only complicate any attempt towards understanding and designing them. Nevertheless, on analyzing the reported eutectic compositions and the binary eutectics that are discussed in this chapter, four criteria seem to play a crucial role in forming eutectic compositions over the expected cocrystals. They are 1. Lack of auxiliary interactions. 2. Misfit or mismatch of components. 3. Molecular symmetry. 4. Structural similarity.

Lack of auxiliary interactions: This criterion is best illustrated through Benzamide-Benzoic acid eutectic. In 2008 Singh et. al.[33], reported the benzamide-benzoic acid eutectic which was used as a model for understanding the thermodynamic and microstructural features of eutectics. In 2009, Brittain[51] claimed to have made a cocrystal between benzamide and benzoic acid based on the minor differences in the product phase in IR and PXRD spectra. In 2011, Seaton and coworkers[38] revisited this group of molecules and showed that the lack of auxiliary interactions that support the major acid-amide heterosynthon in the benzamide-benzoic acid system resulted in the formation of eutectic instead of cocrystal. In the absence of additional supporting interactions, cohesive interactions dominate the adhesive forces favoring the eutectic formation. They have supported this hypothesis by forming cocrystals of benzamide with various derivatives of benzoic acid like 3-nitro benzoic acid and pentafluoro benzoic acid etc (Figure 5.15). Here the auxiliary hydrogen bonds augment the primary acid-amide synthon, strengthening the heteromeric interactions for cocrystal formation. For similar reasons, paracetamol-cloperastine hydrochloride[52] also forms a eutectic.

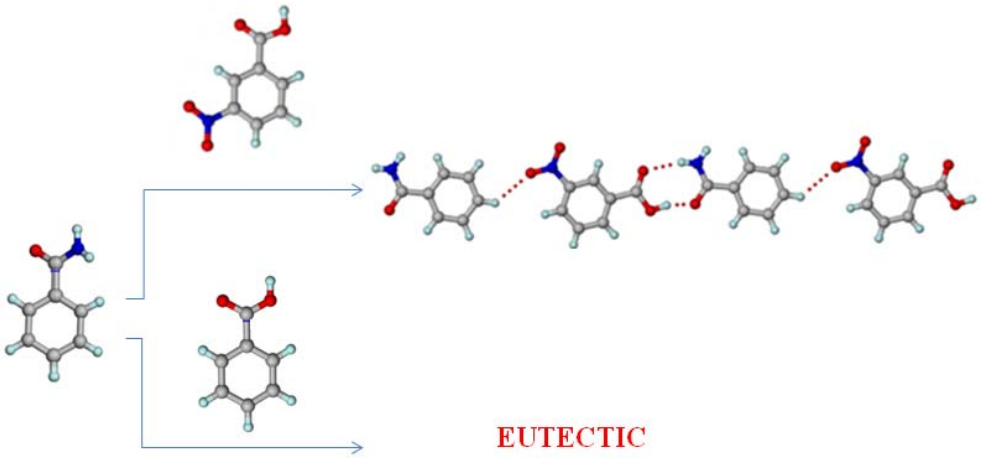

Figure 5.15 Here the nature of the product obtained on reacting benzoic acid and 3-nitrobenzoic acid separately with benzamide is depicted. In the case of 3-nitro benzoic acid-benzamide system, the primary acid-amide synthon is supported by auxiliary C–H···O interactions leading to a cocrystal. Whereas the absence of auxiliary interactions favored eutectic formation in benzamide-benzoic acid system (Adapted from ref.38).

Misfit or mismatch of components: The homomeric interactions in a crystal structure align the molecules in a precise manner in order to form a minimum energy arrangement. During cocrystallization, this solid state assembly is forced to combine with that of a second component. In the process of cocrystal formation, the parent lattice arrangement may be retained in certain cases, wherein the second component may be inserted into the lattice of first component as a spacer or it may be disrupted in order to form a totally different solid state assembly[53]. In those cases where one of the components is predisposed to retain its lattice structure during cocrystallization, the second component with appropriate shape, size and functional groups can form a cocrystal. When there is a misfit or mismatch between the components it leads to a eutectic where the two components behave as a conglomerate of solid solutions. This criterion may be exemplified through Itraconazole-Succinic acid cocrystal[5b] and Itraconazole-Phenol Eutectic. Park and coworkers[10f] illustrated that Itraconazole and phenol in 2% (w/w) ratio forms a eutectic which was shown to enhance the cell permeability of Itraconazole. Analyzing the crystal structure of Itraconazole[54] reveal that the molecules are arranged in a centrosymmetric dimer like motif (Figure 5.16a). When it is

combined with phenol, the coformer neither has any strong functional groups to disrupt the supramolecular assembly of Itraconazole in order to form a cocrystal with novel solid state assembly nor does it have the appropriate size or shape to fit into the voids, acting as a spacer. Therefore due to misfit and mismatch between the components the Itraconazole-phenol system forms a eutectic. In the case of Itraconazole-succinic acid system, although succinic acid do not have the ideal functional groups to disrupt the solid state assembly of parent molecule, it has the ideal size and shape to fit into the parent lattice with minimum changes to its molecular conformation. As a result succinic acid formed a cocrystal with Itraconazole (Figure 5.16b).

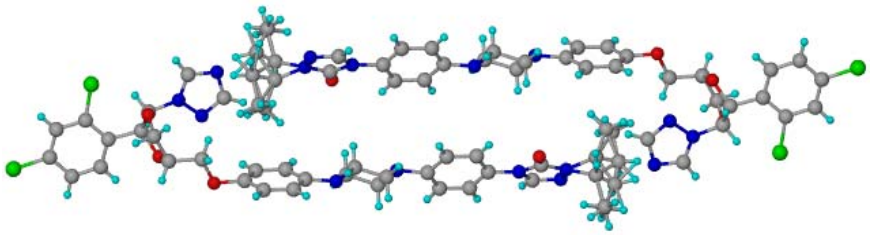

(a)

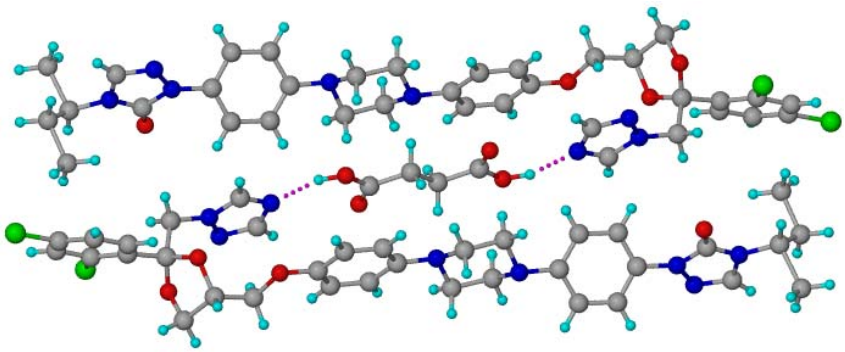

(b)

Figure 5.16a) The individual molecules in Itraconazole crystal structure are held together in a centrosymmetric dimer like arrangement. This structure is disordered at the triazolone ring. **b)** Succinic acid coformer had the appropriate shape, size and functional groups to fit into the solid state assembly through O–H··N interactions with minimum changes to the molecular conformation of Itraconazole, resulting in a cocrystal. Whereas phenol does not qualify any of the above morphological or structural criteria for cocrystal formation, hence it results in a eutectic (Adapted from ref. 54 and 5b respectively).

Molecular symmetry: Internal symmetry in one of the reacting components seems to favor eutectic formation. This criterion may be best illustrated through curcumin-resorcinol cocrystal[25b] and curcumin-hydroquinone eutectic (Figure 5.17). During our earlier attempts to form cocrystals of curcumin we obtained a 1:1 cocrystal with resorcinol. Later, in order to expand the structural landscape[55] of curcumin we performed mechanochemical grinding with other GRAS coformers. In the process we obtained a eutectic with hydroquinone as described in previous sections of this chapter.

Since resorcinol and hydroquinone are structural isomers, there are no additional auxiliary interactions in resorcinol that favor the cocrystal formation which are absent in hydroquinone. Although we cannot rule out the misfit-mismatch criterion as a plausible reason for cocrystal formation with resorcinol and a eutectic with hydroquinone, one other prominent feature that differentiates them is the molecular symmetry. Although the role of molecular symmetry in eutectic formation is not clear, yet internal symmetry in the components of reported eutectic compositions intrigued us to look at it as a plausible criterion. Even in the other reported eutectic systems, molecular symmetry was observed in either one of the components, like tartaric acid in curcumin-L-tartaric acid eutectic (in this chapter), succinic acid in Griseofulvin-succinic acid eutectic[10d] etc. Cherukuvada et. al.[10d] had shown that various attempts to form ternary cocrystals of Pyrazinamide and Isoniazid with succinic acid and fumaric acid separately resulted only in eutectics of binary cocrystals (scheme 5.2). This was also reasoned to the internal symmetry of succinic acid and fumaric acid coformers. Although it is evident that this criteria is system specific, since there are many reported cocrystals with these coformers, further experiments needs to be undertaken to understand the conditions under which this criteria becomes crucial for eutectic formation.

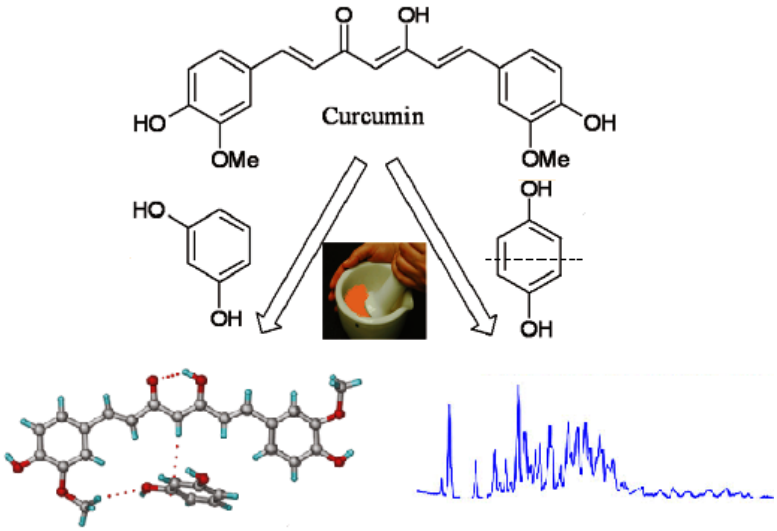

Figure 5.17 While resorcinol formed a cocrystal with curcumin during mechanochemical grinding experiments, its structural isomer hydroquinone formed a eutectic. The internal symmetry of the hydroquinone coformer in addition to the misfit-mismatch criteria seemed to favor the eutectic formation (Adapted from ref. 25b).

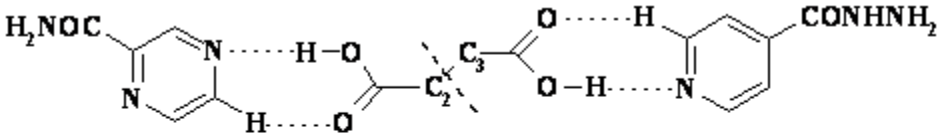

Pyrazinamide (PZA) Dicarboxylic acid Isoniazid (INH)

Succinic acid (SA): C_2—C_3

Fumaric acid (FA): C_2=C_3

Scheme 5.2 Proposed scheme for the formation of ternary cocrystals of Pyrazinamide, and Isoniazid with succinic acid and fumaric acid separately. The internal symmetry of the coformer molecules might have played a role in inhibiting the formation of ternary cocrystal (Adapted from ref. 10a).

Molecular similarity: One common feature that brings together Lidocaine-Prilocaine eutectic[14] and curcumin-ferulic acid eutectic is the structural similarity of their individual components (scheme 5.3). Lidocaine and Prilocaine have a common methyl phenyl

acetamide moiety and 4-hydroxy-3-methoxy phenyl prop-2-ene-one is the common skeleton of curcumin and ferulic acid. While seeding with structurally similar compounds is known to result in novel polymorphs[56], it is still preliminary to conclude that grinding compounds with similar molecular skeleton would result in a eutectic composition. Since cocrystals with structurally similar compounds are reported in literature[57], it would be interesting to study the conditions under which such type of compounds would form a eutectic.

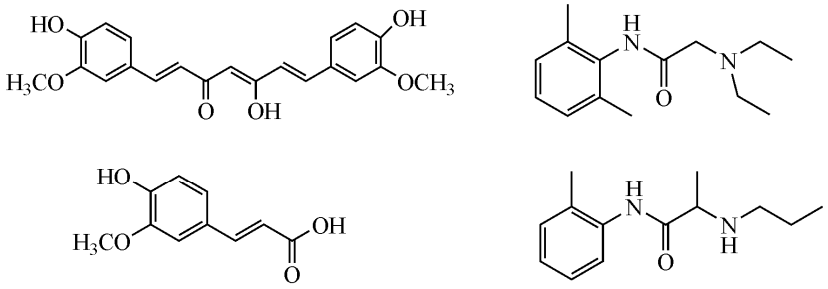

(a) (b)

Scheme 5.3a) Molecular structures of curcumin and ferulic acid and **b)** lidocaine and prilocaine. The structural similarity between the components might have resulted in eutectic formation.

The lack of appropriate characterization tools have distanced researchers from looking at eutectics as a serious alternative for solubility enhancement of poorly soluble drugs. The above criteria were put forth based on the observations made while analyzing the reported eutectic compositions and from our own experience with curcumin binary eutectics. Although systematic experiments needs to be done before seriously considering the above criteria as rules for forming eutectics, nevertheless, they can be invaluable to a certain extent as design strategies in selecting compounds for eutectic formation. Since cocrystals are known to grow from the eutectic melts of two component systems, it would be pertinent to understand the role of kinetic and thermodynamic factors apart from the structural features that favor eutectics in some cases and cocrystals in the others. This understanding may be helpful in analyzing the microstructure of eutectics which would enhance its importance as a promising alternative for solubility enhancement of poorly soluble drugs.

In addition, it is possible to characterize eutectic mixtures using the atomic pair distribution function (PDF) approach[42]. It is used to study the local structure of materials. PDF is obtained from a total scattering powder diffraction pattern via a fourier transform. Since the total scattering is composed of Bragg as well as diffuse scattering contributions, it contains local, medium range and long range structural information. But this requires high intensity X-ray sources which are not available in laboratory diffractometers routinely. However, it is only a matter of time that high intensity X-rays will be available for routine characterization of solid forms. Another technique that might be helpful in understanding the nature of eutectic composition is EXAFS[59] (Extended x-ray absorption fine-structure spectroscopy). It is used to determine the distances, coordination number, and the nature of the neighbors of the absorbing atoms. Therefore it may be helpful in understanding the short range interactions in eutectic mixtures.

5.5 Conclusions

Mechano-chemical grinding of curcumin with GRAS coformers resulted in the formation of binary eutectics with higher solubility and faster dissolution rates. The formation of eutectics, instead of the expected cocrystals, is not totally surprising since mechano-chemical grinding can which can induce long range order to form cocrystals can also form eutectic compositions stabilized by weak, short-range interactions. The solitary confirmatory test for eutectic formation is the lowering of melting point and a single endotherm in DSC. The absence of more than one melting peak in DSC confirmed that there was no further transformation to cocrystal or unreacted solid phase. The intrinsic dissolution rates of binary eutectic compositions were 3–11 times faster and AUC values 2–6 times higher than pure curcumin and three compounds, CUR–NAM, CUR–FA and CUR–HQ, are superior to the previously studied curcumin–resorcinol cocrystal. IDR, PD and AUC values of binary eutectics were higher than that of pure crystalline curcumin. The ultimate aim of the work was to increase curcumin solubility through physical form modification, and this objective was achieved through binary eutectic compositions. The exact multi-component physical form, such as salt, cocrystal, or eutectic, is not that relevant so long as the product exhibits

improved pharmacokinetic properties and good stability. Our binary eutectic compositions were found to be stable in ambient conditions of 35°C and 40% RH for over 6 months. Given their crystalline nature they are less likely to undergo spontaneous phase transformations compared to amorphous forms. Hence eutectics confer both solubility and stability advantage, similar to cocrystal counterparts.[39] Our results show that mechano-chemical grinding can induce eutectic formation in addition to the several examples of cocrystals reported in the literature. It is advisable to check solid form screen products by DSC and confirm eutectic phases.

5.6 Experimental Section

Curcumin was obtained from local suppliers and coformers (purity > 99.8%) were purchased from Sigma-Aldrich (Hyderabad, India). Solvents (purity > 99%) were purchased from Hychem Laboratories (Hyderabad, India). Water filtered through a double deionized purification system (Aqua DM, Bhanu, Hyderabad, India) was used for all experiments.

Preparation of eutectic compositions Curcumin and the coformer were taken in a stoichiometric ratio and subjected to solid-state grinding in a mortar-pestle for 15 min. The resultant ground product was characterized and used in next experiments.

^{1}H NMR spectroscopy All ground products were characterized by ^{1}H NMR to confirm their stoichiometry. Proton NMR spectra were recorded on Bruker Avance 400 MHz spectrometer (Bruker-Biospin, Karlsruhe, Germany). Chemical shifts are quoted in δ scale and J coupling in Hz.

CUR-NAM (1:2). ^{1}H NMR (DMSO-d_6): 3.82 (6H, s), 6.04 (1H, s), 6.76 (2H, d, J 16), 6.82 (2H, d, J 8), 7.15(2H, d, J 8), 7.31 (2H, s), 7.47 (2H, d, J 7), 7.51 (2H, d, J 16), 7.60 (2H, dd, J 7,5), 8.18 (4H, d, J 8), 8.68 (2H, d, J 5), 9.0 (2H, s). OHs (CUR) exchange in solvent.

CUR–FA (1:1). ^{1}H NMR (DMSO-d_6): 3.82 (9H, s), 6.05 (1H, s), 6.37 (1H, d, J 16), 6.72 (1H, d, J 8), 6.76 (2H, d, J 16), 6.82 (2H, d, J 8), 7.05 (1H, d, J 8), 7.15 (2H, d, J 8), 7.26

(1H, s), 7.31 (1H, s), 7.49 (1H, d, J 16), 7.55 (2H, d, J 16). OHs (CUR and FA) and COOH (FA) exchange in solvent.

CUR–HQ (1:1). ^{1}H NMR (DMSO-d_6): 3.81 (6H, s), 6.05 (1H, s), 6.54 (4H, s), 6.71 (2H, d, J 8), 6.81 (2H, d, J 16), 7.14 (2H, d, J 8), 7.28 (2H, s), 7.54 (2H, d, J 16), 8.72 (2H, s). OHs (CUR) exchange in solvent.

CUR–PHBA (1:1). ^{1}H NMR (DMSO-d_6): 3.82 (6H, s), 6.05 (1H, s), 6.69 (2H, d, J 8), 6.76 (2H, d, J 16) 6.81 (2H, d, J 8), 7.14 (2H, d, J 8), 7.29 (2H, s), 7.55(2H, d, J 16), 7.78 (2H, d, J 8), 9.72 (1H, s), 10.29 (1H, s). OHs (CUR) exchange in solvent.

CUR–TA (1:1). ^{1}H NMR (DMSO-d_6): 3.82 (6H, s), 4.31 (2H, s), 6.07 (1H, s), 6.76 (2H, d, J 16), 6.83 (2H, d, J 8), 7.15 (2H, d, J 8), 7.3 (2H, s), 7.55 (2H, d, J 16), 9.78 (2H, s), enolic OH (CUR) and COOH (TA) exchange in solvent.

Dissolution and solubility measurements: IDR experiments on curcumin eutectic compositions were performed in 40% ethanol–water medium at a particular λ_{max} (CUR 430 nm, CUR–NAM 428 nm, CUR–FA 428 nm, CUR–HQ 429 nm, CUR–PHBA 428 nm, CUR–TA 430 nm) for each compound. The procedure is similar to that described in chapter 3.

For powder dissolution studies of curcumin and its eutectic mixtures, the starting solids were sieved in standard mesh sieves to provide samples with particle size range 25 μm < PSD < 75 μm and then directly poured into 500 mL of the dissolution medium (40% ethanol–water), and paddle rotation was fixed at 150 rpm. Dissolution experiments were continued up to 4 h at 37 ºC. At regular intervals, 5 mL of the dissolution medium was withdrawn and replaced by an equal volume of fresh medium to maintain a constant volume. The AUC (area under the curve) was calculated using the linear trapezoidal rule of drug bioavailability.[25b,58]

5.7 References

1. (a) S. R. Byrn, R. R. Pfeiffer and G. G. Stowell, *Solid-State Chemistry of Drugs*, SSCI, West Lafayette, IN, 1999 (b) H. G. Brittain, *Physical Characterization of Pharmaceutical Solids*, Marcel Dekker Inc. NY, 1995. (c) Y. Qiu, Y. Chen and G.G.Z. Zhang, *Developing Solid Oral Dosage Forms: Pharmaceutical Theory and Practice*, First ed. Academic Press, NY, 2009.
2. D. Hörter and J. B. Dressman, *Adv. Drug Del. Rev.,* 1997, **25**, 3-14.
3. C. R. Gardner, C. T. Walsh, Ö. Almarsson, *Nat. Rev. Drug Disc.,* 2004, **3**, 926-934.
4. S. M. Berge, L. D. Bighley and D. C. Monkhouse, *J. Pharm. Sci.,* 1977, **66**, 1–19.
5. (a) S. L. Childs, L. J. Chyall, J. T. Dunlap, V. N. Smolenskaya, B. C. Stahly, G. P. Stahly, *J. Am. Chem. Soc.*, 2004, **126**, 13335–13342. (b) J. F. Remenar, S. L. Morissette, M. L. Peterson, B. Moulton, J. M. MacPhee, H. R. Guzmán, Ö. Almarsson, *J. Am. Chem. Soc.,* 2003, **125**, 8456–8457. (c) N.R. Goud, S. Gangavaram, K. Suresh, S. Pal, S. G.Manjunatha, S. Nambiar and A. Nangia, *J. Pharm. Sci.,* 2012, **101**, 664-680. (d) N. Schultheiss and A. Newman, *Cryst. Growth Des.,* 2009, **9**, 2950-2967.
6. N. Clavaguera, J. Saurina, J. Lheritier, J. Masse, A. Chauvet, M. T. Clavaguera-Mora, *Thermochim. Acta,* 1997, **290**, 173-180.
7. A. T. M. Serajuddin, *J. Pharm. Sci.,* 1999, **88**, 1058–1066.
8. V. M. Rao, M. Nerurkar, S. Pinnamaneni, K. Raghavan, *Int. J. Pharm*., 2006 **319**, 98–106.
9. J. Li, H. Xiao, J. Li, Y.-P. Zhong, *Int. J. Pharm.*, 2004, **278**, 329–342.
10. (a) S. Cherukuvada and A. Nangia, *CrystEngComm*, 2012, **14**, 2579-2588. (b) A. Górniak, A. Wojakowska, B. Karolewicz and J. Pluta, *J. Therm. Anal. Calorim.,* 2011, **104**, 1195-1200. (c) D. Liu, X. Fei, S. Wang, T. Jiang and D. Su, *Asian J. Pharm. Sci.*, 2006, **1**, 213-221. (d) W. L. Chiou and F. Niazi, *J. Pharm. Sci.,* 1976, **65**, 1212. (e) K. Sekiguchi and N. Obi, *Chem. Pharm. Bull*., 1961, **9**, 866-872. (f) C. W. Park, H. M. Mansour, T. O. Oh, J. Y. Kim, J. M. Ha, B. J. Lee, S. C. Chi, Y. S. Rhee and E. S. Park, *Int. J. Pharm*., 2012, **436**, 652-658. (g) P. W. Stott, A. C. Williams and B. W. Barry, *J. Control Release*, 1998, **50**, 297-308.

11. M. D. Moore and P. L. D. Wildfong, *J. Pharm. Innov.,* 2009, **4**, 36-49.
12. (a) W. L. Chiou and S. Riegelman, *J. Pharm. Sci*, 1971, **60**, 1281-1302. (b) F. Cilurzo, P. Minghetti, A. Casiraghi and L. Montanari, *Int. J. Pharm*., 2002, **242**, 313-317. (c) M. C. Gohel and L. D. Patel, *Drug Dev. Ind. Pharm.,* 2003, **29**, 299.
13. (a) http://en.wikipedia.org/wiki/Eutectic_system; (b) A. Karaipekli and A. Sari, *J. Indus. Engi. Chem*., 2010, **16**, 767 (c) L. Shilei, Z. Neng and F. Guohui, *Ener. Build.*, 2006, **38**, 708.
14. (a) B. F. J. Broberg, H. C. A. Evers, *US Pat*., 4529601, 1985. (b) J. G. Castillo, *US Pat.,* 5993836, 1999.
15. H. Hatcher, R. Planalp, J. Cho, F. M. Torti and S. V. Torti, *Cell Mol. Life Sci.* 2008, **65**, 1631–1652.
16. (a) G. B. Mahady, G. B. Pendland, G. Yun, Z. Z. Lu, *Anticancer Res.,* 2002, **22**, 4179-4181 (b) A. J. Ruby, G. Kuttan, K. D. Babu, K. N. Rajasekharan, R. Kuttan, *Cancer Lett.,* 1995, **94**, 79-83. (c) L. K. Wolf, *Chem. Eng. News*, 2012, **90**, 44-46
17. S. Qureshi, A. H. Shah and A. M. Ageel, *Planta. Med.,* 1992, **58**, 124-127.
18. (a) C. D. Lao, M. T. Ruffin, D. Normolle, D. D. Heath, S. I. Murray, J. M. Bailey, M. E. Boggs, J. Crowell, C. L. Rock and D. E. Brenner, *BMC Complement Altern. Med.,* 2006, **6**, 10-13. (b) C. H. Hsu and A. L. Cheng, *Adv. Exp. Med. Biol*., 2007, **595**, 471-480.
19. (a) R. A. Sharma, H. R. McLelland, K. A. Hill, C. R. Ireson, S. A. Euden, M. M. Manson, M. Pirmohamed, L. J. Marnett, A. J. Gescher and W. P. Steward, *Clin. Cancer Res.,* 2001, **7**, 1894-1900. (b) R. A. Sharma, S. A. Euden, S. L. Platton, D. N. Cooke, A. Shafayat, H. R. Hewitt, T. R. Marczylo, B. Morgan, D. Hemingway, S. M. Plummer, M. Pirmohamed, A. J. Gescher and W. P. Steward, *Clin. Cancer Res.,* 2004, **10**, 6847-6854.
20. A. L. Cheng, C. H. Hsu, J. K. Lin, M. M. Hsu, Y. F. Ho, T. S. Shen, J. Y. Ko, J. T. Lin, B. R. Lin, M. S. Wu, H. S. Yu, S. H. Jee, G. S. Chen, T. M. Chen, C. A. Chen, M. K. Lai, Y. S. Pu, M. H. Pan, Y. J. Wang, C. C. Tsai, C. Y. Hsieh, *Anticancer Res.*, 2001, **21**, 2895-2900.
21. Y. J. Wang, M. H. Pan, A. L. Cheng, L. L. Lin, Y. S. Ho, C. Y. Hsieh and J. K. Lin, J. *Pharm. Biomed. Anal.,* 1997, **15**, 1867–1876.

22. (a) P. Anand, A. B. Kunnumakkara, R. A. Newman, B. B. Aggarwal, *Mol. Pharmaceutics*, 2007, **4**, 807-818 (b) B. Antony, B. Merina, V. S. Iyer, N. Judy, K. Lennertz, S. A. Joyal, *Ind. J. Pharm. Sci.,* 2008, **70**, 445-449.
23. (a) F. Zhang, G. K. Koh, D. P. Jeansonne, J. Hollingworth, P. S. Russo, G. Vincente, R. W. Stout and Z. Liu, *J. Pharm. Sci.*, 2011, **100**, 2778-2789. (b) N. K. Gupta, V. K. Dixit, *J. Pharm. Sci.,* 2011, **100**, 1987–1995.
24. (a) M. Pudipeddi and A. T. M. Serajuddin, *J. Pharm. Sci.,* 2005, **94**, 929. (b) W. C. Schinzer, M. S. Bergren, D. S. Aldrich, R. S. Chao, M. J. Dunn, A. Jeganathan, L. M. Madden, *J. Pharm. Sci.,* 1997, **86**, 1426-1431.
25. (a) P. Sanphui, N. R. Goud, U. B. R. Khandavilli, S. Bhanoth and A. Nangia, *Chem Commun,* 2011 **47**, 5013–5015 (b) P. Sanphui, N. R. Goud, U. B. R. Khandavilli, and A. Nangia, *Cryst. Growth Des.,* 2011, **11**, 4135–4145.
26. GRAS chemicals list may be accessed at www.fda.gov/Food/FoodIngredientsPackaging/GenerallyRecognizedasSafeGRAS/GRASSubstancesSCOGSDatabase/default.htm
27. C. J. Yang, C. S. Wang, J. Y. Hung, H. W. Huang, Y. C. Chia, P. H. Wang, C. F. Weng and M. S. Huang, *Lung Cancer.,* 2009, **66**, 162-168.
28. (a) A. V. Trask and W. Jones, *Top. Curr. Chem.,* 2005, **254**, 41–70. (b) N. Shan, F. Toda and W. Jones, *Chem Commun*, 2002, 2372-2373. (c) T. Friščić and W. Jones, *Cryst. Growth Des.,* 2009, **9**, 1621-1637.
29. (a) D. Law, W. Wang, E. A. Schmitt, Y. Qiu, S. L. Krill and J. J. Fort, *J. Pharm. Sci.*, 2003, **92**, 505-515 (b) X. Yuan and A. C. Capomacchia, *Pharm. Dev. Technol.,* 2005, **1**, 1–10.
30. A. Fahr and X. Liu, *Exp. Opin. Drug Deliv.,* 2007, **4**, 403–416.
31. M. Bi, S. J. Hwang and K. R. Morris, *Thermochim. Acta,* 2003, **404**, 213-226.
32. (a) D. R. Askeland and P. P. Fulay, *Essentials of Materials Science and Engineering,* Second ed., Cengage Learning, Canada, 2009. (b) W. D. Callister Jr., *Fundamentals of Material Science and Engineering*, Fifth Ed., John Wiley & Sons, NY, 2001.
33. S. S. Das, N. P. Singh, T. Agrawal, P. Gupta, S. N. Tiwari and N. B. Singh, *Mol. Cryst. Liq. Cryst.*, 2009, **501**, 107–124.

34. S. L. Childs, G. P. Stahly and A. Park, *Mol. Pharmaceutics*, 2007, **4**, 323-338.
35. D. J. Berry, C. C. Seaton, W. Clegg, R. W. Harrington, S. J. Coles, P. N. Horton, M. B. Hursthouse, R. Storey, W. Jones, T. Friščić and N. Blagden, *Cryst. Growth Des.,* 2008, **8**, 1697-1712.
36. M. K. Stanton and A. Bak, *Cryst. Growth Des.,* 2008, **8**, 3856-3862.
37. A. V. Trask, D. A. Haynes, W. D. S. Motherwell and W. Jones, *Chem Commun*, 2006, 51-53.
38. C. C. Seaton and A. Parkin, *Cryst. Growth Des.,* 2011, **11**, 1502-1511.
39. K. Chadwick, R. Davey and W. Cross, *CrystEngComm*, 2007, **9**, 732-734.
40. E. Lu, N. Rodríguez Hornedo and R. Suryanarayanan, *CrystEngComm,* 2008, **10**, 665-668.
41. (a) R. M. Silverstein, *Spectrometric Identification of Organic Compounds*. 6th Ed.; John Wiley & Sons, Inc.: New York, 2002. (b) E. Smith and G. Dent, *Modern Raman Spectroscopy, A Practical Approach*, John Wiley: New York, 2005. (c) F. G. Vogt, J. S. Clawson, M. Strohmeier, A. J. Edwards, T. N. Pham and S. A. Watson, *Cryst. Growth Des.,* 2009, **9**, 921.
42. T. Proffen, K. L. Page, S. E. McLain, B. Clausen, T. W. Darling, J. A. Tencate, S. Y. Lee, E. Ustundag, *Z. Kristallogr.* 2005, **220**, 1002-1008.
43. N. B. Singh, S. S. Das, N. P. Singh and T. Agrawal, *J. Cryst. Growth*, 2008, **310**, 2878-2884
44. S. L. Childs, N. Rodríguez-Hornedo, L. S. Reddy, A. Jayasankar, C. Maheshwari, L. McCausland, R. Shipplett and B. C. Stahly, *CrystEngComm*, 2008, **10**, 856–864.
45. J. B. Dressman, G. L. Amidon, C. Reppas and V. P. Shah, *Pharm. Res.,* 1998, **15**, 11–22.
46. L. X. Yu, A. S. Carlin, G. L. Amidon and A. S. Hussain, *Int. J. Pharm*. 2004, **270**, 221-227.
47. (a) N. Jain, S. H. Yalkowsky, *J. Pharm. Sci.,* 2001, **90**, 234-252 (b) D. J. Good, N. Rodríguez-Hornedo, *Cryst. Growth Des.*, 2009, **9**, 2252–2264.
48. K. Stanton, R. C. Kelly, A. Colletti, M. Langley, E. J. Munson, M. L. Peterson, J. Roberts and M. Wells, *J. Pharm. Sci*., 2011, **100**, 2734-2743.

49. (a) G. R. Desiraju, J. J. Vittal, A. Ramanan, *Crystal Engineering. A Textbook,* World Scientific Publishing, Singapore, 2011 (b) G. R. Desiraju, *Crystal Engineering. The Design of Organic Solids*. Elsevier, 1989 (c) G. R. Desiraju, *Angew. Chem., Int. Ed. Engl*., 1995, **34**, 2311.
50. (a) M. C. Etter, J. C. Macdonald and J. Bernstein, *Acta Crystallogr. Sect. B,* 1990, **46**, 256 (b) M. C. Etter and S. M. Reutzel, J. *Am. Chem. Soc*., 1991, **113**, 2586.
51. H. G. Brittain, *Cryst. Growth Des.,* 2009, **9**, 2492-2499.
52. Y. Sakata, E. Tanabe, T. Sumikawa, S. Shiraishi, Y. Tokudome and M. Otsuka, *Int. J. Pharm.,* 2007, **335**, 12-19.
53. S. G. Fleischman, S. S. Kuduva, J. A. McMahon, B. Moulton, R. D. B. Walsh, N. Rodríguez-Hornendo and M. J. Zaworotko, *Cryst. Growth Des.,* 2003, **3**, 909.
54. O. M. Peeters, N. M. Blaton, C. J. de Ranter, *Acta Crystallogr. Sect. C*, 1996, **52**, 2225.
55. (a) A. Mukherjee, P. Grobelny, T. S. Thakur and G. R. Desiraju, *Cryst. Growth Des*., 2011, **11**, 2637 (b) R. Dubey, M. S. Pavan and G. R. Desiraju, *Chem. Commun.,* 2012, **48**, 9020.
56. E. H. Lee, S. R. Byrn and M. T. Carvajal, *Pharm. Res.,* 2006, **23**, 2375.
57. E. Shefter and P. Sackman, *J. Pharm. Sci.,* 1971, **60**, 282.
58. G. C. Viscomi, M. Campana, M. Barbanti, F. Grepioni, M. Polito, D. Confortini, G. Rosini, P. Righi, V. Cannata and D. Braga, *CrystEngComm*, 2008, **10**, 1074–1081.
59. (a) A. M. Beale and B. M. Weckhuysen, *Phys. Chem. Chem. Phys.*, 2010, **12**, 5562-5574. (b) S. Cammelli, D. L. Hecht, C. Degueldre, J. Bertsch and R. Frahm, *J. Phys. Conf. Ser.,* 2009, **190**, 12027.

CHAPTER SIX

NOVEL COCRYSTALS OF SULFACETAMIDE

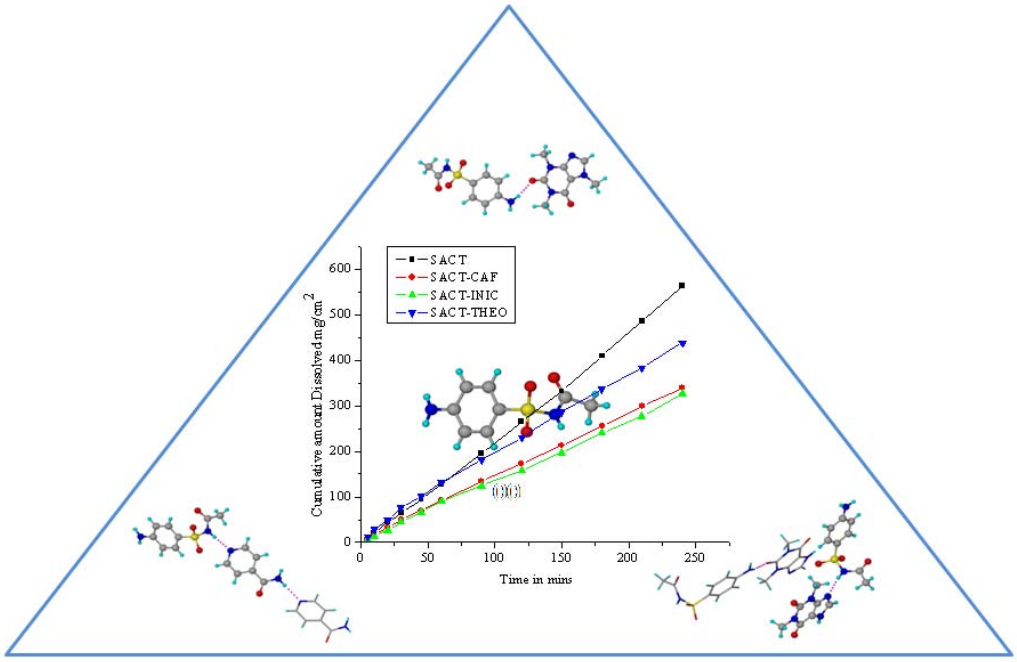

The antibacterial drug sulfacetamide was screened with pharmaceutically acceptable coformers to discover solid forms with low solubility. Cocrystals with INIC and CAF exhibited 0.64 and 0.68 times the IDR of parent drug. The SACT-CAF cocrystal with low solubility and good stability may be a suitable candidate for making an extended release formulation of SACT to improve its therapeutic efficacy.

6.1 Introduction

The subject of Crystal Engineering[1] has enabled the design and development of cocrystals[2] with superior properties compared to their parent compounds. Today, these supramolecular materials have wide range of applications as molecular semiconductors[3a], optical materials[3b], fluorescent[3c] and phosphorescent materials[3d], media for chiral synthesis[3e] apart from improving mechanical properties[3f,g]. Turning on the phosphorescence[3d] of phenanthrene by cocrystallizing it with 1,4, dibromotetrafluorobenzene or conferring unexpected elasticity[3g] to caffeine on complexing with 4-chloro-3-nitrobenzoic acid, are representative examples of cocrystals.

Nevertheless, this group of supramolecular solid forms has primarily garnered the attention of academic and industrial chemists with their ability to modulate physicochemical properties of Active pharmaceutical ingredients (APIs) as 'Pharmaceutical cocrystals'[4]. They are the emerging means for developing an optimal pharmaceutical formulation with implications in improving the manufacturability, storage stability and in vivo delivery of drug substances[5]. Nangia and coworkers[6] have reported the remarkable improvement in the hydrolytic stability of Temozolomide by forming cocrystals with oxalic acid and succinic acid. They showed that while Temozolomide degraded within a week during stability studies at accelerated ICH conditions of 40°C and 75% humidity, its cocrystals were intact for 28 weeks by PXRD analysis. Trask et. al.[7] highlighted the importance of cocrystallization in addressing the hydration problems of caffeine. They have reported that unlike caffeine, its cocrystals especially with oxalic acid showed complete stability to humidity over several weeks. The antipyretic drug paracetamol has pure tableting properties. Jones and coworkers[8] have shown that cocrystallizing paracetamol with various coformers has significantly improved its tabletability and the best case of paracetamol-theophylline cocrystal was proposed as a good replacement for paracetamol in the market. Apart from these pharmaceutical applications, cocrystals are more popular among the scientific community because of their ability to enhance the solubility of poorly soluble drugs[9]. Various groups all over the world have used this advantage of cocrystals in enhancing the solubility of BCS Class II and Class IV drugs. Basavoju et. al.[9c] improved the solubility of Indomethacin by

forming a cocrystal with saccharin. They have shown through powder dissolution studies that the powder dissolution rate of indomethacin-saccharin cocrystal was higher by ~3 times compared to the reference drug. Nangia and coworkers[9b] improved the poor solubility of furosemide by forming a cocrystal with caffeine which showed 6 times higher IDR compared to furosemide in 10% EtOH-water solution. Remenar and colleagues[9a] have reported that the Itraconazole-L-Malic acid cocrystal showed 20 fold higher dissolution rate compared to crystalline Itraconazole and comparable solubility to that of the marketed form (as amorphous Itraconazole Sporanox beads).

This application of cocrystals primarily towards solubility enhancement of poorly soluble drugs is not surprising since 40% of the marketed drugs have solubility problems and about 80-90% of drugs in the R&D pipeline could fail due to low solubility[10]. However, about 60% of the currently marketed drug molecules have moderate to high solubility. Although higher solubility of a drug is essential for therapeutic efficacy, sometimes it comes with the undesired effects of lower bioavailability due to short half-life resulting in faster systemic elimination. This necessitates frequent administration of dosage in order to maintain optimal drug concentration in blood, leading to drug-patient incompatibility. Therefore modified release versions[11] are often formulated for high soluble drugs in order to improve their bioavailability, lower the dosage rate, leading to better therapeutic utility. In this age of patent cliffs[12], repatentability of patent expired drugs is also achieved by introducing controlled release formulations of existing immediate release products with better therapeutic efficacy. This is an attractive financial option for pharmaceutical companies to extend their patent rights. Augmentin XR (Glaxosmithkline)[13a] and Ecosprin (USV)[13b] are the early examples of this option which might soon become a trend. Different methods like polymer assisted matrix tablets[14a], hot melt extrusion[14b], and compression coated matrix tablets[14c] etc are commonly used to prepare extended release formulations of drug molecules. These matrix tablets allow slow but steady release of the drug molecule for extended availability and better efficacy. Remington et. al.[15] has noted that preparing a less soluble form of a highly soluble drug is a facile method for producing extended release dosage forms. Through the process of cocrystallization, the hydrogen bonding patterns of high soluble drugs can be modified with appropriate coformers to lower their solubility. This may

be useful in lowering the solubility of the drug which in turn improves the circulation time of the drug and enhance its bioavailability. In this regard, the work of Smith et. al[16] on Epigallocatechin-3-gallate (EGCG) is noteworthy. EGCG is a highly water soluble (20mg/mL) bioflavonoid, extensively studied in the past decade as a therapeutic potential for various cancers. But due to its poor bioavailability resulting from faster metabolism, it is not yet approved as a drug. Smith and colleagues made cocrystals of EGCG which showed low solubility compared to the parent molecule (Figure 6.1a). They intended to study the effect of reducing the solubility on the pharmacokinetic profile of EGCG. They have found that the relative bioavailability of EGCG-Isonicotinic acid-trihydrate and EGCG-Isonicotinic acid is 1.53 and 1.18 times higher compared to EGCG (Figure 6.1b). Thus they have shown that the bioavailability of EGCG is improved by lowering its solubility through cocrystallization.

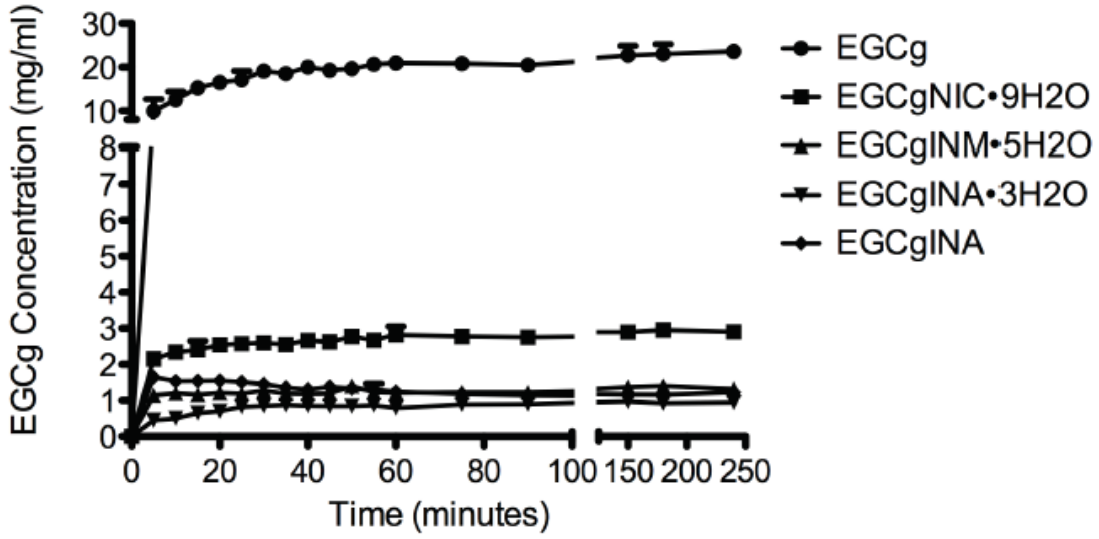

Figure 6.1a) Dissolution profile of EGCG and its cocrystals in water. The graph indicates that all the cocrystals have far lower dissolution rate compared to the parent molecule (Adapted from ref. 16).

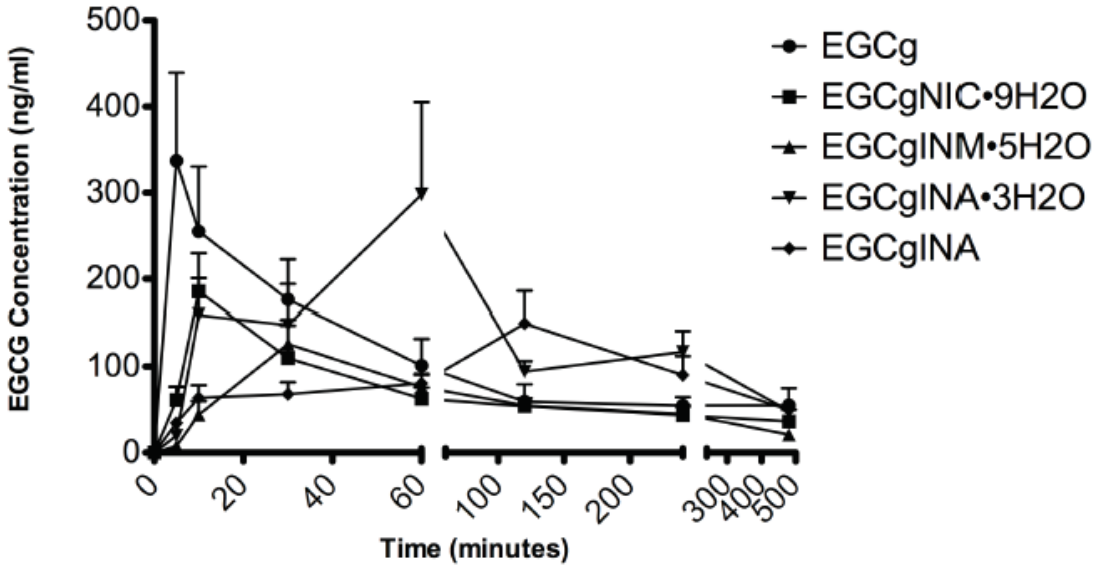

Figure 6.1b) Pharmacokinetic profile of EGCG and its cocrystals. The relative bioavailability of EGCgINA.$3H_2O$ and EGCgINA cocrystals are 1.53 and 1.18 times higher compared to EGCG (Adapted from ref. 16).

Although not with an intention of studying the effect on bioavailability, certain literature reports showed that the solubility of drugs can be lowered by making cocrystals. Childs et. al.[17a] reported that the solubility of Fluoxetine hydrochloride (11.4 mg/mL) was lowered by forming a cocrystal with benzoic acid (5.6mg/mL). Aakeroy et. al.[17b] showed that sebacic acid and dodecanedioic acid coformers could lower the solubility of hexamethylenebisacetamide, an anti-cancer drug by the virtue of their extended aliphatic chain. Apart from the studies of Zaworotko and group on EGCG, there are no literature reports dedicated towards addressing the rapid metabolic issues of high soluble drugs by making low solubility cocrystals. However if seriously investigated this ability of cocrystals might provide a promising solution for addressing the poor bioavailability of highly soluble drugs resulting from their rapid metabolism and low half-lives. It is this solubility lowering ability of cocrystals we wish to highlight in this chapter.

6.2 Literature reports on Sulfacetamide

Sulfacetamide (SACT, hereafter) belongs to the class of sulfonamide antibiotics. It is a frontline drug for the treatment of various ocular infections like trachoma, blepheritis, conjunctivitis and corneal ulcer. It has been investigated as a therapeutic agent for the treatment of pityriasis versicolor and rosacea[18]. Recent reports indicate that it may also act as antifungal drug by a CYP51A1-independent mechanism[19]. It is a bacteriostatic agent with similar activity against both Gram-positive and Gram-negative bacteria. It systematically inhibits bacterial synthesis of dihydrofolic acid by preventing condensation of pteridine with aminobenzoic acid through competitive inhibition of the enzyme dihydropteroate synthetase[20]. It has high solubility of 12.5mg/mL[21]. As a result, the therapeutic efficacy of SACT in treating eye infections is severely limited by physiological constraints such as tear flow and reflex blinking which results in considerable drug loss. The washout rate reduces the concentration of drug to one-tenth of its starting value in 4-20mins after administration[22]. Therefore only a few percent of the administered drug is absorbed by the eye and therefore duration of the therapeutic action is quiet short. This necessitates frequent administration of dose for maintaining optimal therapeutic levels of drug which is often incompatible with patients. In literature, extended release modifications of SACT in the form of bioadhesive microspheres[22a], polymeric nanosuspensions[22b] are used to increase its residence time on the ocular surface by releasing the drug slowly for an extended period of time. Nonetheless, SACT is still marketed in its native form.

6.3 Preparation of sulfacetamide cocrystals

In order to address the issue of rapid drop in the concentration of SACT at the site of action we resorted to cocrystallization strategy. We have explored the structural landscape[23] of SACT through cocrystallization methods with an idea that the resulting pharmaceutical cocrystals would have the appropriate hydrogen bonding patterns for lowering the solubility of the parent molecule which inturn might act as an extended release version of the drug for increasing its residence time on the ocular surface leading to better therapeutic efficacy.

Using mechanochemical grinding[24], slurry grinding and solution crystallization techniques we have screened SACT with various coformers which resulted in cocrystals with theophylline (THEO), isonicotinamide (INIC), caffeine (CAF), 4,4′-bipyridine (BIP) and a salt with 4-aminopyridine (4AP) (Scheme 6.1). These cocrystals were characterized by various thermal, spectroscopic and diffraction methods. The implications of cocrystal formation on the solubility and dissolution of SACT are discussed in this chapter.

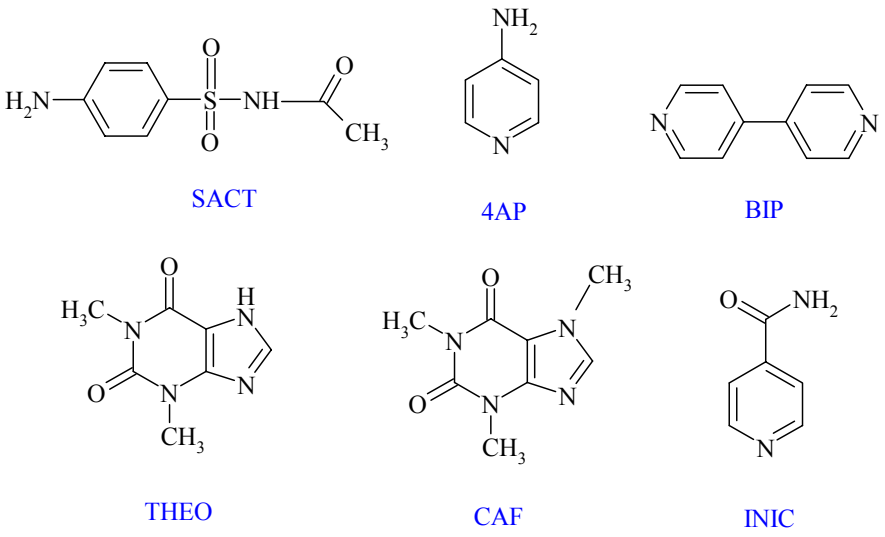

Scheme 6.1 Sulfacetamide and coformers discussed in this study. Compound abbreviations are used throughout the paper.

6.4 Results and Discussion

Supramolecular synthon[25] strategy guided by hydrogen bonding rules[26] has been the primary design element for the construction of multicomponent cocrystals since its introduction by Desiraju in 1995[25a]. Based on the nature of functional groups in a drug molecule, coformers with complementary functional moieties are chosen in order to design cocrystals with robust synthons. Primary functional groups in SACT are the amide and amine moieties. In literature, -COOH, -$CONH_2$, N-oxide, pyridine etc. functional moieities were chosen to form

synthons with amide containing molecules[27]. Therefore, in order to obtain cocrystals, we combined SACT with coformers containing above functional moieties. A complete list of all the coformers used to form cocrystals are shown in experimental section (Table 6.8) Surprisingly, we did not obtain any cocrystals with –COOH containing coformers which have 48% synthon probability with amide functional groups[28], but instead we obtained cocrystals with amide and pyridine coformers which have a CSD probability of 35% and 4% respectively[28]. In addition the cocrystals obtained in this study exhibited variable stoichiometry in the asymmetric unit. SACT-CAF (1:1), SACT-INIC (1:2), SACT-THEO (2:2), SACT-BIP (1:0.5) and SACT-4AP (1:1). As a result these cocrystals have different Z''[29] values in their crystal structures.

Presence of multiple molecules in the asymmetric unit (Z') has been a matter of huge interest in the crystallographic community[30]. Numerous opinions like fossil relics of the stable form[30a], crystal on the way[30a], synthon frustration[30c], steric hindrance[30b], internal symmetry[30d], donor acceptor imbalance[30c] etc. were hypothesized to be the reasons for the occurrence of this phenomenon. Similar criteria were proposed for the occurrence of variable Z'' cocrystals[29,30,31]. Z'' defines the number of crystallographically nonequivalent molecules in the asymmetric unit. This quantity is important because it gives the number of entities that have to be positioned and oriented differently. For compound structures like hydrates the Z'' >1 even as the Z' =1. Crystallographic parameters (Table 6.1) clearly indicates the diversity in Z'' of SACT cocrystals apart from the commonly observed Z'' = 2 structures. Although SACT has three acceptor and donor atoms, various factors like the internal symmetry of the coformer molecules, donor acceptor imbalance due to differences in acid-base strengths of participating atoms, strained conformation of SACT in its cocrystals are plausible reasons for its variable Z'' structures. This aspect is discussed along with the crystal structure description of the cocrystals. The hydrogen bonding parameters of all the SACT cocrystals are listed in Table 6.2.

Table 6.1 Crystallographic Parameters of SACT Cocrystals

	SACT-BPN (1:0.5)	SACT-CAF (1:1)	SACT-INIC (1:2)	SACT-THEO (2:2)	SACT-4AP (1:1)
Emp form.	$C_{13}H_{14}N_3O_3S$	$C_{16}H_{20}N_6O_5S$	$C_{20}H_{22}N_6O_5S$	$C_{15}H_{18}N_6O_5S$	$C_{13}H_{16}N_4O_3S$
Form wt	292.33	408.44	458.50	394.41	308.36
Cryst syst	Monoclinic	Monoclinic	Monoclinic	Triclinic	Monoclinic
Sp gr	$P2_1/n$	$P2_1/c$	$P2_1/n$	$P\bar{1}$	$P2_1/c$
T/K	298(2)	100(2)	298(2)	100(2)	298(2)
a/Å	11.6469(9)	7.1821(6)	10.7667(4)	8.6640(7)	7.7413(7)
b/Å	10.4670(6)	30.430(3)	9.7508(4)	14.9675(13)	17.8726(16)
c/Å	12.4421(9)	8.8188(7)	21.1014(7)	15.3632(15)	11.0065(10)
α/º	90	90	90	110.234(2)	90
β/º	116.510(10)	107.6790(10)	96.176(3)	106.3650(10)	97.8790(10)
γ/º	90	90	90	97.2830(10)	90
Z	4	4	4	4	4
Z''	1.5	2	3	4	2
V/Å^3	1357.31(17)	1836.3(3)	2202.45(14)	1737.1(3)	1508.5(2)
Rflns collect	4882	18761	7836	18179	15456
Unique rflns	2315	3579	3762	6823	2992
Obsd rflns	1910	3358	3002	5929	2698
Parameters	183	269	318	525	211
R_1	0.0404	0.0436	0.0407	0.0505	0.0496
wR_2	0.1131	0.1158	0.1057	0.1297	0.1226
GOF	1.035	1.074	1.065	0.953	1.191

Table 6.2 Hydrogen bond parameters of SACT cocrystals. O–H, N–H and C–H distances are neutron-normalized to 0.983, 1.009 and 1.083Å respectively

D–H···A	D···A (Å)	H···A (Å)	D–H···A (°)	symmetry code
		SACT-BPN (1:0.5)		
N1–H1B···O3	3.008(3)	2.44	124	3/2–x, –1/2+y,1/2–z
N2–H2···N3	2.889(3)	2.10	153	1/2–x, 1/2+y,1/2–z
C2–H2A···O1	2.956(3)	2.60	103	--[a]
C8–H8A···O2	3.399(4)	2.44	178	1/2–x, 1/2+y,1/2–z
		SACT-CAF (1:1)		
N1–H1A···N5	2.842(2)	2.12	175	1+x,y,1+z
N2–H2A···O1	2.991(2)	2.18	172	x,y, –1+z
N2–H2B···O5	2.941(3)	2.07	170	1–x, –y, –z
C6–H6···O1	2.936(2)	2.59	102	--[a]
C13–H13···O3	3.197(3)	2.28	163	–1+x,1/2–y, –1/2+z

C15–H15B···O4	2.755(3)	2.29	108	--[a]
		SACT-INIC (1:2)		
N1–H1···N3	2.852(2)	2.00	177	1/2–x, –1/2+y,1/2–z
N2–H2A···O3	2.920(3)	2.06	166	–x, –y, –z
N2–H2B···N2	3.109(4)	2.49	131	–x,1–y, –z
N4–H4A···O5	3.092(2)	2.26	169	1–x, –y, –z
N4–H4B···N5	2.982(2)	2.11	179	–1/2+x,1/2–y, –1/2+z
N6–H6A···O4	2.941(3)	2.03	168	1–x,1–y, –z
N6–H6B···O5	2.961(2)	2.15	164	1–x, –y, –z
C8–H8A···O1	3.142(3)	2.48	126	1/2–x, –1/2+y,1/2–z
C10–H10···O5	3.369(3)	2.44	173	1–x, –y, –z
C13–H13···O2	3.299(3)	2.54	139	x,1+y,z
		SACT-THEO (2:2)		
N1–H1···N11	2.797(3)	2.00	165	2–x, –y,1–z
N2–H2A···O1	3.026(3)	2.17	171	–1+x,y,z
N2–H2B···O10	2.868(3)	2.04	169	1–x,1–y,1–z
N3–H3A···O5	2.969(3)	2.13	174	1+x,y,z
N3–H3B···O8	2.886(3)	2.07	157	2–x,1–y,1–z
N4–H4···N7	2.812(3)	2.00	163	–1+x,y,z
N8–H8D···O6	2.791(3)	1.95	174	–1+x,y,z
N12–H12A···O3	2.803(3)	1.95	177	1–x, –y,1–z
C2–H2···O2	2.896(3)	2.52	104	--[a]
C8–H8A···O4	3.344(3)	2.51	143	x, –1+y,z
C14–H14···O4	2.943(3)	2.58	103	--[a]
C16–H16A···O4	3.184(3)	2.55	123	1–x,1–y, –z
C21–H21···O4	3.137(3)	2.37	137	1–x,1–y, –z
C21–H21···O6	3.251(3)	2.43	145	1–x,1–y, –z
C22–H22B···O7	2.739(3)	2.30	106	--[a]
C23–H23A···O8	3.316(3)	2.49	142	1 –x,1 –y,1 –z
C28–H28···O2	3.200(2)	2.50	130	x,y,1+z
C28–H28···O3	3.307(3)	2.43	153	x,y,1+z
C29–H29B···O9	2.722(3)	2.37	100	--[a]
C30–H30A···O10	2.761(3)	2.37	103	--[a]
		SACT-4AP(1:1)		
N2–H2A···O1	3.146(3)	2.41	153	1–x, –1/2+y,1/2–z
N2–H2B···O2	2.999(4)	2.19	166	x,1/2–y,1/2+z
N3–H3A···N1	2.783(3)	1.87	178	1–x, –1/2+y,1/2–z
N4–H4A···O3	2.806(3)	1.97	164	1+x,y,z
C2–H2···O2	2.914(3)	2.54	105	--[a]
C5–H5···O3	3.337(3)	2.46	157	x,1/2–y,1/2+z

--[a] = Intramolecular hydrogen bond

6.4.1 Crystal Structure Description

Sulfacetamide-4,4′-bipyridine (SACT-BPN) cocrystal This crystal structure was solved and refined in $P2_1/c$ space group. It contains 1 molecule of SACT and half molecule of BPN in the asymmetric unit. Shift from the usually observed Z″=2 molecules in this structure is ascribed to the internal symmetry of the BPN coformer. SACT molecules are aligned along the 2_1 screw axis connected through N–H···O (N1···O3, 2.44Å, 124°) hydrogen bonds. Such screw related helices of SACT molecules are bridged by BPN coformer molecules through a one point N–H···N (N2···N3, 2.10Å, 153°) hydrogen bonds on both sides (Figure 6.2a). Collectively these hydrogen bonds extend the SACT and BPN molecules along the 2D lattice. A one point C–H···O hydrogen bond between methyl proton and $O_{sulfonamide}$ atoms of SACT molecules in adjacent layers confer additional stability to the crystal lattice (Figure 6.2b and 6.2c).

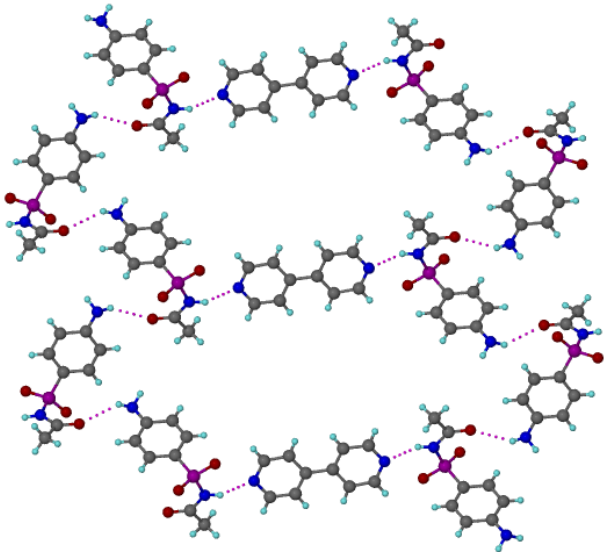

Figure 6.2a) 2_1 screw related SACT molecules bridged by BPN molecules.

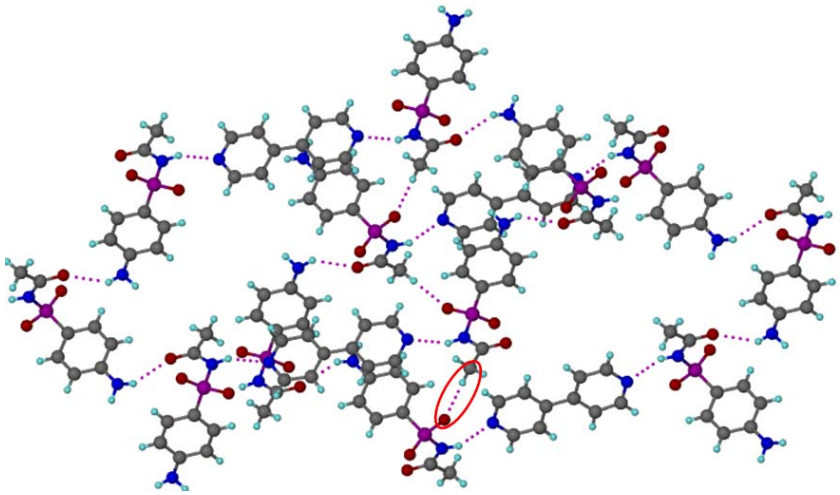

Figure 6.2b) Adjacent layers connected through C–H···O hydrogen bonds (highlighted by a circle, top view).

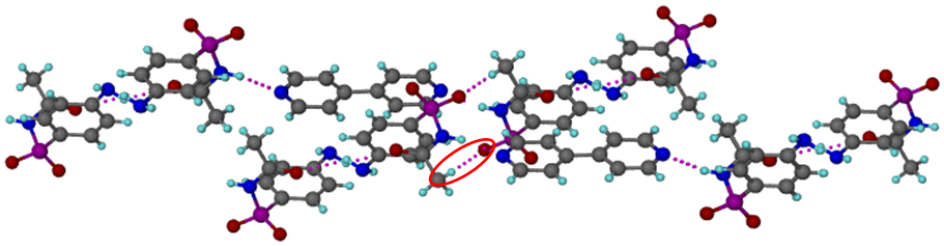

Figure 6.2c) Adjacent layers connected through C–H···O hydrogen bonds (highlighted by a circle, side view).

Sulfacetamide-caffeine (SACT-CAF) cocrystal This 1:1 stoichiometric cocrystal was obtained from its ethanol solution by slow evaporation method. It was solved and refined in $P2_1/c$ space group with the commonly observed Z″ value of 2 in its asymmetric unit. Here the SACT molecules are connected to each other through a one point N–H···O hydrogen bond (N2···O1, 2.18Å, 172°) extending as a 1D chain along the *C*-axis. Adjacent layers of these 1D chains of SACT molecules are bridged by two CAF molecules connecting them through N–H···O and N–H···N hydrogen bonds (N2···O5, 2.07Å, 170° and N1···N5, 2.12Å,

175°) (Figure 6.3a). These discrete units are connected through C–H···O hydrogen bonds (C13···O3, 2.28Å, 163°) extending them along the 2D lattice (Figure 6.3b).

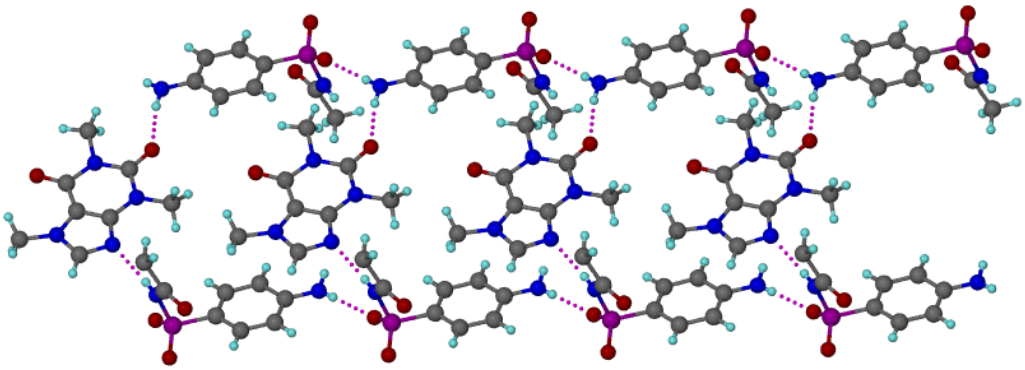

Figure 6.3a) Linear chains of SACT molecules bridged through CAF coformer molecules (only one layer of CAF molecules are shown for clarity).

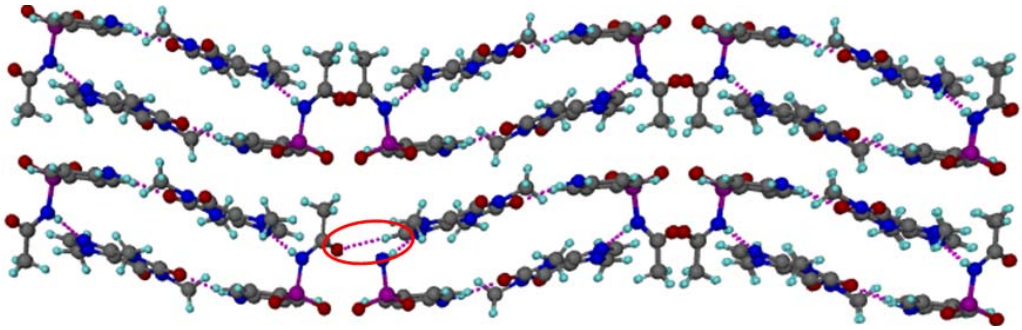

Figure 6.3b) Discrete units of SACT and CAF molecules are connected through C–H···O hydrogen bonds (marked by a circle). Few atoms are deleted for clarity.

Sulfacetamide-isonicotinamide (SACT-INIC) cocrystal Initially, single crystals of this 1:2 cocrystal was obtained on crystallizing 1:1 molar ratio of SACT and INIC along with some crystals of SACT from toluene-ethyl acetate solvent mixture. When the interacting molecules try to attain a balance between fulfilling all the hydrogen bonding interactions of major acceptors and donors with efficient packing, such unexpected stoichiometry was observed[30c]. In this cocrystal, in order to fulfill the donors and acceptors of INIC, another

molecule of INIC is included in the asymmetric unit. This cocrystal was optimized by crystallizing SACT and INIC in 1:2 ratio which resulted in complete conversion of the starting materials to the cocrystal. Unlike the previous structures, SACT molecules in this cocrystal form a dimer like discrete units connected by a N–H···O hydrogen bond (N2···O3, 2.06Å, 166°). As shown in Figure 6.4a, one type of crystallographically non-equivalent INIC molecules extend these discrete SACT units through a one point N–H···N hydrogen bond (N1···N3, 2.00Å, 177°), which inturn are connected by a dimeric unit of the other non-equivalent INIC molecules through N–H···N hydrogen bonds (N4···N5, 2.11Å, 179°). The dimeric unit of INIC molecules are held together by an $R^2_2(8)$ ring motif (N6···O5, 2.15Å, 164°). These one dimensional units of SACT and INIC molecules are connected to each other through a one point N–H···O (N6···O4, 2.03Å, 168°) hydrogen bond between the crystallographically nonequivalent INIC molecules (Figure 6.4b).

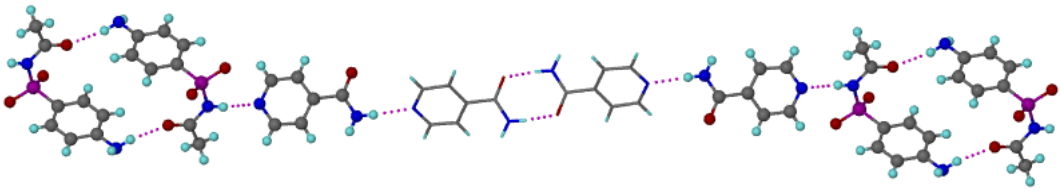

Figure 6.4a) Discrete SACT molecules connected through INIC molecules. The crystallographically nonequivalent INIC molecules are distinguished by capped stick and ball-stick models.

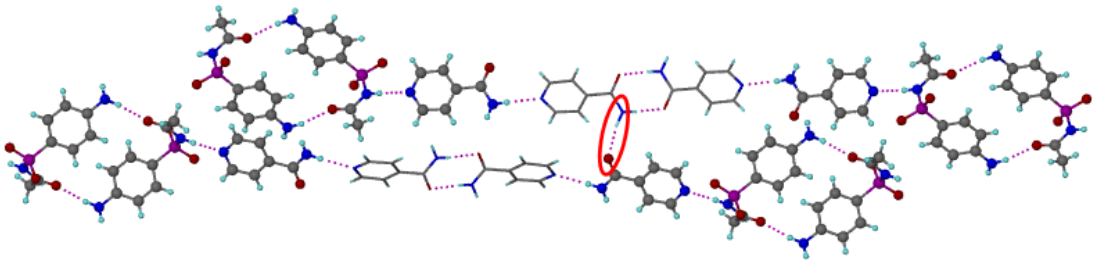

Figure 6.4b) One point N–H···O hydrogen bonds connects the one dimensional units of SACT and INIC molecules (highlighted by a circle).

Sulfacetamide-theophylline (SACT-THEO) Cocrystal This 1:1 cocrystal with two symmetry independent molecules of each component was obtained when stoichiometric amounts of SACT and THEO were dissolved in i-PrOH and evaporated at ambient conditions. Like the SACT-INIC cocrystal, even in this crystal structure an attempt to balance hydrogen bonding interactions with packing efficiency resulted in 2 molecules each of SACT and THEO in the asymmetric unit. In the crystal structure, one molecule each of the crystallographically nonequivalent SACT and THEO molecules pair up through hydrogen bonding interactions in a manner similar to the SACT-CAF cocrystal resulting in discrete units. These crystallographically nonequivalent pairs of SACT and THEO molecules resemble the distinct entities of 1:1 cocrystal domains alternating each other (Figure 6.5a) and connected through C–H···O (C8···O4, 2.51Å, 143°) hydrogen bonds. The SACT molecules extend as a chain along *a*-axis through one point N–H···O (N3···O5, 2.13Å, 174° in one pair and N2···O1, 2.17Å, 171° in other pair) hydrogen bond. Adjacent chains of SACT molecules are inturn connected by THEO molecules through N–H···O (N3···O8, 2.07Å, 157°, N8···O6, 1.95Å, 174° in one pair and N2···O10, 2.04Å, 169°, N12···O3, 1.95Å, 177° in other pair) and N–H···N (N4···N7, 2.00Å, 163° in one pair and N1···N11, 2.00Å, 165° in other pair) hydrogen bonds (Figure 6.5b).

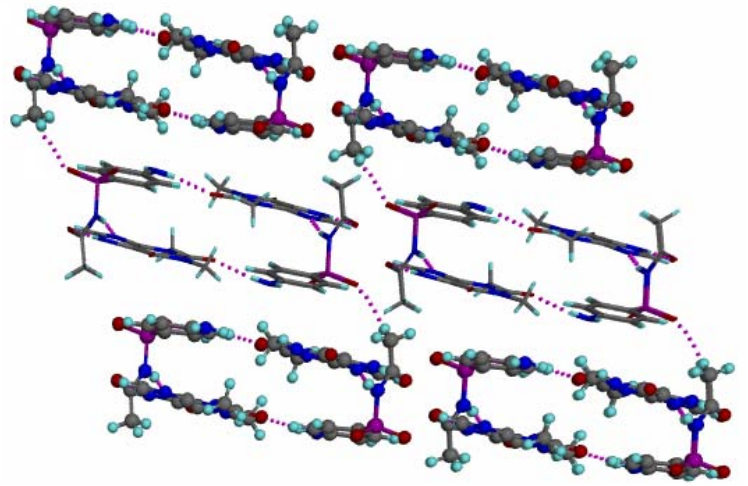

Figure 6.5a) Discrete pairs of SACT and THEO molecules alternate each other, connected through C–H···O hydrogen bonds.

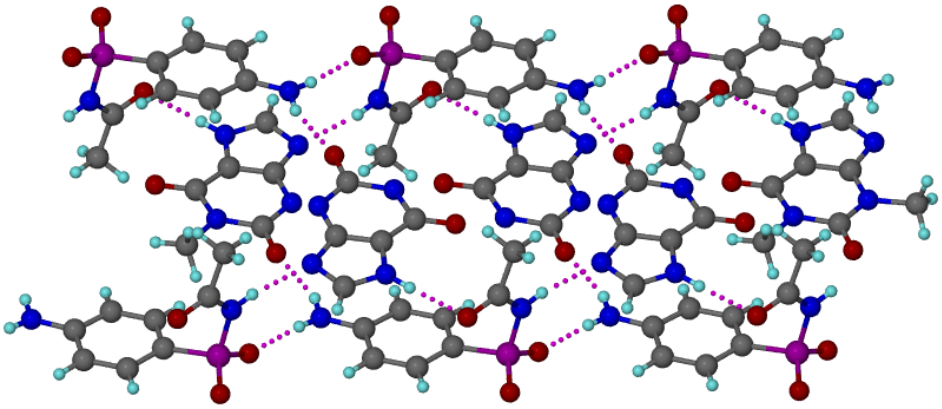

Figure 6.5b) Linear chains of SACT molecules bridged through THEO coformer molecules.

Sulfacetamide-4-aminopyridine (SACT-4AP) salt Solution crystallization of SACT and 4AP molecules in 1:1 stoichiometry resulted in a salt with proton transfer from amide N–H of SACT to pyridyl nitrogen of 4AP. The amide nitrogen is connected to electron withdrawing carbonyl and sulfonyl groups on either side. As a result the amide proton behaves as acid (pK_a = 4.3) in the presence of the basic nitrogen of 4AP (pK_a = 8.95) resulting in proton transfer. In tune with the 'Rule of three[32]', the ΔpK_a value (ΔpK_a = 4.65) is in the range of salt formation. In this crystal structure the 2_1 screw related SACT molecules are held together by N–H···O (N2···O2, 2.19Å, 166°) hydrogen bonds. These screw related SACT tapes are connected by 4AP molecules through one point N–H···N^- (N3···N1, 1.87Å, 178°) hydrogen bond on one side and N–H···O (N4···O3, 1.97Å, 164°) hydrogen bond on the other side (Figure 6.6).

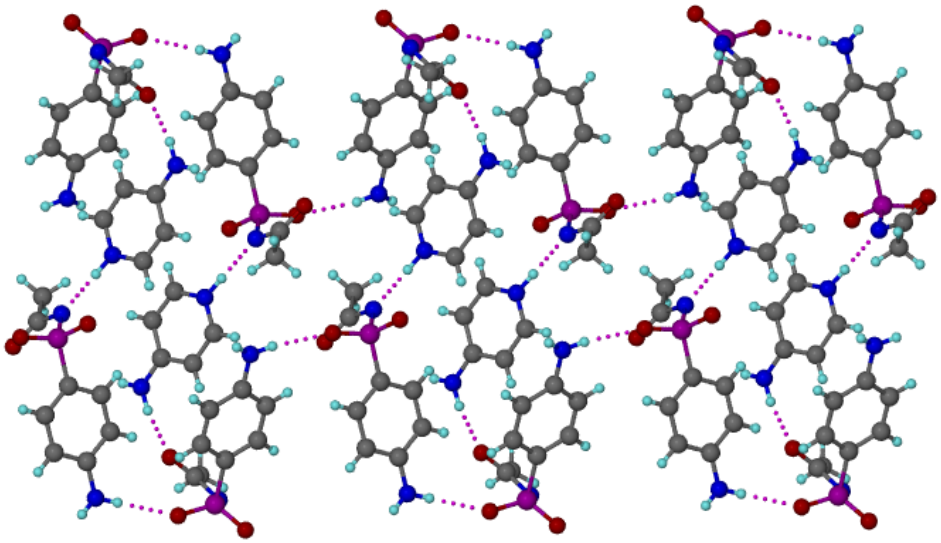

Figure 6.6 2_1 tapes of SACT molecules are connected by 4AP molecules through N–H···O and N–H···N^- hydrogen bonds.

6.4.2 Thermal Analysis

DSC analyses of SACT cocrystals showed unique thermal behavior in comparison to their starting materials (Figure 6.7). All the cocrystals exhibited single melting endotherm thereby acting as a purity indicator for the bulk cocrystal material prepared for various other characterizations. Unlike certain reported cocrystal systems[4a, 33], we did not observe any correlation between the melting points of the SACT cocrystals with those of their respective coformers (Table 6.3). In the DSC thermograms of SACT, SACT-CAF and SACT-THEO cocrystals an extra decomposition hump in addition to the usual melting endotherm was observed. SACT is known to undergo hydrolytic degradation[15,34] at higher temperatures to sulfanilamide and acetic acid (Scheme 6.2). The observed decomposition peak in the thermal experiments is probably due to this degradation.

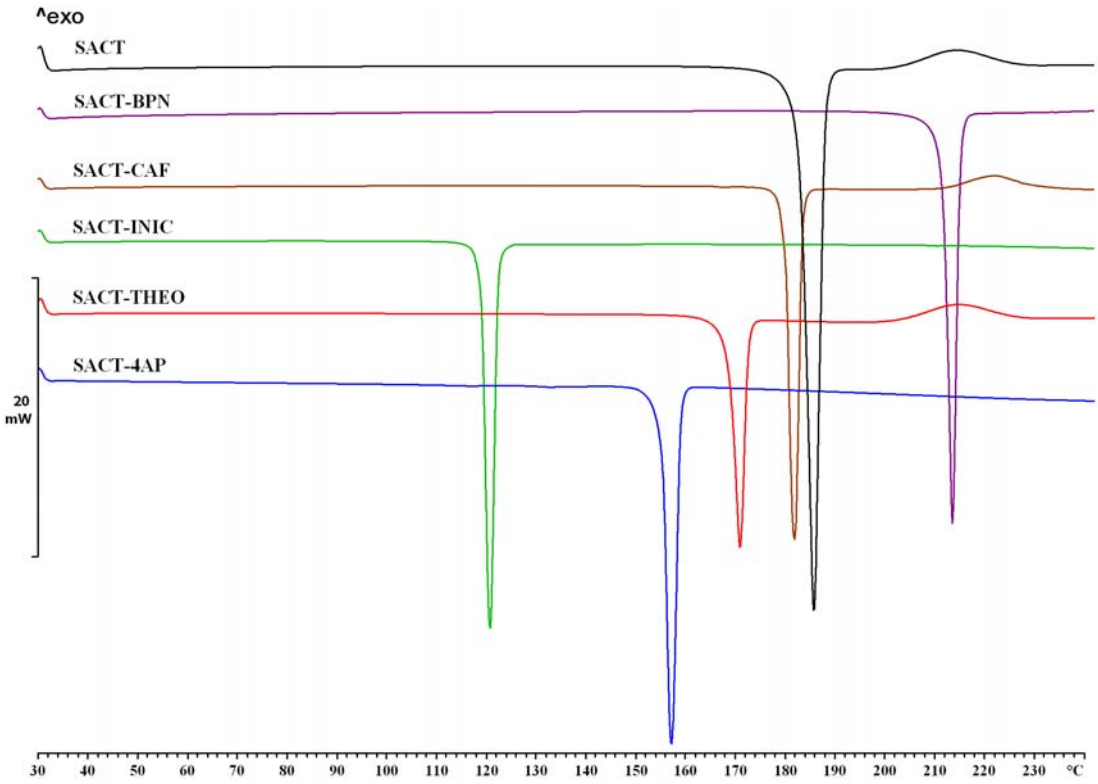

Figure 6.7 DSC heating curves of SACT and its cocrystals exhibiting unique melting behavior. The decomposition hump in SACT, SACT-CAF and SACT-THEO solid forms is due to the degradation of SACT to sulfanilamide and by-products.

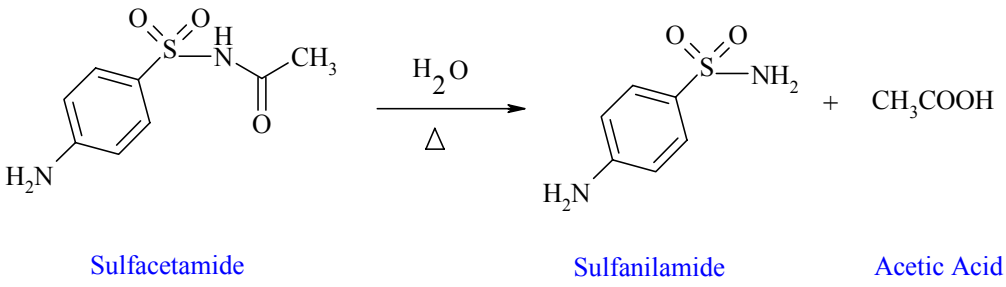

Scheme 6.2 Sulfacetamide is known to undergo hydrolytic degradation at higher temperatures to sulfanilamide and acetic acid.

Table 6.3 Melting points of SACT cocrystals/salt and their coformers.

S.No	SACT cocrystal/salt	Melting Point (°C)	Coformer	Melting Point (°C)
1	SACT-BPN	211–213	4,4'-bipyridine	110–114
2	SACT-CAF	179–181	caffeine	238
3	SACT-INIC	119–121	isonicotinamide	155–157
4	SACT-THEO	169–171	theophylline	272
5	SACT-4AP	156–158	4-aminopyridine	155

6.4.3 Powder X-ray diffraction

Powder diffraction is a reliable technique to establish the novelty of various solid forms through their unique diffraction patterns. It enables easy distinction of the modified solid materials from their individual components[35a]. This technique becomes doubly important in those cases where single crystals are not available for analysis. Recently, its application has been diversified with detection of polymorphic impurity in a mixture of polymorphs, bulk purity of polymorphs, cocrystals or salts, amorphous content in a crystalline material and structure solution of a crystalline material from its powder diffraction data[35]. PXRD was used to establish the bulk purity of SACT cocrystals. The experimental powder patterns of SACT cocrystals showed excellent match when overlayed with their calculated patterns indicating bulk phase purity (Figure 6.8).

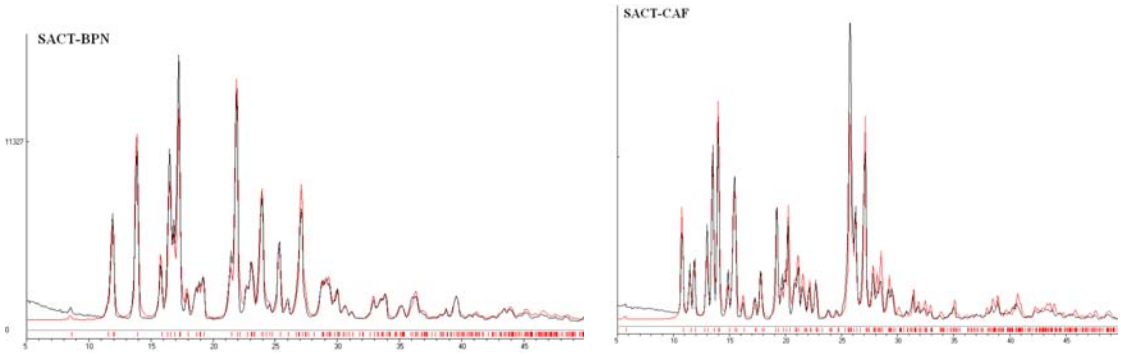

(a) (b)

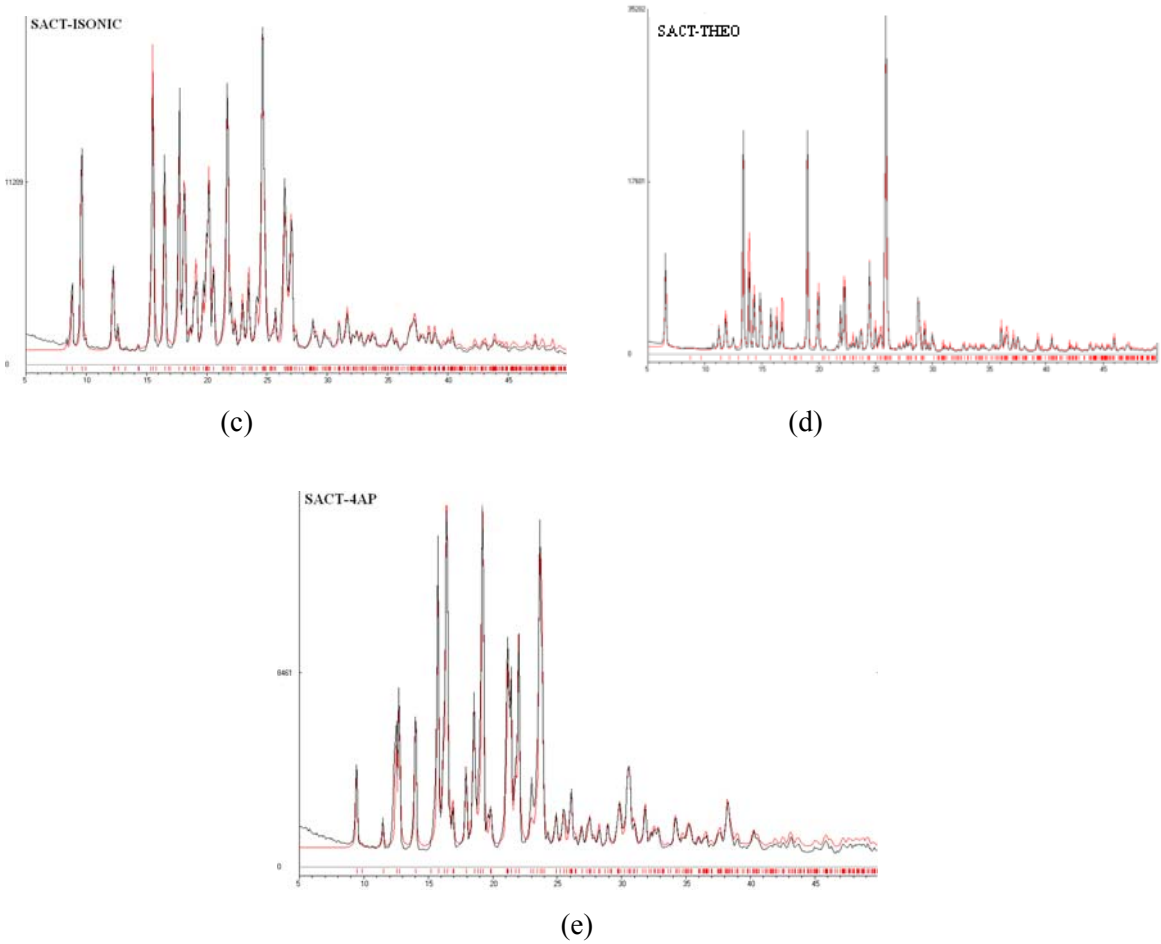

(c) (d)

(e)

Figure 6.8 Overlay of experimental PXRD patterns of SACT solid forms showed good match with their calculated line patterns from the X-ray crystal structures indicating bulk purity and homogeneity.

6.4.4 Spectroscopic analysis

The nature of hydrogen bonding and the extent of ionization can variably influence the vibrational energy levels of compounds on forming cocrystals or salts. IR and Raman instruments are sensitive to such changes, ably identifying and distinguishing novel solid forms from their starting components[36a]. In the IR spectrum of SACT, N–H asymmetric and symmetric stretching frequencies appeared at 3471.2, 3380.7 and 3257.0 cm^{-1}. The amide carbonyl stretch was observed at 1685.7 cm^{-1} and the N-H bending mode at 1596.4 cm^{-1}.

Significant changes in these vibrational modes were observed on forming cocrystal/salt (Figure 6.9). In SACT-BPN cocrystal, the N-H stretching modes shifted to 3475.6, 3375.3 cm^{-1}. While the N-H bending modes moved to 1594.0 cm^{-1}, the amide –C=O stretch appeared at 1704.1cm^{-1}. On forming cocrystal, the C=N stretch of BPN shifted from 1407.3 cm^{-1} to 1409.9 cm^{-1}. Similar differences were also observed in the stretching and bending modes of other cocrystals. While the N-H stretching frequencies appeared at 3441.7, 3358.1 and 3255.8 cm^{-1} in SACT-CAF, they showed up at 3428.4, 3396.6, 3345.9 and 3239.2 cm^{-1} in SACT-INIC and 3471.3 and 3380.8 cm^{-1} in SACT-THEO. The corresponding carboxamide C=O stretch was observed at 1702.0 and 1658.7 cm^{-1} in SACT-CAF, 1697.2 and 1674.2 cm^{-1} in SACT-INIC and 1716.1, 1667.8 cm^{-1} in SACT-THEO. Larger shifts in the N-H stretching frequencies were observed in the case of SACT-4AP where proton transfer from amide N-H to pyridyl nitrogen resulted in salt. The N-H stretching frequencies here were observed at 3444.4, 3422.9, 3350.3 and 3242.0 cm^{-1} and the carboxamide –C=O stretch at 1656.2 cm^{-1} (Table 6.4).

Table 6.4 Major FT-IR vibrational frequencies of (ν_s, cm^{-1}) SACT cocrystals

	N-H stretch	C=O stretch	N-H bend	C=N stretch
SACT	3471.2, 3380.7, 3257.0	1685.7	1596.2	–
BPN	–	–	–	1407.3
SACT-BPN	3475.6, 3375.3	1704.1	1594.0	1409.9
CAF	–	1700.8	–	–
SACT-CAF	3441.7, 3358.1, 3255.8	1702.0, 1658.7	1594.1	–
INIC	3371.2, 3335.4	1677.2	1554.0	–
SACT-INIC	3428.4, 3396.6, 3345.9, 3239.2	1748.0	1593.8, 1554.0	–
THEO	3461.2	1717.2, 1667.8	1567.0	–
SACT-THEO	3471.3, 3380.8, 3257.3	1716.1, 1667.8	1596.3, 1567.4	–
4AP	3436.4, 3301.6	–	1601.7	–
SACT-4AP	3444.2, 3422.9, 3350.3, 3242.0	1656.2	1596.8	–

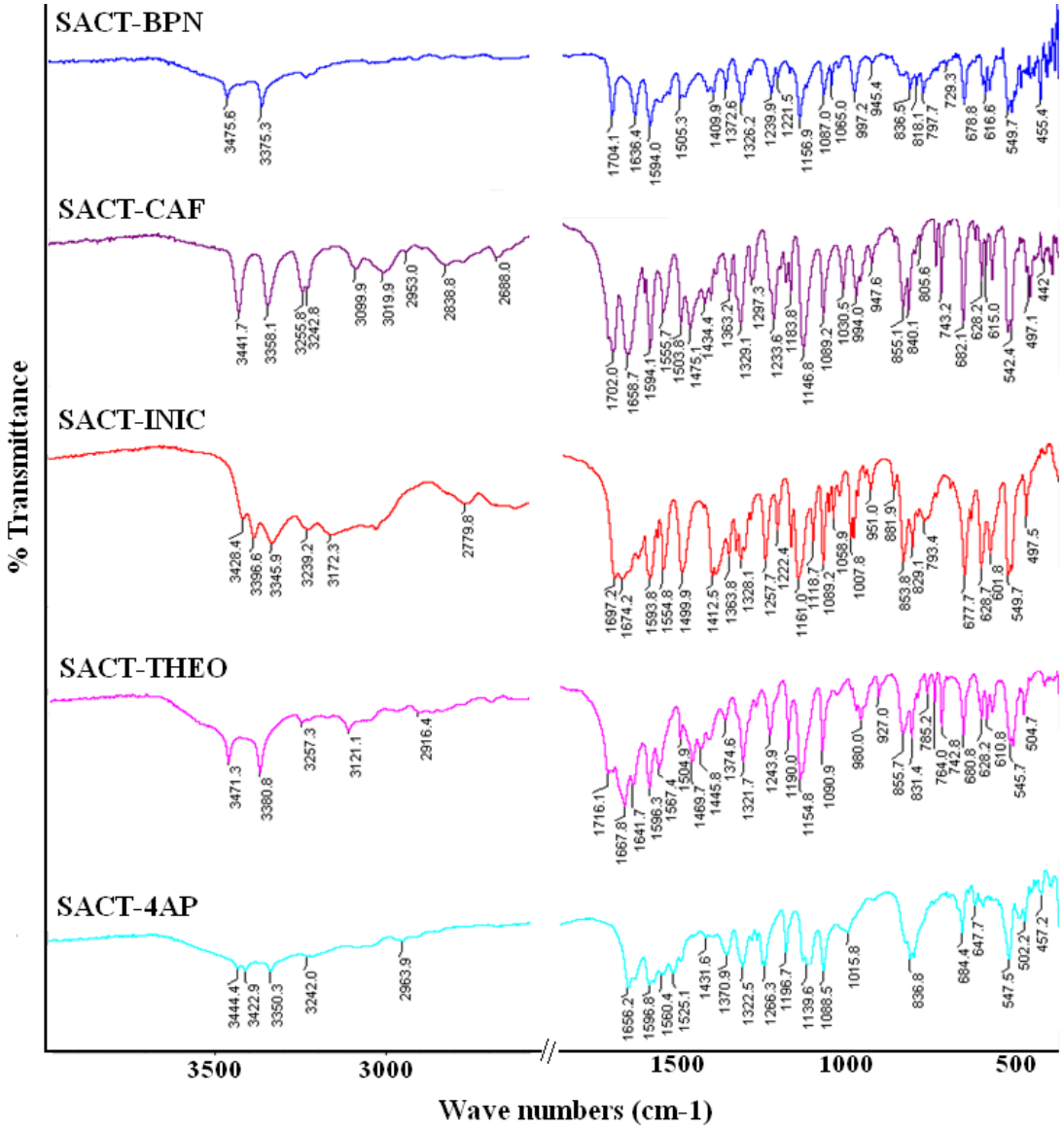

Figure 6.9 Overlay of the IR Spectra of SACT cocrystals

The complementary Raman spectra[36b], where the symmetric stretching frequencies have stronger intensities compared to the asymmetric modes, significant shifts in the Raman intensities on forming cocrystal/salt was observed (Figure 6.10). The Raman intensities for asymmetric and symmetric N-H and –C=O stretching frequencies appeared at 3479.5, 3380.7 and 1688.0 cm^{-1} respectively. These peak positions showed significant shift in the

cocrystals/salt. While the N-H asymmetric and symmetric intensities appeared at 3475.5, 3377.1 in SACT-BPN, 3443.3, 3358.2, 3256.3 in SACT-CAF, 3472.4, 3381.6 cm^{-1} in SACT-THEO and 3445.2, 3426.4, 3354.2, 3243.8 cm^{-1} in SACT-4AP the corresponding –C=O stretch was observed at 1707.1 cm^{-1} in SACT-BPN, 1703.4 cm^{-1} in SACT-CAF, 1699.7 cm^{-1} in SACT-INIC, 1708.3 cm^{-1} in SACT-THEO (Table 6.5).

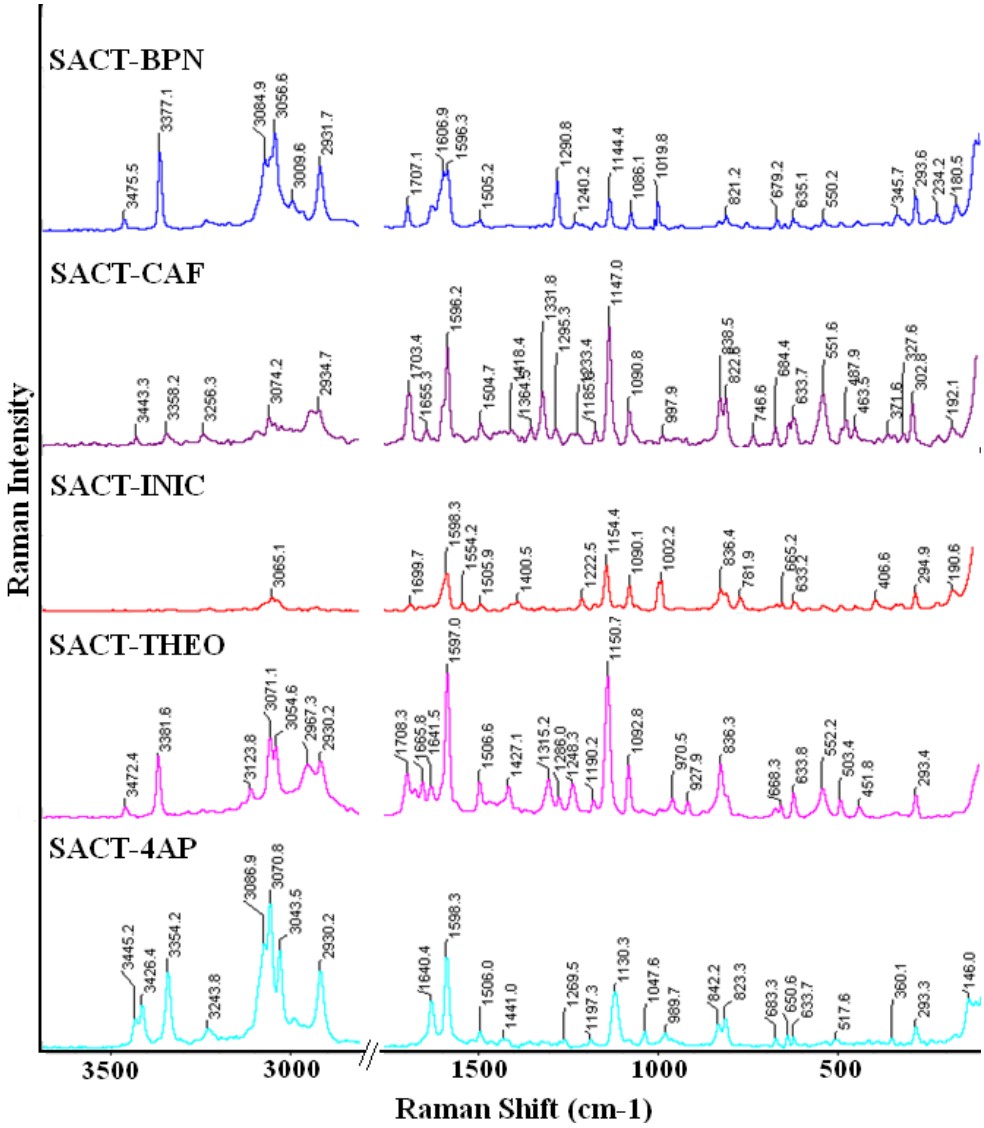

Figure 6.10 Overlay of the Raman Spectra of SACT cocrystals

Table 6.5 Major FT-Raman vibrational frequencies of (ν_s, cm^{-1}) SACT cocrystals

	N-H stretch	C=O stretch	N-H bend	C=N stretch
SACT	3479.5, 3380.7	1688.0	1598.4	–
BPN	–	–	–	1506.2
SACT-BPN	3475.5, 3377.1	1707.1	1596.3	1505.2
CAF	–	1697.4	–	–
SACT-CAF	3443.3, 3358.2, 3256.3	1703.4	1596.2	–
INIC	–	–	1602.2	–
SACT-INIC	–	1699.7	1598.3	–
THEO	3288.2	1705.8,1664.1	1610.9	–
SACT-THEO	3472.4, 3381.6	1708.3	1597.0	–
4AP	3438.3	–	1597.4	–
SACT-4AP	3445.2, 3426.4, 3354.2	1640.3	1598.3	–

ssNMR is a reliable technique for characterizing pharmaceutical solid forms because of its sensitivity to changes in hydrogen bonding interactions and molecular conformation[37]. It is a non-destructive method necessitating minimum amount of sample for characterization. Its nuclear specificity helps in detecting changes in the chemical shift values of local environment. ^{13}C ssNMR analysis of SACT cocrystals showed significant differences in chemical shifts in comparison to their individual components (Figure 6.11). In SACT, the –C=O– carbon showed a chemical shift at δ 171.8 ppm. Due to significant changes in the hydrogen bonding patterns, this peak appeared at varying chemical shifts in cocrystals. It was observed at 170.7 ppm in SACT-BPN, 171.2 ppm in SACT-CAF, 170.5 ppm in SACT-INIC, 171.3 ppm in SACT-THEO and 170.9 ppm in SACT-4AP. Even the other carbon nuclei showed important differences in their chemical shifts essentially distinguishing them from their starting components (Table 6.6).

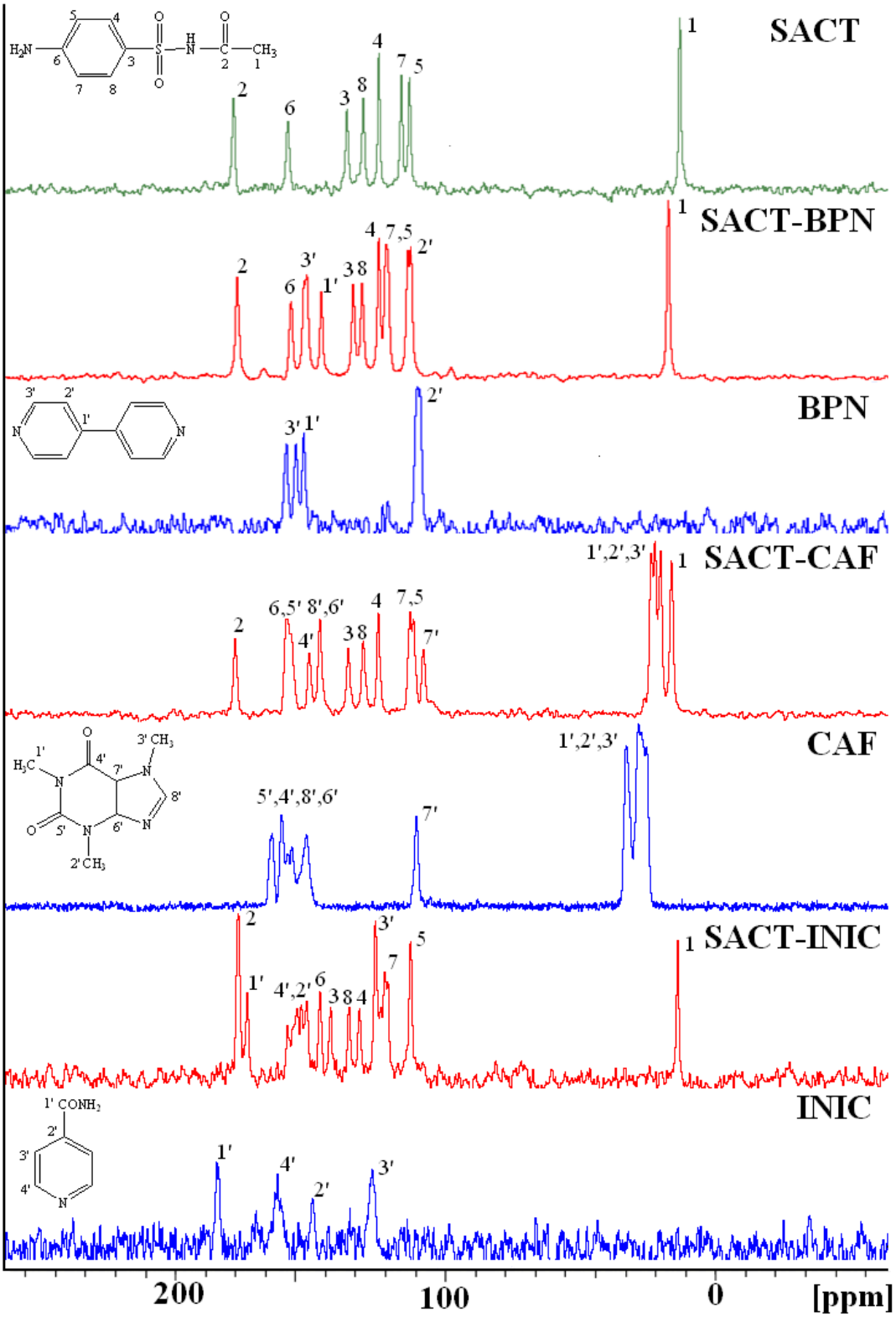
SACT
SACT-BPN
BPN
SACT-CAF
CAF
SACT-INIC
INIC
200
100
0
[ppm]

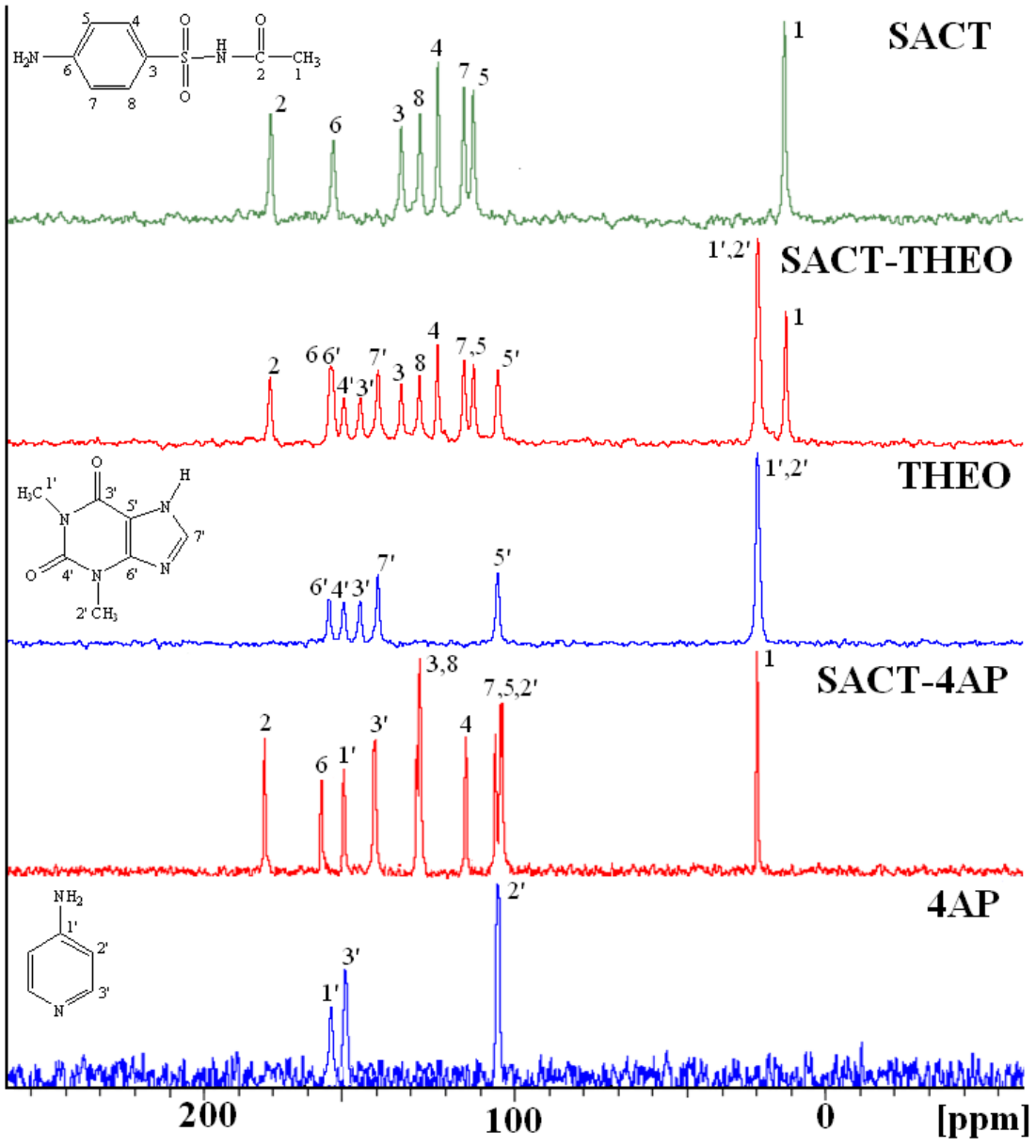

Figure 6.11 ^{13}C ssNMR spectra of SACT cocrystals.

Table 6.6 ss-NMR ^{13}C chemical shifts (δ, ppm) of SACT cocrystals

Carbon	SACT	BPN	SACT-BPN	CAF	SACT-CAF	INIC	SACT-INIC	THEO	SACT-THEO	4AP	SACT-4AP
1	21.2	–	25.1	–	24.6	–	22.5	–	21.5	–	27.7
2	171.8	–	170.7	–	171.2	–	170.5	–	171.3	–	180.5
3	133.6	–	131.4	–	133.2	–	139.4	–	133.7	–	130.5
4	122.9	–	122.9	–	123.1	–	129.6	–	123.1	–	116.9
5	112.5	–	112.0	–	111.3	–	112.5	–	112.7	–	108.3
6	153.5	–	152.4	–	153.8	–	143.0	–	154.3	–	159.9
7	115.2	–	120.4	–	112.5	–	120.1	–	115.4	–	110.9
8	128.2	–	128.6	–	128.2	–	133.2	–	128.4	–	128.9
1′	–	144.1	142.3	32.9	28.3	175.4	167.4	29.7	29.6	154.0	152.4
2′	–	121.2	113.0	33.5	30.1	145.9	147.4, 149.2	29.7	29.6	109.8	107.1
3′	–	149.4	147.3	35.8	31.4	125.8	122.5, 124.3	145.7	145.6	150.8	140.9
4′	–	–	–	152.3	146.3	158.1	150.7, 153.9	150.5	150.4	–	–
5′	–	–	–	155.7	152.1	–	–	105.5	105.5	–	–
6′	–	–	–	147.3	142.8	–	–	154.7	154.3	–	–
7′	–	–	–	110.4	108.0	–	–	140.5	140.4	–	–
8′	–	–	–	148.4	142.8	–	–	–	–	–	–

6.4.5 Solubility and Dissolution

The primary intention behind developing cocrystals of SACT is to address its poor bioavailability at the site of action that is reasoned to its high solubility and rapid elimination. We have surmised that the cocrystals obtained in the process would have the appropriate hydrogen bonding patterns to lower its solubility, which in turn might act as a slow release form, and may be helpful in increasing the residence time of drug at the ocular surface and improve its therapeutic efficacy. Therefore, we have determined the solubility and dissolution of SACT and its cocrystals using HPLC (Experimental section). Given its good aqueous solubility of 12.5mg/mL[21], the solubility and dissolution experiments on SACT and its cocrystals were performed in pH 7 buffer medium and the samples analyzed through HPLC. Equilibrium solubility experiments were performed for 24 hrs by making a supersaturated solution of SACT and its cocrystals separately in buffer media. These experiments showed that while SACT and its cocrystal with CAF are stable to the equilibrium solubility conditions, SACT-INIC and SACT-THEO cocrystals dissociated into their individual components precipitating SACT. The stable SACT-CAF cocrystal showed only about 0.59 times (8.64g/L) the solubility of SACT (14.54g/L), indicating that the thermodynamic solubility of SACT is lowered by forming a cocrystal with caffeine.

Being a kinetic method, Dissolution is helpful in determining the rate at which a particular compound dissolves into a solvent. Intrinsic dissolution rate (IDR) is particularly useful in determining the solubility of metastable forms before they convert to their more stable polymorph/hydrate etc. IDR experiments on SACT and its cocrystals were performed in pH 7 buffer media for 4 hrs by the rotating disk intrinsic dissolution rate (DIDR) method[38] at 37 °C. SACT-INIC showed 0.64 times the IDR of SACT followed by SACT-CAF (x 0.68) and SACT-THEO (x 1). Akin to the solubility experiments, SACT and SACT-CAF were stable at the end of dissolution experiment, but SACT-INIC and SACT-THEO cocrystals dissociated into their individual components precipitating the parent drug. The dissolution rates are correlated to the coformer solubility rather than cocrystal melting points. Unlike certain cocrystal systems[4a], we observed an inverse relationship between the solubility of the coformer and its corresponding cocrystal dissolution rate i.e. coformer with higher solubility

(INIC, 191.7 g/L) produced cocrystal with lower dissolution rate. The Intrinsic dissolution rate curves are displayed in Figure 6.12, and equilibrium solubility values, dissolution rates, melting points, and coformer solubility are listed in Table 6.7. The amount of dissolved SACT after 4 hrs ($AUC_{0\text{-}4h}$) is 64763.6 mg h/L for SACT, 38767.3 mg h/L for SACT-INIC, 41460.9 mg h/L for SACT-CAF, and 55241.6 mg h/L for SACT-THEO. The AUC value, which indicates the total amount of dissolved SACT in a given time period, is the highest for the parent drug. PXRD plots of the residue at the end of the equilibrium solubility and dissolution experiments are shown in Figure 6.13. In summary, the solubility of SACT is modulated by forming cocrystals with CAF, INIC and THEO. SACT-CAF cocrystal showed lower solubility and good stability in the equilibrium solubility and dissolution experiments. With pending in vivo experiments, SACT-CAF cocrystal by the virtue of its low solubility can be a promising candidate to improve the residence time of SACT at the ocular surface resulting in better therapeutic utility.

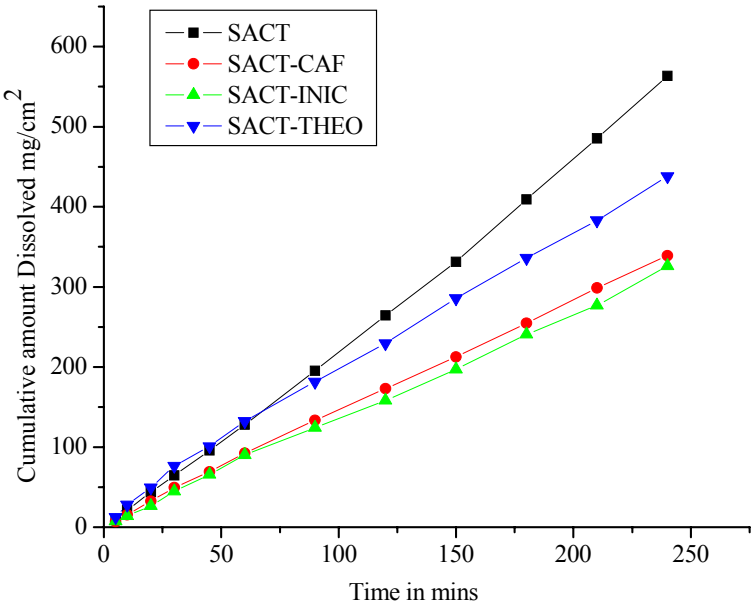

Figure 6.12 Intrinsic dissolution rate curves of SACT and its cocrystals in pH 7 Buffer.

Table 6.7 Intrinsic dissolution rate curves of SACT and its cocrystals along with $AUC_{0\text{-}4h}$ values, melting point of cocrystals and solubility of coformers

Compound	Eq. Solubility (g/L)	IDR in ($mg/cm^2/min$)	$AUC_{0\text{-}4h}$ (mgh/L)	M.P (°C) of cocrystals	Solubility of coformers (g/L)
SACT	14.54	2.18	64763.6	–	–
SACT-CAF	8.64	1.49 (x 0.68)	41460.9	179-181	21.7
SACT-INIC	–	1.39 (x 0.64)	38767.3	119-121	191.7
SACT-THEO	–	2.18 (x 1)	55241.6	169-171	8.3

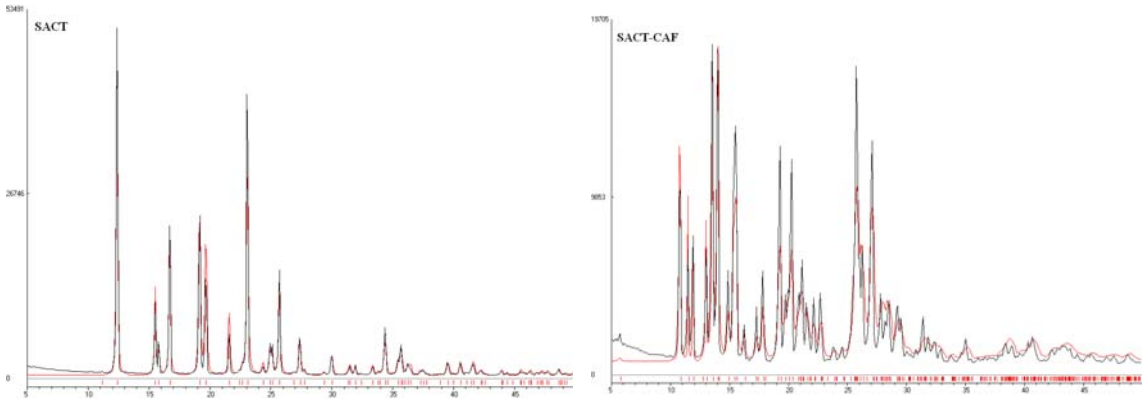

(a) (b)

Figure 6.13a) Representative PXRD pattern of SACT, SACT-INIC and SACT-THEO at the end of equilibrium solubility and dissolution experiments matches very well with SACT when overlayed with its calculated pattern. **b)** Representative PXRD pattern of SACT-CAF at the end of equilibrium solubility and dissolution experiments matches very well with its calculated pattern indicating phase stability.

6.5 Conclusions

Cocrystal screening techniques like mechanochemical grinding, slurry grinding and solution crystallization techniques were used to discover novel cocrystals of SACT with CAF, INIC, THEO and BIP in addition to a salt with 4AP. All the solid forms were characterized by diffraction, thermal and spectroscopic techniques. Crystal structure determination revealed that the cocrystals exhibited variable Z″ structures. Internal symmetry of the coformer and donor-acceptor imbalance were shown to be probable reasons for this occurrence. The solubility and dissolution of SACT and its cocrystals were determined in pH 7 buffer media. Solubility experiments revealed that the stable SACT-CAF cocrystal has low solubility (0.59 times) compared to the parent compound. Given their instability, equilibrium solubility of SACT-INIC and SACT-THEO could not be determined. Dissolution experiments on these cocrystals in the same media showed that SACT-INIC and SACT-CAF has 0.64 times and 0.68 times the IDR of SACT, while SACT-THEO has similar dissolution profile as the reference drug. Stability order was similar to the solubility experiments where only SACT and SACT-CAF were stable while SACT-INIC and SACT-THEO dissociated at the end of dissolution experiments. The primary aim of this work was to reduce the solubility of SACT intended for better therapeutic efficacy and this was achieved through SACT-INIC and SACT-CAF cocrystals. Although the compatibility of SACT cocrystals for ocular administration needs to be ascertained through in vivo studies, but as such the low solubility and good stability of SACT-CAF cocrystal may be useful in addressing the poor residence time and faster elimination issues of SACT. This work also act as a model study for Class I and Class III drugs wherein their poor bioavailability issues due to high solubility and faster elimination may be addressed by forming low solubility cocrystals.

6.6 Experimental Section

SACT and coformers (purity > 99.8%) were purchased from Sigma-Aldrich (Hyderabad, India). Solvents (purity > 99%) were purchased from Hychem Laboratories (Hyderabad,

India) for crystallization experiments. Water and solvents (HPLC grade) were purchased from Merck chemicals (Bangalore, India) for solubility and dissolution experiments.

Table 6.8 List of all the compounds used to form cocrystals with SACT

P-hydroxybenzoic acid	Hydroquinone	Theophylline
Benzamide	Isonicotinic acid	4-aminopyridine
4-methoxybenzoic acid	Nicotinic acid	Thymine
4-nitrobenzoic acid	Isonicotinamide	Urea
Cytosine	Resorcinol	Vanillin
Malonamide	Catechol	Salicylamide
Oxalic acid	4,4′-bipyridine	Succinamide
2,4-dihydroxy benzoic acid	Caffeine	Vanillic acid
Succinic acid	Adipic acid	Glutaric acid
3,5-dihydroxy benzoic acid	Malonic acid	Fumaric acid

Apart from caffeine, theophylline, 4-aminopyridine, isonicotinamide and 4,4′-bipyridine all the other coformers were unsuccessful in making cocrystals with SACT. Preparation methods for the successful candidates are shown below.

Preparation of SACT cocrystals SACT (214.2 mg) and 4,4'-BIP (78.0 mg) in 1:0.5 molar ratio were slurry ground in 5 mL of EtOH for 8 hrs. The formation of cocrystal was confirmed by PXRD and DSC. 30 mg of this material was dissolved in 5 mL EtOH and left for slow evaporation at ambient conditions. Single crystals suitable for X-ray diffraction were obtained after 3-4 days. The same cocrystal was also obtained on manual grinding of SACT and BIP in 1:0.5 stoichiometric ratio for 30 mins.

SACT (214.2 mg) and CAF (194.2 mg) in 1:1 molar ratio were slurry ground in 4 mL of EtOH for 24 hrs. The formation of cocrystal was confirmed by PXRD and DSC. 30 mg of this material was dissolved in 5 mL EtOH and left for slow evaporation at ambient conditions. Single crystals suitable for X-ray diffraction were obtained after 3-4 days. The same cocrystal was also obtained on manual grinding of SACT and CAF in 1:1 stoichiometric ratio for 30 mins.

SACT (214.2 mg) and INIC (244.24 mg) in 1:2 molar ratio were slurry ground in 2.5 mL of toluene and 1.5 ml of EtOAc solvent mixture for 24 hrs. The formation of cocrystal was confirmed by PXRD and DSC. 30 mg of this material was dissolved in 4 mL of 1:1 mixture of toluene and ethyl acetate solvent mixture and left for slow evaporation at ambient conditions. Single crystals suitable for X-ray diffraction were obtained after 4-5 days. The same cocrystal was also obtained on manual grinding of SACT and INIC in 1:2 stoichiometric ratio for 30 mins.

SACT (214.2 mg) and THEO (180.2 mg) in 1:1 molar ratio were slurry ground in 4 mL of i-PrOH for 24 hrs. The formation of cocrystal was confirmed by PXRD and DSC. 30 mg of this material was dissolved in 4 mL of i-PrOH and left for slow evaporation at ambient conditions. Single crystals suitable for X-ray diffraction were obtained after 4-5 days.

SACT (214.2 mg) and 4AP (94.11 mg) in 1:1 molar ratio were manually ground for 30 mins in a mechanochemical grinding experiment. The formation of salt was confirmed by PXRD and DSC. 30 mg of this material was dissolved in 4 mL of EtOH solvent and left for slow evaporation at ambient conditions. Single crystals suitable for X-ray diffraction were obtained after 3-4 days.

X-ray crystallography Crystal structures of SACT-BPN and SACT-INIC cocrystals were collected on CrysAlisPro, Oxford Diffraction Ltd., and the crystal structures of SACT-CAF, SACT-4AP and SACT-THEO cocrystals were collected using Bruker SMART-APEX CCD diffractometer.

Solubility and Dissolution The solubility and dissolution experiments were performed using HPLC method. Prior to estimating solubility and dissolution rates, calibration curves were determined for each compound. Various dilutions of a stock solution of SACT and cocrystals in pH 7 buffer were made and their respective AUC values were determined using HLPC at λ_{max} 254nm (λ_{max} of SACT). By plotting known concentration of each dilution vs. corresponding area, calibration curve for each compound was obtained. HPLC was done on Shimadzu Prominence model LC-20AD equipped with a PDA detector and C-18G column (250 mm x 4.6 mm ID, 5µm particle size and 120Å pore size). Elution was achieved by a

mobile phase made of 85:15 ratio of water with 1% acetic acid: Methanol in an isocratic method. The retention times of standard aqueous solutions of SACT, CAF, THEO and INIC were found to be 8.2, 41.4, 3.6 and 22.2 mins respectively and the same were observed even for the cocrystals. SACT has 73.3, 42.3 and 66.4% contribution in SACT-CAF, SACT-INIC and SACT-THEO cocrystals. The quantification of SACT in test solutions obtained from equilibrium solubility and dissolution experiments were done by comparison of the HPLC peak area with that of the standards. Equilibrium solubility was determined in pH 7 buffer using shake-flask method[39]. Excess amount of powdered material was added to 5 ml of the buffer solution and the resulting suspension was stirred at room temperature for 24hrs. The suspension was filtered through 0.45µ syringe filter and the concentration of the resultant solution determined. Intrinsic dissolution rate (IDR) measurements were carried on a USP-certified Electrolab TDT-08 L dissolution tester by the disk intrinsic dissolution method. For IDR experiments, 500 mg of pure SACT and the cocrystals were taken in the intrinsic attachments and compressed to a 0.5 cm^2 disk using a hydraulic press at a pressure of 2.5 ton $inch^{-2}$ for 5 min. The intrinsic attachments were placed in jars of 900 mL of pH 7 buffer preheated to 37°C and rotated at 150 rpm. 5 ml aliquots were collected at specific time intervals, and concentrations of the aliquots were determined with proper dilution from the predetermined calibration curves. The linear region of the dissolution profile (regression > 0.99) was used to determine the IDR of the compound as [slope of the amount dissolved÷ surface area of the pellet] per unit time. There was no transformation of SACT or cocrystals upon tablet compression as confirmed by PXRD.

6.7 References

1. (a) G. R. Desiraju, J. J. Vittal, A. Ramanan, *Crystal Engineering. A Textbook,* World Scientific Publishing, Singapore, 2011 (b) G. R. Desiraju, *Crystal Engineering. The Design of Organic Solids*. Elsevier, 1989 (c) G. R. Desiraju, *Angew. Chem., Int. Ed. Engl*., 1995, **34**, 2311.

2. (a) G. R. Desiraju, *CrystEngComm*, 2003, **5**, 466 (b) J. D. Dunitz, *CrystEngComm*, 2003, **5**, 506 (c) A. D. Bond, *CrystEngComm*, 2007, **9**, 833-834 (d) A. Parkin, C. J. Gilmore, C. C. Wilson, *Zeitschrift für Kristallographie,* 2008, 223, 430.
3. (a) A. N. Sokolov, T. Friščić and L. R. MacGillivray, *J. Am. Chem. Soc.,* 2006, **128**, 2806-2807 (b) M. Morimoto, S. Kobatake and M. Irie, *Chem Commun*, 2008, 335-337 (c) D. P. Yan, A. Delori, G. O. Lloyd, T. Friščić, G. M. Day, W. Jones, J. Lu, M. Wei, D. G. Evans and X. Duan, *Angew. Chem. Int. Ed.,* 2011, **50**, 12483 (d) X. Pang, H. Wang, X. R. Zhao and W. J. Jin, *CrystEngComm*, 2013, **15**, 2722-2730 (e) L. R. MacGillivray, G. A. Papaefstathiou, T. Friščić, T. D. Hamilton, D. –K, Bučar, Q. Chu, D. B. Varshney, I. G. Georgiev, *Acc. Chem. Res*., 2008, **41**, 280-291 (f) C. Malla Reddy, G. Rama Krishna and S. Ghosh, *CrystEngComm*, 2010, **12**, 2296-2314 (g) S. Ghosh and C. Malla Reddy, *Angew. Chem. Int. Ed.,* 2012, **51**, 10319.
4. (a) N. Schultheiss and A. Newman, *Cryst. Growth Des.,* 2009, **9**, 2950-2967 (b) W. Jones, W. D. S. Motherwell and A. V. Trask, *MRS Bulletin*, 2006, **31**, 875 (c) P. Vishweshwar, J. A. McMahon, J. A. Bis and M. J. Zaworotko, *J. Pharm. Sci*., 2006, **95**, 499.
5. (a) S. R. Byrn, R. R. Pfeiffer and G. G. Stowell, *Solid-State Chemistry of Drugs*, SSCI, West Lafayette, IN, 1999 (b) H. G. Brittain, *Physical Characterization of Pharmaceutical Solids*, Marcel Dekker Inc. NY, 1995. (c) Y. Qiu, Y. Chen and G.G.Z. Zhang, *Developing Solid Oral Dosage Forms: Pharmaceutical Theory and Practice*, First ed. Academic Press, NY, 2009.
6. N. J. Babu, P. Sanphui and A. Nangia, *Chem. Asian J.,* 2012, **7**, 1-13.
7. A. V. Trask, W. D. S. Motherwell and W. Jones, *Cryst. Growth Des*., 2005, **5**, 1013-1021.
8. S. Karki, T. Friščić, L. Fábián, P. R. Laity, G. M. Day and W. Jones, *Adv. Mater.,* 2009, **21**, 3905-3909.
9. (a) J. F. Remenar, S. L. Morissette, M. L. Peterson, B. Moulton, J. M. MacPhee, H. R. Guzmán, Ö. Almarsson, *J. Am. Chem. Soc.,* 2003, **125**, 8456–8457. (b) N.R. Goud, S. Gangavaram, K. Suresh, S. Pal, S. G.Manjunatha, S. Nambiar and A. Nangia, *J. Pharm. Sci.,* 2012, **101**, 664-680. (c) S. Basavoju, D. Boström and S. P.

Velaga, *Pharm. Res.,* 2008, **25**, 530-541 (d) P. Sanphui, S. S. Kumar and A. Nangia, *Cryst. Growth Des.,* 2012, **12**, 4588.

10. A. M. Thayer, *Chem. Eng. News*, 2010, **88**, 13-18.
11. (a) X. Chen, H. Wen and K Park, in *Oral Controlled Release Formulation Design and Drug Delivery: Theory and Practice*, H.Wen and K. Park, Eds., John Wiley and Sons, Inc., 2010. (b) P. De Haan and C. F. Lerk, *Pharmaceutisch Weekbald*, 1984, **6**, 57-67.
12. (a) R. Mullin, *Chem. Eng. News,* 2012, **90**, 15. (b) M. May, *Nature Med*., 2009, **15**, 1243 (c) L. F. Joseph and J. M. Hale, *Pharm. Times,* 2012, **78**, 124.
13. (a) N. G. Das and S. K. Das, *Formulation Fill and Finish*, 2003, 10. (b) P. M. Brooks, M. S. Roberts and B. Patel, *Br. J. Clin. Pharmacol.,* 1978, **5**, 337-339.
14. (a) D. Patel, B. Patel, H. Patel and C. Patel, *J. Young Pharm*., 2011, **3**, 176-180. (b) A. Almeida, L. Brabant, F. Siepmann, T. De Beer, W. Bouquet, L. Van Hoorebeke, J. Siepmann, J. P. Remon and C. Vervaet, *Eur. J. Pharm. Biopharm.,* 2012, **82**, 526-533 (c) B. K. Nanjwade, S. R. Mhase and F. V. Manvi, *Trop. J. Pharm. Res.,* 2011, **10**, 375-383.
15. A. R. Gennaro, *Remington: The Science and Practice of Pharmacy*, 20th Ed., Lippincott Williams and Wilkins, NY, 2000.
16. A. J. Smith, *Modulating the Pharmacokinetics of Bioflavonoids*, Ph.D Thesis, University of South Florida page 67-68.
17. (a) S. L. Childs, L. J. Chyall, J. T. Dunlap, V. N. Smolenskaya, B. C. Stahly and G. P. Stahly, *J. Am. Chem. Soc.,* 2004, **126**, 13335-13342 (b) C. B. Aakeroy, S. Forbes and J. Desper, *J. Am. Chem. Soc.,* 2009, **131**, 17048-17049.
18. (a) C. A. Hull and S. M. Johnson, *Cutis*, 2004, **73**, 425 (b) J. Q. Del Rosso, *Cutis,* 2004, **73**, 29 (c) I. Meghan, B. S. Dubina, B. Alan and M. D. Fleischer Jr., *Arch. Dermatol.,* 2009, **145**, 1027.
19. A. Mastrolorenzo and C. T. Supuran *Met. Based Drugs*, 2000, **7**, 49.
20. G. L. Mandell, J. E. Bennett, R. Dolin, Eds., *Mandell, Douglas, and Bennett's Principles of Infectious Diseases,* NewYork, Churchill Livingstone Inc; 2000.
21. http://www.drugbank.ca/drugs/DB00634

22. (a) D. Sensoy, E. Cevher, A. Sarici, M. Yilmaz, A. Özdamar and N. Bergisadi, *Eur. J. Pharm. Biopharm.,* 2009, **72**, 487-495 (b) B. Mandal, K. S. Alexander, A. T. Riga, *J. Pharm. Pharmaceut. Sci.,* 2010, **13**, 510-523.
23. (a) A. Mukherjee, P. Grobelny, T. S. Thakur and G. R. Desiraju, *Cryst. Growth Des*., 2011, **11**, 2637 (b) R. Dubey, M. S. Pavan and G. R. Desiraju, *Chem. Commun.,* 2012, **48**, 9020.
24. (a) A. V. Trask and W. Jones, *Top Cur. Chem*., 2005, **254**, 41 (b) N. Shan, F. Toda and W. Jones, *Chem Commun,* 2002, **20**, 2372
25. (a) G. R. Desiraju, *Angew. Chem. Int. Ed. Engl.,* 1995, **34**, 2311-2327. (b) C. B. Aakeröy, *Acta Crystallogr. Sect. B,* 1997, **53**, 569-586. (c) B. Moulton and M. Zaworotko, *Chem. Rev*., 2001, **101**, 1629-1658.
26. (a) M. C. Etter, *Acc. Chem. Res*., 1990, **23**, 120-126. (b) M. C. Etter, *J. Phys. Chem*., 1990, **23**, 120-126.
27. (a) A. Nangia and G. R. Desiraju, *Top Curr. Chem*., 1998, **198**, 57 (b) P. Vishweshwar, A. Nangia and V. M. Lynch, *Cryst. Growth Des*., 2003, **3**, 783 (c) N. J. Babu, L. S. Reddy and A. Nangia, *Mol. Pharmaceutics*, 2007, **4**, 417 (d) L. S. Reddy, N. J. Babu, A. Nangia, *Chem Commun*, 2006, 1369.
28. (a) T. Steiner, *Acta Crystallogr*., 2001, **B57**, 103-106 (b) J. A. McMahon, J. A. Bis, P. Vishweshwar, T. R. Shattock, O. L. McLaughlin and M. J. Zaworotko, *Z. Kristallogr.*, 2005, **220**, 340-350 (c) F. H. Allen, W. D. S. Motherwell, P. R. Raithby, G. P. Shields, R. Taylor, *New J. Chem*., 1999, 25-34.
29. B. P. V. Eijck and J Kroon, *Acta Crystallogr., Sect. B*, 2000, **56**, 535-542
30. (a) K. M. Anderson, M. R. Probert, C. N. Whiteley, A. M. Rowland, A. E. Goeta and J. M. Steed, *Cryst. Growth Des.,* 2009, **9**, 1082-1087 (b) A. M. Todd, K. M. Anderson, P. Byrne, A. E. Goeta and J. M. Steed, *Cryst. Growth Des*., 2006, **6**, 1750-1752 (c) K. M. Anderson, A. E. Goeta and J. M. Steed, *Cryst. Growth Des*., 2008, **8**, 2517-2524 (d) H. J. Lehmler, L W. Robertson, S. Parkin and C. P. Brock, *Acta Crystallogr., Sect. B*, 2002, **B58**, 140-147
31. R. Thakuria, S. Cherukuvada and A Nangia, *Cryst. Growth Des.,* 2012, **12**, 3944-3953.

32. (a) C. B. Aakeroy, M. E. Fasulo and J. Desper, *Mol. Pharmaceutics*, 2007, **4**, 317. (b) B. Sarma, N. K. Nath, B. R. Bhogala and A. Nangia, *Cryst. Growth Des*., 2009, **9**, 1546. (c) S. L. Childs, G. P. Stahly and A Park, *Mol. Pharmaceutics,* 2007, **4**, 323. (d) A. J. Cruz-Cabeza, *CrystEngComm,* 2012, **14**, 6362.
33. (a) W, Jones W. D. S. Motherwell and A. V. Trask, *MRS Bull.,* 2006, **31**, 875. (b) M. K. Stanton and A. Bak, *Cryst. Growth Des*., 2008, **8**, 3856. (c) M. K. Stanton, S. Tufekcic, C. Morgan and A. Bak, *Cryst. Growth Des*., 2009, **9**, 1344.
34. (a) T. Ahmad, *Pharmazie*, 1982, **37**, 559-561.
35. (a) K. D. M. Harris, M. Tremayne and B. M. Kariuki, *Angew. Chem. Int. Ed*., 2001, **40**, 1626-1651. (b) K. D. Harris, M. Tremayne, P. Lightfoot and P. G. Bruce, *J. Am. Chem. Soc.,* 1994, **116**, 3543-3547 (c) E. Y. Cheung, S. J. Kitchin, K. D. M. Harris, Y. Imai, N. Tajima and R. Kuroda, *J. Am. Chem. Soc.,* 2003, **125**, 14658-14659.
36. (a) R. M. Silverstein, *Spectrometric Identification of Organic Compounds*. 6th Ed.; John Wiley & Sons, Inc.: New York, 2002. (b) E. Smith and G. Dent, *Modern Raman Spectroscopy, A Practical Approach*, John Wiley: New York, 2005.
37. (a) F. G. Vogt, J. S. Clawson, M. Strohmeier, A. J. Edwards, T. N. Pham and S. A. Watson, *Cryst. Growth Des.,* 2009, **9**, 921. (b) D. Braga, L. Maini, G. de Sanctis, K. Rubini, F. Grepioni, M. R. Chierotti and R. Gobetto, *Chem – Eur. J*., 2003, **9**, 5538.
38. L. X. Yu, A. S. Carlin, G. L. Amidon and A. S. Hussain, *Int. J. Pharm*., 2004, **270**, 221.
39. T. Higuchi, K. A. Connors, *Adv. Anal. Chem. Instrum*., 1965, **4**, 117.

CHAPTER SEVEN

RELATIVE STABILITY OF ATOVAQUONE POLYMORPHS

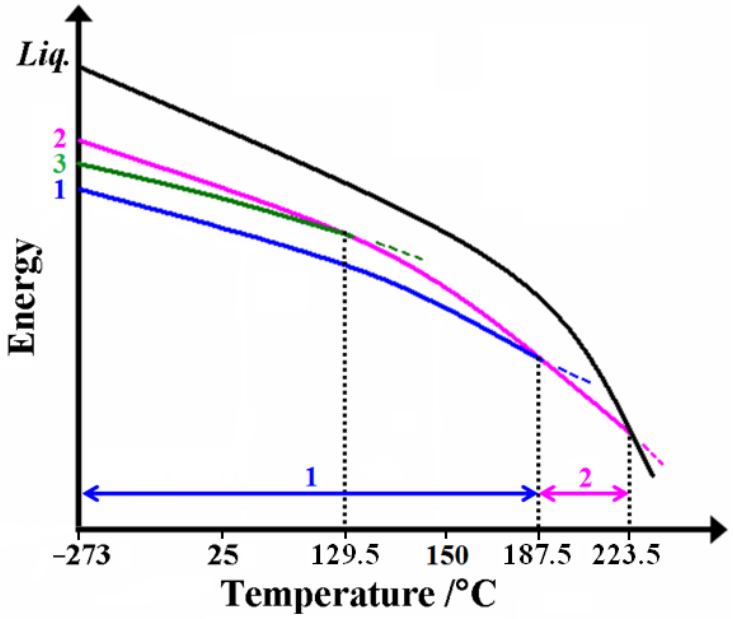

Schematic energy vs temperature diagram to show the relative stability and phase transformation of ATV polymorphs. At -273°C form 1 is the stable phase. Form 1 is the stable modification between 25-187.5°C since form 2 and form 3 converted to form 1 in slurry and grinding experiments. The transition points at 187.5°C and 129.5°C is due to the conversion of form 1 and form 3 to form 2 on heating. Form 2 is the stable phase above 187.5°C and upto its melting temperature at 223.5°C.

7.1 Introduction

According to the widely accepted definition of McCrone[1], a polymorph is "*a solid crystalline phase of a given compound resulting from the possibility of at least two different arrangements of the molecules of that compound in solid state*". The first report on polymorphism in the area of crystallography is credited to Mitscherlich[2] (1822, 1823) who identified different crystal structures of the same compound in several arsenate and phosphate salts. Since then it continues to occupy a prominent place in the field of solid state chemistry. Today the interest in polymorphism has brought together supramolecular chemists, material scientists and biochemists with its wide range of applications in pharmaceutical[1,3], electronic[4] and biological membranes[5].

From the beginning of the last century, polymorphism of drugs has been an area of immense importance in pharmaceutical industry. Although identical in chemical composition, polymorphs differ in bioavailability, solubility, dissolution rate, chemical and physical stability, melting point, color, filterability, density, flow properties etc[1,3,6]. For instance, Chloramphenicol, a broad spectrum antibiotic is marketed as its prodrug, palmitate ester which converts to the active compound in the small intestine[7a]. Of the three polymorphic forms of Chloramphenicol palmitate, Form C is highly unstable and form A has low biological activity because it is slowly hydrolyzed to the active component. It was found that the maximum blood levels attained with 100% form B is about 7 times greater than with 100% form A polymorph and that with mixtures of A and B the blood levels vary in proportion to the percentage of B in suspension[7b,c] (Figure 7.1). This observation not only highlights the effect of polymorphism on in vivo bioavailability of drug molecules but also establishes the importance of marketing the optimal polymorph for better therapeutic utility. In addition, the recent patent litigations concerning the marketing rights of anti-ulcer drug Ranitidine[8a], where the original inventor Glaxo was able to ward off competition from generic companies by patenting an additional form II apart from the marketed form I, or the unfortunate withdrawal of anti-retroviral drug Ritonavir[8b] form the market by Abbott laboratories because of the unexpected crystallization of the more stable polymorph (and so less soluble) which compromised on the oral bioavailability, has only enhanced the priority

for polymorphism in terms of thorough screening for obtaining all the possible polymorphs of a drug molecule and establishing their stability relationships. Inefficient screening of polymorphs of a drug molecule might lead to unreliable physicochemical properties which can compound the financial woes of pharmaceutical companies during advanced stages of drug development. Conversely, a thorough understanding of solid state properties has implications in candidate selection for drug development, formulation, and may qualify for independent patent protection, effectively extending the marketable life of an active pharmaceutical ingredient[3c,6a] (API).

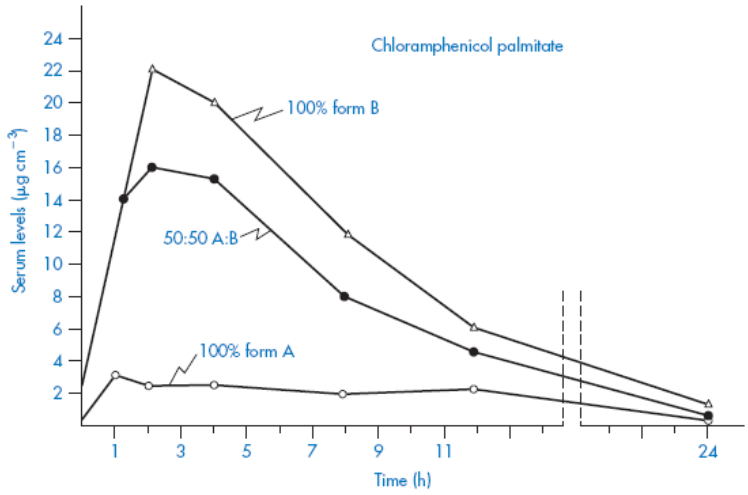

Figure 7.1 Comparison of serum levels (μg cm^{-3}) obtained with suspensions of Chloramphenicol palmitate after oral administration of a dose equivalent to 1.5g of Chloramphenicol (Adapted from ref. 7c).

In literature various analytical techniques were used to discover novel polymorphs of a drug molecule and understand the phase relationship between them in order to optimize the thermodynamic modification. Nangia and coworkers[9a] used solvent less methods like melt crystallization and sublimation to discover novel polymorphs of 1,1-bis(4-hydroxyphenyl) cyclohexane. McArdle et. al.[9b] discovered novel polymorphs of Bicifadine hydrochloride using ATR-IR, ATR-NIR in addition to powder diffraction and thermal methods. Spiegeleer and colleagues[9c] estimated the relative amounts of three crystal forms of a benzimidazole drug from its finished formulations using FT-Raman spectroscopy. Dharmayat et. al.[9d]

monitored the polymorphic transformation of L-glutamic acid using combined on-line video microscopy and X-ray diffraction. Using FT-Raman spectroscopy Byrn and coworkers[9e] estimated the transition temperature for the enantiotropic polymorphic system of Flufenamic acid from its transformation kinetics. Apart from these well known methods much of the research effort is now placed on utilizing novel techniques to discover, characterize and establish the phase stability of polymorphs. Techniques like Solid-state NMR[10a], Terahertz spectroscopy[10b] and Atomic force microscopy[10c] come under this category. Understanding the relative stability of polymorphs is highly beneficial in those cases where the more stable polymorph is not necessarily the optimal modification for marketing the drug. At times a metastable polymorph needs to be stabilized because of its therapeutic advantage. For instance, the anthelminthic drug Mebendazole exists in three forms[11]. While form A is more stable followed by form B and Form C, their therapeutic effect does not follow the same order. While Form A is inactive, Form B is toxic with only form C having the ideal physicochemical properties to confer drug efficacy. Therefore this metastable form C was stabilized and marketed as the drug[11b]. In essence, the above literature reports stress the importance of thorough screening for all the polymorphs of a drug molecule. They highlight the necessity of understanding the stability relationships between the polymorphs using various analytical techniques in order to avoid undue phase transformations and in the process develop the ideal polymorph for optimal drug delivery.

7.2 Literature reports on Atovaquone

Atovaquone (ATV hereafter), trans-2-[4-(4-chlorophenyl) cyclohexyl]-3-hydroxy-1,4-naphthalenedione (Scheme 7.1) belongs to the naphthoquinones family and is a lipophilic analogue of ubiquinone (coenzyme Q), an important component of the mitochondrial electron transfer system in cells. It is a popular anti-pneumocystic with specific activity against *Pneumocystis carinii*[12a], and a potent antimalarial drug[12b]. The antimalarial activity of ATV has been attributed to its interference with mitochondrial electron transport in the parasite, specifically at the cytochrome C reductase complex[13], that results in a collapse of the mitochondrial activity. It is manufactured and sold as anti-pneumocystic under the brand

name *mepron*[14], in both liquid and suspension forms. It has been commercially available from GlaxoSmithKline since 2000 as malarone[15] (sometimes abbreviated A+P) for its anti-malarial activity. Various patents disclose the synthesis of different naphthaquinone derivatives and microfluidised particles of ATV to increase bioavailability[16]. Other literature reports describe the generation of four different polymorphic modifications of ATV and their stability relationship[17]. Malpezzi et. al.[18a] reported the thermal analysis of form 1 and form 2 polymorphs and showed that form 2 is the thermodynamic phase. Later Reitveld et. al.[18b] reported through Energy-Temperature diagrams that form 1 is the stable polymorph and not form 2. (Form 1 has the lowest Gibbs free energy). Recently Nayak et. al.,[18c] reported crystal structures and binding studies of ATV and its derivatives with cytochrome bc1 coenzyme.

The article of Malpezzi et. al. appeared when our study on ATV polymorphs was in final stages. The results obtained in our study suggested a different stability order to that proposed by Malpezzi et. al. Based on the phase transformation studies on the known ATV polymorphs along with a novel polymorph (form 3) under different conditions such as polymorphic seeds, mechanical stress (grinding), solvent, and temperature, the relative stability order of ATV polymorphs was found to be: at absolute zero form 1 < form 3 < form 2, at ambient temperature form 1 < form 3 < form 2, whereas at high temperature form 2 < form 1 < form 3. Apart from this, both form 1 and form 2 were characterized by X-ray crystal structure analysis at 100K and their molecular overlay confirmed them as packing polymorphs. Furthermore, during solubility study of ATV polymorphs, it was noted that the molar absorptivities (or molar extinction coefficients) of polymorphs differ from each other just as other physico-chemical properties. In addition a novel salt form of ATV with PIP was discovered in order to address the poor solubility of this BCS class II drug.

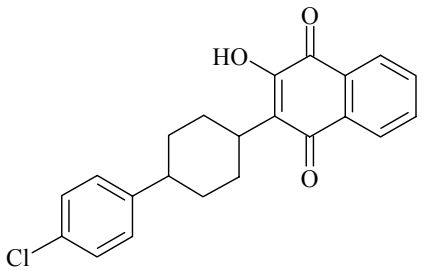

Scheme 7.1 Molecular structure of ATV

7.3 Crystallization of ATV Polymorphs

Commercial ATV is in the form 1 polymorphic modification (PXRD pattern match in Figure 7.2) and the material was used for all experiments of this study. All ATV polymorphs were reproduced in macroscopic amounts in pure state as confirmed by their experimental PXRD profile match with that of the calculated lines from the X-ray crystal structures in case of form 1 and form 2 and through consistent reproducibility and characterization in case of form 3 where single crystals are not available for overlay (Figure 7.2). Form 1 polymorph was obtained as blocks exclusively from dilute acetonitrile and nitromethane. Form 2 was obtained as plates from common solvents such as i-propanol, THF, dioxane, hexane etc. Form 3 was obtained only by crash cooling of a DCM solution of form 1 in liquid nitrogen. HSM snapshots to depict the differences in crystal morphologies of form 1 and form 2 are discussed later (Figure 7.12). A saturated solutions of acetonitrile resulted in the crystallization of form 2 instantly which when left for evaporation for few more days resulted in the appearance of form 1 crystals at the expense of form 2 phase. Kinetic methods like melting and sublimation consistently gave form 2. These kinetic methods and crystallization from saturated solutions already indicate that form 2 is a metastable phase. In all, ATV polymorphs form 1 and form 2 were obtained both exclusively and concomitantly from several solvents whereas form 3 was generated by crash cooling.

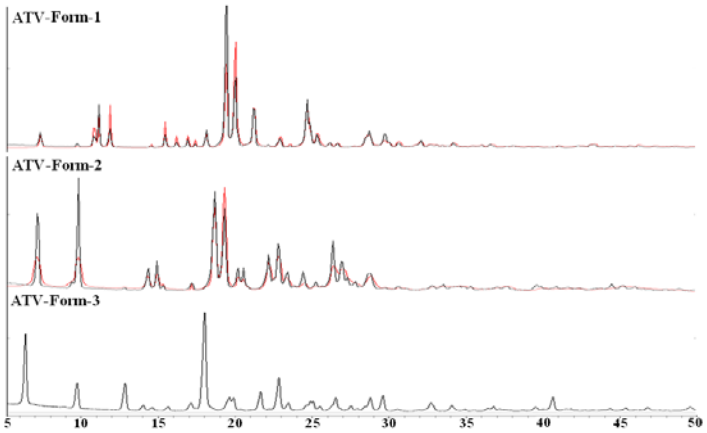

Figure 7.2 Form 1 and form 2 experimental patterns showed good match with their calculated lines indicating bulk purity. Form 3 purity was confirmed by PXRD and DSC.

7.4 Crystal structure analysis of ATV polymorphs

While the crystal structures of ATV polymorphs form 1 and form 2 were reported by Malpezzi et. al. and Nayak et. al., the latter group also disclosed the crystal structure of the cis-isomer of the parent drug. Several other derivatives of ATV were also documented by these groups. Surprisingly, there are no reports on the pharmaceutical multicomponent solid modifications like cocrystals or salts of ATV for addressing its poor solubility. In this study we have redetermined the crystal structures of Form 1 and form 2 at 100K and solved to a higher accuracy. Crystal structure of Form 3 could not be obtained. Several attempts to grow the single crystals of form 3 invariably resulted in form 2 or form 1 due to solvent mediated phase transformation during crystallization. Nevertheless, its uniqueness was established by its consistent powder pattern and its characteristic DSC heating curve. In addition, we also obtained the first pharmaceutical bicomponent solid modification of ATV in the form of 1:0.5 PIP salt. The crystal structure parameters of form 1, 2, and PIP salt are listed in Table 7.1 and their hydrogen bonding parameters in Table 7.2. For the sake of continuity in studying the phase relationships between ATV polymorphs, crystal structure of ATV-PIP and its other characterizations are discussed in section 7.9.

Table 7.1 Crystallographic parameters of ATV polymorphs and salt

	Form 1	Form 2	ATV-PIP
Chemical formula	$C_{22}H_{19}ClO_3$	$C_{22}H_{19}ClO_3$	$C_{24}H_{24}ClNO_3$
Crystal system	Monoclinic	Monoclinic	Triclinic
Space group	$P2_1/n$	$P2_1/c$	$P\bar{1}$
T/K	100	100	298
a/Å	5.8614(5)	12.4281(13)	9.0999(15)
b/ Å	18.1209(16)	5.1921(6)	10.3082(14)
c/ Å	16.4844(15)	27.550(3)	12.0950(18)
α/°	90	90	95.989(12)
β/°	96.131(1)	91.957(2)	110.290(14)
γ/°	90	90	101.192(13)
V/A° ^{3}	1740.9(3)	1776.7(3)	1025.6(3)
D_{calc}/g cm^{-3}	1.400	1.371	1.327
Total Reflns.	17654	17147	7629
Unique Reflns	3407	3492	4192
Observed Reflns	3251	2930	1430
R_1[I>2σ(I)]	0.0358	0.0554	0.0634

Table 7.2 Hydrogen bond parameters of ATV polymorphs and salt. O–H, N–H and C–H distances are neutron-normalized to 0.983, 1.009 and 1.083Å respectively

Interaction	D···A (Å)	H···A (Å)	D–H···A (°)	symmetry code
		Form 1		
O2–H2···O1	2.6728(14)	2.16(1)	110.7	[a]
O2–H2···O1	2.7348(14)	1.89(4)	141.7	1–x,1–y, –z
C11–H11···O2	2.7898(16)	2.28(6)	106.2	[a]
C16–H16B···O3	2.9980(16)	2.35(8)	116.1	[a]
		Form 2		
O2–H2···O1	2.651(2)	2.12(2)	111.9	[a]
O2–H2···O1	2.782(2)	1.92(7)	143.8	1–x,3–y, –z
C11–H11···O2	2.828(3)	2.31(2)	107.1	[a]
C12–H12A···O3	3.079(3)	2.40(1)	119.3	[a]
C15–H15A···O3	3.424(2)	2.36(5)	165.2	1–x,1/2+y,1/2–z
C16–H16B···O3	3.122(3)	2.46(2)	118.1	[a]
		ATV-PIP		
N1–H20A···O1	2.685(4)	1.68(4)	153.3	1–x,1–y, –z
N1–H21A···O2	2.656(5)	1.64(4)	161.2	2–x,1–y, –z
N1–H21A···O3	3.001(4)	2.35(3)	118.4	2–x,1–y, –z
C9–H9A···O2	3.101(5)	2.48(2)	122.1	[a]
C10–H10···O1	2.861(4)	2.37(2)	110.0	[a]
C11–H11B···O2	3.166(5)	2.57(3)	120.2	[a]
C23–H23A···O3	3.031(5)	2.50(2)	114.1	2–x,1–y, –z
C23–H23B···O2	3.190(5)	2.50(2)	128.1	x,1+y,z

[a] = Intramolecular hydrogen bond

Form 1 crystallized in $P2_1/n$ space group with one molecule (Z'=1) in the asymmetric unit. Centrosymmetric O–H···O dimer with $R^2_2(10)$ graph set notation[19] is the prominent hydrogen bonding interaction in this crystal structure. It connects the adjacent ATV molecules through O-H···O hydrogen bonding (O2-H2···O1, 2.735Aº, 144.69º) extending them along the 1D plane (Figure 7.3a). These ATV dimers are stacked in an anti-parallel fashion in the adjacent layers along the crystallographic *b*-axis forming a zig-zag chain motif. (Figure 7.3b & c). The 2nd carbonyl moiety on the other side of the naphthaquinone ring does not take part in the hydrogen bonding.

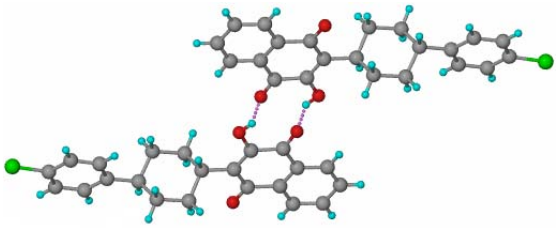

Figure 7.3a) Centrosymmetric O–H···O dimers connects the adjacent ATV molecules.

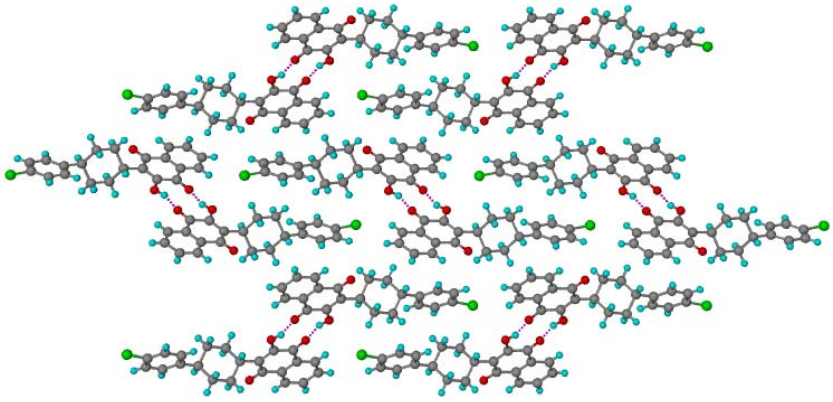

Figure 7.3b) Dimeric ATV molecules arranged in an anti-parallel fashion in the adjacent layers.

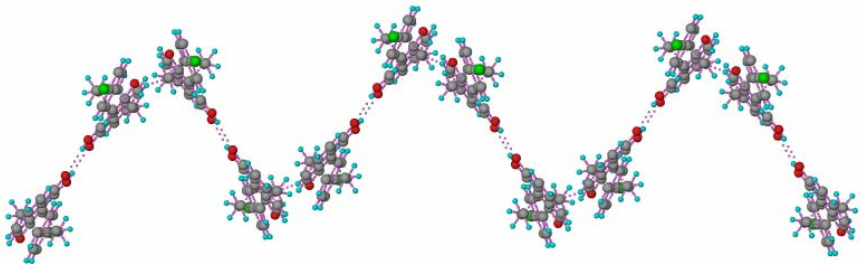

Figure 7.3c) Adjacent layers of dimeric ATV molecules are connected through close packing interactions, resembling a zig-zag motif.

ATV form 2 crystallizes in monoclinic $P2_1/c$ space group with one molecule in the asymmetric unit. Similar to the form 1 crystal structure, the centrosymmetric O–H···O dimer

(O2-H2···O1, 2.782Aº, 146.84º) with graph set notation $R^2_2(10)$ is the prominent motif here. It connects the adjacent ATV molecules extending them along the 1D plane. But unlike form 1 these centrosymmetric dimers extend in space through C-H-O one point synthon (C15-H15···O3, 3.424Aº, 165.80º) apart form the close packing interactions (Figure 7.4a). The ATV dimers within the 1D layer and the 2D sheet propagate in a parellel fashion along the *bc*-plane (Figure 7.4b).

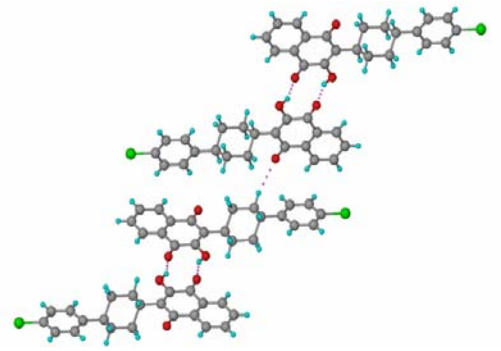

Figure 7.4a) Form 2 ATV dimers extend through C–H···O interaction.

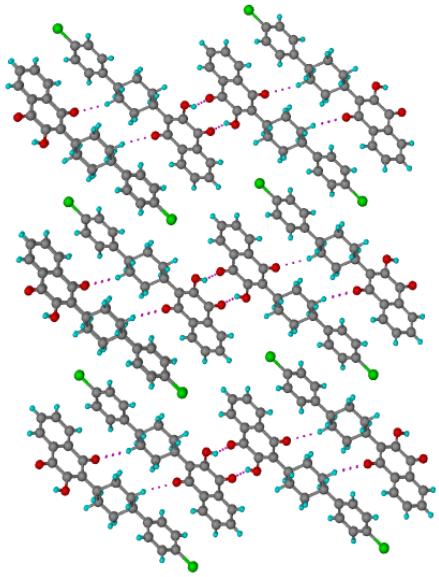

Figure 7.4b) Form 2 dimers arranged in parallel fashion in different layers.

7.5 Spectroscopic Characterization

Diversity in the supramolecular assemblies of various solid forms often results in significant differences in their conformational and hydrogen bonding patterns. These differences directly affect the vibrational stretching frequencies of the functional groups constituting them[20]. IR spectroscopic analysis of ATV polymorphs showed minor but significant differences in the vibrational patterns of their functional groups. While the O–H stretching and bending modes of form 1 appeared at 3376.2 cm^{-1} and 1368.5 cm^{-1}, they were observed at 3377.9 cm^{-1}, 1370.5 cm^{-1} for form 2 and 3369.8 cm^{-1} and 1365.7 cm^{-1} for form 3. The α, β – unsaturated carbonyl appeared at 1659.5 cm^{-1}, 1656.6 cm^{-1} and 1655.5 cm^{-1} for form 1, form 2 and form 3 respectively (Figure 7.5, Table 7.3). Even the other stretching and bending modes varied significantly, distinguishing the polymorphs. Raman spectra are based on the principle of polarizability and consequently the symmetric stretching modes have better intensity compared to their asymmetric counterparts. While the sp^3 C-H Raman shift for form 1 appeared at 2936.4 cm^{-1}, it was observed at 2935.6 cm^{-1} and 2930.9 cm^{-1} for form 2 and 3 respectively (Figure 7.6, Table 7.3). The other functional groups showed such minor but significant differences in their raman modes effectively complementing the IR analysis.

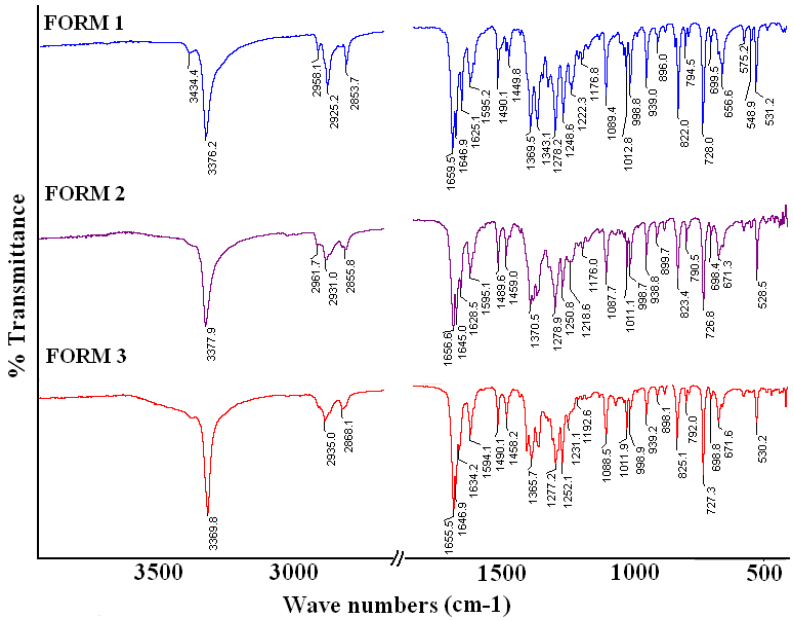

Figure 7.5 IR spectral overlay of ATV polymorphs

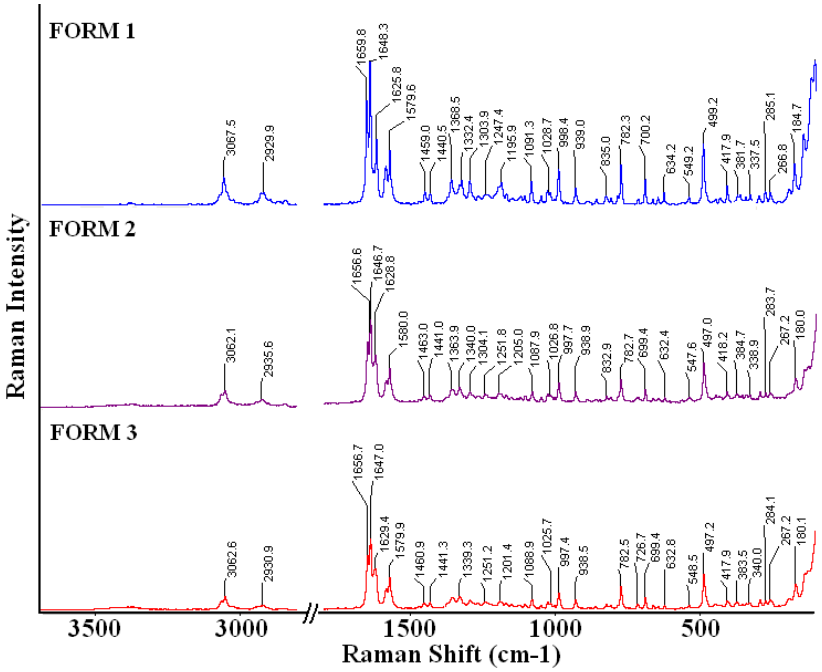

Figure 7.6 Raman spectral overlay of ATV polymorphs

Table 7.3 Major IR and Raman vibrational frequencies of ATV polymorphs (in cm^{-1})

Form/Functional group	Form 1	Form 2	Form 3
		INFRARED	
O-H stretch	3376.2	3377.9	3369.8
sp3 C-H stretch	2925.2	2931.0	2935.0
Carbonyl C=O stretch	1659.5	1656.6	1655.5
O-H bending	1368.5	1370.5	1365.7
C-O stretch	1089.4	1087.7	1088.5
C-Cl stretch	728.0	728.8	727.3
		RAMAN	
Aromatic C-H stretch	3080.9,3067.5	3075.6,3062.1	3075.6,3062.8
sp3 C-H stretch	2936.4	2935.6	2930.9
C=O stretch	1659.8	1656.6	1656.7
C-O stretch	1091.3	1087.9	1088.9
C-Cl stretch	782.3	782.7	782.5

^{13}C ssNMR analysis of ATV polymorphs showed minor but significant differences in their chemical shifts. While the C2 and C9 carbonyl chemical shifts of form 1 appeared at 180.1 and 182.9 ppm, the same carbons showed chemical shifts at 180.5, 181.8 ppm in form 2 and 180.3, 181.6 ppm in form 3. The OH attached C1 carbon appeared at δ 152.2, 151.8, 152.0

ppm in form 1, 2 and 3 respectively (Figure 7.7). Even the other carbon nuclei showed such significant changes between the polymorphs, effectively distinguishing them (Table 7.4).

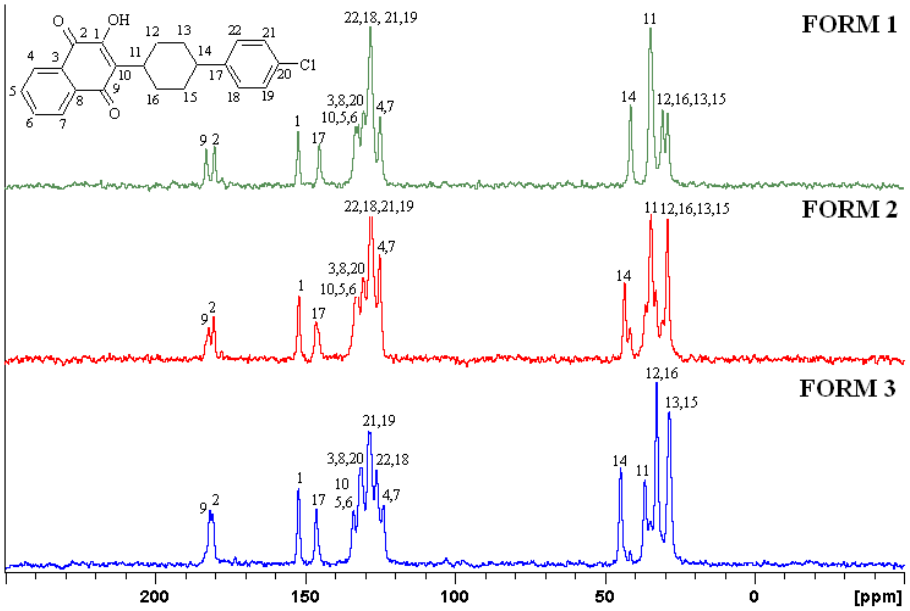

Figure 7.7 ^{13}C ssNMR spectral overlay of ATV polymorphs.

Table 7.4 Chemical shift values of ATV polymorphs (in ppm)

	Form 1	Form 2	Form 3
C15, C13	28.8	28.9	28.2
C16, C12	30.6	32.9	32.6
C11	34.7	36.0	36.5
C14	41.2	43.2	44.6
C22, C18	124.7	124.8	123.7
C4, C7	128.0	126.7	126.0
C21, C19	128.2	127.8	128.7
C3	130.3	129.2	131.2
C8	132.1	130.4	131.2
C20	132.1	131.1	131.6
C10	133.1	132.2	133.7
C6, C5	133.1	133.0	133.7
C17	145.1	146.2	146.1
C1	152.2	151.8	152.0
C2	180.1	180.5	180.3
C9	182.9	181.8	181.6

7.6 Relative stability of ATV Polymorphs

An optimal balance between the hydrogen bonding interactions of donors and acceptors coupled with better packing efficiency would determine the stability of crystal structure. The polymorph which satisfies this criterion will be the stable of the system. Crystal density and packing fraction analysis of ATV polymorphs showed that the calculated density (Form 1, – 1.400 g cm^{-3}, form 2, – 1.371 g cm^{-3}) and packing fraction (form 1, – 71.0 %, form 2, – 69.3 %) of form 1 is higher than that of form 2. According to the density rule[21] proposed by Burger and Ramberger, the form with higher density is the stable modification and the one with lower density is the metastable phase. Application of this rule to the ATV polymorphs shows that form 1 is more stable compared to form 2. In their article, Malpezzi et. al., concluded that this polymorphic system is an exception to density rule, because the less dense form 2 has additional hydrogen bonding interactions compared to form 1 and hence it is the stable polymorph. Although, the presence of additional hydrogen bonds contributes to the stability of a polymorph, this is not the sole criteria to establish its stability. We have shown using further characterization techniques (thermal, slurry and grinding) that in spite of its additional bonding interactions form 2 is the metastable polymorph. Conformational and lattice energy calculations on form 1 and form 2 polymorphs yielded similar result. The overlay of the ATV polymorphs (Figure 7.8) and the list of torsion angles in Table 7.5 suggest that the molecules adopt virtually the same conformation in the two modifications. Nevertheless, the differences are large enough to cause major differences in their packing arrangement hence they can be categorized as a prominent case of packing polymorphism[22]. Conformational energy calculated using Gaussian 03 software and lattice energy calculations performed using cerius[2] software showed that form 1 is stable over form 2 by 2.98 Kcal mol^{-1}.

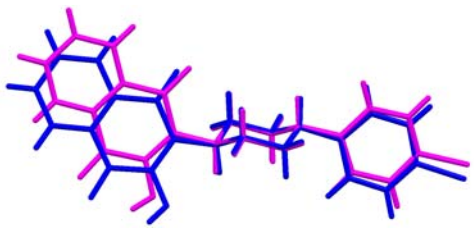

Figure 7.8 Overlay of ATV polymorphs. (Form 1(Blue) and Form 2 (pink)).

Table 7.5 Conformer torsion angles[a] (X-ray structures), conformational energy[b] (Gaussian 03, DFT, B3LYP/6-31G (d, p)) and lattice energy (cerius 2) calculations of ATV Form 1and form 2

Conformer	Form 1	Form 2
τ_1 /°	50.15º	61.20º
τ_2 /°	98.74º	119.62º
τ_3 /°	124.41º	122.73º
τ_4 /°	59.57º	68.41º
Conformational energy (Kcal mol^{-1}) E_{conf}	0	+2.044708
Lattice energy ($Kcalmol^{-1}$) $E_{lattice}$	-46.05875	-45.12125
$E_{total} = E_{lattice}+E_{conf}$	-46.05875	-43.07654

Energy calculations suggest that Form 1 is stable over Form 2 by 2.98 Kcal mol^{-1}

[a] Absolute values of torsion angles are quoted.

[b] The lowest energy conformer is arbitrarily set to 0.

τ_1 = C(9)-C(10)-C(11)-C(16) τ_2 = C(1)-C(10)-C(11)-C(12)

τ_3 = C(15)-C(14)-C(17)-C(18 τ_4 = C(13)-C(14)-C(17)-C(22)

All the ATV polymorphs were further characterized using thermal methods like DSC and HSM (Hot stage microscopy). DSC experiments were performed at a heating rate of 10°C/min (Figure 7.9). DSC heating curve of ATV form 1 showed a transition endotherm at 187.5°C, indicating an enantiotropic relationship with the high temperature phase which goes on to melt at 223.5°C. In order to identify the high temperature phase, we have performed an isothermal DSC experiment where form 1 was heated till 190°C (above phase transition temperature) and allowed to stay at this temperature for 20mins before cooling back to room temperature. At the end of the experiment the aluminum pan containing the sample was cut open and the material was analyzed by IR spectroscopy. The IR peaks matched exactly with those of form 2, confirming it as the high temperature phase (Figure 7.10). DSC heating curve of Form 2 did not show any phase transition before melting at 223.5°C. Similar to form 1, form 3 also showed a phase transition at 129.5°C followed by a melting endotherm around 223.5°C. Hence an isothermal DSC experiment was performed on

form 3, where the sample was heated till 135°C and allowed to stay at this temperature for 20mins. Post this experiment the IR peaks of the material in the DSC pan resembled those of form 2 (Figure 7.11). Based on the Heat of transition rule[21], we could deduce that Form 1 and 3 are enantiotropically related to the high temperature phase form 2, while form 1 and form 3 exhibit monotropic relationship. Since form 1 and form 3 undergo phase transition to form 2, their actual melting enthalpy values could not be known from their DSC heating curves. For such cases, the melting enthalpy was calculated using the equation proposed by J. O. Henck[23a] which was successfully applied to obtain the melting points of various enantiotropic systems[23]. Application of this equation to the ATV polymorphic system (Scheme 7.2) revealed the melting temperature of form 1 as 221.4°C and that of form 3 as 220.4°C (Table 7.6). Based on the Heat of fusion rule[21], the calculated melting point values could be used to infer the stability order of ATV polymorphs. Since form 1 and form 3 undergo phase transition in their respective heating curves to high temperature phase form 2, they are the stable phases below their transition points with form 2 being stable above the transition point in both cases. In accordance with their monotropic relationship form 1 is more stable compared to form 3 over the entire heating range due to its higher melting and enthalpy values.

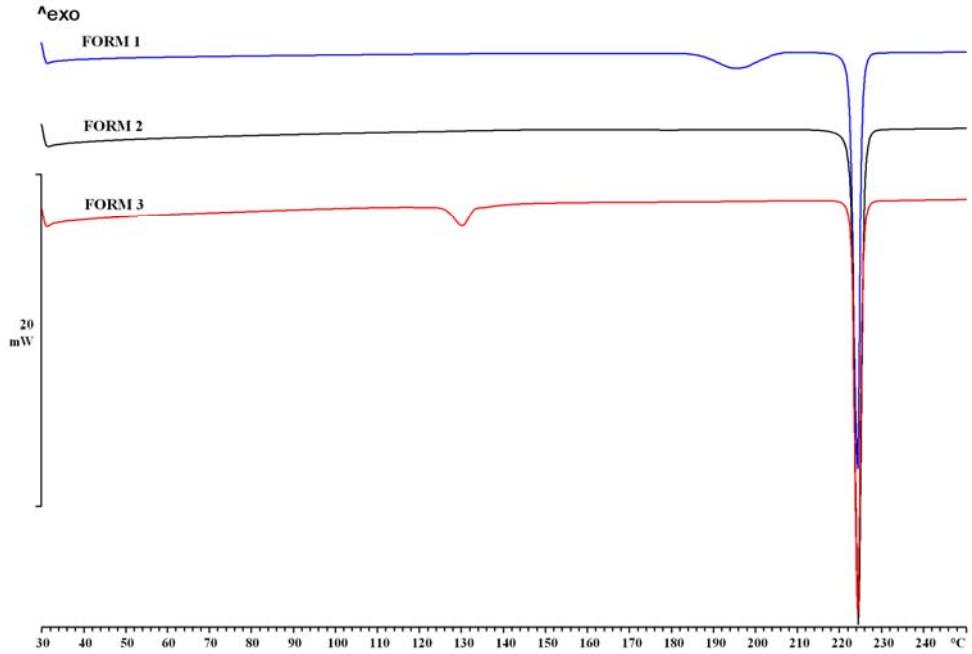

Figure 7.9 DSC analysis of ATV polymorphs

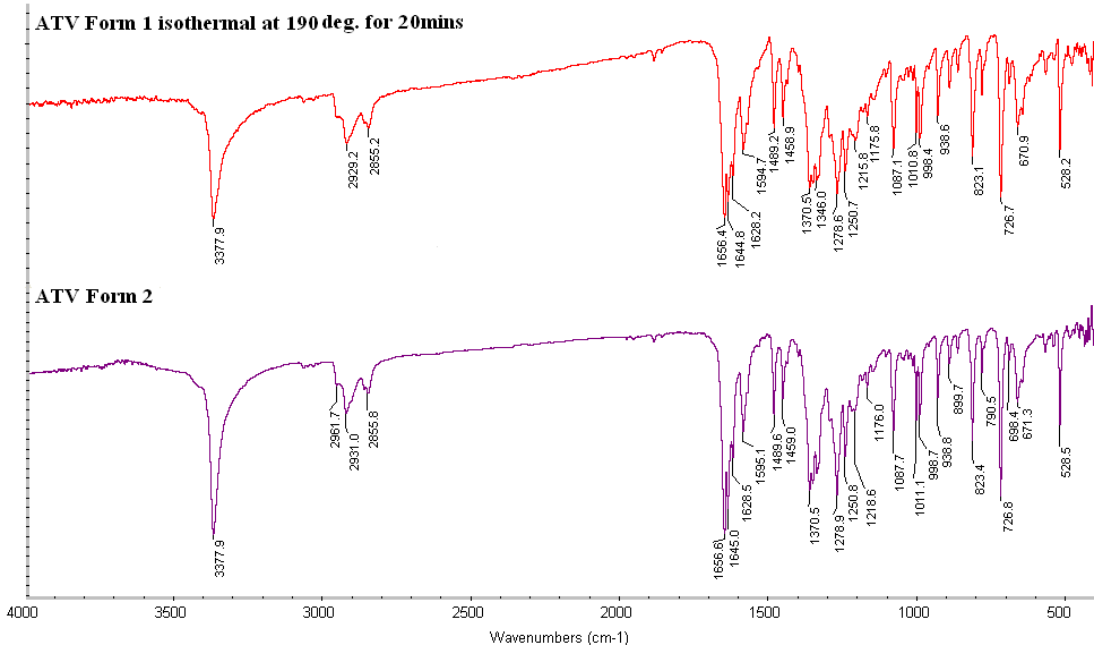

Figure 7.10 IR spectral comparision of Form 1 material after performing DSC till 190ºC and kept isothermal for 20mins, with form 2.

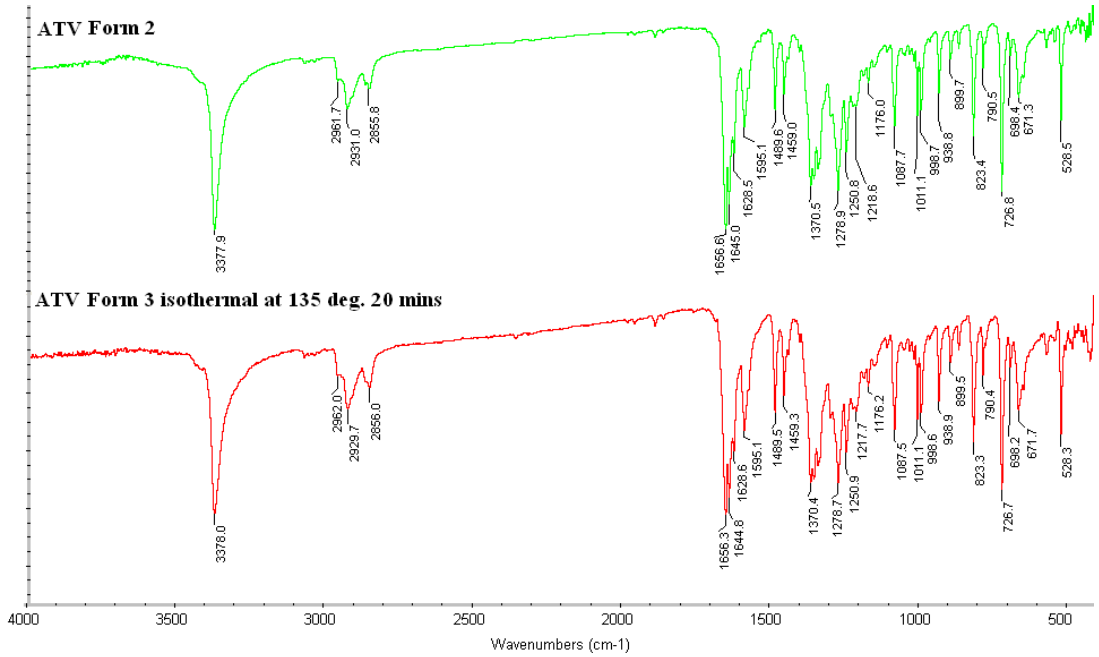

Figure 7.11 IR spectral comparision of form 3 material after performing DSC till 135ºC and kept isothermal for 20mins, with form 2.

Table 7.6 Enthalpy values of ATV polymorphs at a heating rate of 10°C/min.

Form	T_{trs} / °C	ΔH_{trs} (KJ/mol)	T_m/ °C	ΔH_{fus} (KJ/mol)
1	187.5	1.9	221.4*	38.0#
2	--	--	223.5	36.1
3	129.5	0.7	220.4*	36.8#

* Calculation showed in Scheme 7.2. (Ref. 23a)

$\Delta H_{fus\ (form\ 1)} = \Delta H_{fus\ (form\ 2)} + \Delta H_{trs}$

$\Delta H_{fus\ (form\ 3)} = \Delta H_{fus\ (form\ 2)} + \Delta H_{trs}$

Scheme 7.2 Calculation of Melting point of ATV Form 1

$$T_{fus(form\ 1)} = \frac{\Delta H_{fus(form\ 1)} \times T_{fus(form\ 2)} \times T_{trs}}{(\Delta H_{fus(form\ 1)} \times T_{fus(form\ 2)}) + (T_{trs} \times \Delta H_{fus(form\ 2)}) - (T_{fus(form\ 2)} \times \Delta H_{fus(form\ 2)})}$$

$$T_{fus(form\ 1)} = \frac{38.0 \times 223.5 \times 187.5}{(38 \times 223.5) + (187.5 \times 36.1) - (223.5 \times 36.1)} = 221.4° C$$

$\Delta H_{fus(form\ 1)}$ = Enthalpy of fusion of form 1 (Enthalpy of fusion of form 2 + Enthalpy of Transition) = 38.0 kJ/mol

$T_{fus(form\ 2)}$ = Temperature of fusion of form 2 = 223.5°C

T_{trs} = Temperature of transition from form 1 to form 2 = 187.5°C

$\Delta H_{fus(form\ 2)}$ = Enthalpy of fusion of form 2 = 36.1 kJ/mol

$T_{fus(form\ 1)}$ = Temperature of fusion of form 1 (calculated) = 221.4°C

Calculation of Melting point of ATV Form 3

$$T_{fus(form\ 3)} = \frac{\Delta H_{fus(form\ 3)} \times T_{fus(form\ 2)} \times T_{trs}}{(\Delta H_{fus(form\ 3)} \times T_{fus(form\ 2)}) + (T_{trs} \times \Delta H_{fus(form\ 2)}) - (T_{fus(form\ 2)} \times \Delta H_{fus(form\ 2)})}$$

$$T_{fus(form\ 3)} = \frac{36.8 \times 223.5 \times 129.5}{(36.8 \times 223.5) + (129.5 \times 36.1) - (223.5 \times 36.1)} = 220.4° C$$

$\Delta H_{fus(form\ 3)}$ = Enthalpy of fusion of form 3 (Enthalpy of fusion of form 2 + Enthalpy of Transition) = 36.8 kJ/mol

$T_{fus(form\ 2)}$ = Temperature of fusion of form 2 = 223.5°C

T_{trs} = Temperature of transition from form 3 to form 2 = 129.5°C

$\Delta H_{fus(form\ 2)}$ = Enthalpy of fusion of form 2 = 36.1 kJ/mol

$T_{fus(form\ 3)}$ = Temperature of fusion of form 3 (calculated) = 220.4°C.

Hot stage microscopy was used to get a visual evidence of the morphological and thermal events that occurred during the DSC analysis. Due to the non-availability of form 3 crystals HSM experiments were performed only on form 1 and form 2 crystals. As observed in DSC experiments, there were no morphological changes indicating phase transition in the HSM analysis of Form 2 crystals before they melted at 222°C (Figure 7.12a). Whereas the yellowish form 1 crystals faded into a dark crystal with minimum morphological changes between 183-188°C before they went on to melt again at 222°C (Figure 7.12b). A slight change in the melting temperature of the crystals in HSM experiments is not unusual because in DSC, experiments are performed in a closed environment whereas in HSM the crystals are exposed to ambient conditions where the influence of external environmental may cause a slight alteration in the melting point. HSM results suggest that in the absence of significant morphological changes form 2 to form 1 conversion is similar to a single crystal-

single crystal phase transformation[24]. VT-PXRD experiments were performed on form 1 and form 3 to confirm the high temperature phase. However these experiments were not useful because both form 1 and form 3 sublimed at their respective transition temperatures and hence it was not possible to obtain PXRD patterns above these temperatures to identify the high temperature phase.

a) Form 2

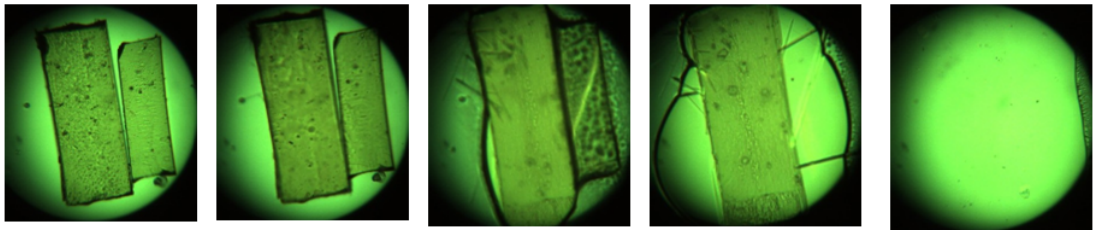

(a)

b) Form 1

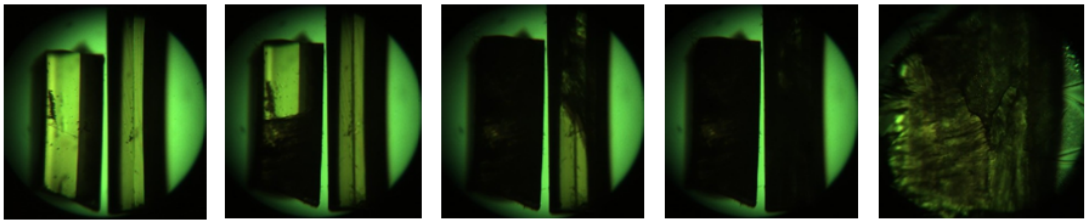

(b)

Figure 7.12 HSM snapshots of ATV polymorphs. **a)** No changes were observed in form 2 crystals. **b)** Form 1 crystals faded by darkening between 183-188°C indicating phase transition.

From the thermal analysis of ATV polymorphs through DSC and HSM experiments we were able to conclude that form 1 is the most stable phase below the transition point followed by

form 3 whereas form 2 is the stable phase above the transition point. Yet phase stability studies at ambient conditions are very important in order to establish the thermodynamic modification of the three forms at ambient conditions. The stable phase at room temperature was determined by subjecting both the forms to slurry and grinding experiments[23a,b,d].

7.7 Solvent Mediated Stability Experiments

Slurry grinding experiments were performed on ATV polymorphs in a protic solvent, Isopropanol and a non-protic solvent, Acetonitrile. This is to understand the effect of solvent on the stability outcome of the solvent mediated experiments. All the polymorphs were slurry grinded separately in both the solvents along with competitive slurry experiments, where a mixture of two forms was taken together in 1:1 stoichiometric ratio. Upon slurry grinding in CH_3CN, pure form 1 was stable for 72 hrs (Figure 7.13a) whereas form 2 converted to form 1 in 4 hrs (Figure 7.13b) and form 3 converted to form 1 in about 8 hrs (Figure 7.13c). In competitive slurry experiment, a mixture of form 1 and form 2 converted to form 1 in 2 hrs (Figure 7.13d), form 1 and form 3 1:1 mixture converted to form 1 in 3 hrs (Figure 7.13e) and a mixture of form 2 and form 3 resembled a mixture of all the three forms after 1 hr which totally converted to form 1 after 2 hrs (Figure 7.13f).

In i-PrOH the transformation rate was slow. In this solvent Form 1 was stable for 1 week (Figure 7.14a), whereas form 2 converted to form 1 in 72 hrs (Figure 7.14b) and form 3 converted to form 1 only after 5 days (Figure 7.14c). In competitive slurry experiments, a mixture of form 1 and form 2 converted to form 1 in 72 hrs (Figure 7.14d), form 1 and form 3 1:1 mixture converted to form 1 in 5 days (Figure 7.14e) and a mixture of form 2 and form 3 converted to form 3 after 3 days which went on to convert completely to form 1 after 5 days (Figure 7.14f). Based on the solvent mediated stability experiments we could demonstrate that form 1 is the thermodynamic phase at room temperature. Since form 2 converted to form 3 in competitive slurry experiment, form 3 is the next stable phase followed by Form 2. This stability relationship was cross checked by performing mechanochemical grinding experiments.

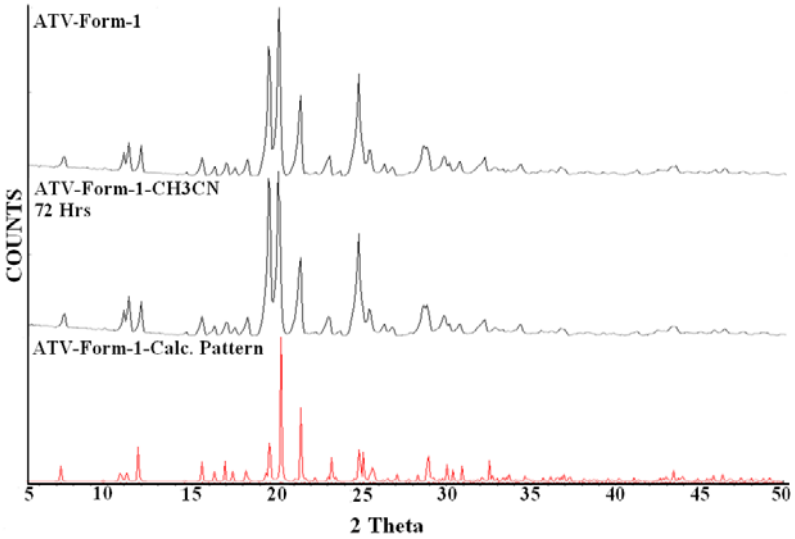

Figure 7.13a) Overlay of experimental PXRD pattern of ATV form 1 (Top) with the experimental PXRD matching with form 1 obtained after slurry grinding form 1 in CH_3CN for 3 days (middle). The calculated pattern of form 1 is shown for comparison (below)**.**

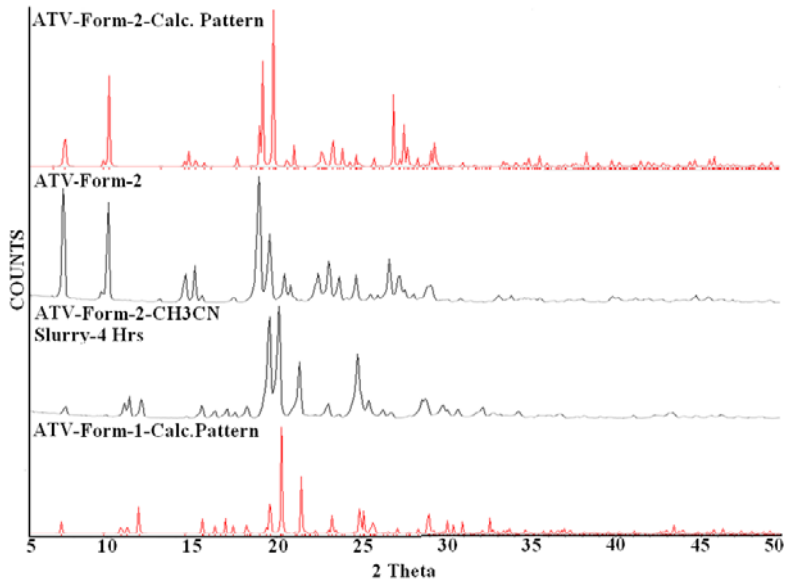

Figure 7.13b) Overlay of experimental PXRD pattern of ATV form 2 (2nd from top) with the experimental PXRD matching with form 1, obtained after slurry grinding form 2 in CH_3CN for 4 hrs (3rd from top). The respective calculated patterns of form 2 and 1 (top and bottom) are shown for comparison.

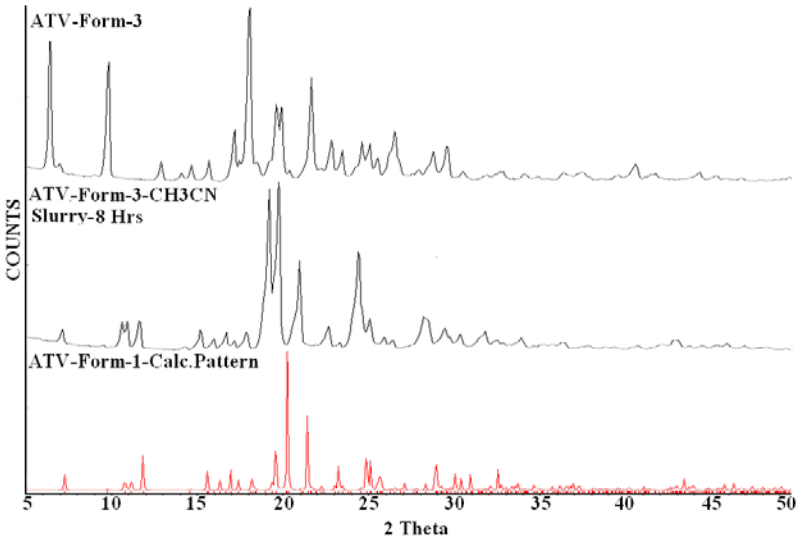

Figure 7.13c) Overlay of experimental PXRD pattern of ATV form 3 (Top) with the experimental PXRD matching with form 1 obtained after slurry grinding form 3 in CH_3CN for 8 hrs (middle). The calculated pattern of form 1 is shown for comparison (below).

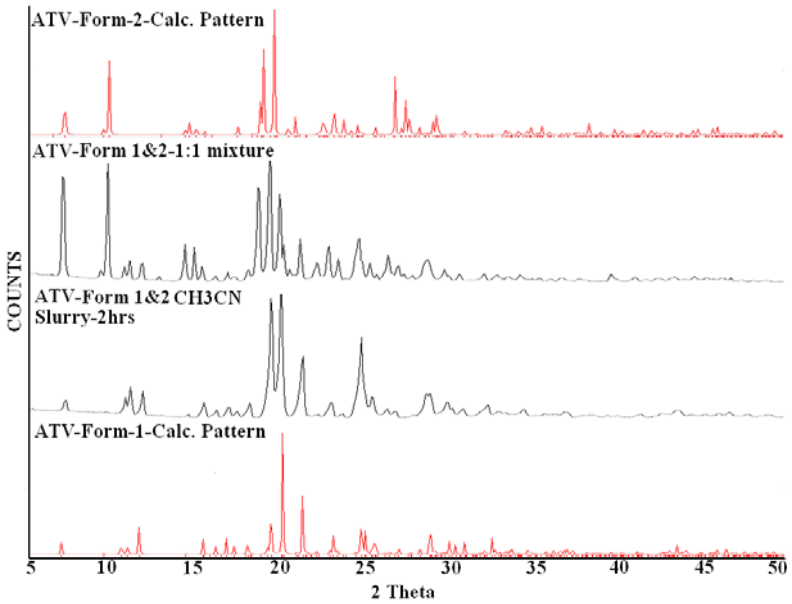

Figure 7.13d) Overlay of experimental PXRD pattern of 1:1 mixture of ATV form 1 and 2(2^{nd} form top) with the experimental PXRD matching with form 1, obtained after slurry grinding the mixture in CH_3CN for 2 hrs (3^{rd} form top). The calculated patterns of form 2 and form 1 are shown for comparison (top and bottom).

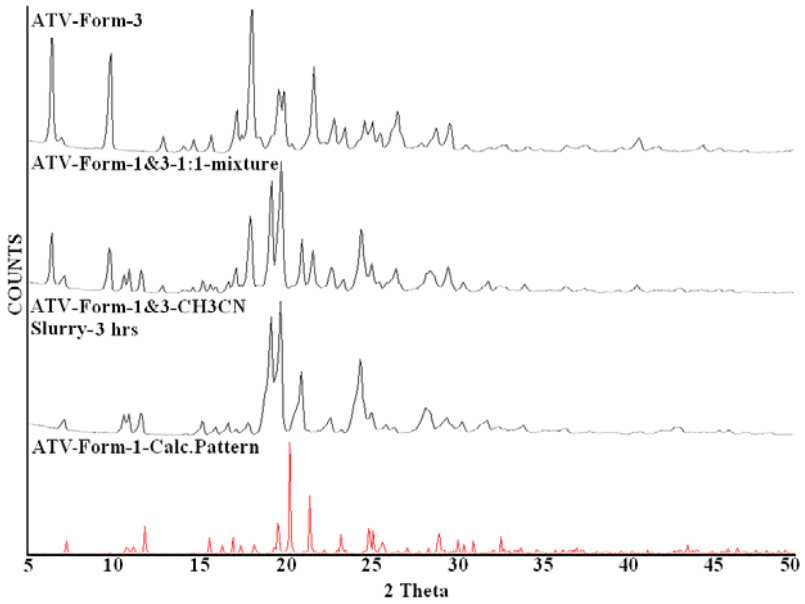

Figure 7.13e) Overlay of experimental PXRD pattern of 1:1 mixture of ATV form 1 and 3(2nd form top) with the experimental PXRD matching with form 1, obtained after slurry grinding the mixture in CH_3CN for 3 hrs (3rd form top). The experimental pattern of form 3 (top) and the calculated pattern of form 1 are shown for comparison (bottom).

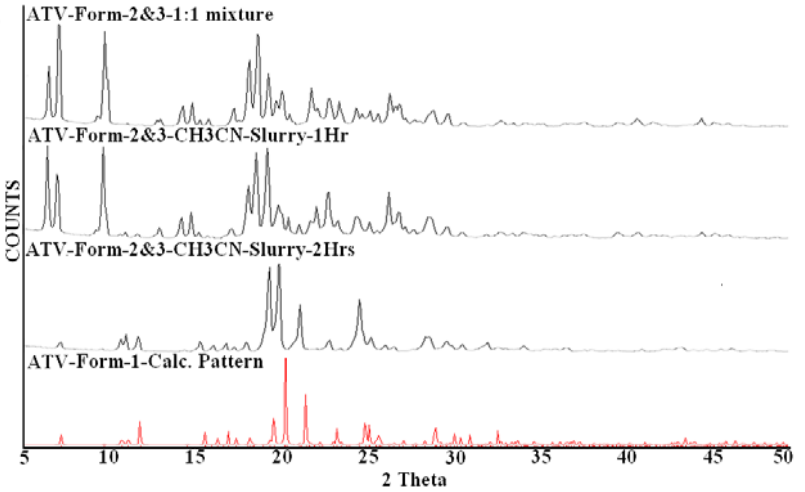

Figure 7.13f) Overlay of experimental PXRD pattern of 1:1 mixture of ATV form 2 and 3(top) with the experimental PXRD matching with all three forms after 1hr (2nd from top), converted completely to form 1 after 2 hrs (3rd form top). The calculated pattern of form 1(bottom) is shown for comparison.

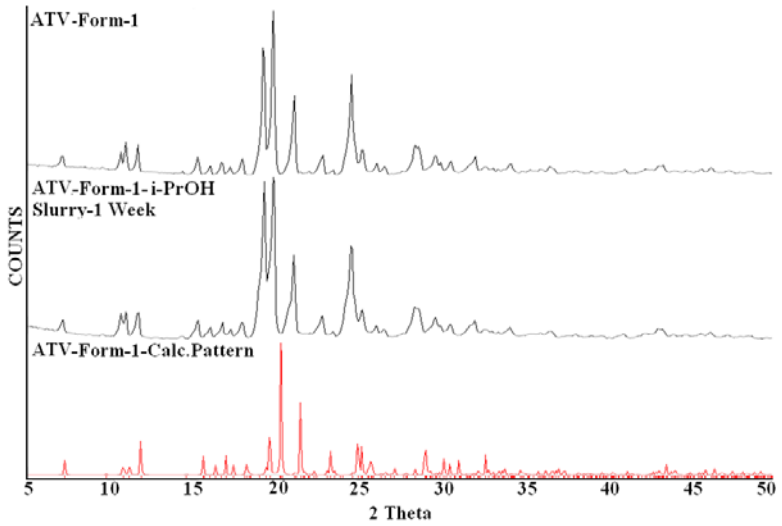

Figure 7.14a) Overlay of experimental PXRD pattern of ATV form 1 (Top) with the experimental PXRD matching with form 1 obtained after slurry grinding form 1 in i-PrOH for 1 week (middle). The calculated pattern of form 1 is shown for comparison (below)**.**

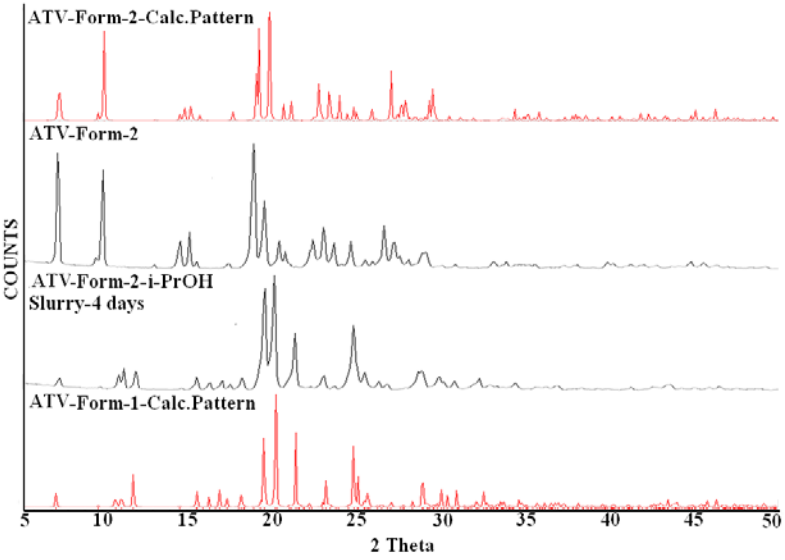

Figure 7.14b) Overlay of experimental PXRD pattern of ATV form 2 (2nd from top) with the experimental PXRD matching with form 1, obtained after slurry grinding form 2 in i-PrOH for 4 days (3rd from top). The respective calculated patterns of form 2 and 1 (top and bottom) are shown for comparison.

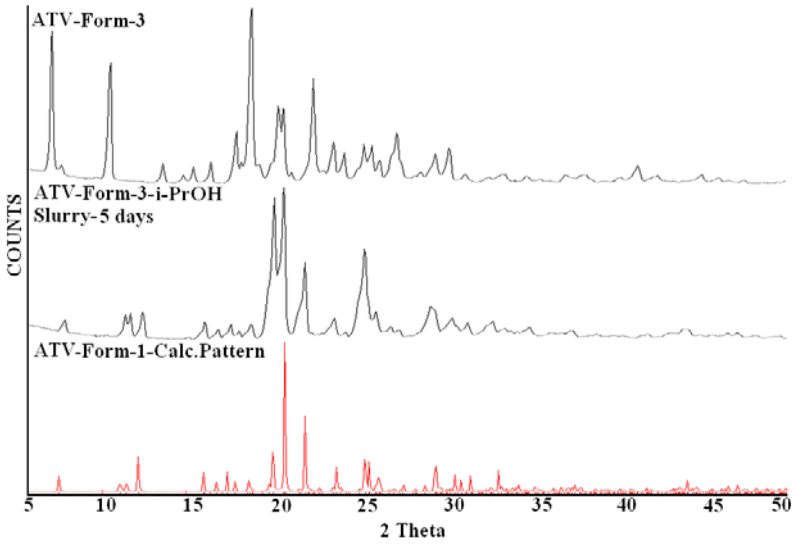

Figure 7.14c) Overlay of experimental PXRD pattern of ATV form 3 (Top) with the experimental PXRD matching with form 1 obtained after slurry grinding form 3 in i-PrOH for 5 days (middle). The calculated pattern of form 1 is shown for comparison (below).

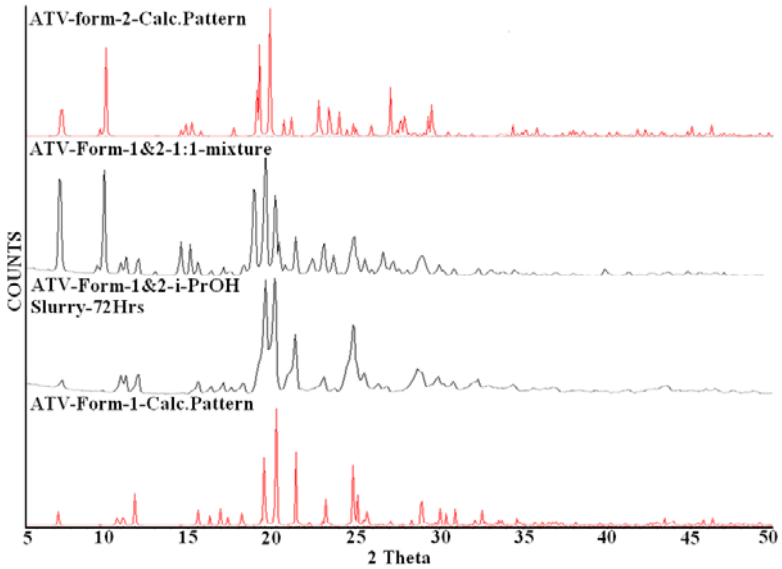

Figure 7.14d) Overlay of experimental PXRD pattern of 1:1 mixture of ATV form 1 and 2(2nd form top) with the experimental PXRD matching with form 1, obtained after slurry grinding the mixture in i-PrOH for 72 hrs (3rd form top). The calculated patterns of form 2 and form 1 are shown for comparison (top and bottom).

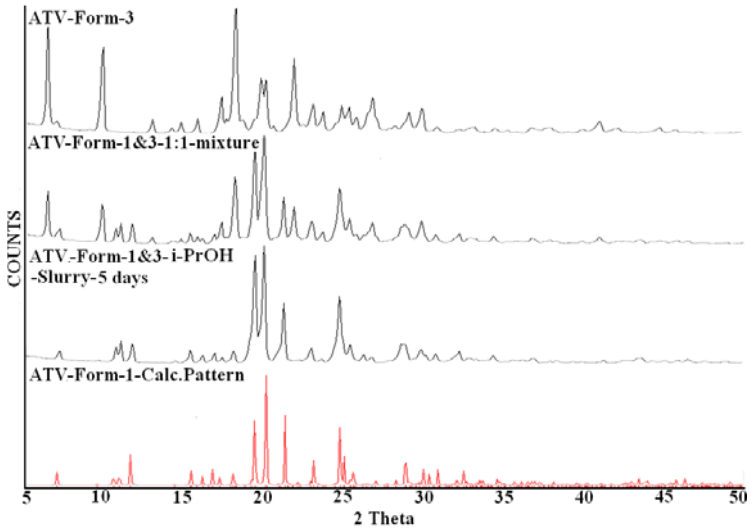

Figure 7.14e) Overlay of experimental PXRD pattern of 1:1 mixture of ATV form 1 and 3(2nd form top) with the experimental PXRD matching with form 1, obtained after slurry grinding the mixture in i-PrOH for 5 days (3rd form top). The experimental pattern of form 3 (top) and the calculated pattern of form 1 are shown for comparison (bottom).

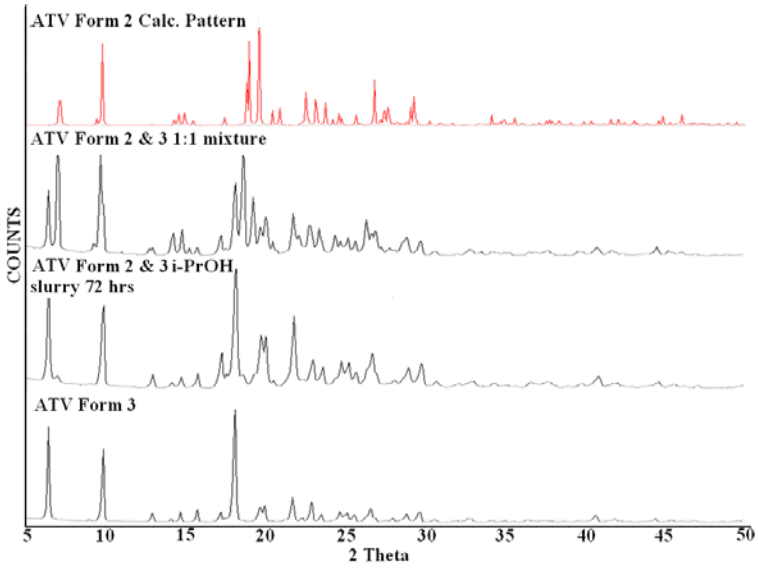

Figure 7.14f) Overlay of experimental PXRD pattern of 1:1 mixture of ATV form 2 and 3(2nd from top) with the experimental PXRD matching with form 3 after slurry grinding the mixture in i-PrOH for 72 hrs. The calculated pattern of form 2 (top) and the experimental pattern of form 3(bottom) are shown for comparison.

7.8 Solid state grinding experiments

Neat grinding of ATV polymorphs individually in a mixer-mill did not show any peaks resembling phase transformation for 8 hrs. All the polymorphs were stable throughout the 8 hr period (Figure 7.15a-c). Nevertheless in competitive grinding experiments, a 1:1 stoichiometric mixture of form 1and form 2 converted to form 1 in 1hr (Figure 7.15d). While a 1:1 mixture of form 1 and form 3 converted to form 1 in 2 hrs (Figure 7.15e), form 2 and form 3 in similar ratio converted to form 3 in 2 hrs (Figure 7.15f). In summary, the grinding experiments ably complemented the solvent mediated stability experiments in establishing form 1 as the thermodynamic phase at room temperature.

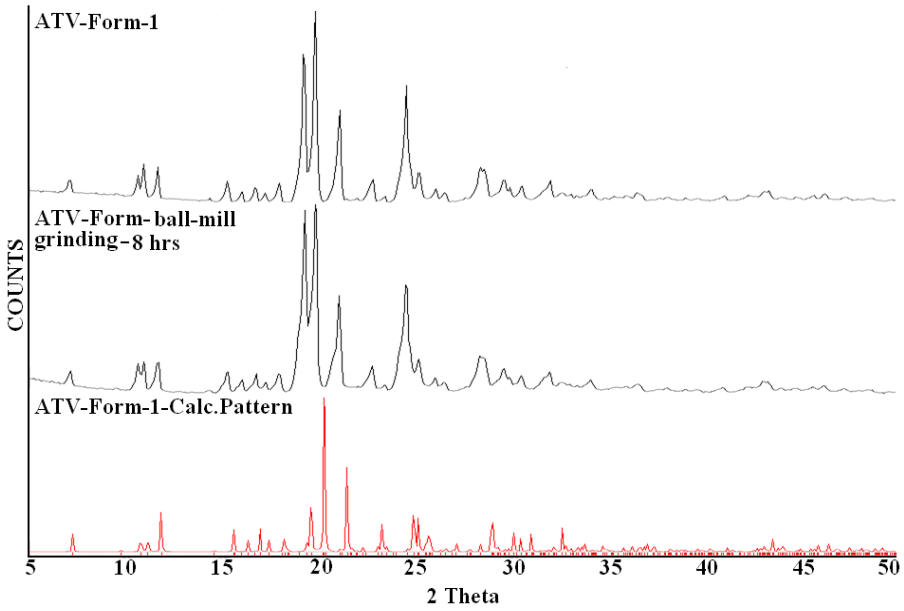

Figure 7.15a) Overlay of experimental PXRD pattern of ATV form 1 (Top) with the experimental PXRD matching with form 1 obtained after ball-mill grinding of form 1 for 8 hrs (middle). The calculated pattern of form 1 is shown for comparison (below).

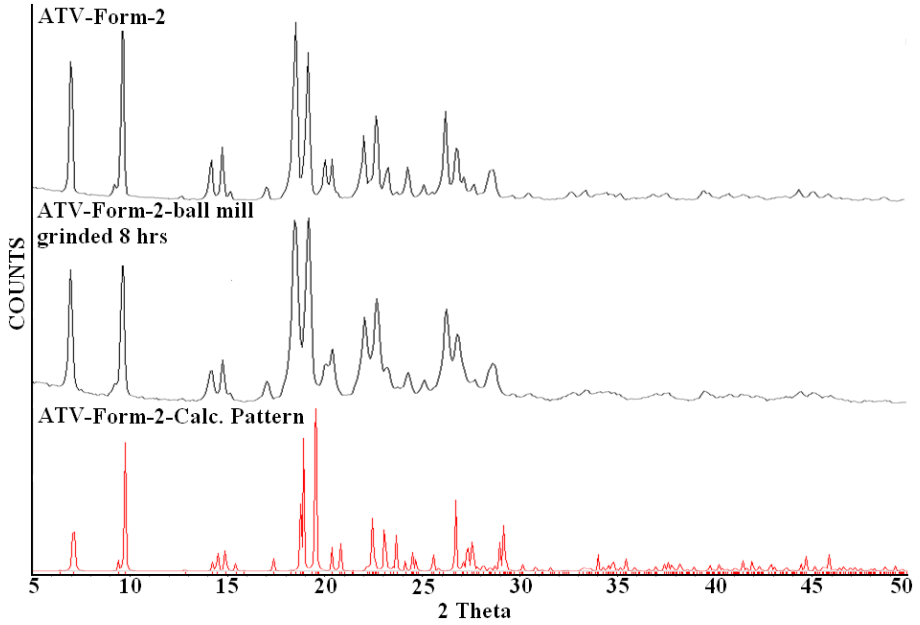

Figure 7.15b) Overlay of experimental PXRD pattern of ATV form 2 (Top) with the experimental PXRD matching with form 2 obtained after ball-mill grinding form 2 for 8 hrs (middle). The calculated pattern of form 1 is shown for comparison (below).

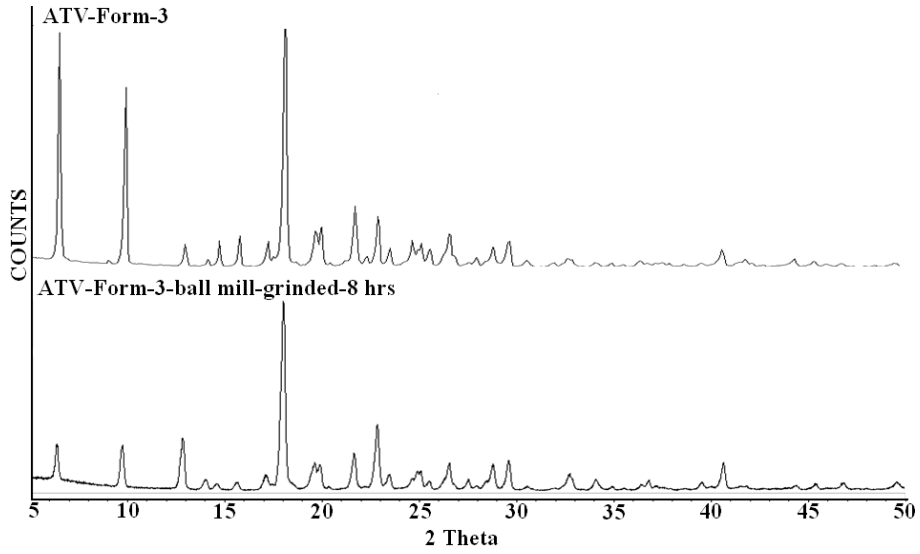

Figure 7.15c) Overlay of experimental PXRD pattern of ATV form 3 (Top) with the experimental PXRD matching with form 3 obtained after ball-mill grinding form 3 for 8 hrs (bottom).

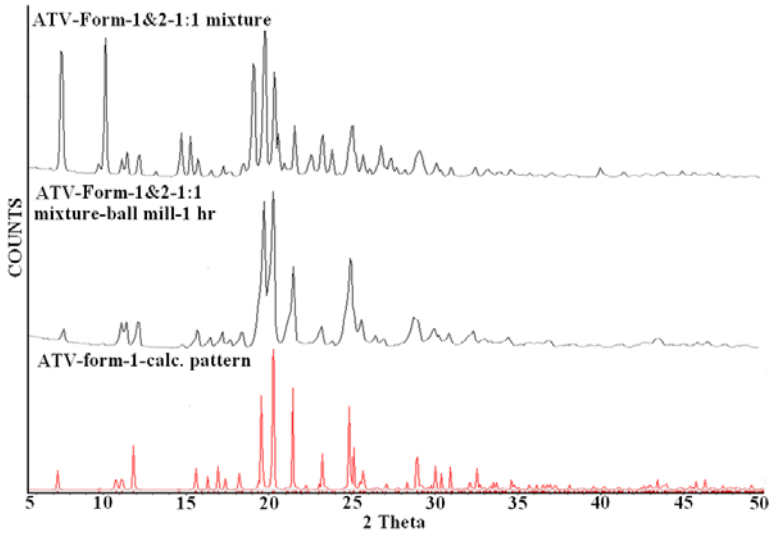

Figure 7.15d) Overlay of experimental PXRD pattern of 1:1 mixture of ATV form 1 and 2(top) with the experimental PXRD matching with form 1, obtained after ball mill grinding the mixture for 1 hr (2nd form top). The calculated pattern of form 1 is shown for comparison (bottom).

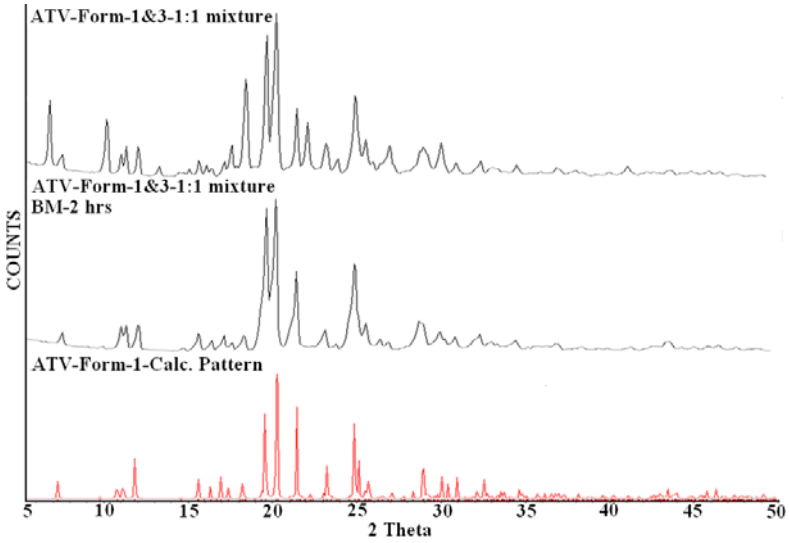

Figure 7.15e) Overlay of experimental PXRD pattern of 1:1 mixture of ATV form 1 and 3(top) with the experimental PXRD matching with form 1, obtained after ball mill grinding the mixture for 2 hrs (2nd form top). The calculated pattern of form 1 is shown for comparison (bottom).

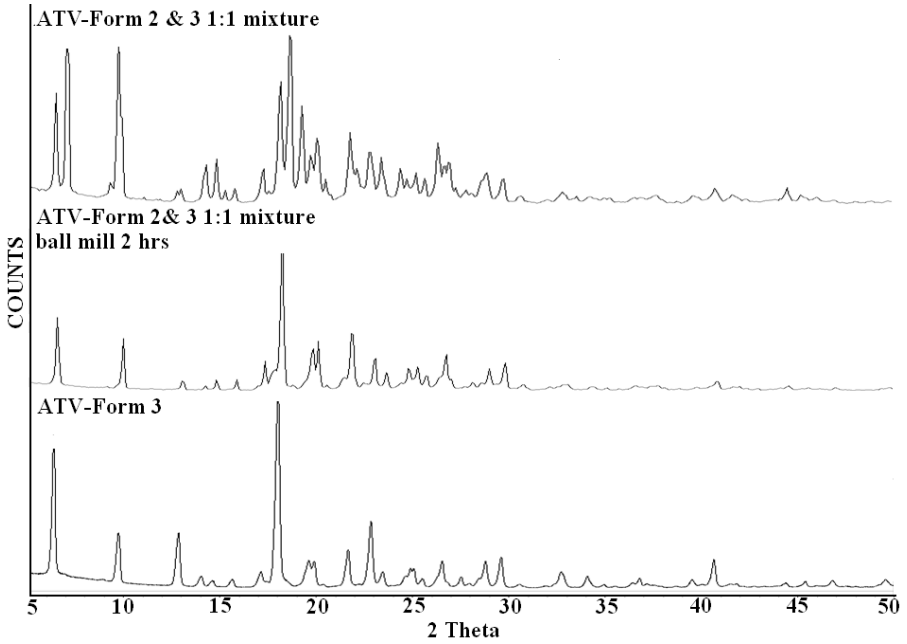

Figure 7.15f) Overlay of experimental PXRD pattern of 1:1 mixture of ATV form 2 and 3 (top) with the experimental PXRD matching with form 3, obtained after ball mill grinding of the mixture for 2 hrs (2nd form top). The experimental pattern of form 3 is shown for comparison (bottom)

A semi-schematic Energy vs Temperature (E-T) diagram consistent with the results obtained through DSC, HSM, slurry and grinding experiments is shown in Figure 7.16. The E-T diagram establishes form 1 as the most stable phase at absolute zero based on the density rule[21]. The conversion of form 2 and 3 to form 1 at ambient conditions is rationalized by the low free energy of form 1 polymorph between 25-187.5°C. Form 3 is shown as the next stable polymorph since form 2 converted to form 3 in slurry and grinding experiments. It is shown to have lower energy till its transition temperature i.e between 25-129.5°C. The phase transition of form 1 to form 2 and form 3 to form 2 are represented through a crossover at 187.5°C and 129.5°C (transition point) respectively and the melting point of form 2 at 223.5°C.

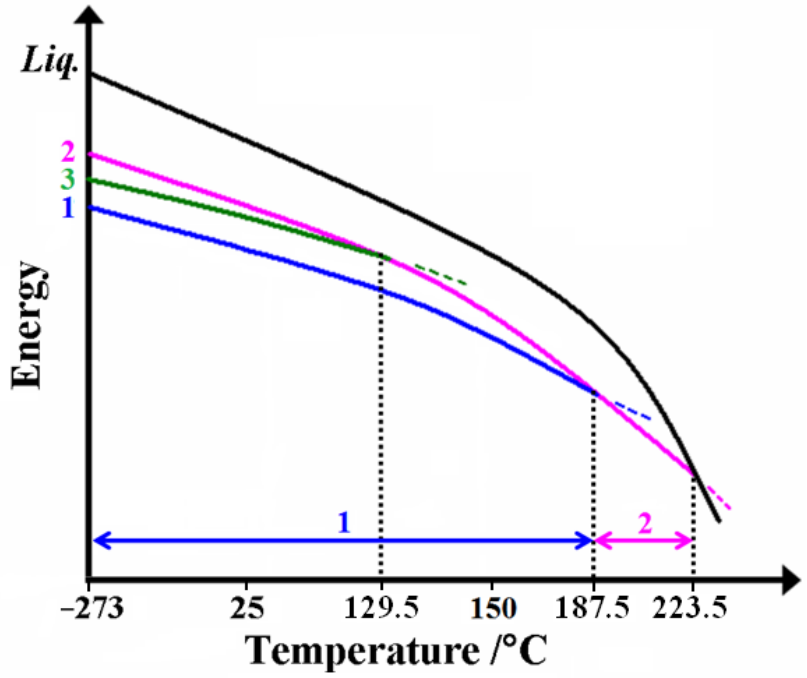

Figure 7.16 Semischematic energy vs temperature diagram to show the relative stability and phase transformation of ATV polymorphs. At -273°C form 1 is the stable phase. Between 25-187.5°C form 1 is the stable modification since form 2 and form 3 converted to form 1 in slurry and grinding experiments. The transition points at 187.5°C and 129.5°C is due to the conversion of form 1 and form 3 to form 2 on heating. Form 2 is the stable phase above 187.5°C before it melts at about 223.5°C. The dashed line indicates that the polymorph has transformed to another phase at that temperature, T_{trs}.

7.9 Pharmaceutical Salt of Atovaquone

In order to address the poor solubility of ATV, mechanochemical grinding of ATV with various GRAS coformers was performed with the intention that the resulting solid forms would enhance the solubility of the parent drug. In the process we obtained a 1:0.5 salt with piperazine from nitromethane solvent with proton transfer occurring from hydroxyl group of naphthaquinone ring to the piperazinyl nitrogen. In the crystal structure the piperazine ring connects the adjacent layers of ATV molecules through N–H···O (1.68Å, 153.3° and 2.35Å,

118.4°) and N–H···O$^-$ (1.64Å, 161.2°) hydrogen bonds (Figure 7.17). This salt was further characterized through IR (Figure 7.18), Raman (Figure 7.19) and the bulk purity was established through PXRD (Figure 7.20) and DSC (Figure 7.21).

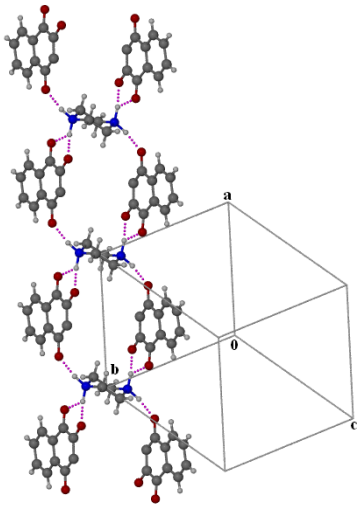

Figure 7.17 Piperazine ring connects adjacent chains of ATV molecules through N–H···O and N–H···O$^-$ hydrogen bonds. Some atoms of ATV molecules are deleted for clarity.

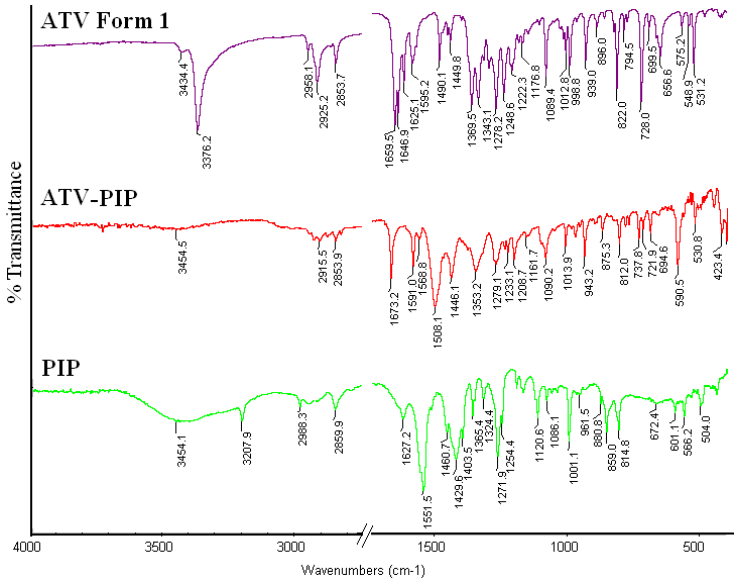

Figure 7.18 IR overlay of ATV-PIP-salt with its starting materials showing significant differences in peak positions.

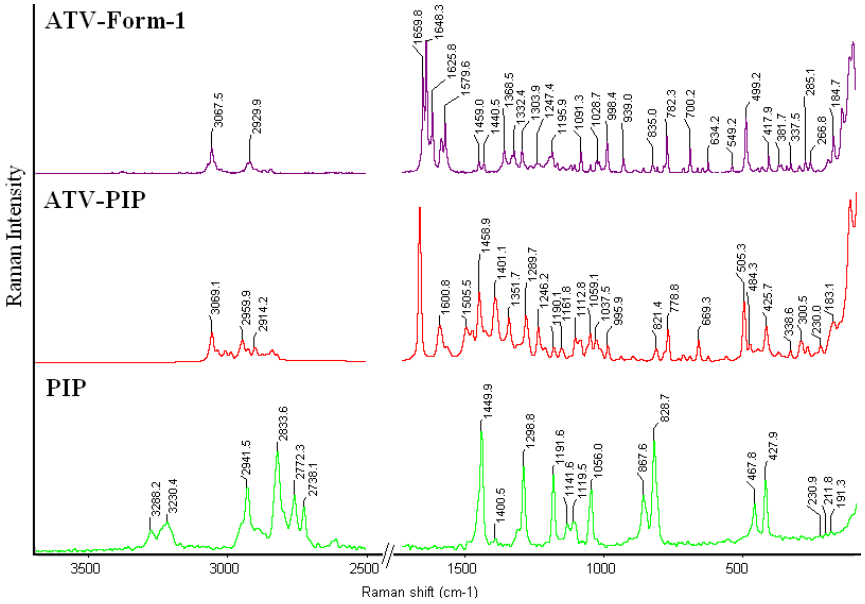

Figure 7.19 Raman overlay of ATV-PIP-salt with its starting materials showing significant differences in peak positions.

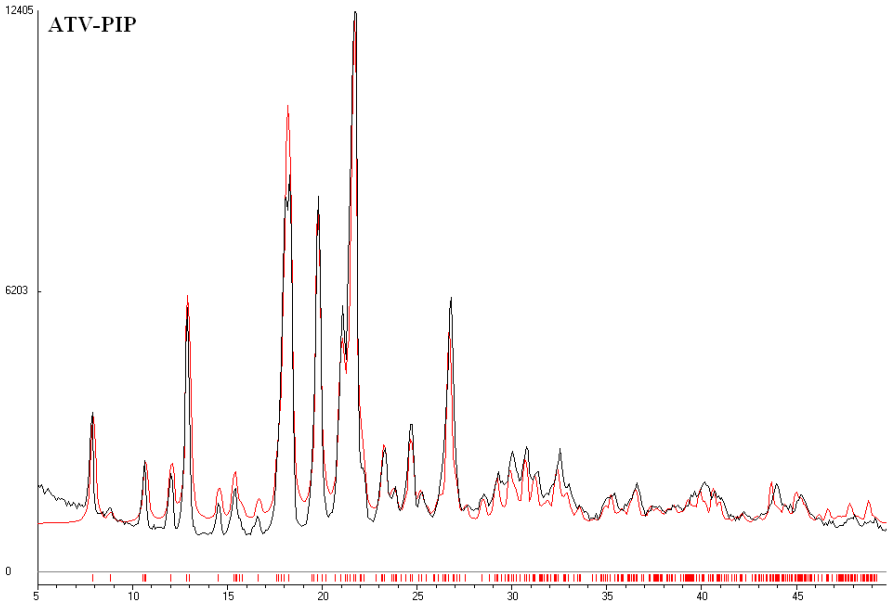

Figure 7.20 Experimental PXRD of ATV-PIP-salt with its calculated pattern showing good match indicating bulk purity.

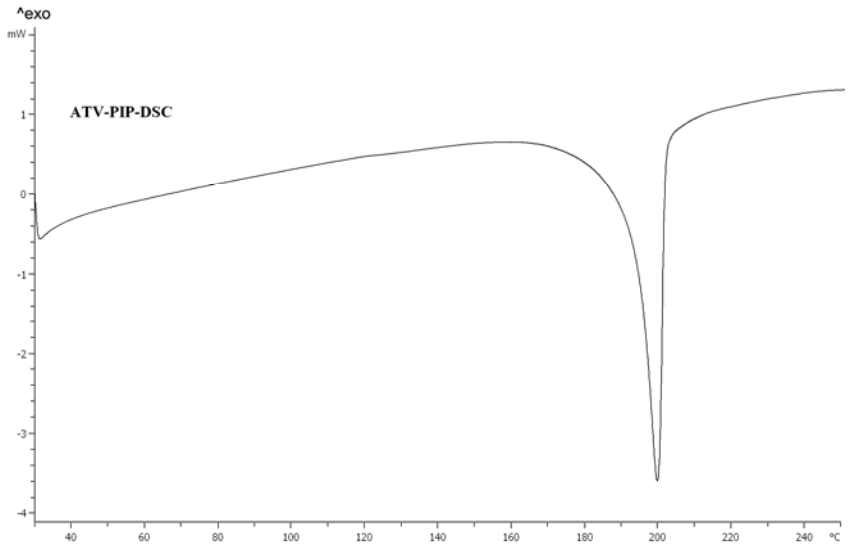

Figure 7.21 DSC analysis of ATV-PIP-salt revealed its melting point as 199.6°C. M.P of ATV form 1 is 221.4°C and that of PIP is 106°C.

Solubility and dissolution of ATV polymorphs and its PIP salt was performed in 60% EtOH water solution to ascertain the solubility advantage of metastable polymorphs and the salt.

7.10 Solubility and Dissolution

ATV is a BCS class II drug with poor solubility of < 2x 10^{-4}mg/mL in water[15]. Hence addressing its poor solubility through modified solid forms of parent compound would enhance its bioavailability and in turn its therapeutic efficacy. Therefore in order to determine the solubility advantage gained on forming solid modifications of ATV, solubility and dissolution studies were performed on the polymorphs and piperazine salt. Due to poor solubility of ATV, solubility experiments were performed in 60% EtOH-water solution. While all the polymorphs were stable at the end of equilibrium solubility experiments, ATV-PIP converted partially to form 1. The stable form 2 and form 3 showed 1.9 and 1.4 times higher solubility compared to ATV form 1 respectively (Table 7.7).

Dissolution experiments were performed on ATV polymorphs and its PIP salt in order to estimate the rate at which the ATV solid forms dissolved into solution. Dissolution

experiments were performed for 6hrs in 60% EtOH-water solution by the rotating disc intrinsic dissolution rate method[25]. ATV form 2, form 3 and ATA-PIP- salt showed 2.1, 1.5 and 17.8 times higher IDR compared to the Form 1 (Figure 7.22). From the solubility experiments we could infer that the ATV polymorphs followed the generally observed trend of metastable polymorphs being more soluble than their stable counterparts and that the ATA-PIP salt with improved solubility could be useful in making a better therapeutic formulation of ATV. PXRD plots of the residue at the end of the equilibrium solubility and dissolution experiment are shown in Figure 7.23.

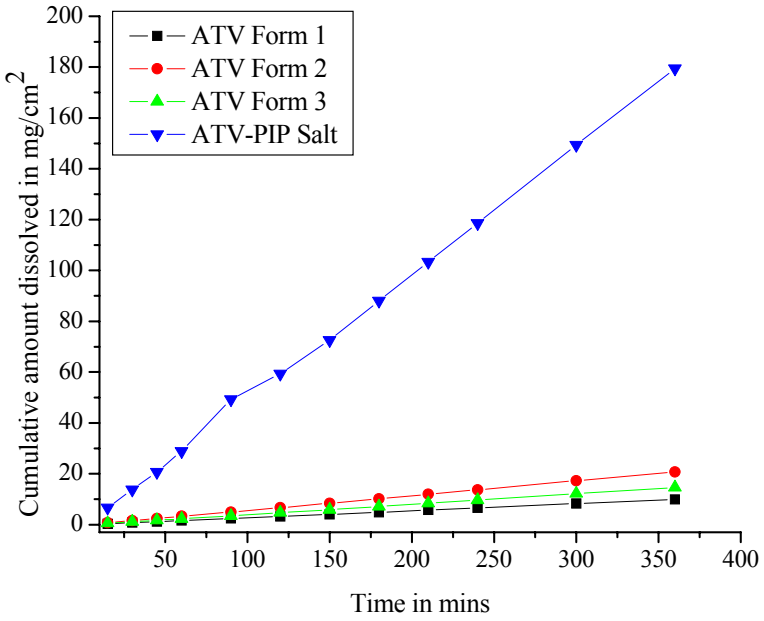

Figure 7.22 Intrinsic dissolution rate curves of ATA polymorphs and its salt with PIP in 60% EtOH-water.

Table 7.7 Intrinsic dissolution rates of ATV polymorphs along with their molar extinction coefficient (ε), and solubility values. The number of times enhancement of IDR and solubility with respect to ATV form 1 is given in parentheses.

Form	Molar extinction coefficient (ε) /mM	Equilibrium solubility (mg/L)	Intrinsic dissolution rate (IDR) mg/cm^2/min (x 10^{-3})
Form 1	26.67	101.71	26
Form 2	23.51	193.48 (x 1.9)	54 (x 2.1)
Form 3	27.52	142.41 (x 1.4)	38 (x 1.5)
ATV-PIP salt	24.61	–	464 (x 17.8)

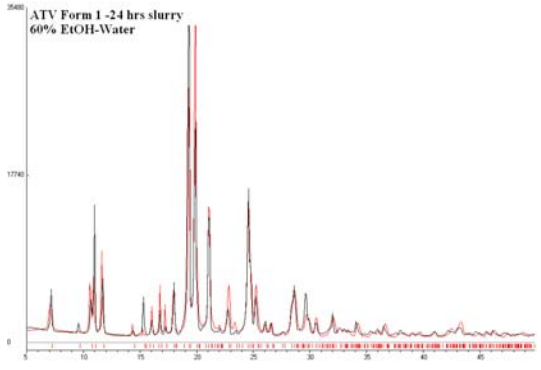

(a)

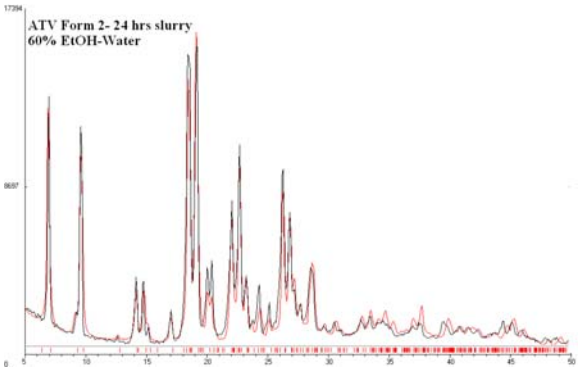

(b)

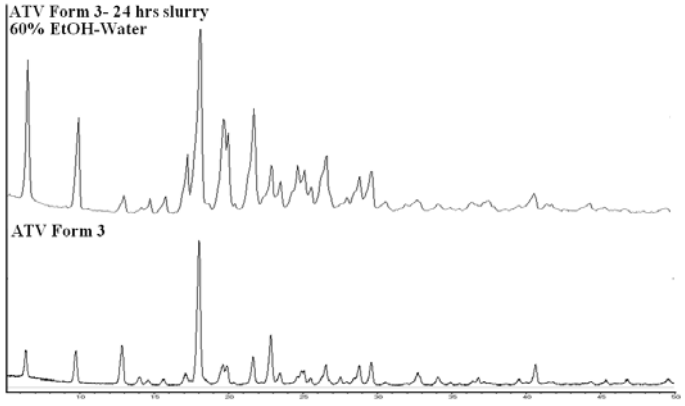

(c)

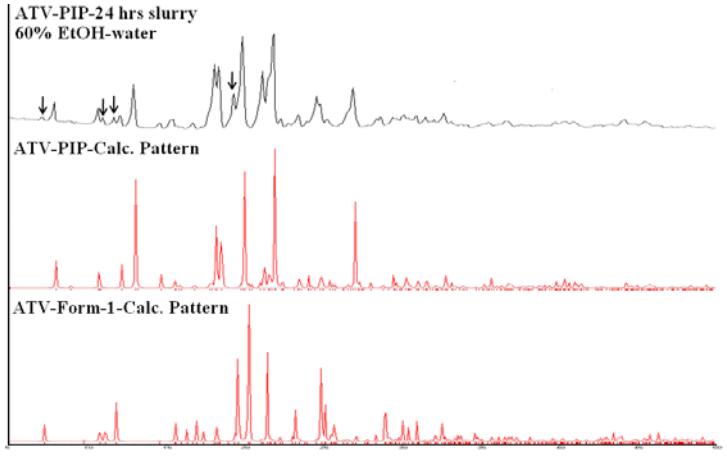

(d)

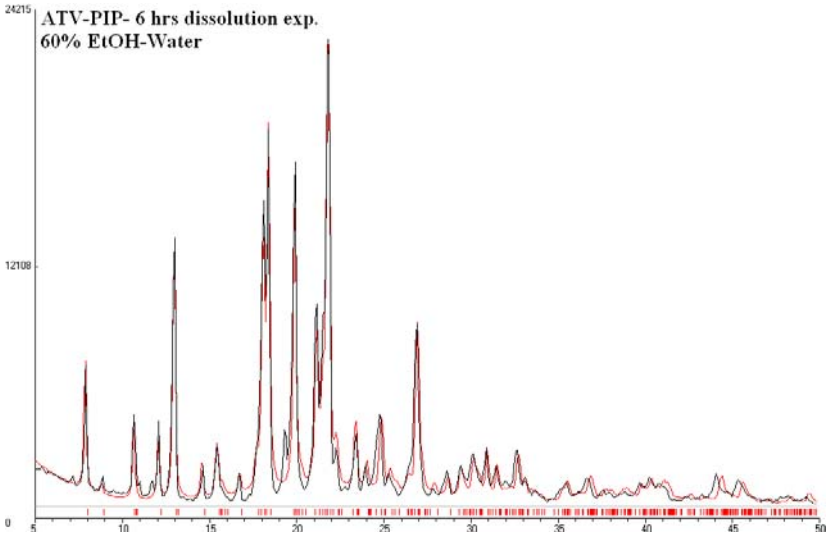

(e)

Figure 7.23 PXRD spectra of **a)** ATV Form 1 **b)** ATV Form 2 **c)** ATV Form 3 at the end of equilibrium solubility experiments showed good overlay with their calculated patterns (with pure experimental spectra in case of form 3) indicating phase stability. Similar stability relationship was observed in their dissolution experiments. **d)** Solubility experiments on ATV-PIP indicated partial conversion to form 1(indicated by arrows), **e)** while it was stable in dissolution experiments showing good overlay with its calculated pattern.

7.11 Conclusions

In this chapter identification, characterization and understanding the stability relationship between three polymorphs of Atovaquone and solubility enhancement through a pharmaceutical salt with piperazine is discussed. All the polymorphs and the piperazine salt were fully characterized by spectroscopic, thermal and diffraction methods. Structural analysis revealed a prominent centrosymmetric O–H···O dimer in form 1 and form 2 polymorphs and N–H··O and N–H···O^- interactions in ATV-PIP salt. Attempts are being made to solve the structure of ATV form 3 from powder data. With minor conformational and synthon differences, this system is shown to be a prominent example of packing polymorphism. Application of thermal methods like DSC and HSM showed that both form 1 and form 3 are enantiotropically related to form 2. In combination with slurry and grinding techniques, we have established form 1 as the thermodynamic phase followed by form 3 and form 2 which is quiet opposite to the stability order proposed by Malpezzi and coworkers. Solubility and Dissolution studies showed that all the polymorphs were stable in 60% EtOH-water media and they followed the generally observed trend of metastable forms being more soluble compared to their stable counterparts. While the metastable Form 2 and form 3 showed 1.9 and 1.4 times more solubility, their IDR values are 2.1 and 1.5 times higher compared to form 1. The novel ATA-PIP salt showed 17.8 times higher IDR compared to the parent compound hinting at the improved solubility on forming salt. In essence we have highlighted the importance of thorough characterization in establishing the stability relationships between the polymorphs. They are important not only in overcoming accidental phase transformations but also in judicious selection of the optimal solid form for maximal drug delivery.

7.12 Experimental Section

Preparation of ATV polymorphs ATV was purchased from commercial suppliers from China. Crystallization of this sample from common solvents like acetonitrile and nitromethane at very dilute concentrations (15mg in 17mL) yielded Atovaquone form 1

crystals. Saturated solution of CH_3CN yielded form 2 immediately. Later, form 1 crystals grew from this solution at the expense of form 2.

Long plates of form 2 suitable for single crystal X-ray analysis was obtained exclusively from Isopropanol, by slow evaporation of 20 mg of the compound dissolved in 8 mL of the solvent.

Form 3 was obtained by the following procedure: 1gram of Form 1 was dissolved in 35mL of Dichloromethane and filtered to remove undissolved particles. The clear solution was either added to a vessel containing liquid nitrogen or the beaker containing Atovaquone solution was immersed in a bath containing liquid nitrogen. Both the procedures resulted in immediate solidification. PXRD and DSC patterns of the solid mass indicated a novel polymorph.

Computations Conformer energies were calculated in Gaussian03 (B3LYP/6-31G (d,p)).[25] Since the observed conformation in the crystal structure is usually different from the gas phase minimized conformer and often higher in energy, constrained optimization of the crystal conformer was carried out by keeping the main torsion angles fixed but allowing bond distances and angles to relax at the nearest local minima (E_{conf}). Lattice energies were computed in Cerius[2] using the COMPASS force field[26]. Crystal structures were minimized (U_{latt}) by allowing small variations in cell parameters but not gross differences between the calculated and experimental crystal lattice.

Phase Transformation Experiment All the slurry and grinding experiments were performed on 100 mg scale with the procedure similar to that used in Chapter 4.

Dissolution and solubility measurements The experimental procedure for performing solubility and dissolution experiments on ATV polymorphs and salt in 60% EtOH-Water and at a λ_{max} of 277 nm is similar to that described in chapter 3.

7.13 References

1. (a) W. C. McCrone, *Physics and chemistry of the organic solid state,* D. Fox, M. M. Labes and A. Weissberger, eds. Wiley Interscience, New York, 1965 (b) J. Haleblian and W. McCrone, *J. Pharm. Sci.*, 1969, **58**, 911.
2. E. Mitscherlich, *Abhl. Akad. Berlin,* 1822-1823, 43.
3. (a) A. Burger, *Topics in Pharmaceutical Sciences*, ed., D. D. Bremer and P. Speiser, Elsevier, Amsterdam, 1983, p.347. (b) J. K. Haleblian, *J. Pharm. Sci*., 1975, **64**, 1269. (c) S. R. Byrn, *Solid State Chemistry of Drugs*, Academic Press, New York, 1982.
4. (a) J. Bernstein, *J. Phys. D; Appl. Phys.,* 1993, **26**, 1366 (b) J. Bernstein and E. Chosen, *Mol. Cryst. Liq. Cryst.,* 1988, **164**, 213.
5. D. A. Mannock, R. N. A. H. Lewis, A. Sen and R. N. McElhaney, *Biochemistry*, 1988, **27**, 6852.
6. (a) J. Bernstein, *Polymorphism in Molecular Crystals*, Oxford University Press, Oxford, 2002 (b) J. Bernstein, *Cryst. Growth Des.,* 2011, **11**, 632-650.
7. (a) A. Koda, S. Ito, S. Itai and K. Yamamoto, *J. Pharm. Sci. Technol. Jpn.,* 2000, **60**, 43-52 (b) A. J. Aiguiar and J. E. Zelmer, *J. Pharm. Sci.*, 1969, **58**, 983. (c) A. T. Florence and D. Attwood, *Physicochemical Principles of Pharmacy*, Pharmaceutical Press, London, UK, 2006.
8. (a) http://findarticles.com/p/articles/mi_m1200/is_8_166/ai_n7069007/pg_1 (b) S. R. Chemburkar, J. Bauer, K. Deming, H. Spiwek, K. Patel, J. Morris, R. Henry, S. Spanton, W. Dziki, W. Porter, J. Quick, P. Bauer, J. Donaubauer, B. A. Narayanan, M. Soldani, D. Riley and K. McFarland, *Org. Process Res. Dev.* 2000, **4**, 413.
9. (a) B. Sarma, S. Roy and A. Nangia, *Chem. Commun.,* 2006, 4918-4920 (b) P. McArdle, K. Gilligan, D. Cunningham and A. Ryder, *Appl. Spectrosc.,* 2005, **59**, 1365 (c) D. Spiegeleer, D. Seghers, R. Wieme, J. Schaubroeck, F. Verpoort, G. Slegers and L. Van Vooren, *J. Pharm. Biomed. Anal.,* 2005, **39**, 275. (d) S. Dharmayat, J. C. De Ande, R. B. Hammond, X. Lai, K. J. Roberts and X. Z. Wang, *J. Cryst. Growth,* 2006, **294**, 35. (e) Y. Hu, H. Wikström, S. R. Byrn and L. S. Taylor, *J. Pharm. Biomed. Anal.,* 2007, **45**, 546.

10. (a) K. S. Dempah, D. H. Barich, A. M. Kaushal, Z. Zong, S. D. Desai, R. Suryanarayan, L. Kirsch and E. J. Munson, *AAPS Pharm. Sci. Tech*., 2013, **14**, 19 (b) K. Ajito, Y. Ueno, H. J. Song, E. Tamechika and N. Kukutsu, *Mol. Cryst. Liq. Cryst.,* 2011, **538**, 33. (c) D. B. Sattin and M. C. Goh, *J. Biol. Phys.,* 2006, **32**, 153.
11. (a) A. Y. Hassan, A. B. Andrei and F. Serban, *Biopolymers*, 2002, **67**, 56 (b) E. Swanepoel, W. Liebenberg and M. M. De Villiers, *E. J. Pharm Biopharm.,* 2003, **55**, 345.
12. (a) W. T. Hughes, W. Kennedy, J. L. Shenep, P. M. Flynn, S. V. Hetherington, G. Fullen, D. J. Lancaster, D. S. Stein, S. Palte, D. Rosenbaum, S. H. T. Liao, M. R. Blum and M. D. Rogers, *J. Infect. Dis.,* 1991, **163**, 843. (b) Y. C. Martin, T. M. Bustard and K. R. Lynn*, J. Med. Chem.,* 1973, **16**, 1089.
13. M. Fry and M. Pudney, *Biochem. Pharmacol.,* 1992, **43**, 1545
14. http://www.rxlist.com/mepron-drug.htm
15. https://www.gsksource.com/gskprm/en/US/adirect/gskprm?cmd=ProductDetailPage&product_id=1244172404936&featureKey=600601
16. (a) A. T. Hudson and A. W. Randall, *US Pat.,* 5053432, 1991 (b) A. R. Dearn, *US Pat.,* 6018080, 2000 (c) M. A. Crasto and A. M. Khan, *US Pat.,* 0105350A1, 2009.
17. (a) V. R. Tarur, *US Pat.,* 0241311A1, 2006. (b) A. Kumar, S. Y. Dike, P. K. Mathur, N. T. Byju, B. Sharma, S. S. Kore, V. S. Buchude and D. Singh, *US pat.,* 2009/0221715 A1, 2009.
18. (a) L. Malpezzi, C. Fuganti, E. Maccaroni, N. Masciocchi and A. Nardi, *J. Therm. Anal. Calorim.,* 2010, **102**, 203-210. (b) R. Ceolin and I. B. Reitveld, *J. Therm. Anal. Calorim.*, 2010, **102**, 203. (c) S. K. Nayak, S. B. Mallik, S. P. Kanaujia, K. Sekar, K. R. Ranganathan, V. Ananthalakshmi, G. Jeyaraman, S. S. Saralaya, K. S. Rao, K. Sridhara, K. Nagarajan and T. N. G. Row, *CrystEngComm,* 2013, **15**, 4871-4884.
19. (a) M. C. Etter, J. C. Macdonald and J. Bernstein, *Acta Crystallogr. Sect. B,* 1990, **46**, 256. (b) M. C. Etter and S. M. Reutzel, J. *Am. Chem. Soc*., 1991, **113**, 2586. (c) J. Bernstein, R. E. Davis, L. Shimoni and N. L. Chang, *Angew. Chem., Int. Ed. Engl*., 1995, **34**, 1555.

20. (a) R. M. Silverstein, *Spectrometric Identification of Organic Compounds*. 6th Ed.; John Wiley & Sons, Inc.: New York, 2002. (b) E. Smith and G. Dent, *Modern Raman Spectroscopy, A Practical Approach*, John Wiley: New York, 2005.
21. A. Burger and R. Ramberger, *Microchim. Acta II*, 1979, 273.
22. D. E. Braun, T. Gelbrich, V. Kahlenberg, G. Laus, J. Wieser and U. J. Griesser, *New J. Chem.,* 2008, **32**, 1677-1685.
23. (a) J. O. Henck, Konformationspolymorphie n-butylsubstituierter Arzneistoffe. Innsbruck: Thesis, p 41 (b) D. E. Braun, T. Gelbrich, V. Kahlenberg, R. Tessadri, J. Weiser and U. J. Griesser, *J. Pharm. Sci*., 2009, **98**, 2010 (c) L. Yu, *J. Pharm. Sci*., 1995, **84**, 966 (c) U. J. Griesser, D. Weigand, J. M. Rollinger, M. Haddow and E. Gstrein, *J. Therm. Anal. Calorim*., 2004, **77**, 511.
24. S. Aitipamula, P. S. Chow and R. B. H. Tan, *CrystEngComm,* 2010, **12**, 3691-3697.
25. L. X. Yu, A. S. Carlin, G. L. Amidon and A. S. Hussain, *Int. J. Pharm*., 2004, **270**, 221.

CHAPTER EIGHT

CONCLUSIONS AND FUTURE PROSPECTS

This thesis deals with the identification, characterization and application of various single and multi-component solid forms of Active pharmaceutical Ingredients (APIs). Extensive studies on various solid forms such as polymorphs (Chapter 5 and 7), salts (Chapter 3), cocrystals (Chapter 1 and 6) and eutectics (Chapter 4) of several APIs were carried out with the intent of understanding and solving the problems associated with them.

In Chapter 2, a novel and reliable heterosynthon for sulfonamide group was engineered using Pyridine-*N*-oxide as complementary hydrogen bond acceptor. This was achieved by cocrystallizing model sulfonamides and a drug molecule, Furosemide with pyridine-*N*-oxides by using the traditional solution crystallization, liquid assisted grinding and slurry grinding methods. These experiments have resulted in six new cocrystals containing sulfonamide and pyridine-*N*-oxide moieties. Crystal structure analysis revealed that the exact geometry of the sulfonamide motif, i.e. discrete N–H···O (D), cyclic motifs $R^2_4(8)$ or $R^2_2(4)$ varied from one structure to another. Nevertheless, the heteromeric N–H···$O_{N\text{-}oxide}$ one-point synthon was the recurring interaction in all the structures. Interestingly, the robust N–H···$O_{N\text{-}oxide}$ heteromeric interaction was successful in breaking the stable homomeric sulfonamide dimer of parent sulfonamides in order to form cocrystals. This novel heterosynthon may be useful in forming drug-drug cocrystals between pyridine-*N*-oxide and sulfonamide or carboxamide containing drug molecules.

Aceclofenac (ACF) is a poorly soluble non-steroidal anti-inflammatory drug (NSAID) prone to degradation in strongly acidic/basic conditions. In Chapter 3, novel salts and salt hydrates of ACF were discovered using mild coformers in order to improve its solubility without affecting its stability. Mechanochemical grinding and slurry grinding resulted in salts with

cytosine, lysine, γ-aminobutyric acid and piperazine apart from a cocrystal with bipyridine and a salt hydrate with piperazine. All the salts were characterized by thermal, spectroscopic and diffraction techniques. The intrinsic dissolution rate of highly soluble ACF-LYS is 135 times, solubility is 156 times, and AUC value 127 times higher than that of the reference crystalline drug. Solid form stability at accelerated ICH conditions of 40ºC and 75% RH showed that ACF-LYS is stable for over 8 months. ACF-LYS appears to be a promising salt for further preclinical studies.

The primary aim of Chapter 4 was to explore the structural diversity and determine the stability relationship of polymorphs of a molecule belonging to a rarely polymorphic group of $–SO_2NHCO–$ skeleton containing molecules. This was achieved by the discovery of two polymorphs of a cocrystal involving sulfacetamide (SACT) and acetamide (ACT). Structural analysis showed differences in N–H···O hydrogen bonding and packing modes in these forms. Interestingly, the synthon patterns observed in these polymorphs are quite different from those reported for this group of molecules containing SO_2–NH–C=O functional moiety. A thorough characterization using various thermal, spectroscopic and diffraction techniques established SACT-ACT form 2 as the thermodynamic phase and the form 1 as the metastable kinetic modification.

In Chapter 5, novel binary eutectic compositions of curcumin were discovered using mechanochemical grinding technique. Although the initial interest was to develop novel cocrystals of curcumin for addressing its poor solubility, cogrinding curcumin with various GRAS coformers resulted in eutectic mixtures with nicotinamide (1:2), ferulic acid (1:1), hydroquinone (1:1), tartaric acid (1:1) and p-hydroxybenzoic acid (1:1). The eutectic nature of the compositions was confirmed by a lower melting point and a single endotherm in DSC. The excess thermodynamic functions of these eutectic mixtures were exploited by performing solubility and dissolution studies. The intrinsic dissolution rates of binary eutectic compositions were 3–11 times faster and AUC values 2–6 times higher than pure curcumin and the IDR of three compounds, CUR–NAM, CUR–FA and CUR–HQ, are superior to the previously studied curcumin–resorcinol cocrystal. Since the exact multi-component physical form, such as salt, cocrystal, or eutectic, is not that relevant as long as

the product exhibits improved pharmacokinetic properties and good stability, the eutectic compositions studied here conferred solubility advantage and they were also found to be stable at ambient conditions of 35°C and 40% RH for over 6 months. Our results also show that mechanochemical grinding can induce the generation of eutectic compositions in addition to cocrystal formation.

Sulfacetamide is a highly soluble sulfonamide antibiotic used in the treatment of ocular infections. Due to high solubility in water physiological constraints such as tear flow resulted in considerable drug loss resulting in poor residence time and low bioavailability at the site of action. In Chapter 6, cocrystallization of sulfacetamide (SACT) with various GRAS coformers was performed with the intention that the resulting cocrystals would have the appropriate hydrogen bonding interactions to lower the solubility of SACT which in turn might improve its residence time at the site of action and increase its therapeutic efficacy. Mechanochemical grinding resulted in cocrystals of SACT with caffeine (CAF), theophylline (THEO), isonicotinamide (INIC) and 4,4′-bipyridine (BIP) and a salt with 4-amino pyridine (4AP). The stable SACT-CAF cocrystal has low solubility (0.59 times) compared to the parent drug. Dissolution experiments on these cocrystals showed that SACT-INIC and SACT-CAF have 0.64 times and 0.68 times the IDR of SACT, while SACT-THEO has similar dissolution profile as the reference drug. Although the compatibility of SACT cocrystals for ocular administration needs to be ascertained through in vivo studies, but as such the low solubility and good stability of SACT-CAF cocrystal may be useful in addressing the poor residence time and faster elimination issues associated with sulfacetamide drug.

In Chapter 7, we have characterized and determined the stability relationship between three polymorphs of anti-pneumocystic drug Atovaquone apart from improving its solubility through a piperazine salt. Structural analysis revealed a prominent centrosymmetric O–H···O dimer in the polymorphs, whereas the dimer was disrupted in the salt through N–H··O and N–H···O^- interactions. Thermal methods like DSC and HSM showed that both form 1 and form 3 are enantiotropically related to form 2. In combination with slurry and grinding techniques, we have established form 1 as the thermodynamic phase followed by form 3 and

form 2 which is quiet opposite to the stability order proposed by Malpezzi and coworkers who concluded that form 2 is the thermodynamic form. Solubility and dissolution experiments revealed that the novel ATA-PIP salt showed 17.8 times higher IDR compared to the parent compound. In essence the importance of thorough characterization in establishing the stability relationships between the polymorphs was highlighted.

Future prospects

The novel sulfonamide-pyridine-*N*-oxide heterosynthon discussed in this thesis may be applied to form drug-drug cocrystals between *N*-oxide and sulfonamide containing drug molecules which may synergistically influence each other in improving their therapeutic efficacy. It would also be interesting to test the robustness of this heterosynthon in the presence of other competing donor functional groups like –OH, $-NH_2$, -COOH etc. The eutectic microstructure is poorly understood in organic eutectic materials. It is a current challenge to dissect and analyze the local domain structure of these compounds. Nevertheless, techniques like atomic pair distribution function (PDF) approach and extended X-ray absorption fine-structure spectroscopy (EXAFS) are used to understand local structure of materials and may be useful in understanding the internal crystal lattice of eutectic compositions. Neutron vibrational spectroscopy, which was used in conjunction with density functional approach to determine the structure of amorphous AlB_4H_{11}, may also be informative in understanding the structure of organic eutectic compositions. Further polymorphism in eutectics would be an altogether new area with large scope for exploration. In addition, it would be interesting to test experimentally the observations made in section 5.4.5 of chapter 5 regarding the role of auxiliary interactions, misfit or mismatch of components, internal symmetry and structural similarity in eutectic formation. The solubility lowering ability of cocrystals with the intent of improving bioavailability of parent molecule was explored in chapter 6. It may be further explored with BCS class I and class III compounds having poor bioavailability issues due to high solubility and faster elimination. It would be interesting to see the effect of cocrystallization on the bioavailability of such drug molecules since this aspect of cocrystals is less explored.

ABOUT THE AUTHOR

Nagula Rajesh Goud, eldest son of Mr. N. Laxman Goud and Mrs. N. Rama Devi, was born at Metpalli, Karimnagar District, Andhra Pradesh, India. He received primary education at Raghavendra Convent High School, Metpalli, and did his secondary education (VII to X Std.) at Sri Satya Sai Gurukulam, Rajahmundry. He completed Intermediate (Bi. P. C.) at Sri Satya Sai Higher Secondary School, Puttaparthi. He pursued B. Sc. (B. Z. C.) and M. Sc. (Chemistry) from Sri Satya Sai Institute of Higher Learning, Puttaparthi. He qualified GATE examination in February 2007. In 2008, he was awarded 'Junior Research Fellowship' (JRF) by Council for Scientific and Industrial Research (CSIR), New Delhi, upon qualifying CSIR-UGC-JRF National Entrance Examination. He, then, joined Prof. Ashwini Nangia's Research Group, School of Chemistry, University of Hyderabad, as a PhD Student and was upgraded as a 'Senior Research Fellow' (SRF) in 2010.

LIST OF PUBLICATIONS

1. Crystal Structures of Norfloxacin Hydrates.
   Saikat Roy, **N. Rajesh Goud**, N. Jagadeesh Babu, Javed Iqbal, Anil K. Kruthiventi and Ashwini Nangia.
   Cryst. Growth & Des **2008**, *8*, 4343–4346.

2. Synergistic Pharmaceutical Cocrystals.
   Ashwini Nangia, Anil K. Kruthiventi, Saikat Roy, **N. Rajesh Goud,** Jaggavarapu Satyanarayana Reddy, Javed Iqbal. PCT-WO 2009/136408 A1.

3. Sulfonamide–Pyridine–*N*–Oxide Cocrystals.
   N. Rajesh Goud, N. Jagadeesh Babu and Ashwini Nangia.
   Cryst. Growth & Des **2010**, *11*, 1930–1939.

4. Novel Polymorphs of Curcumin
   Palash Sanphui, **N. Rajesh Goud**, U. B. Rao Khandavilli, Sreenu Bhanoth and Ashwini Nangia,. Indian patent, **2010**, Application no. 3190/CHE/2010.

5. Fluoroquinolone Salts with Carboxylic Acids.
   J.Satyanarayana Reddy, Saraswatula Viswanadha Ganesh, Ravikumar Nagalapalli, Rambabu Dandela, K. Anand Solomon, K. Anil Kumar, **N. Rajesh Goud** and Ashwini Nangia.
   J. Pharm Sci. **2011**, *100*, 3160–3176.

6. New Polymorphs of Curcumin
   Palash Sanphui, **N. Rajesh Goud**, U. B. Rao Khandavilli, Sreenu Bhanoth and Ashwini Nangia.
   Chem.Commun. **2011**, *47*, 5013-5015.

7. Fast Dissolving Curcumin Cocrystals
   Palash Sanphui, **N. Rajesh Goud**, U. B. Rao Khandavilli and Ashwini Nangia
   Cryst. Growth & Des **2011**, *11*, 4135–4145.

8. Novel Furosemide Cocrystals and Selection of High Solubility Drug Forms.
   N. Rajesh Goud, Swarupa Gangavaram, Kuthuru Suresh, Sharmistha Pal, Sulur G.Manjunatha, Sudhir Nambiar, and Ashwini Nangia.
   J. Pharm Sci. **2012,** *101*, 664–680.

9. Fast Dissolving Eutectic Compositions of Curcumin.
   N. Rajesh Goud, Kuthuru Suresh, Palash Sanphui and Ashwini Nangia.
   Int. J. Pharm. **2012,** *439*, 63-72.

10. Solubility and Stability Advantage of Aceclofenac Salts.
    N. Rajesh Goud, Kuthuru Suresh and Ashwini Nangia.
    Cryst. Growth Des. **2013**, *13*, 1590-1601.

11. Polymorphism in Sulfacetamide-Acetamide Cocrystal
    N. Rajesh Goud and Ashwini Nangia (Manuscript Communicated)

12. Novel Cocrystals of Sulfacetamide
    N. Rajesh Goud, Ronak Ali Khan and Ashwini Nangia (Manuscript under preparation)

13. Relative Stability of Atovaquone Polymorphs
    N. Rajesh Goud and Ashwini Nangia (Manuscript under preparation)

14. Highly Solubility Sodium and Potassium Salt Hydrates of Furosemide
    Swarupa Gangavaram, U. B. Rao Khandavilli, **N. Rajesh Goud**, S. Raghavender, Suryanarayan Cherukuvada, Sharmistha Pal, Sulur G.Manjunatha, Sudhir Nambiar, and Ashwini Nangia. (Manuscript under preparation)

15. Isostructural Cocrystals of Andrographolide – Addressing Chemical Instability and Poor Solubility
    Kuthuru Suresh, **N. Rajesh Goud** and Ashwini Nangia (Manuscript under preparation)

16. Polymorphs, Salts and Cocrystals: What's in a name?

S. Aitipamula, R. Banerjee, A. K. Bansal, K. Biradha, M. L. Cheney, A. R. Chowdhury, G. R. Desiraju, A. G. Dikundwar, R. Dubey, N. Duggirala, P. P. Ghogale, S. Ghosh, P. K. Goswami, **N. Rajesh Goud**, R. R. K. R. Jetti, P. Karpinski, P. Kaushik, D. Kumar, V. Kumar, B. Moulton, A. Mukherjee, G. Mukherjee, A. S. Myerson, V. Puri, A. Ramanan, T. Rajamannar, C. M. Reddy, N. Rodriguez-Hornedo, R. D. Rogers, T. N. Guru Row, P. Sanphui, N. Shan, G. Shete, A. Singh, C. C. Sun, J. A. Swift, R. Thaimattam, T. S. Thakur, R. K. Thaper, S. P. Thomas, S. Tothadi, V. R. Vangala, N. Variankaval, P. Vishweshwar, D. R.Weyna and M. J. Zaworotko.

Cryst. Growth Des., 2012, **12**, 2147-2152.

PARTICIPATION IN SYMPOSIA & CONFERENCES

1. Participated in the **1st Indo-US Bilateral Workshop** on **"Pharmaceutical Cocrystals and Polymorphs"** held at Hotel Regaalis, Mysore, India, during February 8-11, 2009.
2. Participated in the "**38th National Seminar on Crystallography"** held at University of Mysore, Mysore, India, during February 11-13, 2009.
3. Presented a poster entitled **"Sulfonamide-Pyridine-*N*-Oxide Cocrystals"** at the **International Conference on the Chemistry of Organic Solid state (ICCOSS) XX** held at Indian Institute of Science, Bengaluru, India, during June 26-30, 2011.
4. Presented a poser entitled **"Novel Solid Forms of Furosemide and Selection of High Solubility Drug Forms"** at the 2nd Indo-US Bilateral Workshop on "**Evolution of Solid State Science in Pharmaceutical Industry"** held at Gurgaon, New Delhi, during February 2-4, 2012.
5. Delivered an oral presentation entitled **"Novel Solid Forms of Furosemide and Selection of High Solubility Drug Forms"** at the **Chemfest 2012** held at University of Hyderabad, Hyderabad, India, during February 25-26, 2012.